Supplementary Information for

Late-stage Deuteration of Arenes in D_2O Exclusively Driven by Single-atom Pt Sites under Visible Light

Jie Xu[1,2], Xin-Yuan Wu[1,2], Rui Cao[1,2], Da Zhao[3], Xi-Zhong Song[4], Huan Chen[5], Wen-Wei Li[1,2], Tingrui Pan[6], K.M. Liew[7], Flemming Besenbacher[8], Yi-Tao Dai[1,2,4]*

[1]State Key Laboratory of Precision and Intelligent Chemistry, School of Chemistry and Materials Science, School of Nano Science and Technology, University of Science and Technology of China; Hefei, Anhui 230026, China

[2]Suzhou Key Laboratory of Water Environment Science and Technology, Suzhou Institute for Advanced Research, University of Science and Technology of China; Suzhou, Jiangsu 215123, China

[3]School of Chemical Sciences, University of Chinese Academy of Sciences; Beijing 101408, China

[4]Jiangxi Fangzhu Pharmaceutical Co., Ltd.; Xinyu, Jiangxi 338000, China

[5]Peric Technology Co., Ltd.; Handan, Hebei 056027, China

[6]Institute of Biopharmaceutical and Health Engineering (iBHE), Tsinghua Shenzhen International Graduate School, Tsinghua University; Shenzhen 518055, China

[7]Department of Architecture and Civil Engineering, Centre for Nature-Inspired Engineering, City University of Hong Kong; Hong Kong, China

[8]Interdisciplinary Nanoscience Center (iNANO), Aarhus University; DK-8000 Aarhus C, Denmark

*Corresponding author. Email: yitaodai@ustc.edu.cn

Table of Contents

1. General information

Unless otherwise noted, all reagents, substrates, and solvents were obtained from commercial suppliers (including Bidepharm: https://www.bidepharm.com/; Leyan: https://www.leyan.com/; Aladdin: https://www.aladdin-e.com/; Macklin: https://www.macklin.cn/; Energy: https://www.energy-chemical.com/; Sinopharm: https://www.sinoreagent.com/) and used without further purification. NMR spectra were recorded on a Bruker spectrometer at 400 MHz (^{1}H NMR), 92 MHz (^{2}H NMR), 376 MHz (^{19}F NMR). Chemical shifts were reported relative to tetramethylsilane, D_2O 4.79 ppm for ^{1}H), $CDCl_3$ (7.26 ppm for ^{1}H), DMSO-d_6 (2.50 ppm for ^{1}H). The following abbreviations (or combinations thereof) were used to explain multiplicities: s = singlet, d = doublet, t = triplet, q = quartet, m = multiplet, br = broad. Coupling constants, *J*, were reported in the Hertz unit (Hz). All measurements were carried out at room temperature unless otherwise stated. The ^{1}H NMR of the substrates was measured directly without further purification. The degree of deuterium incorporation was determined by the decrease of ^{1}H NMR signal intensities in comparison with the unlabeled one. To get a precise integration by quantitative NMRs, we did as follows: (1) Checking for a proper phase correction. (2) Making appropriate baseline correction (baseline must be flat and, most importantly, situated at zero value of the vertical (y) axis). (3) Always using the same integration region, the width of which is defined by a constant multiple of the signal half-width. (4) Using the signals of the undeuterated C–H positions as internal references, which have equal intensities in contrast to reactants. In cases where deuterium exchange happened at all the C(sp^2)–H positions without the unlabeled parts as internal references, *e.g.*, **8b**, **9b**, and **35b-38b**, we introduced an internal standard 1,4-dioxane to identify the deuterium content of products.

2. Photocatalyst preparation

Raw Materials: the following noble-metals, semiconductors and solvents were obtained from commercial suppliers: $H_2PtCl_6 \cdot xH_2O$ (Energy, 99.9%), K_2PdCl_4 (Aladdin, ≥99.95% metals basis), $RuCl_3 \cdot 3H_2O$ (Macklin, 98%), $RhCl_3 \cdot 3H_2O$ (Macklin, 99.95% metals basis), $IrCl_3 \cdot 3H_2O$ (Energy, 98%), $AuCl_3$ (Aladdin, ≥99.9% metals basis), Pt/C (Energy, 10% Pt), TiO_2-R (Aladdin, commercial rutile, 99.8% metals basis), Nb_2O_5 (Macklin, 99.99% metals basis), $SrTiO_3$ (Macklin, 99.5% metals basis), $BiVO_4$ (Energy, 99.9% metals basis), BiOCl (Aladdin, ≥99%), $Ti(OBu)_4$ (Aladdin, ≥99%), EtOH (Sinopharm, Ar, ≥99.7%), $NH_3 \cdot H_2O$ (Sinopharm, Ar), *i*-PrOH (Macklin, HPLC purity ≥99.9%), Melamine (Macklin, 99.8%).

2.1 Preparation of TiO_2-h

Firstly, 30 mL $Ti(OBu)_4$ was added to 100 mL absolute ethanol, which was stirred on a thermostatic stirrer for 10 min to form a uniform light-yellow solution. Then, 10 mL deionized water was added to the above solution dropwise. After 1 h stirring, the suspension was filtered through a funnel. The obtained solid was washed with deionized water 3 times and then dried at 70 °C for 12 h. The sample was transferred to a ceramic crucible and placed in a muffle furnace, which was heated at 500 °C for 2 h (at a heating rate of 10 °C/min). After cooling down, TiO_2-h as a white powder was obtained.

2.2 Preparation of Pt_n/TiO_2-h

According to the literature[1], 300 mg TiO_2-h was dispersed in 10 mL deionized water with 4.4 mg $H_2PtCl_6 \cdot xH_2O$ and was stirred at room temperature. Then, the reactor was illuminated for 1 h with a 365 nm LED lamp. After irradiation, the light grey solids were collected via centrifugation and further washed with ethanol and water. After drying, the sample **Pt_n/TiO_2-h** was obtained.

2.3 Preparation of other photocatalysts (Metal/Semiconductor)

In_2O_3: it was prepared according to the literature[2]. 7 mmol $In(NO_3)_3 \cdot 6H_2O$ were dissolved in 50 mL deionized water under stirring. Then, $NH_3 \cdot H_2O$ was added dropwise until no further precipitation occurred. The resulting white slurry was then placed in a thermostatic water bath and aged at 80 °C for 1 h. Later, the product was separated by centrifugation. The sediment was washed twice with deionized water and then twice with ethanol before drying for 5 h at 60 °C. Finally, the

dried sediment was transferred to a crucible, heated at 350 °C for 3 h in a muffle furnace at a heating rate of 5 °C/min.

C_3N_4: it was prepared by a typical pyrolysis method with melamine as the precursor. The sample was transferred to a ceramic crucible and placed in a muffle furnace, which was heated at 550 °C for 2 h (at a heating rate of 2 °C/min). After cooling down, yellow powders of C_3N_4 were obtained.

According to the synthesis method of Pt_1/TiO_2-h, 500 mg semiconductor powders and required amounts of noble-metal salts were added in a 20 mL water-isopropanol solution (volume ratio of deionized water : *i*-PrOH = 5 : 1) under stirring for 30 min. Then the mixture was irradiated with a 410 nm LED lamp under Ar atmosphere at room temperature. After 10 h irradiation, the photocatalyst was collected via centrifugation and further washed with water. After drying in a vacuum oven, photocatalysts of **M/TiO_2-h** or **Pt/Semiconductors** were obtained. The metal loading was tuned by introducing different amounts of noble-metal salts. Specifically, Pd_1/TiO_2-h, Rh/TiO_2-h, Ir/TiO_2-h, Au/TiO_2-h, Pt/TiO_2-R, Pt/Nb_2O_5, Pt/$SrTiO_3$, Pt/C_3N_4, Pt/In_2O_3, Pt/$BiVO_4$, and Pt/BiClO were prepared accordingly.

3. Photocatalyst characterizations

3.1 X-ray diffraction (XRD)

XRD data were collected on all samples using a Rigaku smartlab X-ray diffractometer equipped with a Cu Kα source (40 kV, 200 mA; λ=1.54178 Å). The XRD patterns were recorded using the conventional θ-2θ geometry (Bragg-Brentano). A scan range from 20 to 80 ° with a step size of 0.02 ° and a scan rate of 20 °/min was employed.

3.2 Electron microscopy

Scanning electron microscope (SEM) images were collected on GeminiSEM 500. Transmission electron microscopy (TEM) images were collected on JEM-2100 Plus. High-resolution TEM (HRTEM) images and energy-dispersive X-ray spectroscopy (EDS) elemental mapping were obtained on JEM-F200. Aberration-corrected high-angle annular dark-field scanning transmission electron microscopy (AC HAADF-STEM) analysis was performed on JEOL JEM-ARM200F operated at 200 kV equipped with a Gatan Quantum 965 image filter system.

3.3 Inductively coupled plasma-mass spectrometry (ICP-MS)

The metal loadings of photocatalysts were precisely analyzed by an inductively coupled plasma mass spectrometer (ICP and Agilent 720ES). For each measurement, a 100 mg sample was dissolved in the mixture of aqua regia and HF for analysis.

3.4 UV-Vis diffuse reflectance spectroscopy (UV-Vis DRS) and photoluminescence (PL)

The UV-Vis DRS profiles were recorded on a PerkinElmer Lambda 365 UV-Vis spectrophotometer at r.t. with $BaSO_4$ (spectroscopy grade) as reference. For each measurement, a 100 mg sample was loaded for analysis. According to the Kubelka-Munk theory, Tauc plots of a direct semiconductor can be drawn by plotting $[F(R)\cdot hv]^2$ versus hv (incident photon energy)^3, where $F(R) = (1\text{-}R)^2/(2R)$ with R as the measured reflectance. To investigate the possible interaction between 4-methoxyphenol and photocatalyst samples, 0.5 mg 4-methoxyphenol was directly mixed with dry sample powders, which were subsequently analyzed by the spectrophotometer to obtain UV-Vis DRS data.

Steady-state PL spectra under control conditions were recorded on a Cary Eclipse fluorescence spectrophotometer using the excitation wavelength of 320 nm. In detail, 1 mg photocatalyst sample was well dispersed in 2 mL D_2O for steady-state PL tests.

3.5 Transient photocurrent

Transient photocurrent tests were performed in a three-electrode system using a CHI660E. Firstly, 10 mg photocatalyst was dispersed in 1 mL Nafion/ethanol solution, which was then sonicated for 30 min to prepare a homogeneous catalyst ink. Subsequently, 0.3 mL catalyst ink was deposited on a clean highly oriented pyrolytic graphite (HOPG) electrode, which was then dried in air for 30 min to serve as the working electrode (WE). Finally, the photocurrent was measured in a 0.5 M Na_2SO_4 electrolyte with Pt mesh as a counter electrode (CE) and Ag/AgCl as a reference electrode (RE). Meanwhile, a timer was used to control the on-off intervals of light irradiation (410 nm, 300W Xe lamp with a filter).

3.6 In situ mass spectrometry

To identify the gas composition during photocatalytic HIE of 4-methoxyphenol in D_2O, the gas phase was analyzed qualitatively and quantitatively using an *in situ* mass spectrometer (MS, PM-QMS, Pro-Tech). Since the system had a well-defined volume and was leak-tight, the quantity of evolved gases can be calculated based on their partial pressure by applying the ideal gas law calibrated with the MS sensitivity factor. The *in situ* MS system can be employed to monitor the evolution of several gases (e.g., H_2, HD, D_2) all at once.

3.7 Fourier transform infrared spectroscopy (FT-IR)

3.7.1 Diffuse reflectance infrared Fourier transform spectroscopy (DRIFTS) analysis

DRIFTS experiments were conducted using the Praying Mantis accessory (Harrick) in a Nicolet iS20 spectrometer equipped with an MCT detector. The fresh powder sample (e.g., TiO_2-h, Pt_1/TiO_2-h, and organic substrates mixed with Pt_1/TiO_2-h) was placed in the catalytic reaction chamber equipped with a three-window dome (two ZnSe windows and one quartz window) and coupled with a temperature controller for heating. Firstly, the sample was heated from R.T. to 120 °C for 30 min under Ar flow (20 mL/min) to remove the adsorbed water molecules. After the sample was cooled down to r.t. under Ar flow, IR spectra were recorded.

3.7.2 *In situ* DRIFTS analysis

DRIFTS As shown in Supplementary Fig. 29, an *in situ* DRIFT setup was home-built to investigate the HIE process at the surface of the photocatalyst. The setup consisted of the following parts: (1) a Nicolet iS20 spectrometer equipped with an MCT detector and a Praying Mantis™ HVC accessory enclosed with a three-window dome (Harrick Scientific Products, Inc.) as the reaction chamber; (2) an ATC temperature controller with a cooling water circulating system; (3) a 410 nm LED lamp for light irradiation; (4) Ar as carrier gas introduced by a mass flow controller (MFC). To study the possible reaction pathway during the HIE reaction of phenol, *in situ* DRIFTS experiments were conducted as follows: Initially, the fresh powder sample (e.g., Pt_1/TiO_2-h) was loaded in the reaction chamber. Then, the sample was heated at 120 °C for 30 min under Ar flow (20 mL/min) to remove the adsorbed water. After cooling down to room temperature, phenol vapor was introduced into the chamber via a syringe. Later, the sample was flushed with Ar flow (20 mL/min) for 10 min to remove physically adsorbed phenol. IR spectra were recorded in dark and

light irradiation, respectively. To investigate the dynamic changes under light irradiation in the presence of D_2O, sufficient D_2O vapor was introduced into the chamber via a syringe. Subsequently, photocatalysts covered with phenol and D_2O molecules in the closed chamber were irradiated by a 410 nm LED lamp. Simultaneously, IR spectra were recorded repeatedly with a certain time interval.

3.8 X-ray Absorption Spectroscopy (XAS)

3.8.1 XAS measurements and data processing

The X-ray absorption spectra at the Pt L_3-edge were recorded at the XAS station (BL14W1) of the Shanghai Synchrotron Radiation Facility (SSRF). The electron storage ring was operated at 3.5 GeV. Using Si (311) double-crystal monochromator, the data collection was carried out in fluorescence excitation mode for Pt L_3-edge XAFS. All spectra were collected in ambient conditions. By using the third ionization chamber, standard samples including Pt foil and PtO_2 were measured simultaneously for energy calibrations. The beam size was limited by the horizontal and vertical slits with an area of 1 × 4 mm^2 during XAFS measurements. The as-obtained, raw XAFS data were processed using WinXAS version 3.1.

3.8.2 XAS data analysis

The EXAFS data were processed according to the standard procedures using the Athena and Artemis implemented in the IFEFFIT software packages. The EXAFS spectra were obtained by subtracting the post-edge background from the overall absorption and then normalizing with respect to the edge-jump step. Subsequently, the $\chi(k)$ data of Fourier were transformed to real (R) space using a hanning windows (dk=1.0 $Å^{-1}$) to separate the EXAFS contributions from different coordination shells. To obtain the quantitative structural parameters around central atoms, least-squares curve parameter fitting was performed using the ARTEMIS module of IFEFFIT software packages.

The following EXAFS equation was employed:

$$\chi(k) = \sum_j \frac{N_j S_o^2 F_j(k)}{k R_j^2} \exp[-2k^2\sigma_j^2] \exp[\frac{-2R_j}{\lambda(k)}] \sin[2k R_j + \phi_j(k)]$$

S_0^2 is the amplitude reduction factor, $F_j(k)$ is the effective curved-wave backscattering amplitude, N_j is the number of neighbors in the j^{th} atomic shell, R_j is the distance between the X-

ray absorbing central atom and the atoms in the j^{th} atomic shell (backscatterer), λ is the mean free path in Å, $\phi_j(k)$ is the phase shift (including the phase shift for each shell and the total central atom phase shift), σ_j is the Debye-Waller parameter of the j^{th} atomic shell (variation of distances around the average R_j). The functions $F_j(k)$, λ, and $\phi_j(k)$ were calculated with the ab initio code FEFF8.2. The coordination numbers of model samples were fixed as the nominal values. The obtained S_0^2 was fixed in the subsequent fitting. While the internal atomic distances R, Debye-Waller factor δ^2, and the edge-energy shift ΔE_0 were allowed to run freely.

3.9 High-resolution Mass Spectrometry (HRMS)

The HRMS analysis was recorded on a Thermo Fisher Scientific Q-Exactive mass spectrometer using the ESI (electrospray ionization) model (Analyzer: Orbitrap). Accurate masses were reported for the molecular ion + hydrogen ([M+H$^+$]) or molecular ion - hydrogen ([M-H$^+$]). For each measurement, 50% methanol and 50% water were used as the mobile phase.

3.10 Electron Paramagnetic Resonance (EPR)

EPR measurements were performed at an EMXplus electron paramagnetic resonance spectrometer to investigate possible radicals with 5,5′-dimethyl-1-pyrroline-N-oxide (DMPO) as the radical scavenger. First, in the glove box, a suspension with 25 mg photocatalysts and 0.1 mmol DMPO in 1 mL D_2O was prepared. Then, a certain amount of the suspension was sucked into a capillary (inner diameter of 0.9 mm). After sealing one end of the capillary, it was transferred to an EPR quartz tube (inner diameter of 4 mm) with a leak-tight cap. Later, the EPR tests were performed with the suspension in the quartz tube irradiated by a 410 nm LED lamp. In addition, the suspension without light irradiation was tested with EPR as well for comparison.

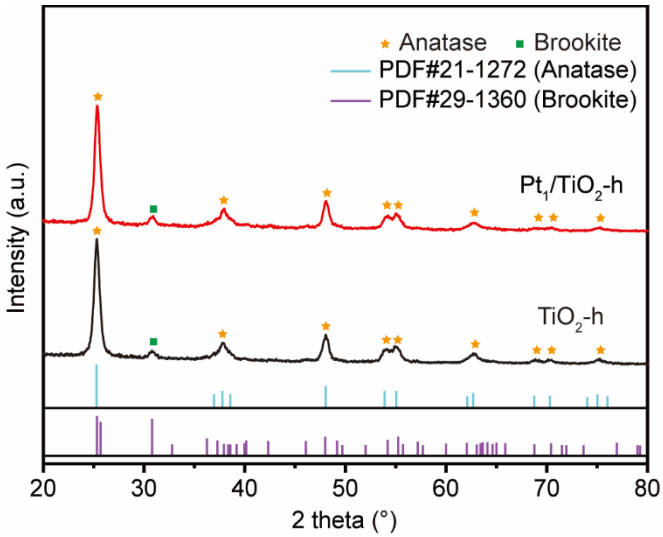

Supplementary Figure 1. XRD patterns of TiO_2-h and Pt_1/TiO_2-h. The standard JCPDS cards of anatase (PDF#21-1272) and brookite (PDF#29-1360) TiO_2 were incorporated for comparison.

In comparison with the pristine homemade TiO_2 (TiO_2-h), the XRD pattern of the sample loaded with Pt (Pt_1/TiO_2-h) showed that there was no significant change in crystal phases without the observation of diffraction peaks attributed to Pt nanoparticles.

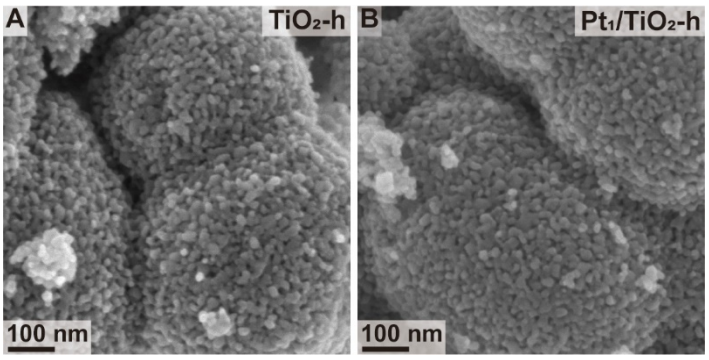

Supplementary Figure 2. SEM images of (A) TiO_2-h and (B) Pt_1/TiO_2-h.

The SEM data of TiO_2-h showed the aggregation of spherical particles, with the particle size ranging between 15-25 nm. Moreover, there is no significant change in morphology for the sample loaded with Pt (Pt_1/TiO_2-h) in comparison with pristine TiO_2-h.

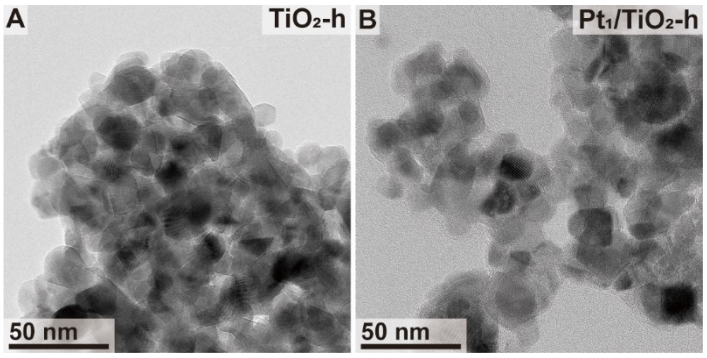

Supplementary Figure 3. TEM images of (A) TiO_2-h and (B) Pt_1/TiO_2-h.

To further clarify the microstructures of the photocatalysts, we conducted TEM characterizations. TEM images revealed that TiO_2-h has a well-defined nanoparticle structure and no significant change in morphology appeared after loading Pt via the photo-deposition method. Moreover, no Pt nanoparticles were detected.

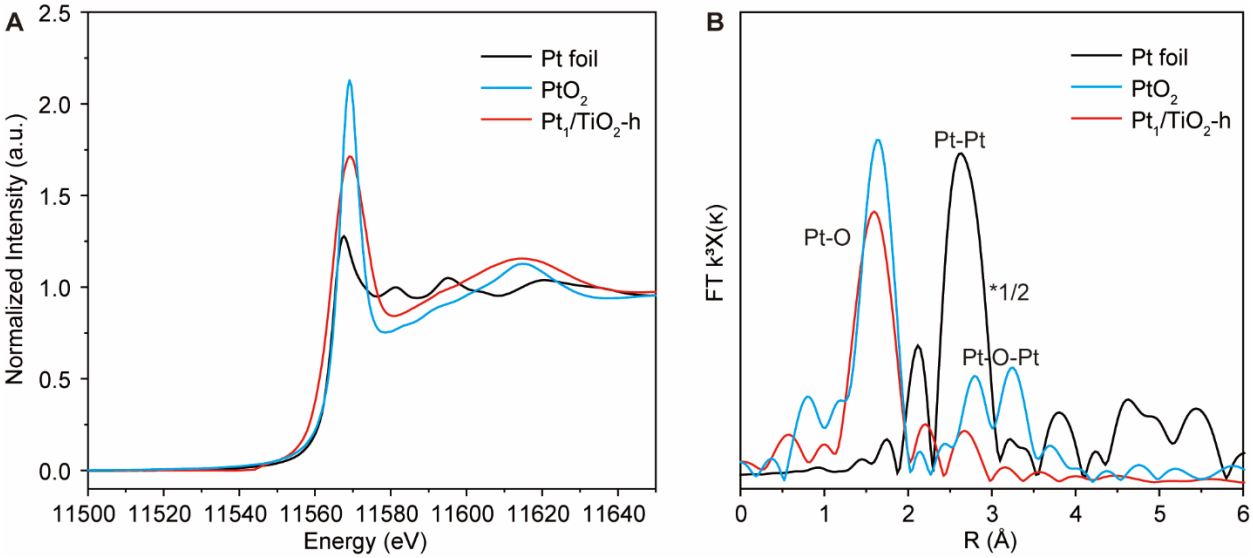

Supplementary Figure 4. (A) X-ray absorption near-edge structure (XANES) of Pt L_3-edge for Pt_1/TiO_2-h catalyst with reference materials Pt foil and PtO_2. (B) Fourier transforms of k^3-weighted Pt L_3-edge EXAFS experimental data for Pt foil, PtO_2, and Pt_1/TiO_2-h.

The electronic properties of Pt species in Pt_1/TiO_2-h were studied by XANES spectroscopy with Pt foil and PtO_2 as reference samples. As shown in Supplementary Fig. 4A, XANES spectra displayed that the intensity of the white line peak for Pt_1/TiO_2-h was located between that of Pt foil and PtO_2, indicating the existence of $Pt^{\delta+}$ rather than Pt^0 ($0<\delta<4$). Besides, the near-edge structure of Pt_1/TiO_2-h was similar to that of the PtO_2 reference. The low-intensity oscillations directly following the near-edge region indicated the short-range and low-coordinate environment of Pt on TiO_2-h.

For Pt_1/TiO_2-h there was only one notable peak at 1.6 Å from the Pt–O contribution without the appearance of a signal at 2.6 Å from the Pt–Pt contribution (Supplementary Fig. 4B), confirming the dominant presence of atomically dispersed Pt atoms in Pt_1/TiO_2-h.

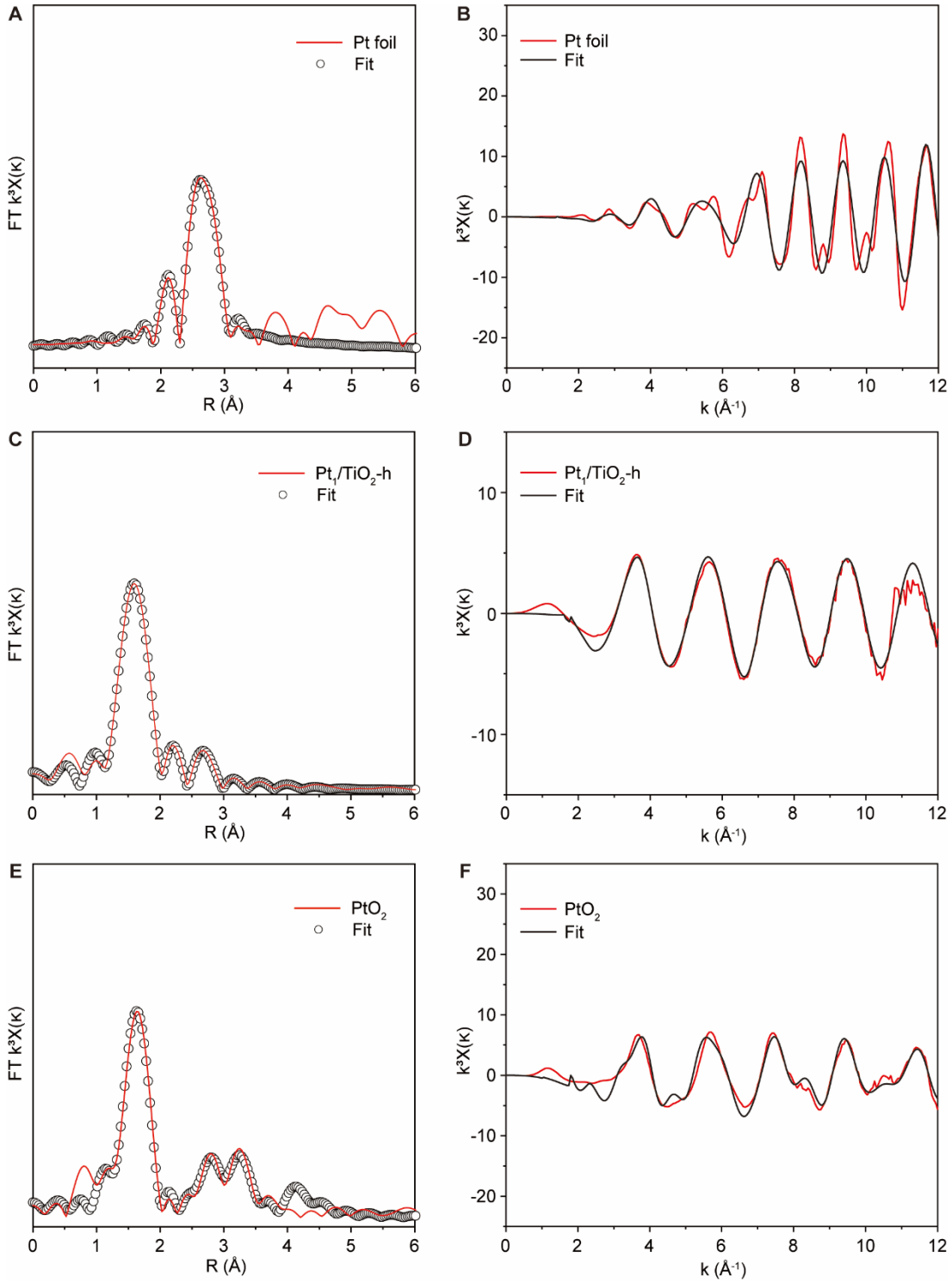

Supplementary Figure 5. EXAFS R space fitting curves (circle) and the experimental ones (red line), k space fitting curves (red line) and the experimental ones (black line) of (A, B) Pt foil, (C, D) Pt_1/TiO_2-h and (E, F) PtO_2, respectively.

Supplementary Table S1. EXAFS fitting parameters at the Pt L_3-edge EXAFS fitting. (S_0^2=0.87 from Pt foil)

Sample	Scattering path	CN	R (Å)	δ^2(Å^2)	ΔE_0 (eV)	R factor
Pt foil	Pt-Pt	12	2.76 ± 0.01	0.0046	4.1 ± 1.0	0.0026
PtO_2	Pt-O	6	2.02 ± 0.01	0.0059	4.9 ± 1.0	0.0054
	Pt-O-Pt	8	3.31 ± 0.01	0.0067		
Pt_1/TiO_2-h	Pt-O	4.6 ± 0.1	2.01 ± 0.01	0.0052	5.3 ± 1.0	0.0059

S_0^2 is the amplitude reduction factor; CN is the coordination number; R is interatomic distance (the bond length between central atoms and surrounding coordination atoms); δ^2 is Debye-Waller factor (a measure of thermal and static disorder in absorber-scatterer distances); ΔE_0 is edge-energy shift (the difference between the zero kinetic energy value of the sample and that of the theoretical model). R factor is used to value the goodness of the fitting. Error bounds that characterize the structural parameters obtained by EXAFS spectroscopy were estimated as N ± 20%; R ± 1%; δ^2 ± 20%.

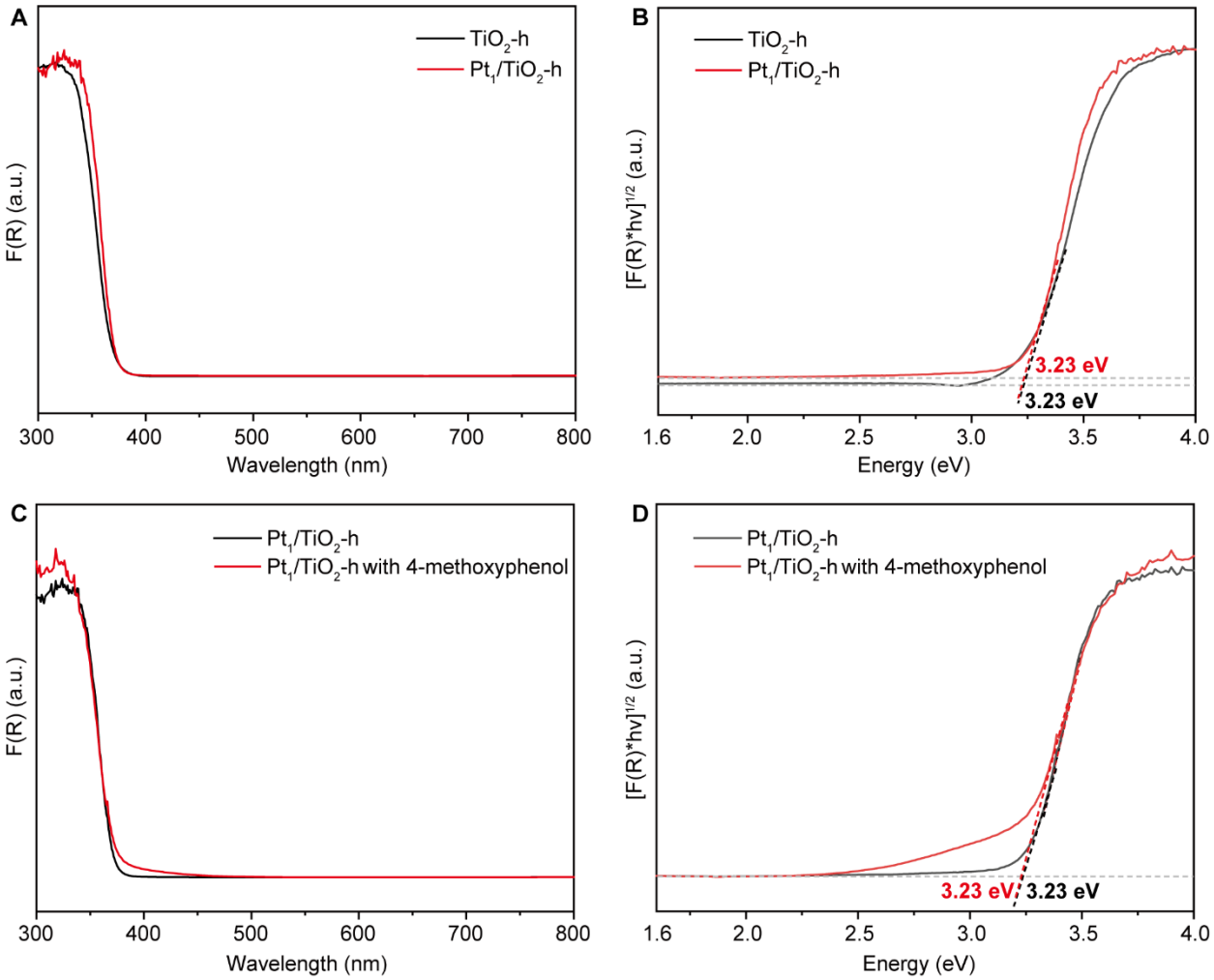

Supplementary Figure 6. (A) UV-Vis DRS and (B) Tauc plots of TiO_2-h and Pt_1/TiO_2-h. (C) UV-Vis DRS and (D) Tauc plots of Pt_1/TiO_2-h with the adsorption of 4-methoxyphenol.

Supplementary Fig. 6A showed that TiO_2-h exhibited good light absorption in the ultraviolet region (<400 nm) and limited light absorption in the visible region (>400 nm). After Pt loadings, the sample Pt_1/TiO_2-h presented the same absorption edge as TiO_2-h. Based on UV-Vis DRS and Tauc plots, the main bandgap of Pt_1/TiO_2-h was the same as that of TiO_2-h (3.23 eV). Furthermore, the adsorption of 4-methoxyphenol onto the surface of Pt_1/TiO_2-h extended the absorption spectrum of Pt_1/TiO_2-h to the visible-light region (~470 nm, Supplementary Fig. 6C). It originated from the surface complexation between heteroatom-containing substrates (e.g., O, N, or S) and TiO_2[4]. Specifically, the surface complex via weak coordination could create new electron donor levels above the valence band of TiO_2 from the 2p orbital of N/O, resulting in visible light response.

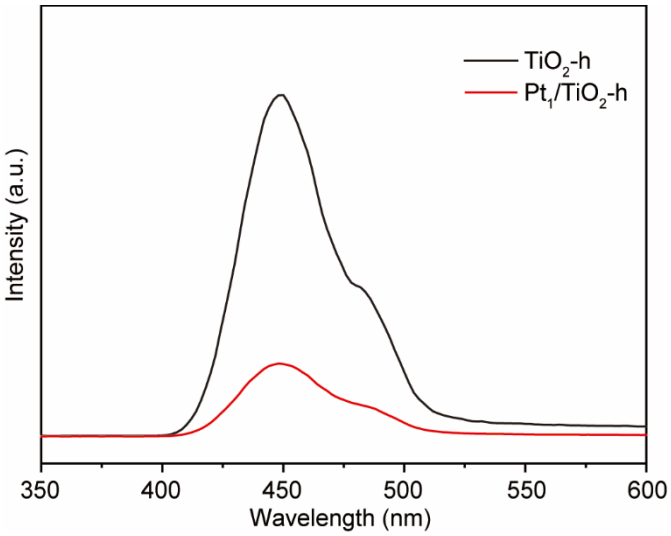

Supplementary Figure 7. PL spectra of TiO_2-h and Pt_1/TiO_2-h.

As shown in Supplementary Fig. 7, TiO_2-h and Pt_1/TiO_2-h samples exhibited a broad peak at 450 nm in PL spectra, which can be attributed to the irradiative recombination of electrons and holes from the conduction band (CB) and valence band (VB), respectively. The Pt_1/TiO_2-h sample showed a lower peak intensity than pristine TiO_2-h, indicating the suppressed charge recombination because of the electron reservoir ability from loaded Pt species. Thus, more photogenerated charges could be available on the surface of the Pt_1/TiO_2-h photocatalyst.

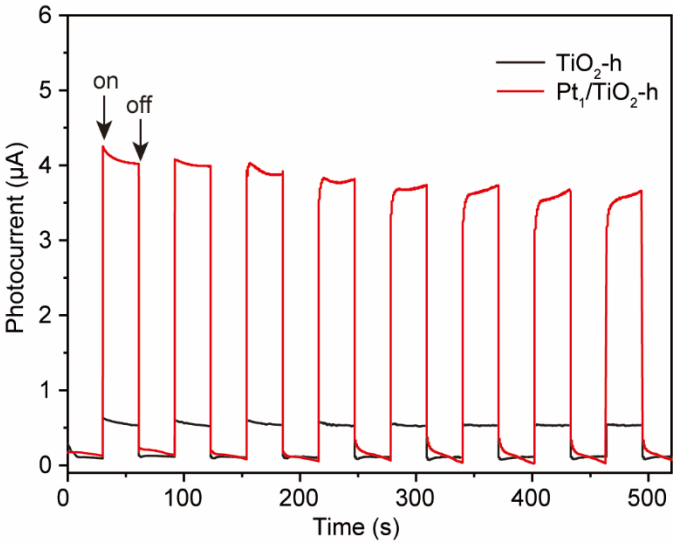

Supplementary Figure 8. Photocurrent analysis of TiO_2-h and Pt_1/TiO_2-h

As shown in Supplementary Fig. 8, the photocurrent of the Pt_1/TiO_2-h sample is approximately 7 times that of the TiO_2 sample, indicating that the loading of Pt significantly enhances the separation efficiency of photo-generated charge carriers in the sample.

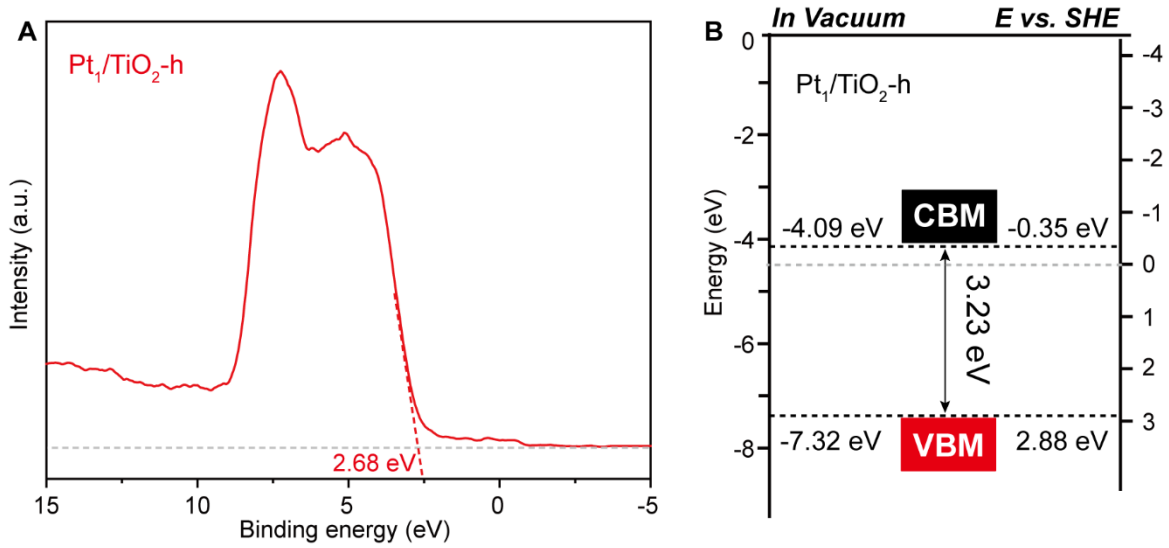

Supplementary Figure 9. (A) Valence band spectrum from XPS of Pt_1/TiO_2-h. (B) Estimated conduction band minimum (CBM) and valence band maximum (VBM) of Pt_1/TiO_2-h.

Considering UV-Vis DRS and Tauc plots in Supplementary Fig. 6, the bandgap of Pt_1/TiO_2-h was 3.23 eV. According to the valence band spectrum from XPS, the E_{VBS} value of Pt_1/TiO_2-h was 2.68 eV. Based on the calculation equation (1), the E_{VBM} and E_{CBM} (*vs.* SHE, pH = 0) of Pt_1/TiO_2-h were calculated to be 2.88 V and -0.35 eV, respectively.

Specifically, the valence band maximum (VBM) position was calculated as follows:

$$E_{VBM}\ (SHE) = E_{VBS} + \text{Work function } (\Phi) - 4.44 \qquad \text{equation (1)}$$

E_{VBM} (SHE): VBM position *vs.* SHE, pH = 0; E_{VBS}: Cutoff energy from valence band spectrum of XPS; Φ: Work function of the sample (4.64 eV for anatase TiO_2[5]).

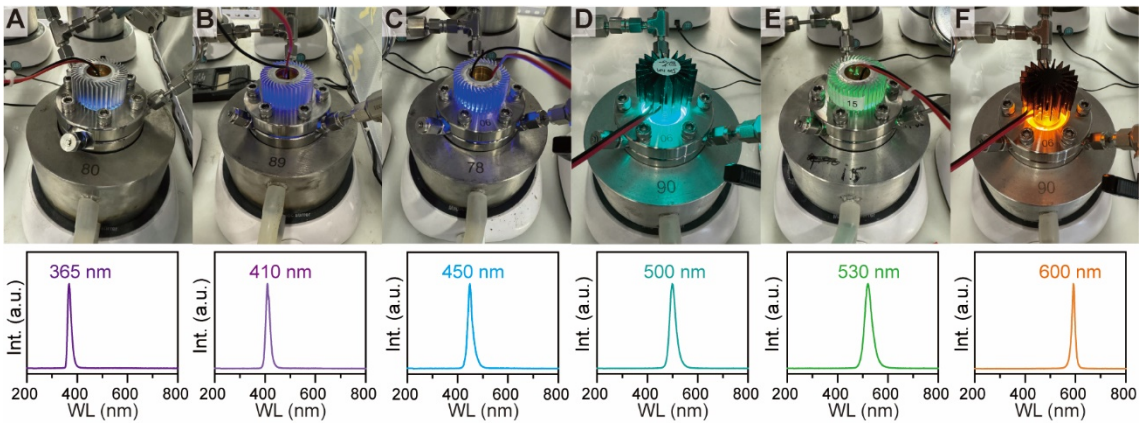

Supplementary Figure 10. Images of the homemade batch-mode photocatalytic reactors under LED light irradiation with different wavelengths. (A) 365 nm; (B) 410 nm; (C) 450 nm; (D) 500 nm; (E) 530 nm; (F) 600 nm.

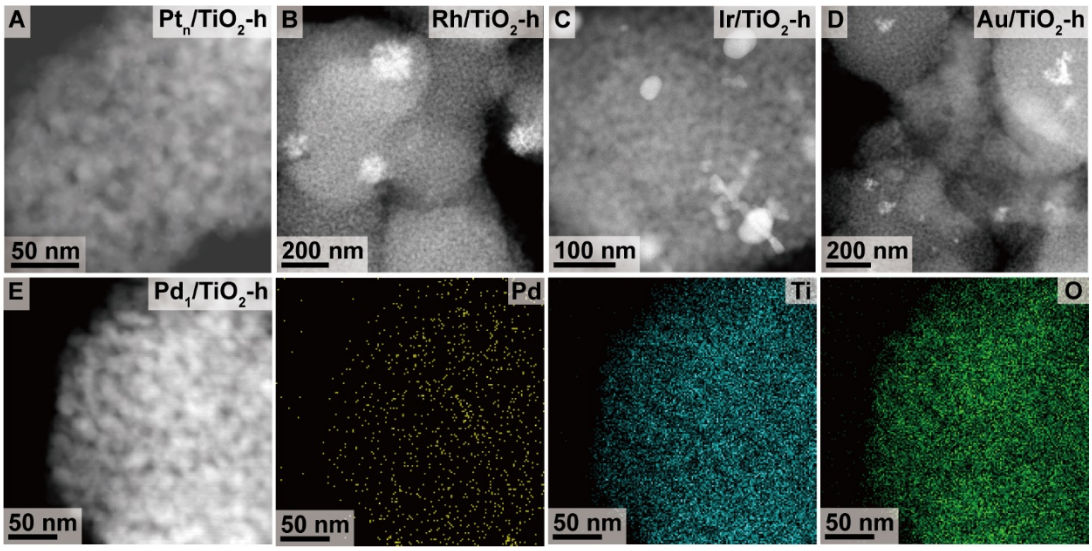

Supplementary Figure 11. STEM images of different photocatalysts. (A) Pt_n/TiO_2-h; (B) Rh/TiO_2-h; (C) Ir/TiO_2-h; (D) Au/TiO_2-h, (E) Pd_1/TiO_2-h.

Based on STEM analysis in Supplementary Fig. 11, the particles size of Pt in Pt_n/TiO_2-h was about 1-5 nm; the particles size of Rh in Rh/TiO_2-h was about 100-200 nm; the particles size of Ir in Ir/TiO_2-h was about 20-50 nm; the particles size of Au in Au/TiO_2-h was about 20-200 nm; the Pd_1/TiO_2-h sample showed that Pd species were homogeneously loaded on TiO_2-h without the presence of Pd nanoparticles.

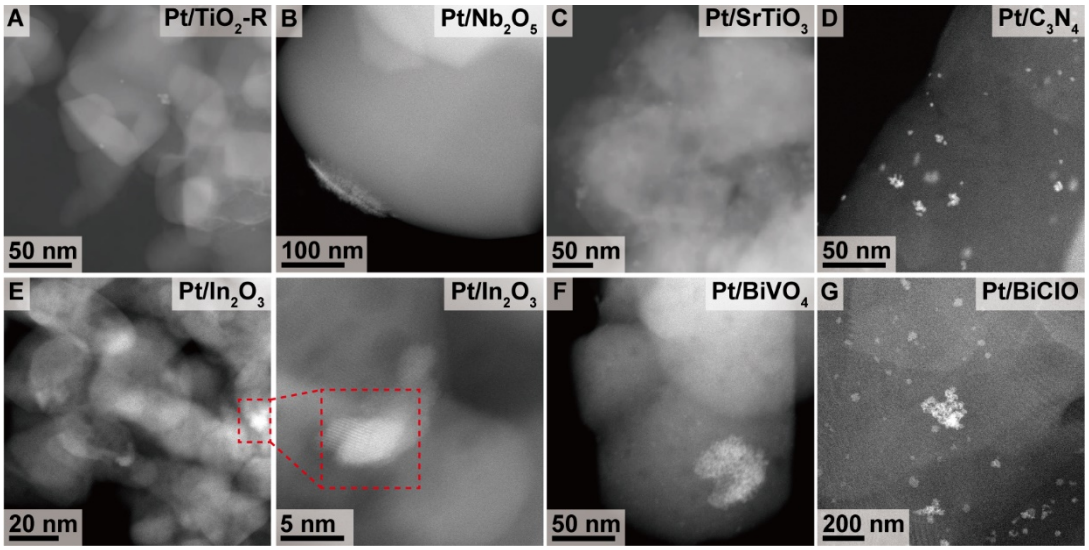

Supplementary Figure 12. STEM images of different photocatalysts. (A) Pt/TiO_2-R; (B) Pt/Nb_2O_5; (C) Pt/$SrTiO_3$; (D) Pt/C_3N_4; (E) Pt/In_2O_3; (F) Pt/$BiVO_4$; (G) Pt/BiOCl.

Based on STEM analysis in Supplementary Fig. 12, the particles size of Pt in Pt/TiO_2-R was about 1-10 nm; the particles size of Pt in Pt/Nb_2O_5 was about 20-150 nm; the particles size of Pt in Pt/$SrTiO_3$ was about 5-25 nm; the particles size of Pt in Pt/C_3N_4 was about 2-15 nm; the particles size of Pt in Pt/In_2O_3 was about 2-10 nm; the particles size of Pt in Pt/$BiVO_4$ was about 10-50 nm; the particles size of Pt in Pt/BiOCl was about 10-200 nm.

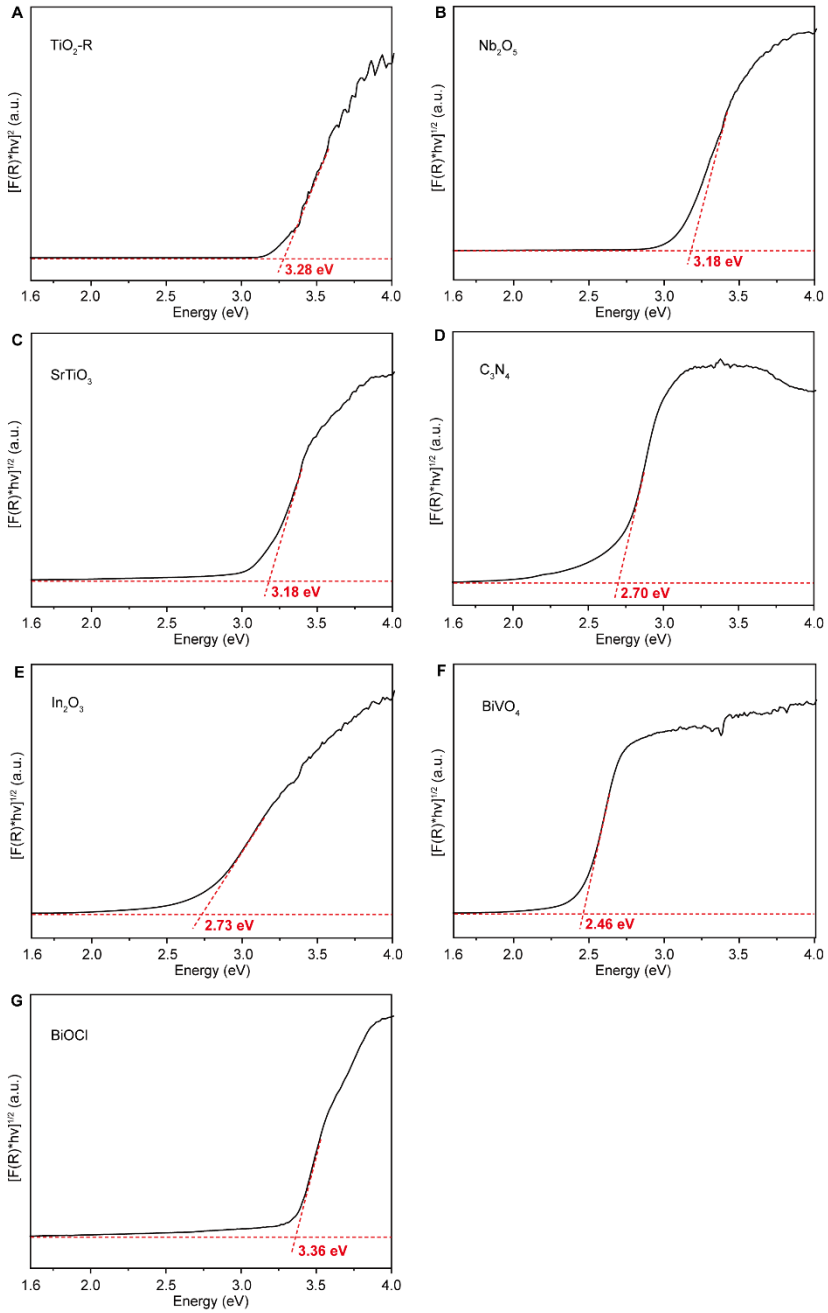

Supplementary Figure 13. The optical absorption analysis of various semiconductors. (A) TiO_2-R. (B) Nb_2O_5. (C) $SrTiO_3$. (D) C_3N_4. (E) In_2O_3. (F) $BiVO_4$. (G) BiOCl.

Based on Tauc plots (Supplementary Fig. 13), the bandgaps of TiO_2-R, $SrTiO_3$, Nb_2O_5, C_3N_4, In_2O_3, $BiVO_4$, and BiOCl were estimated to be 3.28, 3.18, 3.18, 2.70, 2.73, 2.46, and 3.36 eV, respectively.

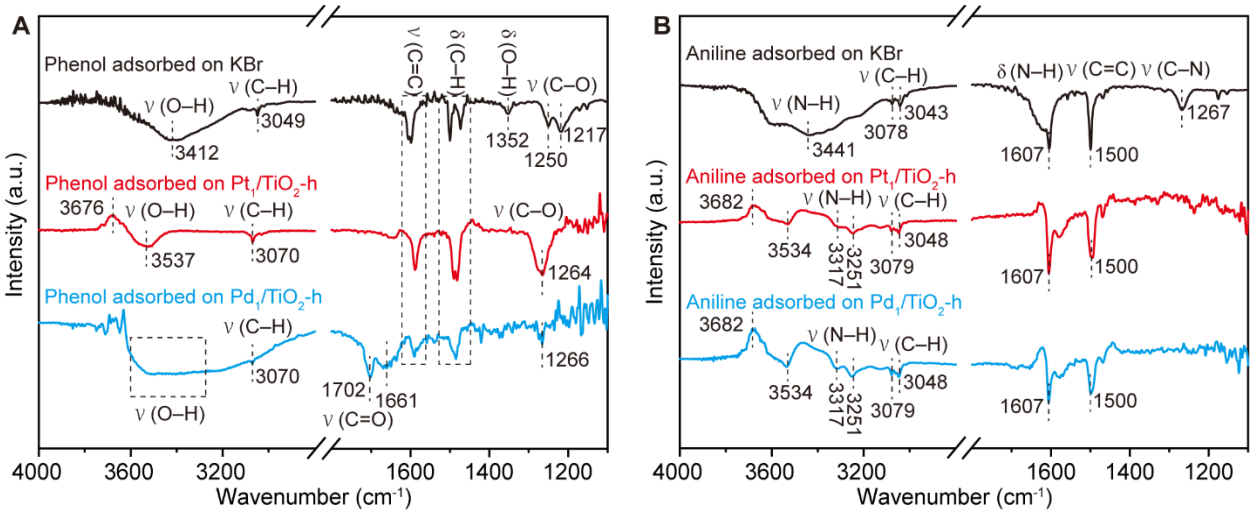

Supplementary Figure 14. (A) DRIFTS data of phenol adsorbed on KBr, Pt_1/TiO_2-h, and Pd_1/TiO_2-h; (B) DRIFTS data of aniline adsorbed on KBr, Pt_1/TiO_2-h, and Pd_1/TiO_2-h.

In contrast to the DRIFTS data of phenol adsorbed on Pt_1/TiO_2-h, two new signals (1702/1661 cm^{-1}) were observed for the case of the phenol adsorbed on Pd_1/TiO_2-h (Supplementary Fig. 14A), which might be ascribed to the C=O stretching mode[6,7]. This indicated that by-products were formed on the surface of Pd_1/TiO_2-h, which blocked the HIE reaction sites for phenol and D_2O. Moreover, the IR spectra of aniline adsorbed on Pt_1/TiO_2-h and Pd_1/TiO_2-h were basically the same (Supplementary Fig. 14B), which indicated that the low reactivity of aniline over Pd_1/TiO_2-h may be due to the lack of the N-heteroarene motif in substrates.

4. Photocatalytic properties of Pt_1/TiO_2-h in HIE reactions

Initially, we employed 4-methoxyphenol as a model substrate to investigate photocatalytic HIE over Pt_1/TiO_2-h. After a series of optimization experiments, the deuterated product was obtained in high D incorporation (95%) by using 0.7 wt.% Pt_1/TiO_2-h as the photocatalyst, D_2O as the solvent, irradiated with 450 nm LED under Ar atmosphere at room temperature for 6 h. The control tests (no photocatalyst, no light, no Pt deposition, or in air) showed that the HIE of arenes could not occur in the absence of light and SA photocatalysts. Besides, the addition of 200 μL D_2 (~8 μmol) presented no significant effect on the HIE reaction. Even with external heating (100 °C), only trace D incorporation can be obtained in the dark.

Supplementary Table S2. The photocatalytic performance of Pt_1/TiO_2-h for the H/D exchange reaction of 4-methoxyphenol in D_2O, including the unsuccessfully deuterated substrates.

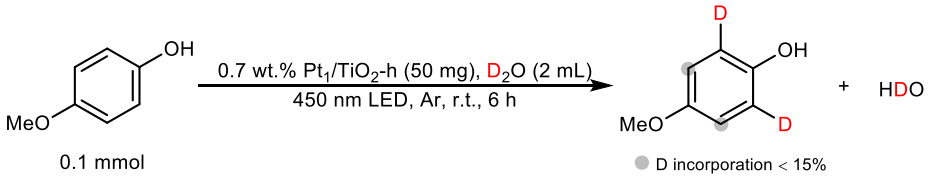

0.1 mmol

D incorporation < 15%

Entry	Variation from the standard conditions[a]	D incorporation (%)[d]
1	None (standard condition)	**95**
2	No photocatalyst	0
3	No light	0
4	No platinum co-catalyst	0
5	Air	0
6	Add 200 μL D_2 (~8 μmol)	95
7	In dark, 100 °C instead of r.t.	trace(<5)

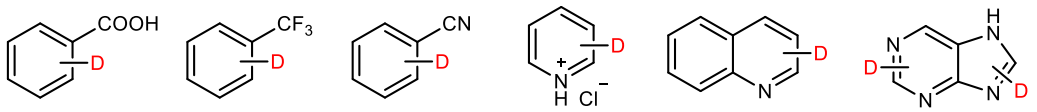

n.d.[b] n.d.[b] n.d.[b] n.d.[c] n.d.[c] n.d.[c]

[a]Standard conditions: 4-methoxyphenol (0.1 mmol), 0.7 wt.% Pt_1/TiO_2-h (50 mg), D_2O (2.0 mL), 450 nm LED (30 mW/cm^2), Ar (1 bar), r.t., 6 h; [b]D_2O (1.6 mL), acetone (0.4 mL), 410 nm LED (60 mW/cm^2); [c]410 nm LED (60 mW/cm^2); [d]D incorporation determined by quantitative ^{1}H NMR: decrease of the signal corresponding to the aromatic protons, using the methoxy proton signals as internal calibration.

The concentration of HDO after reactions was determined by quantitative ^{1}H NMR. Firstly, we performed the ^{1}H NMR analysis of D_2O without 4-methoxyphenol after 6 h light irradiation as the blank test, using 1,4-dioxane as internal calibration. Then, we obtained the ^{1}H NMR spectra of the reaction solution after HIE under standard conditions with 1,4-dioxane for internal calibration. In principle, when 0.1 mmol of 4-methoxyphenol was deuterated with the D incorporation of 95%, 0.32 mmol HDO would be generated. From the NMR results, we calculated the actual molar number of increased HDO to be 0.30 mmol, which was slightly lower than the theoretical value. This may be due to HDO partially adsorbed by the photocatalyst during HIE reactions and characterization errors of ^{1}H NMR.

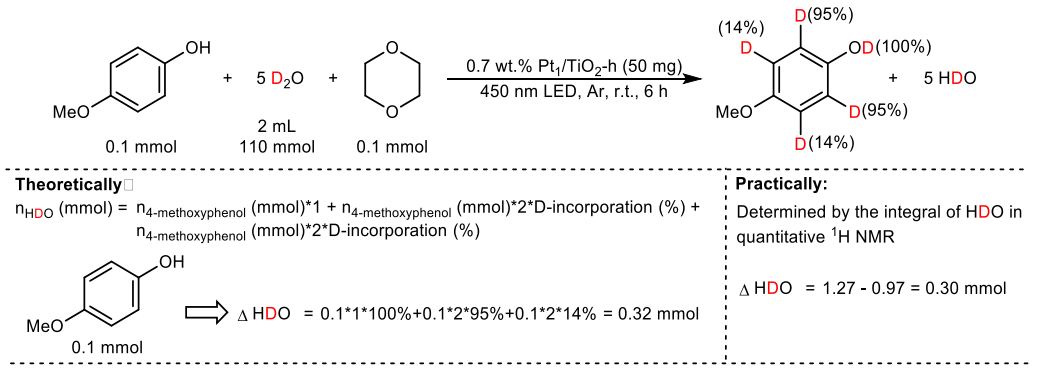

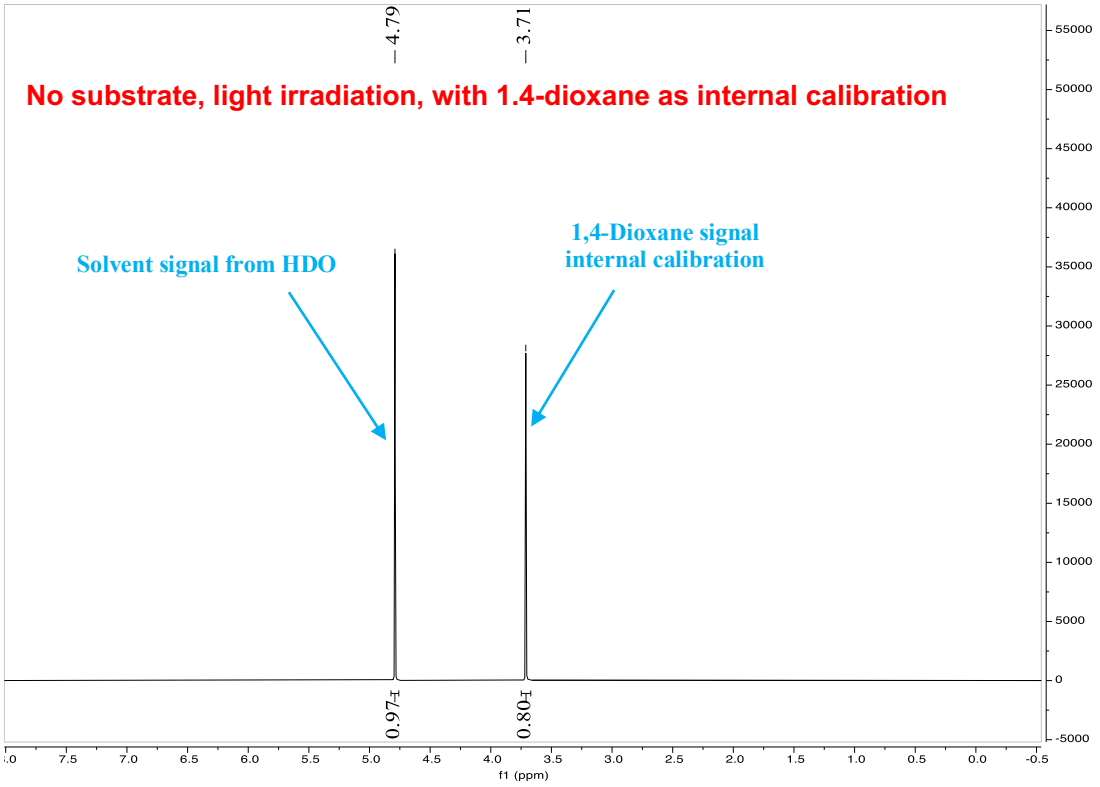

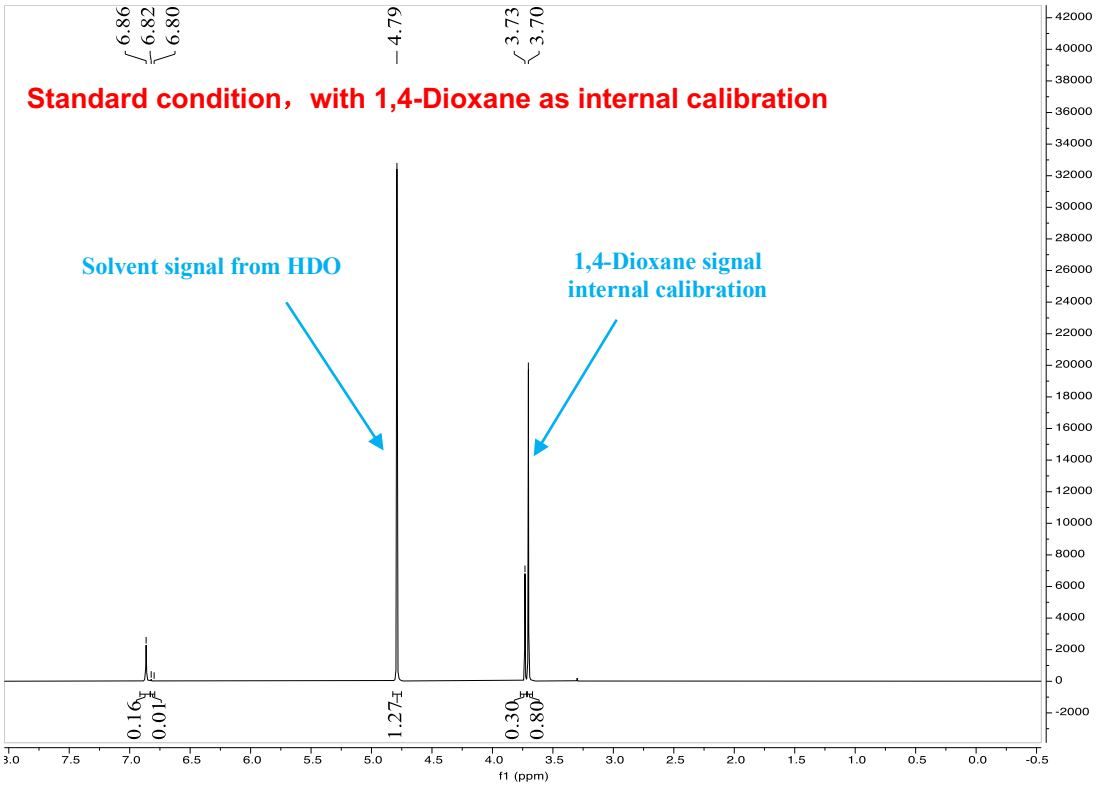

^{2}H NMR (92 MHz, D_2O) of the **1b** product:

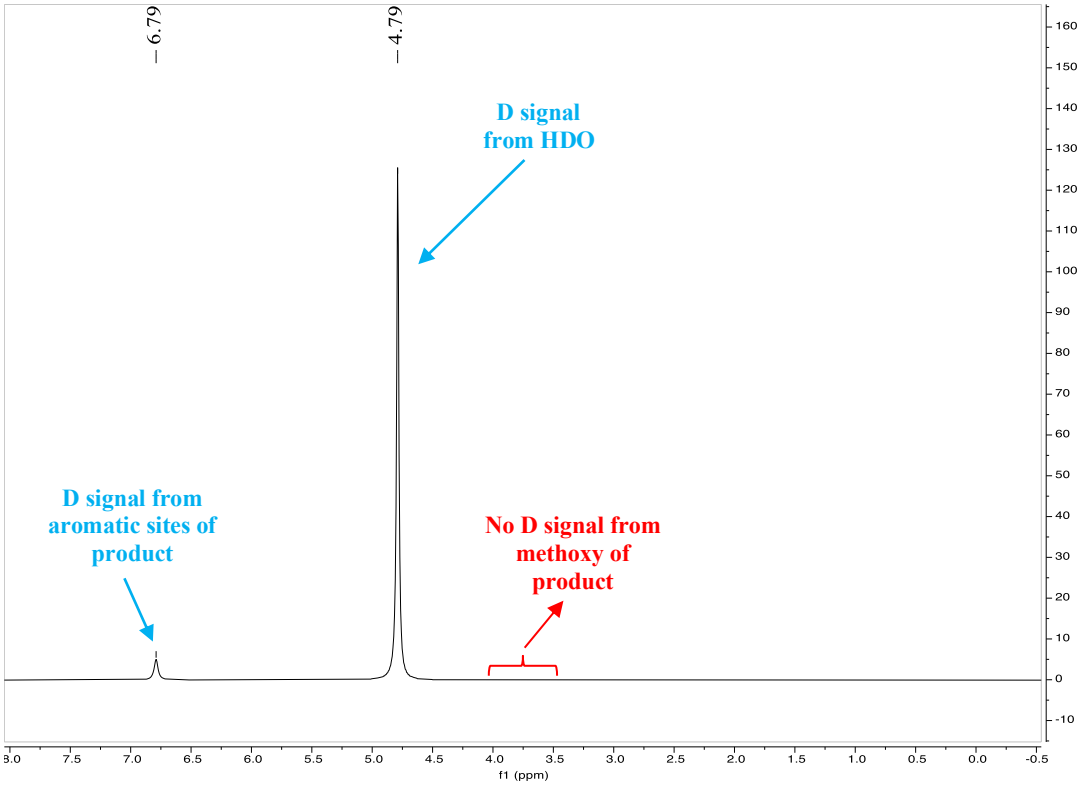

^{2}H NMR spectra of the **1b** product indicated that only C–H bonds at aromatic sites were deuterated. Deuterium incorporation of **1b**: 2.18 D/molecule (^{1}H-NMR), 2.00 D/molecule [**HRMS** (ESI)].

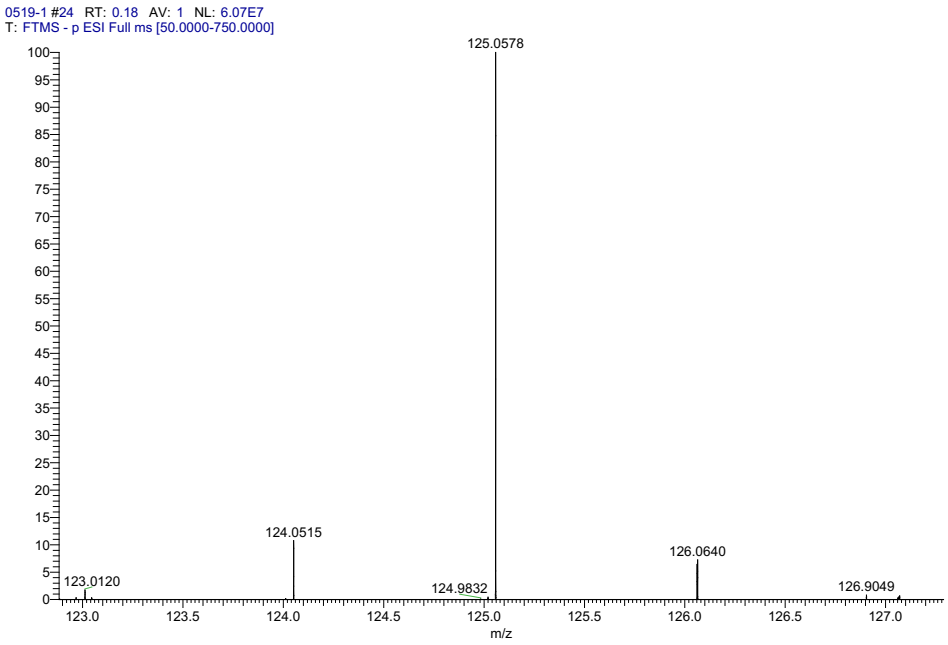

123.0452 ($C_7H_7O_2^-$, 0%), 124.0515 ($C_7H_6DO_2^-$, 9%), 125.0578 ($C_7H_5D_2O_2^-$, 83%), 126.0640 ($C_7H_4D_3O_2^-$, 7%), 127.0702 ($C_7H_3D_4O_2^-$, 1%).

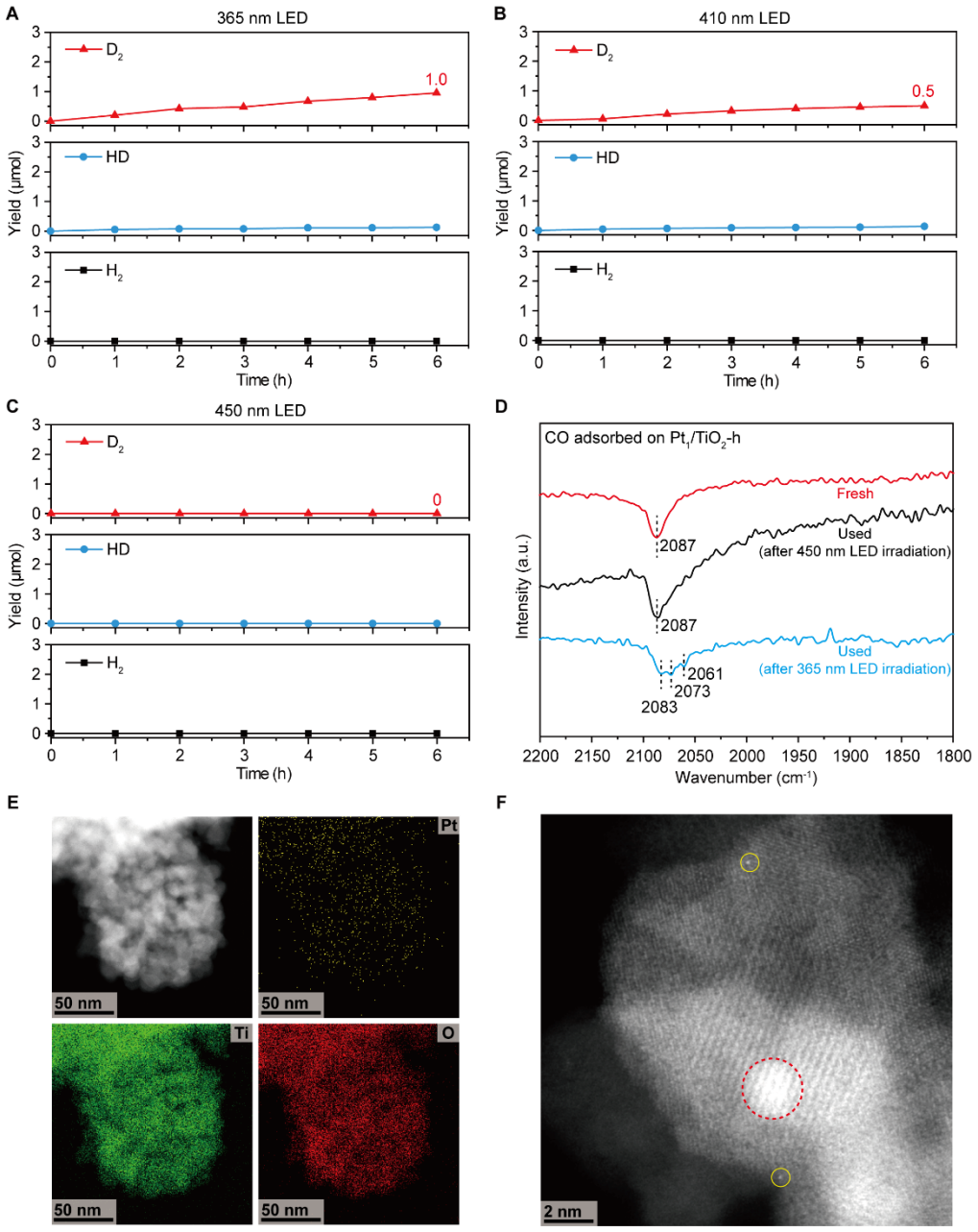

Supplementary Figure 15. (A) Yield of D_2, HD and H_2 under 365 nm LED light irradiation with Pt_1/TiO_2-h; (B) Yield of D_2, HD and H_2 under 410 nm LED light irradiation with Pt_1/TiO_2-h; (C) Yield of D_2, HD and H_2 under 450 nm LED light irradiation with Pt_1/TiO_2-h; (D) DRIFTS data of CO adsorbed on fresh and used Pt_1/TiO_2-h samples; (E) STEM-EDS elemental mapping of used Pt_1/TiO_2-h sample under 365 nm LED irradiation; (F) AC HAADF-STEM image of used Pt_1/TiO_2-h sample under 365 nm LED irradiation (Pt atoms and Pt clusters indicated by yellow circles and red circles, respectively).

In situ MS showed 1.0 and 0.5 μmol D_2 were detected under 365 nm and 410 nm LED irradiation, respectively. Furthermore, no D_2 was detected under 450 nm LED irradiation. Besides, the control experiments indicated that the introduction of more D_2 (~8 μmol) presented no effect on the HIE reaction (Supplementary Table S2, Entry 6). Therefore, we reasoned that the microstructure of SA photocatalyst may change under UV irradiation, which consequently led to a relatively low D incorporation (56%). The DRIFTS data showed the presence of multiple CO adsorption peaks on Pt_1/TiO_2-h sample after UV irradiation (Supplementary Fig. 15D), which might be ascribed to CO adsorbed on Pt single atoms and Pt clusters[8,9]. Meanwhile, the AC HAADF-STEM image also confirmed the formation of Pt clusters (Supplementary Fig. 15F).

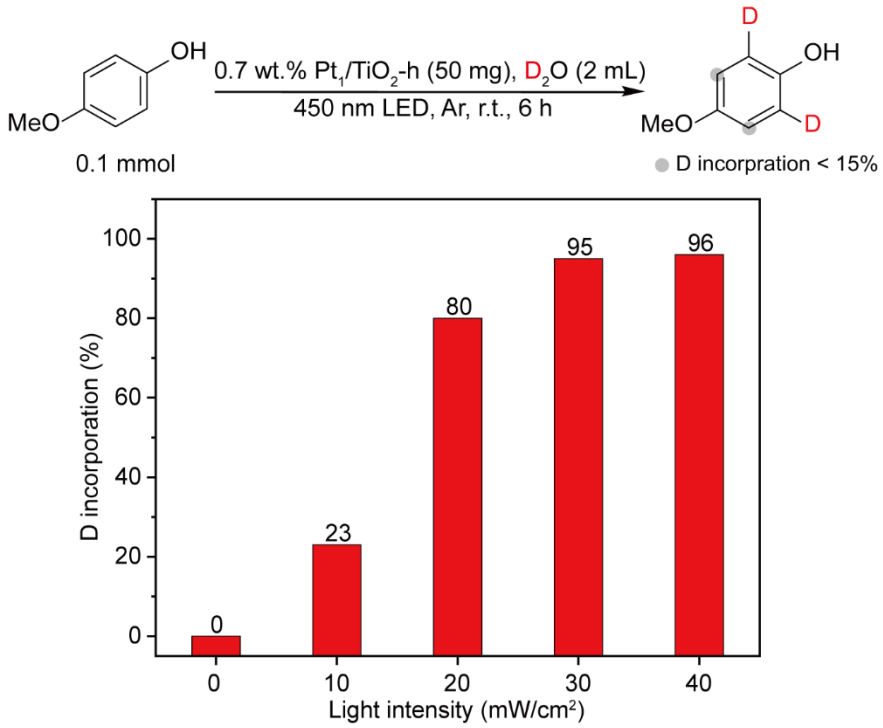

Supplementary Figure 16. Photocatalytic deuterium incorporation of 4-methoxyphenol in D_2O over 0.7 wt.% Pt_1/TiO_2-h under 450 nm irradiation with different light intensity. Reaction conditions: 4-methoxyphenol (0.1 mmol), photocatalyst (50 mg), D_2O (2.0 mL), 450 nm LED (0-50 mW/cm^2), Ar (1 bar), r.t., 6 h.

Under blue light irradiation (450 nm LED), the D incorporation gradually increased (from 0 to 95%) with the light intensity from 0 to 30 mW/cm^2. Higher light intensity of 40 mW/cm^2 slightly increased the D incorporation from 95% to 96%, indicating the light saturation. Thus, we chose 30 mW/cm^2 as the optimal light intensity.

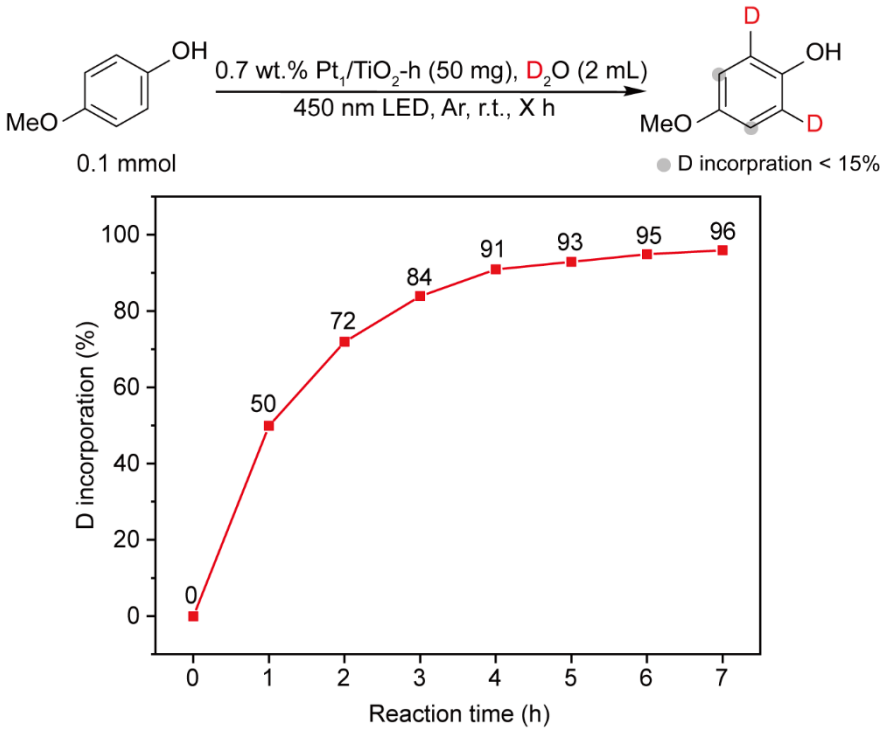

Supplementary Figure 17. Photocatalytic deuterium incorporation of 4-methoxyphenol in D_2O over 0.7 wt.% Pt_1/TiO_2-h under 450 nm irradiation with different reaction time. Reaction conditions: 4-methoxyphenol (0.1 mmol), photocatalyst (50 mg), D_2O (2.0 mL), 450 nm LED (30 mW/cm^2), Ar (1 bar), r.t., 0-7 h.

The D incorporation showed a growth trend with the reaction time. Specifically, within 3 hours, the D incorporation rose rapidly to 84%. Then, the deuteration rate slowed down from 3 to 7 h (from 84% to 96% D incorporation), because the collision probability between active sites of photocatalysts and unlabeled molecules decreased dramatically as most reactants were deuterated. The satisfactory deuteration (95% D incorporation) was realized after 6 h irradiation. Thus, we chose 6 h as the optimal reaction time.

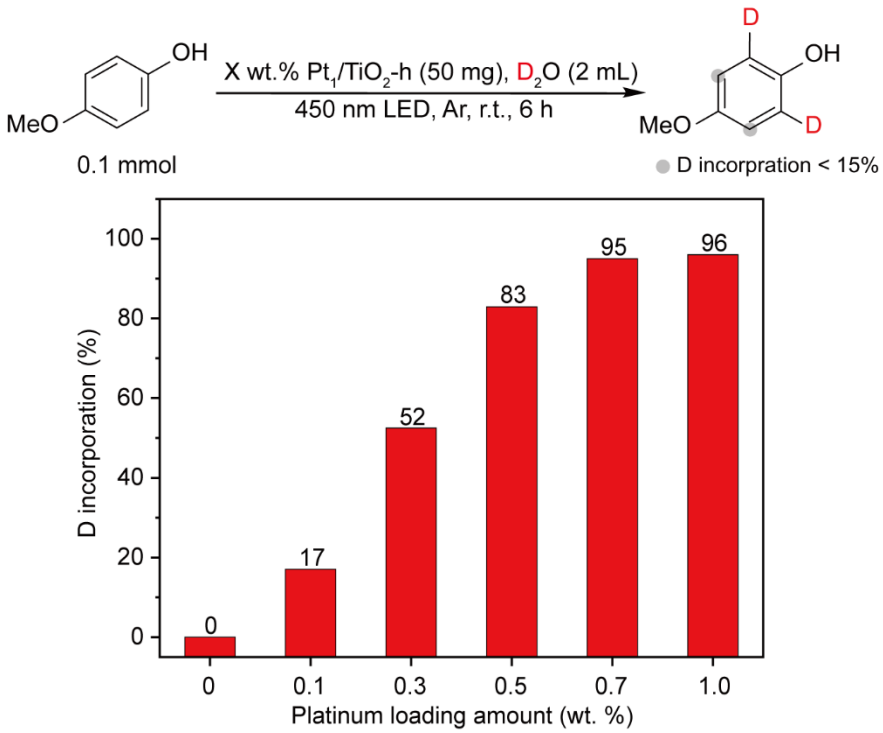

Supplementary Figure 18. Photocatalytic deuterium incorporation of 4-methoxyphenol in D_2O under 450 nm irradiation over photocatalyst Pt_1/TiO_2-h with different Pt loading amounts. Reaction conditions: 4-methoxyphenol (0.1 mmol), photocatalyst (50 mg), D_2O (2.0 mL), 450 nm LED (30 mW/cm^2), Ar (1 bar), r.t., 6 h.

With the increase of Pt loadings from 0 to 0.7 wt.%, the D incorporation showed a growth trend, reaching 95% for 0.7 wt.% Pt_1/TiO_2-h. However, more Pt loading (1.0 wt.%) slightly increased the D incorporation from 95% to 96%. It implied that part of the Pt species in Pt_1/TiO_2-h with a higher loading of 1 wt.% may exist as inactive clusters or nanoparticles. Accordingly, we chose the Pt loading amount of 0.7 wt.% for the following studies.

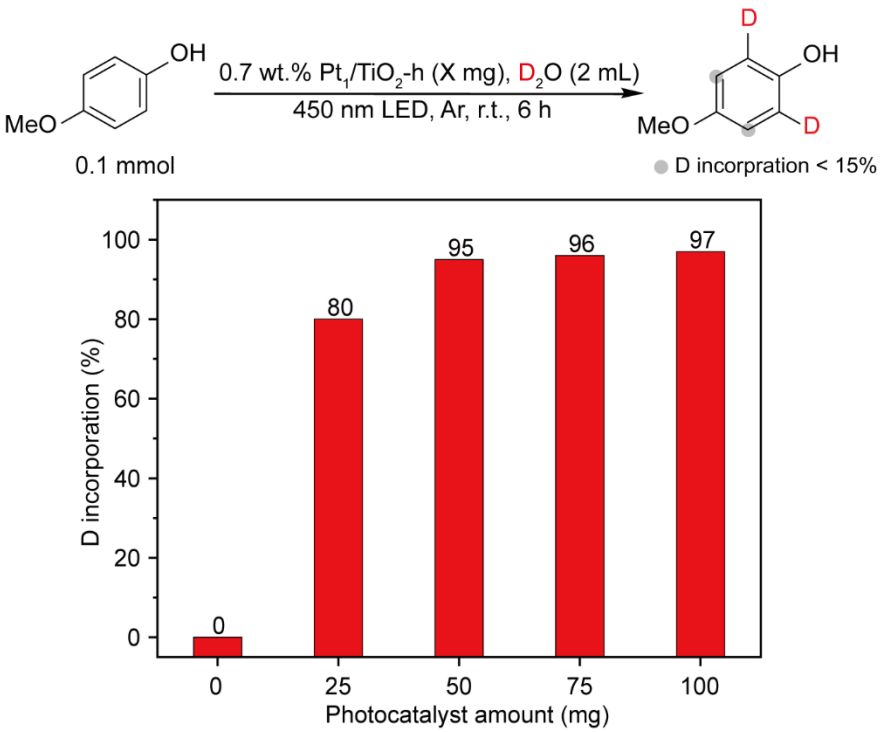

Supplementary Figure 19. Optimization of photocatalyst amount. Reaction conditions: 4-methoxyphenol (0.1 mmol), 0.7 wt.% Pt_1/TiO_2-h (0-100 mg), D_2O (2.0 mL), 450 nm LED (30 mW/cm^2), Ar (1 bar), r.t., 6 h.

With the increase of photocatalyst amount from 0 to 100 mg, the D incorporation showed a growth trend. With the dose of 50 mg photocatalyst, the D incorporation increased rapidly up to 95%. The deuteration level reached a plateau (95% to 97% D incorporation) when adding more photocatalysts (from 50 to 100 mg). Considering the cost of Pt metal, we chose the photocatalyst amount of 50 mg for the following studies.

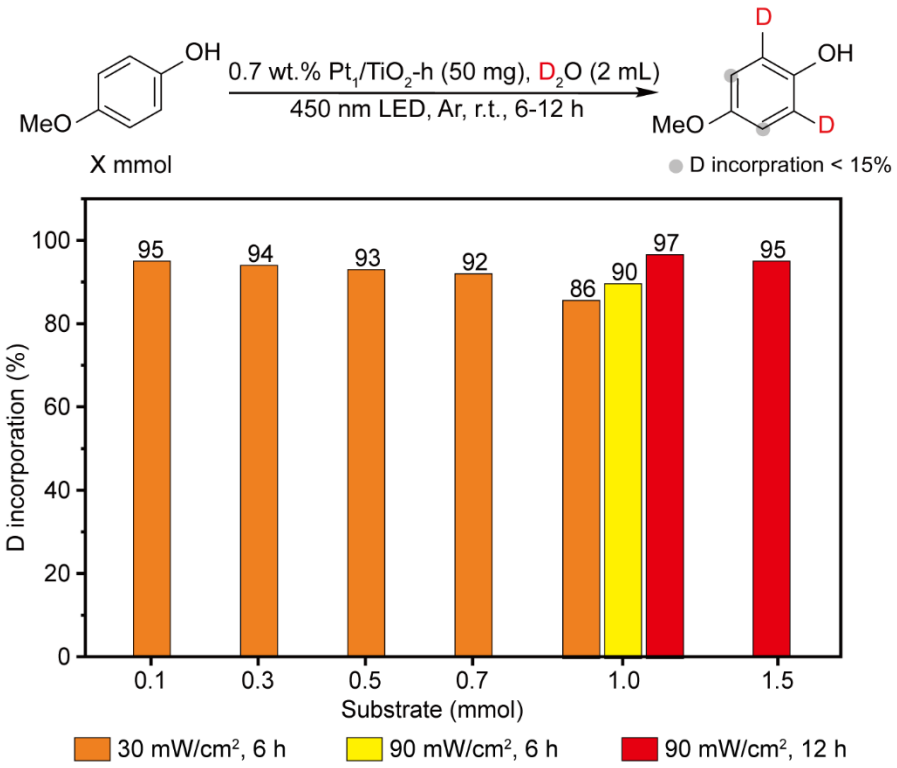

Supplementary Figure 20. Photocatalytic deuterium incorporation of 4-methoxyphenol in D_2O over different substrate concentrations. Reaction conditions: 4-methoxyphenol (0.1-1.5 mmol), photocatalyst (50 mg), D_2O (2.0 mL), 450 nm LED (30-90 mW/cm^2), Ar (1 bar), r.t., 6-12 h.

When the substrate amount was increased from 0.1 to 0.7 mmol, there was no significant decrease in D incorporation (95%-92%). The deuteration performance became poor after adding 1.0 mmol substrate. Fortunately, a higher light intensity of 90 mW/cm^2 and prolonged reaction time (from 6 to 12 h) could realize decent D incorporation (95%-97%) for the cases with 1.0 and 1.5 mmol substrate.

Supplementary Table S3. Pt loading amounts of photocatalysts based on ICP-mass analysis.

Photocatalyst	Pt loading amount （wt.%）
0.7 wt.% Pt_1/TiO_2-h (Fresh)	0.54
0.7 wt.% Pt_1/TiO_2-h (used)	0.53

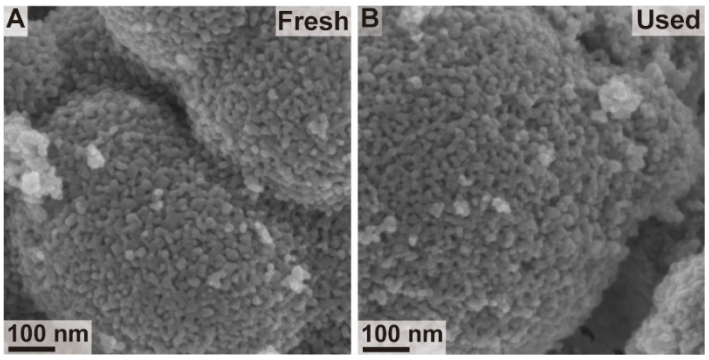

Supplementary Figure 21. SEM images of (A) fresh 0.7 wt.% Pt_1/TiO_2-h and (B) the used photocatalyst after 1 round recycling test.

The SEM images showed that the particle size and morphology of the used photocatalyst Pt_1/TiO_2-h had no significant change after 1 round recycling test.

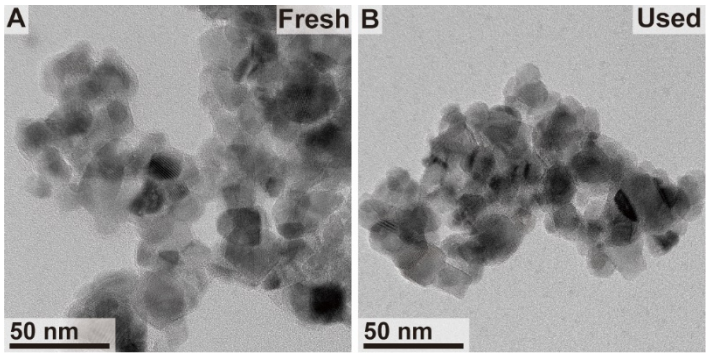

Supplementary Figure 22. TEM images of (A) fresh 0.7 wt.% Pt_1/TiO_2-h and (B) the used photocatalyst after 1 round recycling test.

The TEM images showed that the particle size and morphology of the used photocatalyst Pt_1/TiO_2-h had no significant change after 1 round recycling test as well. Additionally, no Pt nanoparticles were observed.

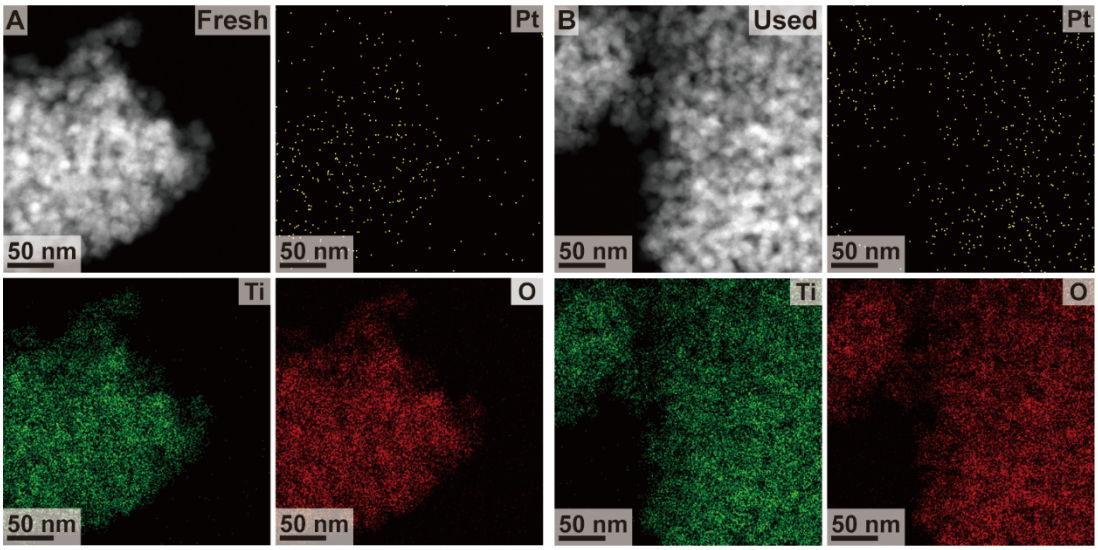

Supplementary Figure 23. STEM-EDS elemental mapping of (A) fresh 0.7 wt.% Pt_1/TiO_2-h and (B) the used photocatalyst after 1 round recycling test.

The STEM-EDS elemental mapping showed that the distribution of elements Pt, Ti, and O in the used photocatalyst Pt_1/TiO_2-h was similar to that of the fresh sample. The main Pt species in the used photocatalyst after 1 round recycling test still presented as the SA state.

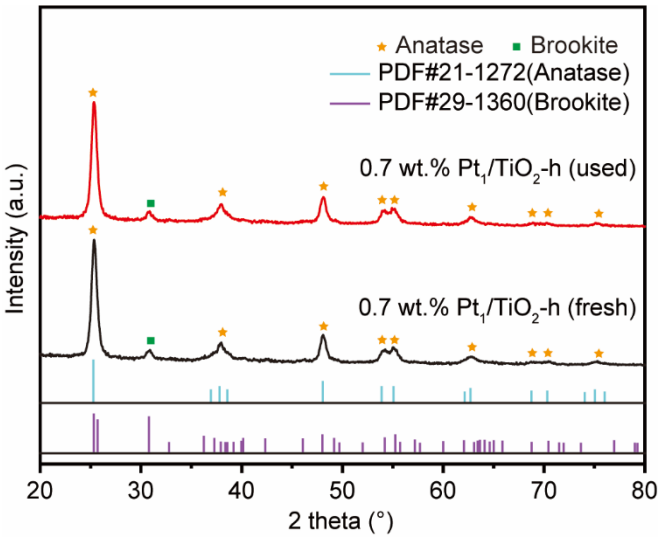

Supplementary Figure 24. XRD patterns of fresh 0.7 wt.% Pt_1/TiO_2-h and the used photocatalyst after 1 round recycling test. The standard JCPDS cards of anatase (PDF#21-1272) and brookite (PDF#29-1360) TiO_2 were incorporated for comparison.

The XRD pattern of the used photocatalyst after 1 round recycling test was the same as that of the fresh sample. Moreover, no peaks attributed to Pt nanoparticles were detected.

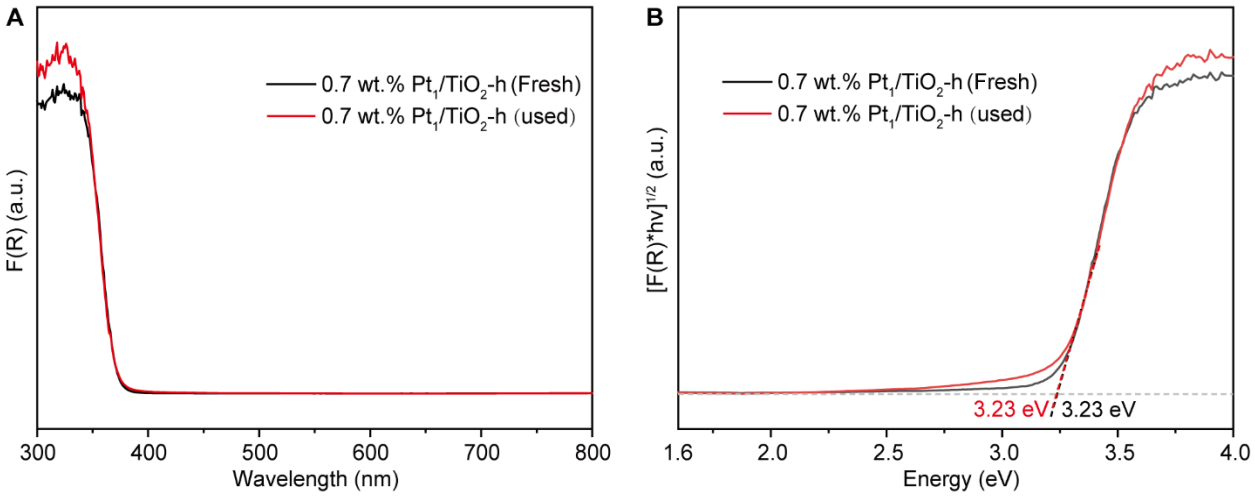

Supplementary Figure 25. (A) UV-Vis DRS and (B) Tauc plots of fresh 0.7 wt.% Pt_1/TiO_2-h and the used photocatalyst after 1 round recycling test.

The optical absorption capability of the used photocatalyst 1 round recycling test was similar to that of the fresh sample with the bandgap unchanged at 3.23 eV.

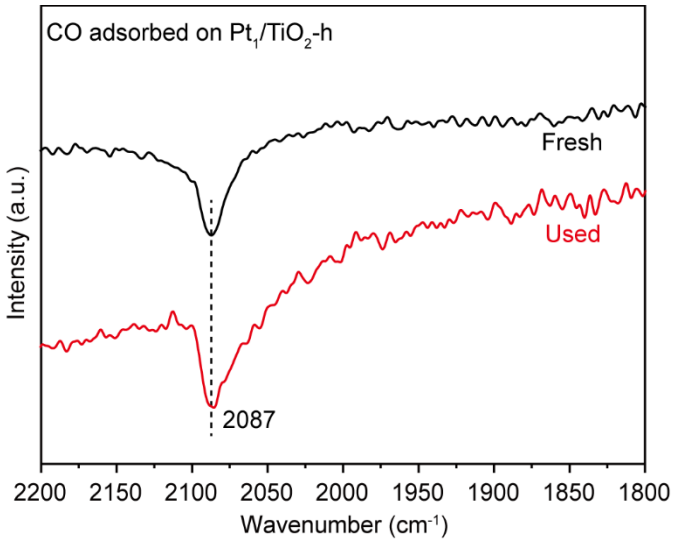

Supplementary Figure 26. DRIFTS data of CO adsorbed on fresh 0.7 wt.% Pt_1/TiO_2-h and the used photocatalyst after 1 round recycling test.

For the used SA photocatalyst with CO adsorbed (red line), the main IR band was the same to the case of the fresh one, implying the preservation of SA Pt sites after photocatalytic tests.

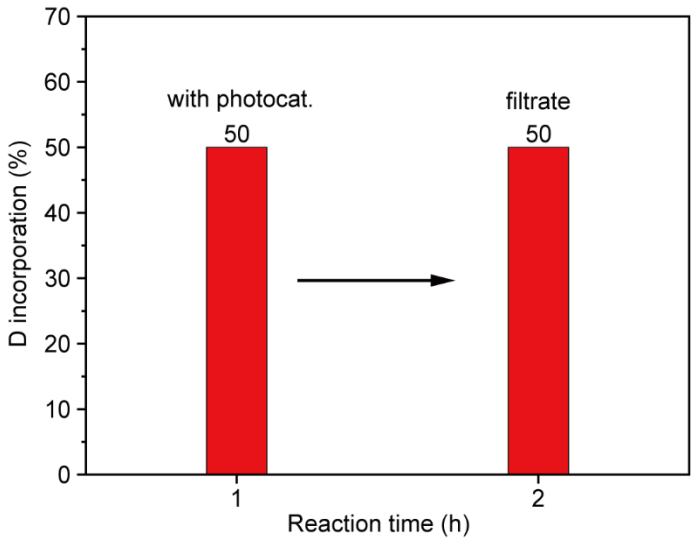

Supplementary Figure 27. The reaction results of the hot filtration test.

After 1 h light irradiation under standard reaction conditions, the SA photocatalyst was removed by filtration. The filtrate was irradiated for another 1 h. Since no increase in D incorporation was observed, the soluble active species could be ruled out. It confirmed that the heterogeneous SA photocatalyst drove the HIE of arenes in D_2O, excluding the contribution from any homogeneous catalysis.

5. Mechanistic studies

Supplementary Table S4. Control experiments.

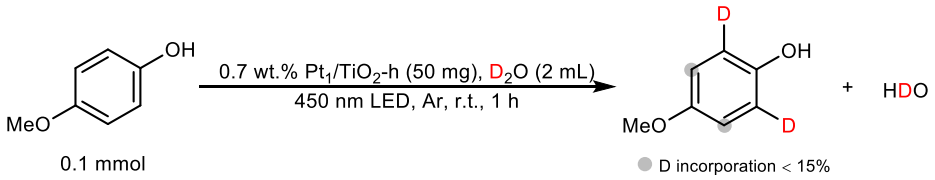

Entry	Variation from the standard conditions[a]	D incorporation (%)[d]
1	None (standard condition)	**50**
2	Add NaOH (0.1 equiv.)	0
3	Add NaCl (0.1 equiv.)	48
4	Add HCl (0.1 equiv.)	0
5	Add HNO_3 (0.1 equiv.)	0

[a]Standard conditions: 4-methoxyphenol (0.1 mmol), 0.7 wt.% Pt_1/TiO_2-h (50 mg), D_2O (2.0 mL), 450 nm LED (30 mW/cm^2), Ar (1 bar), r.t., 1 h; [b]D incorporation determined by quantitative ^1H NMR: decrease of the signal corresponding to the aromatic protons, using the methoxy proton signals as internal calibration.

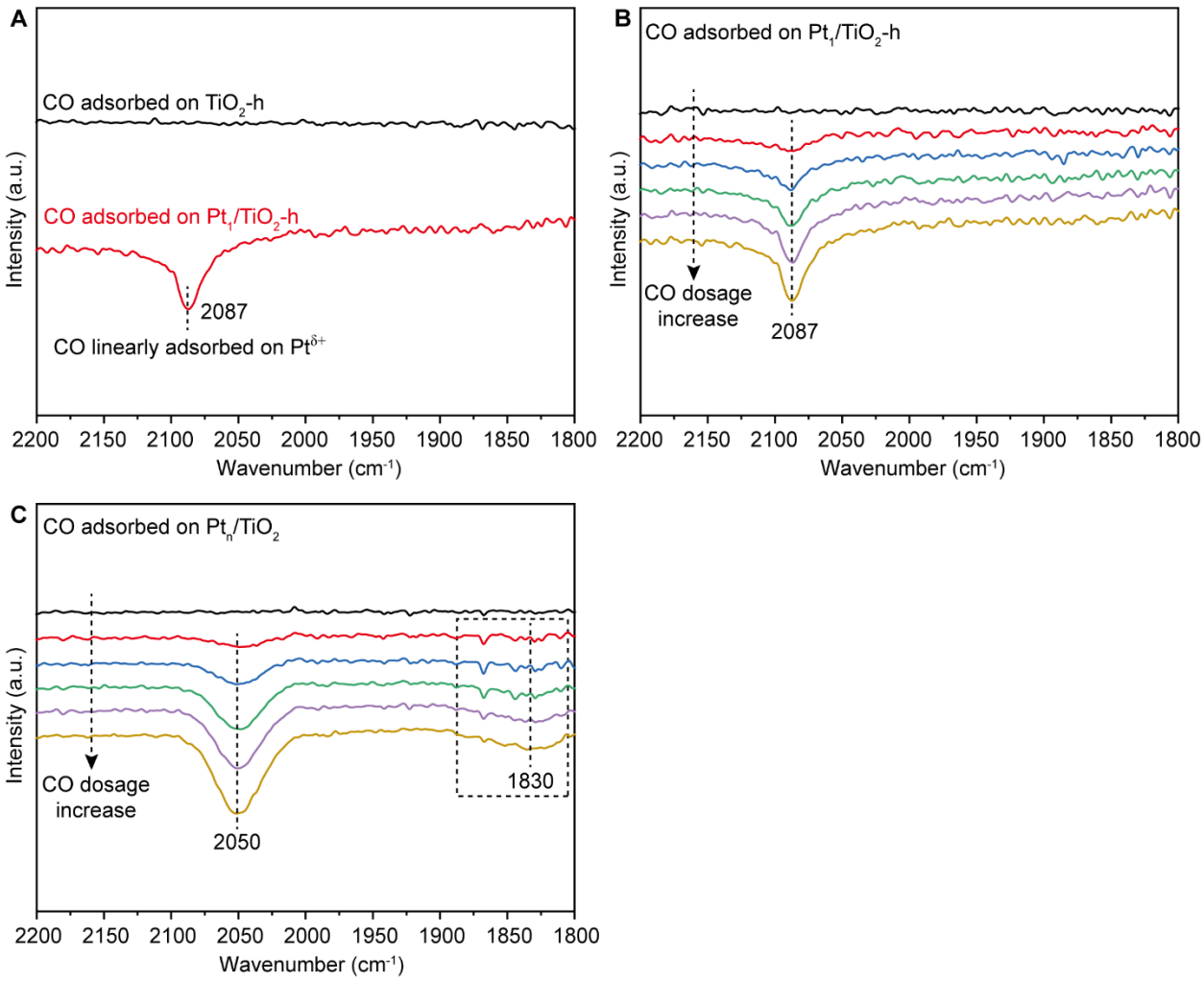

Supplementary Figure 28. (A) DRIFTS data of CO adsorbed on TiO_2-h and 0.7 wt.% Pt_1/TiO_2-h. (B) DRIFTS data of CO adsorbed on 0.7 wt.% Pt_1/TiO_2-h with CO dosage increase. (C) DRIFTS data of CO adsorbed on 0.7 wt.% Pt_n/TiO_2 with CO dosage increase.

The dominant IR band located at 2087 cm^{-1} can be assigned to the linear CO adsorption at SA $Pt^{\delta+}$ sites on Pt_1/TiO_2-h (Supplementary Figs. 28A and 28B)[8,10,11]. For comparison, the DRIFTS analysis of CO adsorbed on Pt_n/TiO_2 sample was conducted (Supplementary Fig. 28C), in which the bands centered at 2050 and 1830 cm^{-1} correspond to the linear and multiple-bonded CO adsorption at Pt NPs, respectively[8].

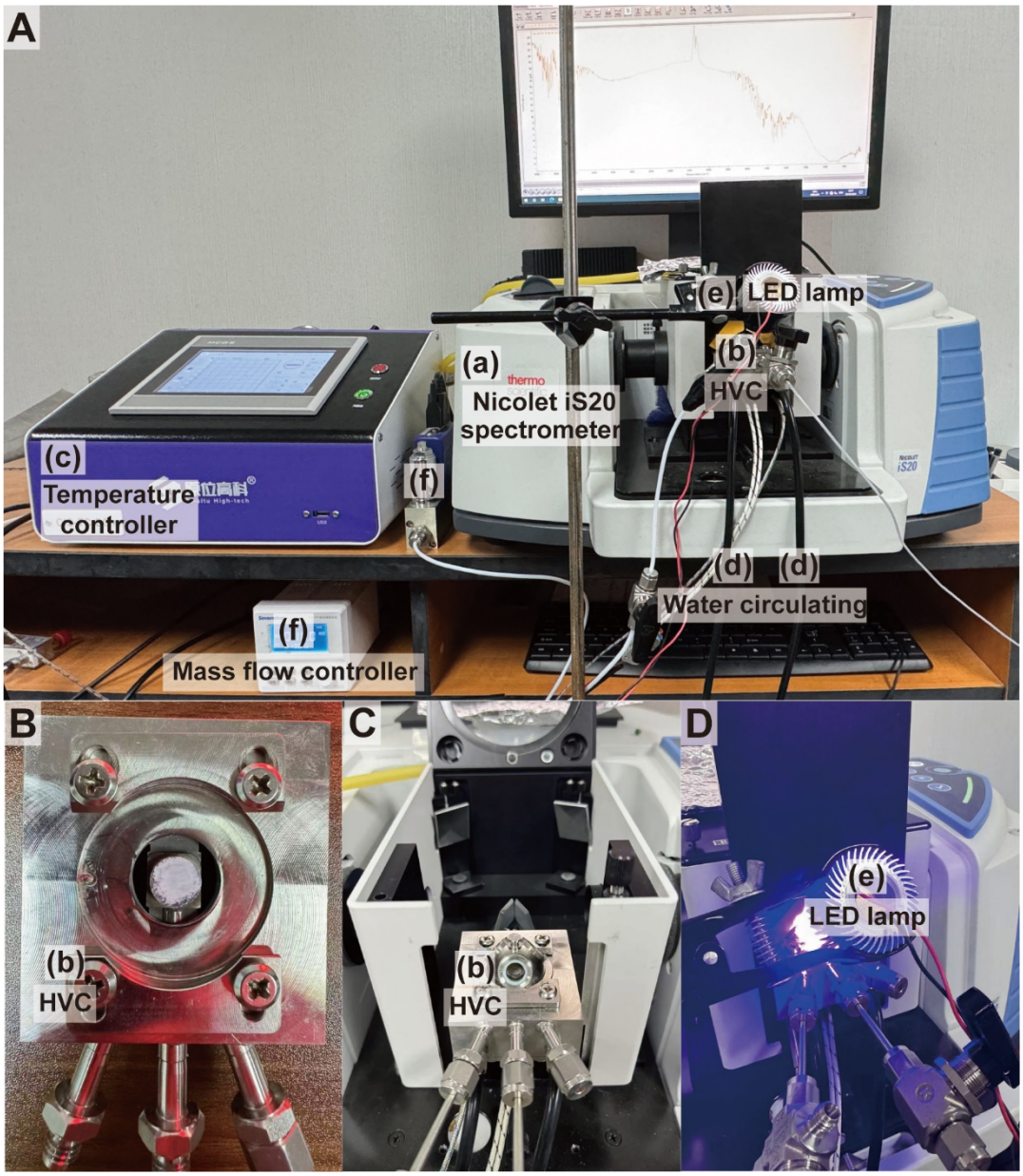

Supplementary Figure 29. Photographs of (A) *in situ* DRIFT setup; (B) HVC loaded with fresh Pt_1/TiO_2-h powder sample; (C) Praying Mantis™ HVC accessory enclosed with a three-window dome; (D) HVC with light irradiation from 410 nm LED.

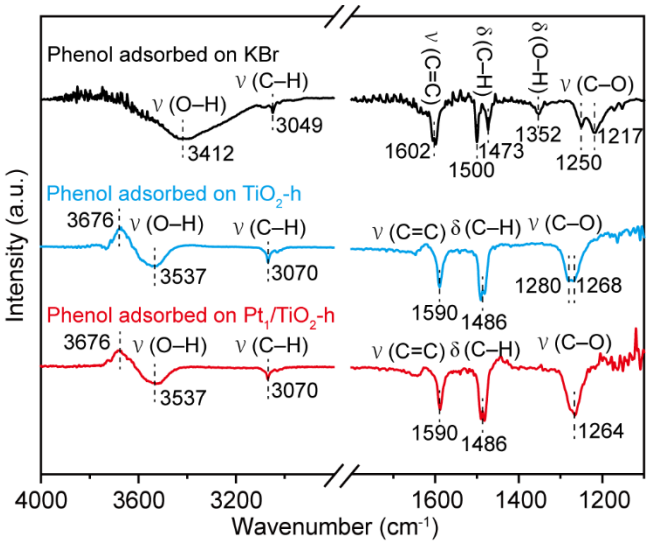

Supplementary Figure 30. DRIFTS data of Phenol adsorbed on KBr, TiO_2-h, and Pt_1/TiO_2-h. Except for the data of phenol adsorption on KBr, all spectra used the DRIFTS data of clean catalyst sample as the background.

As shown in Supplementary Fig. 30, in contrast to the phenol adsorbed on KBr, a blue shift was observed for the C–O stretching mode for the case of the phenol adsorbed on TiO_2-h (from 1217/1250 to 1268/1280 cm^{-1})[12]. Particularly, the O–H bending vibrational peak at 1352 cm^{-1} in phenol disappeared upon the adsorption on TiO_2[13]. This indicated the dissociation of phenolic hydroxyl group on TiO_2 with the formation of Ti-phenolate. Meanwhile, the in-plane C=C stretching vibrational and C–H bending vibrational peaks also slightly changed (from 1473/1500/1602 to 1486/1590 cm^{-1})[14]. The broad IR absorption band centered at 3412 cm^{-1} originated from the hydrogen bonded O–H groups from phenol on KBr. In contrast, the broad band at 3537 cm^{-1} manifested the stretching mode of O–H groups from the dissociation of phenol on TiO_2. The adsorption of phenol was also suggested by the negative band at 3676 cm^{-1}, which was attributed to the terminal OH groups on TiO_2[15].

After loading with Pt, the SA $Pt^{\delta+}$ sites captured the reactant molecules (Phenol) via the coordination between Pt and O atoms, which was evidenced by the red-shifted absorption band of C–O vibration in reactants (from 1280 to 1264 cm^{-1}) in contrast to the bare TiO_2[12,16].

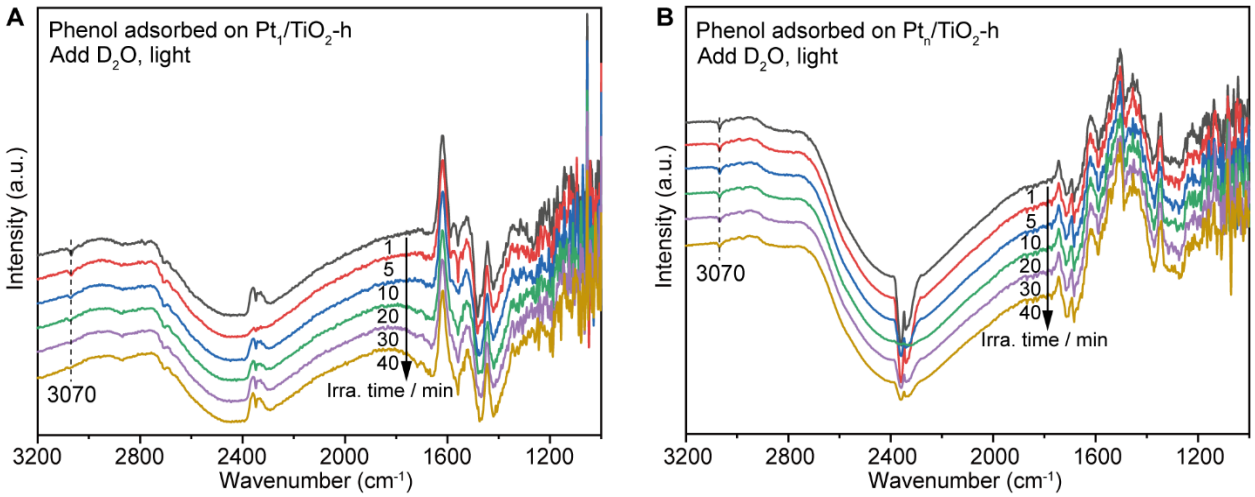

Supplementary Figure 31. DRIFTS data of *in situ* photocatalytic HIE reaction over (A) Pt_1/TiO_2-h and (B) Pt_n/TiO_2-h.

After D_2O was introduced to the cell of DRIFTS, the absorption band belonging to aromatic C(sp^2)–H (at 3070 cm^{-1})[12,16] gradually weakened with irradiation time using Pt_1/TiO_2-h (Supplementary Fig. 31A). It could be ascribed to the H/D exchange step with D_2O. Notably, the DRIFTS data of phenol-d_5 adsorbed on KBr and Pt_1/TiO_2-h showed the stretching vibration of aromatic C–D bonds was around 2283 cm^{-1}, and the bending vibrational of C–D bonds was around 1380 cm^{-1} (Supplementary Fig. 32). However, due to the overlap of CO_2 and D_2O signals (Supplementary Fig. 33), the peak corresponding to C–D bonds could not be directly observed. Instead, no changes occurred during light irradiation for Pt_n/TiO_2-h with phenol and D_2O adsorbed (Supplementary Fig. 31B).

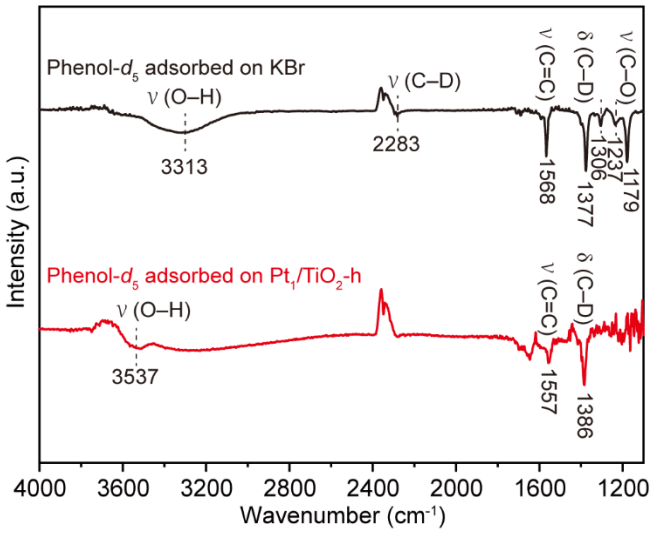

Supplementary Figure 32. DRIFTS data of phenol-d_5 adsorbed on KBr and Pt_1/TiO_2-h.

As shown in Supplementary Fig. 32, the black line represented the DRIFTS data of phenol-d_5 adsorbed on KBr. The absorption band at 2283 cm^{-1} could be attributed to the stretching vibration of aromatic C–D bonds in Phenol-d_5, accompanied by the bending vibration of C–D bonds (at 1377 cm^{-1})[12,16]. The red line showed the IR signals of phenol-d_5 adsorbed on Pt_1/TiO_2-h. Notably, the stretching vibration of C–D bonds failed to be clearly observed due to the interference from CO_2. Only the possible bending vibration of C–D bonds was detected at 1386 cm^{-1}.

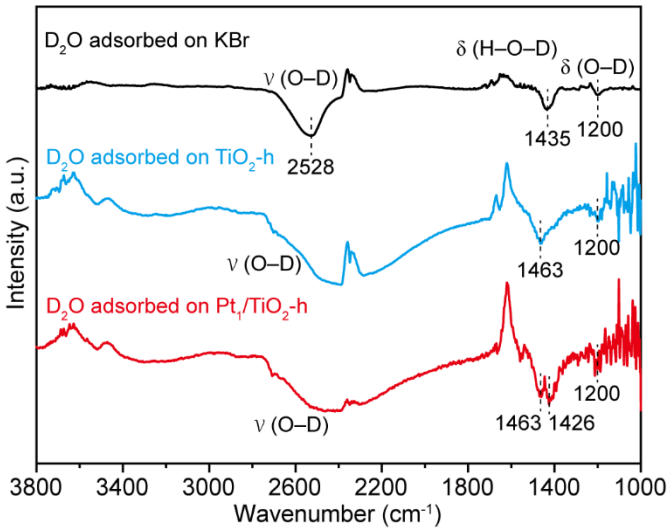

Supplementary Figure 33. DRIFTS data of D_2O adsorbed on KBr, TiO_2-h, and Pt_1/TiO_2-h. Except for the data of D_2O adsorption on KBr, all spectra used the DRIFTS data of clean catalyst sample as the background.

As shown in Supplementary Fig. 33, the dominant IR band located at 2528 cm^{-1} can be assigned to the asymmetric stretching vibrational of the O–D groups from D_2O on KBr, accompanying the bending vibrational of H–O–D and O–D at 1435 cm^{-1} and 1200 cm^{-1}. In contrast to the D_2O adsorbed on KBr, a broader peak was observed for the O–D stretching mode for the case of D_2O adsorbed on TiO_2-h and Pt_1/TiO_2-h. Meanwhile, the H–O–D bending vibrational peak also slightly blue shifts (from 1435 to 1463 cm^{-1}). This might indicate the dissociation of D_2O on TiO_2-h and Pt_1/TiO_2-h with the formation of Ti-OD[17,18].

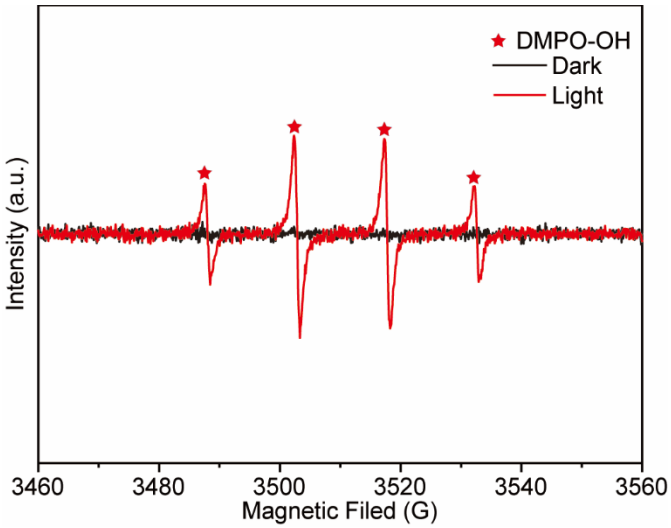

Supplementary Figure 34. EPR spectra of the suspension samples in D_2O with or without light irradiation.

Characteristic signals from hydroxyl radicals were clearly observed in the EPR spectra of the suspension containing Pt_1/TiO_2-h in D_2O under light irradiation[19], which were absent in the case without illumination. Thus, hydroxyl radicals would be produced in the reaction system during photocatalytic HIE. Additionally, the fluctuation of the baseline appeared probably due to the presence of solid photocatalysts in the solution during EPR tests. The hydroxyl radicals could originate from the oxidation of D_2O or surface hydroxyl groups on TiO_2-h by photo-generated holes. Besides, the hydroxyl radicals may play the role of oxidizing the partially reduced sites of $Pt^{\delta*}$ back to $Pt^{\delta+}$ in the photocatalytic cycle.

6. Gram-scale synthesis and synthetic applications

6.1 Gram-scale synthesis of deuterated 2,6-dimethylaniline (13b)

In comparison with the reaction in a 20 mL stainless-steel autoclave (0.1 mmol reactant, 50 mg photocatalyst, 2 mL D_2O), the reactant amount was scaled up to **1000 times** (100 mmol) by use of a homemade glass photoreactor (250 mL, as shown in Supplementary Fig. 35A and 35B). In a 250 mL Schlenk bottle with a fitted magnetic stirrer, 2.0 wt.% Pt_1/TiO_2-h (5.0 g) and 2,6-dimethylaniline (12.1 g, 100 mmol) were added. Then, the bottle was flushed with the Schlenk Line in Ar atmosphere for 3 times. Subsequently, D_2O (180 mL, 9931 mmol) was introduced. Later, it was placed into a homemade light box (equipped with 410 nm LED strips) and irradiated for 48 h. Additionally, the temperature of the reaction after 48 h irradiation was detected to be around 60-70 ºC, which came from the absorption of photon energy and the heat released from the LED strips when working. At the end of the reaction, the suspension was centrifuged to obtain the used photocatalyst and supernatant, which was then extracted with ethyl acetate (50 mL × 3). The organic phases were dried with anhydrous Na_2SO_4. After removing ethyl acetate in vacuo, the desired product was obtained.

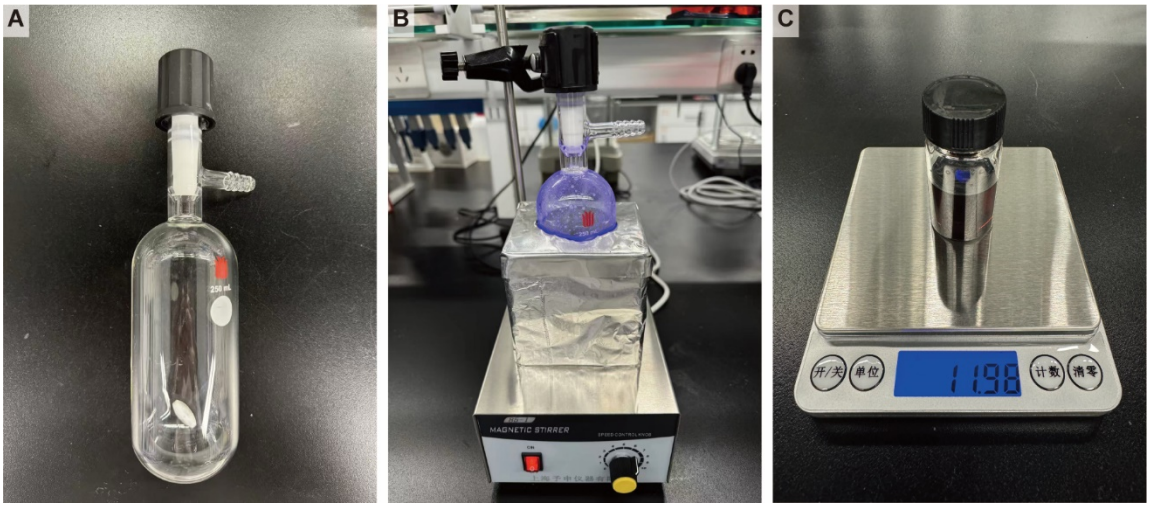

Supplementary Figure 35. (A) 250 mL Schlenk bottle. (B) 250 mL batch-mode photoreactor equipped with 410 nm LED strips covered by Al foils. (C) The isolated product of deuterated 2,6-dimethylaniline (11.98 g).

HRMS analysis of the deuterated 2,6-dimethylaniline (13b)

Deuterium incorporation of **13b**: 3.51D/molecule (^{1}H-NMR), 3.39 D/molecule [HRMS (ESI)].

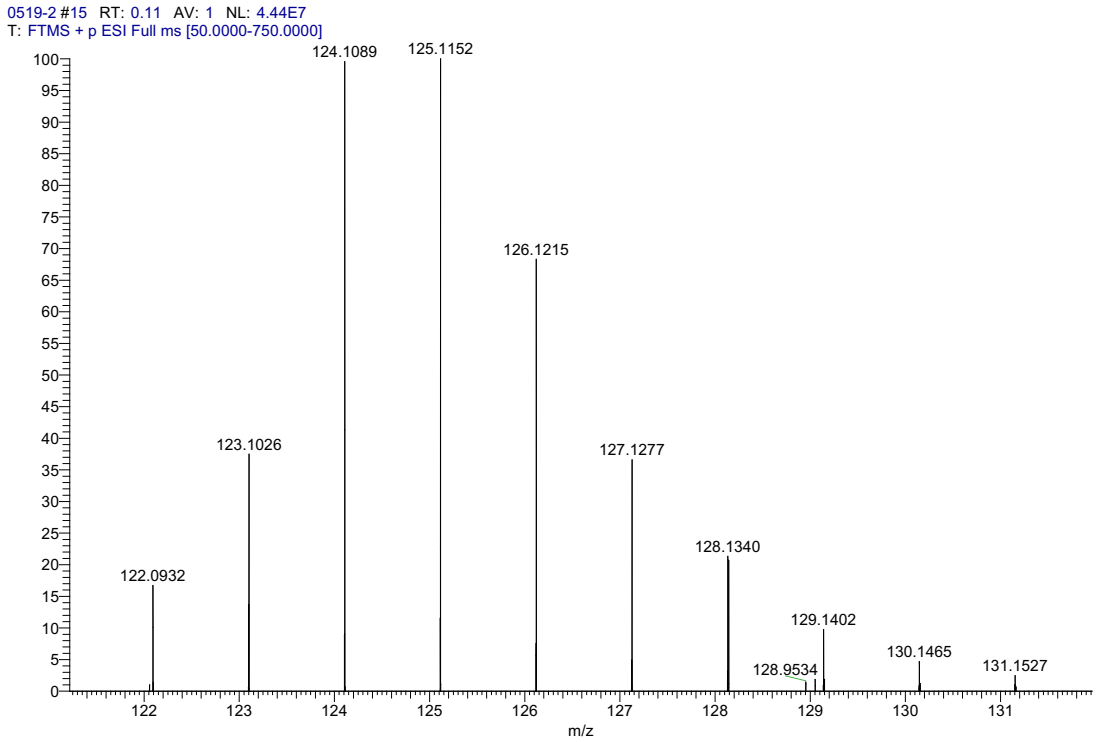

122.0964 ($C_8H_{11}N + H^+$, 0%), 123.1026 ($C_8H_{10}DN + H^+$, 11%), 124.1089 ($C_8H_9D_2N + H^+$, 25%), 125.1152 ($C_8H_8D_3N + H^+$, 26%), 126.1215 ($C_8H_7D_4N + H^+$, 17%), 127.1277 ($C_8H_6D_5N + H^+$, 10%), 128.1340 ($C_8H_5D_6N + H^+$, 6%), 129.1402 ($C_8H_4D_7N + H^+$, 3%), 130.1465 ($C_8H_3D_8N + H^+$, 2%), 131.1527 ($C_8H_2D_9N + H^+$, 1%).

6.2 Procedure for the synthesis of D-labeling drugs

Procedure for synthesis of [D] Lidocaine[20,21]:

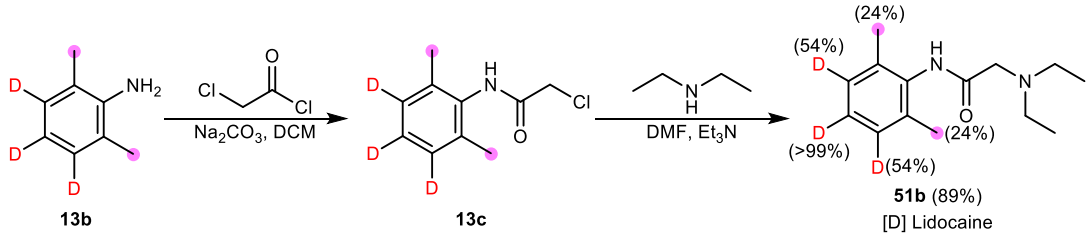

Step 1: In an over dried schlenk tube, Chloroacetyl chloride (2.2 mmol) was slowly added to a suspension of deuterated 2,6-dimethylaniline **13b** (2 mmol) and Na_2CO_3 (2.2 mmol) in DCM (4 mL) at 0 °C. After stirring the solution at room temperature for 3 h, the solution was concentrated and the product **13c** was obtained by flash column chromatography on silica gel.

Step 2: In an over dried schlenk tube, **13c** (1.1 mmol), Diethylamine (1 mmol), and Et_3N (1.1 mmol) were added in DMF (4 mL). After stirring the solution at 99 °C for 24 h, the reaction solution was concentrated and the product **51b** ([D] Lidocaine) was obtained by flash column chromatography on silica gel.

Procedure for synthesis of [D] Nefiracetam[21]:

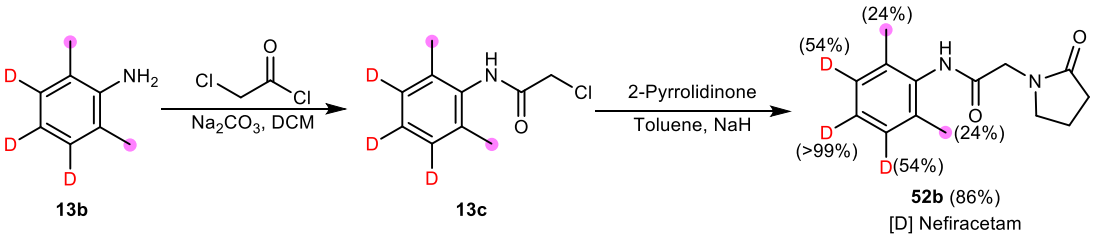

Step 1: In an over dried schlenk tube, Chloroacetyl chloride (2.2 mmol) was slowly added to a suspension of deuterated 2,6-dimethylaniline **13b** (2 mmol) and Na_2CO_3 (2.2 mmol) in DCM (4 mL) at 0 °C. After stirring the solution at room temperature for 3 h, the solution was concentrated and the product **13c** was obtained by flash column chromatography on silica gel.

Step 2: In an over dried schlenk tube, 2-Pyrrolidinone (2.5 mmol) was slowly added to a suspension of NaH (4 mmol) and Toluene (3 mL) at 30 °C. After stirring the solution at 30 °C for 2 h, the product **13c** (1 mmol) obtained in step 1 was added. The reaction mixture was stirred at 60-70 °C for another 2 h, the reaction solution was concentrated and the product **52b** ([D] Nefiracetam) was obtained by flash column chromatography on silica gel.

Procedure for synthesis of [D] Clortoluron[22]:

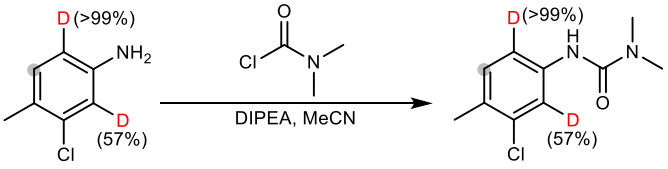

In an over dried schlenk tube, dimethylcarbamoyl chloride (1.2 mmol) was added dropwise to a solution of deuterated aniline derivatives **24b** (1 mmol) in MeCN (10 mL) at room temperature. Then DIPEA (1 mmol) was added slowly to the reaction mixture. After stirring the solution at 100 ^{o}C in an oil bath for 24 h, the reaction solution was concentrated and the product **53b** ([D] Clortoluron) was obtained by flash column chromatography on silica gel.

Procedure for synthesis of [D] Fluometuron[22]:

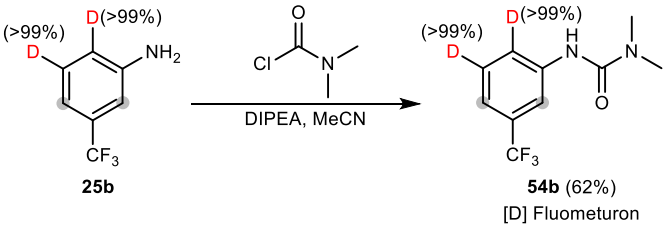

In an over dried schlenk tube, dimethylcarbamoyl chloride (1.2 mmol) was added dropwise to a solution of deuterated aniline derivatives **25b** (1 mmol) in MeCN (10 mL) at room temperature. Then DIPEA (1 mmol) was added slowly to the reaction mixture. After stirring the solution at 100 ^{o}C in oil bath for 24 h, the reaction solution was concentrated and the product **54b** ([D] Fluometuron) was obtained by flash column chromatography on silica gel.

7. NMR analysis of substrates and products

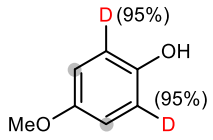

1b

Reaction conditions: 0.7 wt.% Pt_1/TiO_2-h (50 mg), substrate (12.4 mg, 0.1 mmol), D_2O (2 mL), 450 nm LED (30 mW/cm^2), Ar (1 bar), r.t., 6 h. The product **1b** was obtained (Selectivity > 99%, detected by ^{1}H NMR).

Feed material 1a: ^{1}H NMR (400 MHz, D_2O) δ 6.90 – 6.86 (m, 2H), 6.85 – 6.81 (m, 2H), 3.75 (s, 3H).

Product 1b: ^{1}H NMR (400 MHz, D_2O) δ 6.93 (s, 1.67H), 6.88 (d, J = 8 Hz, 0.10H), 3.80 (s, 3H).

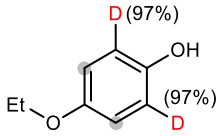

2b

Reaction conditions: 0.7 wt.% Pt_1/TiO_2-h (50 mg), substrate (13.8 mg, 0.1 mmol), D_2O (2 mL), 450 nm LED (30 mW/cm^2), Ar (1 bar), r.t., 6 h. The product **2b** was obtained (Selectivity > 99%, detected by ^{1}H NMR).

Feed material 2a: ^{1}H NMR (400 MHz, D_2O) δ 6.93 – 6.89 (m, 2H), 6.87 – 6.83 (m, 2H), 4.05 (q, J = 12, 8 Hz, 2H), 1.34 (t, J = 8 Hz, 3H).

Product 2b: ^{1}H NMR (400 MHz, D_2O) δ 6.87 (s, 1.79H), 6.78 (d, J = 16 Hz, 0.05H), 4.01 (q, J = 16, 8 Hz, 2H), 1.30 (t, J = 8 Hz, 3H).

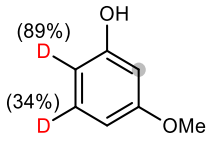

3b

Reaction conditions: 0.7 wt.% Pt_1/TiO_2-h (50 mg), substrate (12.4 mg, 0.1 mmol), D_2O (2 mL), 410 nm LED (95 mW/cm^2), Ar (1 bar), r.t., 6 h. The product **3b** was obtained (Selectivity > 99%, detected by ^{1}H NMR).

Feed material 3a: ^{1}H NMR (400 MHz, D_2O) δ 7.19 (t, *J* = 8 Hz, 1H), 6.55 – 6.49 (m, 2H), 6.45 (t, *J* = 4 Hz, 1H), 3.75 (s, 3H).

Product 3b: ^{1}H NMR (400 MHz, D_2O) δ 7.24 – 7.19 (m, 0.63H), 6.58 – 6.56 (m, 1H), 6.52 (t, *J* = 4 Hz, 0.10H), 6.49 (d, *J* = 4 Hz, 0.84H), 3.78 (s, 3H).

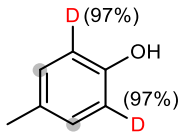

4b

Reaction conditions: 0.7 wt.% Pt_1/TiO_2-h (50 mg), substrate (10.8 mg, 0.1 mmol), D_2O (2 mL), 450 nm LED (30 mW/cm^2), Ar (1 bar), r.t., 6 h. The product **4b** was obtained (Selectivity > 99%, detected by ^{1}H NMR).

Feed material 4a: ^{1}H NMR (400 MHz, D_2O) δ 7.13 (d, *J* = 8 Hz, 2H), 6.83 – 6.79 (m, 2H), 2.24 (s, 3H).

Product 4b: ^{1}H NMR (400 MHz, D_2O) δ 7.12 (s, 1.62H), 6.80 (d, *J* = 8 Hz, 0.06H), 2.24 (s, 3H).

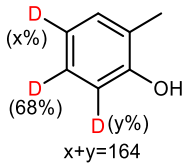

5b

Reaction conditions: 0.7 wt.% Pt_1/TiO_2-h (50 mg), substrate (10.8 mg, 0.1 mmol), D_2O (2 mL), 410 nm LED (60 mW/cm^2), Ar (1 bar), 60 °C, 12 h. The product **5b** was obtained (Selectivity > 99%, detected by ^{1}H NMR).

Feed material 5a: ^{1}H NMR (400 MHz, D_2O) δ 7.16 (d, J = 8 Hz, 1H), 7.11 (t, J = 8 Hz, 1H), 6.86 (t, J = 8 Hz, 2H), 2.17 (s, 3H).

Product 5b: ^{1}H NMR (400 MHz, D_2O) δ 7.22 (s, 1H), 7.15 (s, 0.30H), 6.94 – 6.90 (m, 0.33H), 2.21 (s, 3H).

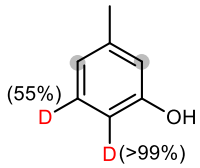

6b

Reaction conditions: 0.7 wt.% Pt_1/TiO_2-h (50 mg), substrate (10.8 mg, 0.1 mmol), D_2O (2 mL), 410 nm LED (95 mW/cm^2), Ar (1 bar), r.t., 6 h. The product **6b** was obtained (Selectivity > 99%, detected by ^{1}H NMR).

Feed material 6a: ^{1}H NMR (400 MHz, D_2O) δ 7.18 (t, J = 8 Hz, 1H), 6.80 (d, J = 8 Hz, 1H), 6.74 (s, 1H), 6.70 (d, J = 8 Hz, 1H), 2.26 (s, 3H).

Product 6b: ^{1}H NMR (400 MHz, D_2O) δ 7.19 (d, J = 8 Hz, 0.43H), 6.81 (t, J = 4 Hz, 0.88H), 6.75 (s, 0.78H), 2.27 (s, 3H).

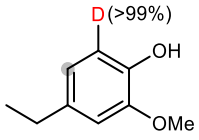

7b

Reaction conditions: 0.7 wt.% Pt_1/TiO_2-h (50 mg), substrate (15.2 mg, 0.1 mmol), D_2O (2 mL), 410 nm LED (60 mW/cm^2), Ar (1 bar), 60 °C, 12 h. The product **7b** was obtained (Selectivity > 99%, detected by ^{1}H NMR).

Feed material 7a: ^{1}H NMR (400 MHz, DMSO-d_6) δ 8.65 (s, 1H), 6.76 (s, 1H), 6.70 (d, J = 8 Hz, 1H), 6.59 (d, J = 8 Hz, 1H), 3.76 (s, 3H), 2.50 (q, J = 16, 4 Hz, 2H), 1.15 (t, J = 8 Hz, 3H).

Product 7b: ^{1}H NMR (400 MHz, D_2O) δ 6.97 (s, 1H), 6.79 (s, 0.85H), 3.86 (s, 3H), 2.58 (q, J = 16, 8 Hz, 2H), 1.18 (t, J = 8 Hz, 3H).

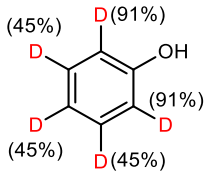

8b

Reaction conditions: 0.7 wt.% Pt_1/TiO_2-h (50 mg), substrate (9.4 mg, 0.1 mmol), D_2O (2 mL), 410 nm LED (60 mW/cm^2), Ar (1 bar), r.t., 12 h. The product **8b** was obtained (Selectivity > 99%, detected by ^{1}H NMR).

Feed material 8a: ^{1}H NMR (400 MHz, D_2O) δ 7.34 (t, J = 8 Hz, 2H), 7.00 (t, J = 8 Hz, 1H), 6.93 (d, J = 8 Hz, 2H).

Product 8b: ^{1}H NMR (400 MHz, D_2O) δ 7.34 (t, J = 4 Hz, 1.04H), 7.02 – 6.98 (m, 0.52H), 6.93 (t, J = 4 Hz, 0.17H).

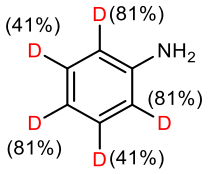

9b

Reaction conditions: 2.0 wt.% Pt_1/TiO_2-h (50 mg), substrate (9.3 mg, 0.1 mmol), D_2O (2 mL), 410 nm LED (60 mW/cm^2), Ar (1 bar), 60 °C, 24 h. The product **9b** was obtained (Selectivity > 99%, detected by ^{1}H NMR).

Feed material 9a: ^{1}H NMR (400 MHz, D_2O) δ 7.24 (t, J = 8 Hz, 2H), 6.90 – 6.85 (m, 3H).

Product 9b: ^{1}H NMR (400 MHz, D_2O) δ 7.24 (t, J = 4 Hz, 1.10H), 6.90 – 6.86 (m, 0.51H).

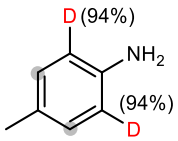

10b

Reaction conditions: 0.7 wt.% Pt_1/TiO_2-h (50 mg), substrate (10.7 mg, 0.1 mmol), D_2O (2 mL), 410 nm LED (60 mW/cm^2), Ar (1 bar), 60 °C, 6 h. The product **10b** was obtained (Selectivity > 99%, detected by ^{1}H NMR).

Feed material 10a: ^{1}H NMR (400 MHz, D_2O) δ 7.09 (d, J = 8 Hz, 2H), 6.79 (d, J = 8 Hz, 2H), 2.23 (s, 3H).

Product 10b: ^{1}H NMR (400 MHz, D_2O) δ 7.09 (s, 1.80H), 6.78 (d, J = 8 Hz, 0.10H), 2.23 (s, 3H).

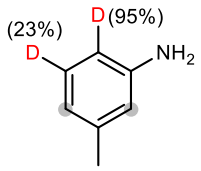

11b

Reaction conditions: 0.7 wt.% Pt_1/TiO_2-h (50 mg), substrate (10.7 mg, 0.1 mmol), D_2O (2 mL), 410 nm LED (60 mW/cm^2), Ar (1 bar), 60 °C, 12 h. The product **11b** was obtained (Selectivity > 99%, detected by ^{1}H NMR).

Feed material 11a: ^{1}H NMR (400 MHz, D_2O) δ 7.14 (t, J = 8 Hz, 1H), 6.72 (t, J = 8 Hz, 2H), 6.67 (d, J = 8 Hz, 1H), 2.26 (s, 3H).

Product 11b: ^{1}H NMR (400 MHz, D_2O) δ 7.16 (d, J = 8 Hz, 0.72H), 6.75 (d, J = 12 Hz, 1.57H), 6.68 (d, J = 8 Hz, 0.04H), 2.27 (s, 3H).

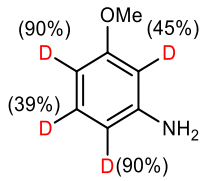

12b

Reaction conditions: 0.7 wt.% Pt_1/TiO_2-h (50 mg), substrate (12.3 mg, 0.1 mmol), D_2O (2 mL), 410 nm LED (60 mW/cm^2), Ar (1 bar), 60 °C, 12 h. The product **12b** was obtained (Selectivity > 99%, detected by ^{1}H NMR).

Feed material 12a: ^{1}H NMR (400 MHz, D_2O) δ 7.17 (t, J = 8 Hz, 1H), 6.49 – 6.46 (m, 2H), 6.45 (t, J = 4 Hz, 1H), 3.78 (s, 3H).

Product 12b: ^{1}H NMR (400 MHz, D_2O) δ 7.18 (s, 0.57H), 6.51 – 6.48 (m, 0.19H), 6.47 (s, 0.47H).

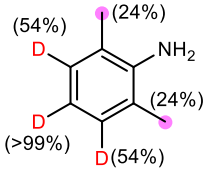

13b

The product **13b** was obtained by gram-scale synthesis (isolated yield 97%).

Feed material 13a: ^{1}H NMR (400 MHz, D_2O) δ 7.06 (d, *J* = 8 Hz, 2H), 6.79 (t, *J* = 8 Hz, 1H), 2.21 (s, 6H).

Product 13b: ^{1}H NMR (400 MHz, D_2O) δ 7.04 (s, 0.85H), 2.19 – 2.15 (m, 4.57H).

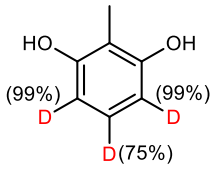

14b

Reaction conditions: 0.7 wt.% Pt_1/TiO_2-h (50 mg), substrate (12.4 mg, 0.1 mmol), D_2O (2 mL), 410 nm LED (60 mW/cm^2), Ar (1 bar), r.t., 12 h. The product **14b** was obtained (Selectivity > 99%, detected by ^{1}H NMR).

Feed material 14a: ^{1}H NMR (400 MHz, D_2O) δ 6.95 (t, *J* = 8 Hz, 1H), 6.47 (d, *J* = 8 Hz, 1H), 2.02 (s, 3H).

Product 14b: ^{1}H NMR (400 MHz, D_2O) δ 6.99 (s, 0.25H), 6.51 (s, 0.02H), 2.06 (s, 3H).

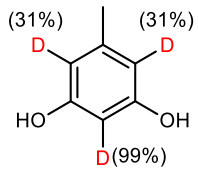

15b

Reaction conditions: 0.7 wt.% Pt_1/TiO_2-h (50 mg), substrate (12.4 mg, 0.1 mmol), D_2O (2 mL), 410 nm LED (60 mW/cm^2), Ar (1 bar), r.t., 12 h. The product **15b** was obtained (Selectivity > 99%, detected by ^{1}H NMR).

Feed material 15a: ^{1}H NMR (400 MHz, D_2O) δ 6.31 (s, 2H), 6.21 (s, 1H), 2.20 (s, 3H).

Product 15b: ^{1}H NMR (400 MHz, D_2O) δ 6.34 (s, 1.24H), 6.23 (s, 0.01H), 2.23 (s, 3H).

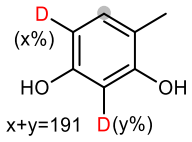

16b

Reaction conditions: 0.7 wt.% Pt_1/TiO_2-h (50 mg), substrate (12.4 mg, 0.1 mmol), D_2O (2 mL), 410 nm LED (60 mW/cm^2), Ar (1 bar), r.t., 12 h. The product **16b** was obtained (Selectivity > 99%, detected by ^{1}H NMR).

Feed material 16a: ^{1}H NMR (400 MHz, D_2O) δ 7.03 (d, J = 8 Hz, 1H), 6.40 (d, J = 8 Hz, 2H), 2.09 (s, 3H).

Product 16b: ^{1}H NMR (400 MHz, D_2O) δ 7.05 (s, 0.90H), 6.42 (d, J = 8 Hz, 0.08H), 2.11 (s, 3H).

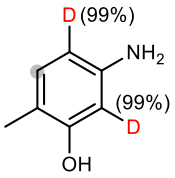

17b

Reaction conditions: 0.7 wt.% Pt_1/TiO_2-h (50 mg), substrate (12.3 mg, 0.1 mmol), D_2O (2 mL), 410 nm LED (60 mW/cm^2), Ar (1 bar), 60 °C, 6 h. The product **17b** was obtained (Selectivity > 99%, detected by ^{1}H NMR).

Feed material 17a: ^{1}H NMR (400 MHz, D_2O) δ 7.00 (d, J = 8 Hz, 1H), 6.38 – 6.36 (m, 2H), 2.10 (s, 3H).

Product 17b: ^{1}H NMR (400 MHz, D_2O) δ 6.99 (s, 0.90H), 6.37 (s, 0.02H), 2.08 (s, 3H).

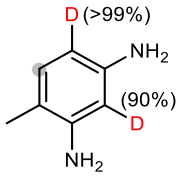

18b

Reaction conditions: 0.7 wt.% Pt_1/TiO_2-h (50 mg), substrate (12.2 mg, 0.1 mmol), D_2O (2 mL), 410 nm LED (60 mW/cm^2), Ar (1 bar), 60 °C, 6 h. The product **18b** was obtained (Selectivity > 99%, detected by ^{1}H NMR).

Feed material 18a: ^{1}H NMR (400 MHz, D_2O) δ 6.94 (d, J = 8 Hz, 1H), 6.33 (d, J = 4 Hz, 1H), 6.29 (dd, J = 8, 4 Hz, 1H), 2.06 (s, 3H).

Product 18b: ^{1}H NMR (400 MHz, D_2O) δ 6.93 (s, 0.88H), 6.32 (s, 0.08H), 2.05 (s, 3H).

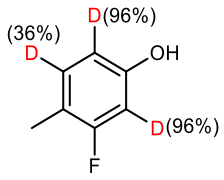

19b

Reaction conditions: 0.7 wt.% Pt_1/TiO_2-h (50 mg), substrate (12.6 mg, 0.1 mmol), D_2O (2 mL), 410 nm LED (60 mW/cm^2), Ar (1 bar), 60 °C, 12 h. The product **19b** was obtained (Selectivity > 99%, detected by ^{1}H NMR).

Feed material 19a: ^{1}H NMR (400 MHz, DMSO-d_6) δ 9.57 (s, 1H), 7.02 (t, J = 8 Hz, 1H), 6.51 – 6.48 (m, 2H), 2.09 (s, 3H); ^{19}F NMR (376 MHz, DMSO-d_6) δ -116.27.

Product 19b: ^{1}H NMR (400 MHz, DMSO-d_6) δ 7.12 (d, J = 8 Hz, 0.63H), 6.63 (d, J = 12 Hz, 0.07H), 2.15 (s, 3H); ^{19}F NMR (376 MHz, DMSO-d_6) δ -116.40.

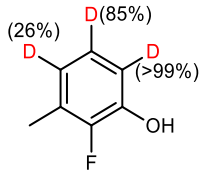

20b

Reaction conditions: 0.7 wt.% Pt_1/TiO_2-h (50 mg), substrate (12.6 mg, 0.1 mmol), D_2O (2 mL), 410 nm LED (60 mW/cm^2), Ar (1 bar), 60 °C, 12 h. The product **20b** was obtained (Selectivity > 99%, detected by ^{1}H NMR).

Feed material 20a: ^{1}H NMR (400 MHz, DMSO-d_6) δ 9.62 (s, 1H), 6.84 (t, J = 8 Hz, 1H), 6.75 (t, J = 8 Hz, 1H), 6.64 (t, J = 8 Hz, 1H), 2.19 (d, J = 4 Hz, 3H); ^{19}F NMR (376 MHz, DMSO-d_6) δ -141.51.

Product 20b: ^{1}H NMR (400 MHz, DMSO-d_6) δ 6.96 (d, J = 8 Hz, 0.15H), 6.81 (d, J = 8 Hz, 0.73H), 2.25 (s, 3H); ^{19}F NMR (376 MHz, DMSO-d_6) δ -142.60.

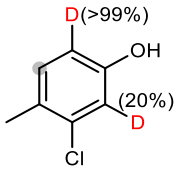

21b

Reaction conditions: 0.7 wt.% Pt_1/TiO_2-h (50 mg), substrate (14.2 mg, 0.1 mmol), D_2O (2 mL), 410 nm LED (60 mW/cm^2), Ar (1 bar), 60 °C, 12 h. The product **21b** was obtained (Selectivity > 99%, detected by ^{1}H NMR).

Feed material 21a: ^{1}H NMR (400 MHz, DMSO-d_6) δ 9.60 (s, 1H), 7.10 (d, J = 8 Hz, 1H), 6.80 (d, J = 4 Hz, 1H), 6.65 (dd, J = 8, 4 Hz, 1H), 2.19 (s, 3H).

Product 21b: ^{1}H NMR (400 MHz, D_2O) δ 7.19 (s, 0.83H), 6.95 (s, 0.75H), 2.26 (s, 3H).

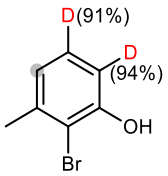

22b

Reaction conditions: 0.7 wt.% Pt_1/TiO_2-h (50 mg), substrate (18.7 mg, 0.1 mmol), D_2O (2 mL), 410 nm LED (60 mW/cm^2), Ar (1 bar), 60 °C, 12 h. The product **22b** was obtained (Selectivity > 99%, detected by ^{1}H NMR).

Feed material 22a: ^{1}H NMR (400 MHz, D_2O) δ 7.18 (t, J = 8 Hz, 1H), 6.94 (d, J = 8 Hz, 1H), 6.88 (d, J = 8 Hz, 1H), 2.40 (s, 3H).

Product 22b: ^{1}H NMR (400 MHz, D_2O) δ 7.17 (d, J = 8 Hz, 0.09H), 6.93 (s, 0.90H), 6.83 (s, 0.06H), 2.39 (s, 3H).

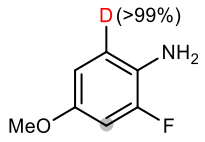

23b

Reaction conditions: 0.7 wt.% Pt_1/TiO_2-h (50 mg), substrate (14.1 mg, 0.1 mmol), D_2O (2 mL), 410 nm LED (60 mW/cm^2), Ar (1 bar), 60 °C, 12 h. The product **23b** was obtained (Selectivity > 99%, detected by ^{1}H NMR).

Feed material 23a: ^{1}H NMR (400 MHz, D_2O) δ 6.91 (t, J = 12 Hz, 1H), 6.80 (dd, J = 12, 4 Hz, 1H), 6.69 (dd, J = 8, 4 Hz, 1H), 3.77 (s, 3H); ^{19}F NMR (376 MHz, DMSO-d_6) δ -128.27.

Product 23b: ^{1}H NMR (400 MHz, D_2O) δ 6.80 (dd, J = 12, 4 Hz, 1H), 6.69 (s, 0.87H), 3.77 (s, 3H); ^{19}F NMR (376 MHz, DMSO-d_6) δ -127.95.

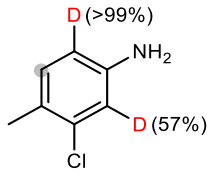

24b

Reaction conditions: 0.7 wt.% Pt_1/TiO_2-h (50 mg), substrate (14.1 mg, 0.1 mmol), D_2O (2 mL), 410 nm LED (60 mW/cm^2), Ar (1 bar), 60 °C, 12 h. The product **24b** was obtained (Selectivity > 99%, detected by ^{1}H NMR).

Feed material 24a: ^{1}H NMR (400 MHz, D_2O) δ 7.13 (d, J = 8 Hz, 1H), 6.91 (d, J = 4 Hz, 1H), 6.71 (dd, J = 8, 4 Hz, 1H), 2.25 (s, 3H).

Product 24b: ^{1}H NMR (400 MHz, D_2O) δ 7.16 (s, 0.88H), 6.95 (s, 0.38H), 2.26 (s, 3H).

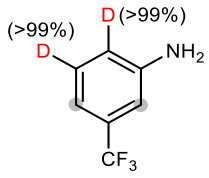

25b

Reaction conditions: 0.7 wt.% Pt_1/TiO_2-h (50 mg), substrate (16.1 mg, 0.1 mmol), D_2O (2 mL), 410 nm LED (60 mW/cm^2), Ar (1 bar), 60 °C, 12 h. The product **25b** was obtained (Selectivity > 99%, detected by ^{1}H NMR).

Considering that **25b** underwent deuterium exchange at all C(sp^2)–H positions without any unlabeled portion serving as an internal reference, we determined the specific D incorporation based on its derivatized product (**54b)**.

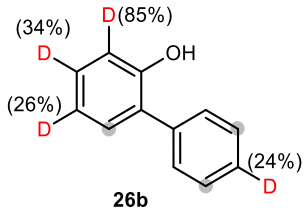

26b

Reaction conditions: 2.0 wt.% Pt_1/TiO_2-h (50 mg), substrate (17.0 mg, 0.1 mmol), D_2O (1.6 mL), acetone (0.4 mL), 410 nm LED (60 mW/cm^2), Ar (1 bar), 60 °C, 24 h. The product **26b** was obtained (Selectivity > 99%, detected by ^{1}H NMR).

Feed material 26a: ^{1}H NMR (400 MHz, DMSO-d_6) δ 9.52 (s, 1H), 7.56 (d, J = 8 Hz, 2H), 7.39 (t, J = 8 Hz, 2H), 7.30 (d, J = 8 Hz, 1H), 7.26 (d, J = 8 Hz, 1H), 7.17 (t, J = 8 Hz, 1H), 6.98 (d, J = 8 Hz, 1H), 6.88 (t, J = 8 Hz, 1H).

Product 26b: ^{1}H NMR (400 MHz, DMSO-d_6) δ 9.49 (s, 1H), 7.53 (d, J = 8 Hz, 2H), 7.41 – 7.37 (m, 1.73H), 7.28 (t, J = 8 Hz, 0.74H), 7.24 (t, J = 4 Hz, 0.94H), 7.16 (d, J = 4 Hz, 0.66H), 6.94 (t, J = 4 Hz, 0.15H), 6.89 – 6.85 (m, 0.73H).

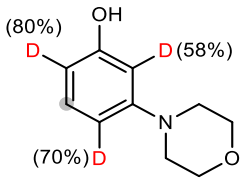

27b

Reaction conditions: 0.7 wt.% Pt_1/TiO_2-h (50 mg), substrate (17.9 mg, 0.1 mmol), D_2O (1.6 mL), acetone (0.4 mL), 410 nm LED (60 mW/cm^2), Ar (1 bar), 60 °C, 12 h. The product **27b** was obtained (Selectivity > 99%, detected by ^{1}H NMR).

Feed material 27a: ^{1}H NMR (400 MHz, $CDCl_3$) δ 7.12 (t, *J* = 8 Hz, 1H), 6.50 (dd, *J* = 8, 4 Hz, 1H), 6.39 (t, *J* = 4 Hz, 1H), 6.35 (dd, *J* = 8, 4 Hz, 1H), 5.10 (s, 1H), 3.86 (t, *J* = 4 Hz, 4H), 3.14 (t, *J* = 4 Hz, 4H).

Product 27b: ^{1}H NMR (400 MHz, $CDCl_3$) δ 7.12 (t, *J* = 4 Hz, 0.88H), 6.50 (d, *J* = 8 Hz, 0.29H), 6.39 (s, 0.41H), 6.35 (d, *J* = 8 Hz, 0.18H), 5.53 (s, 0.29H), 3.86 (t, *J* = 4 Hz, 4H), 3.13 (t, *J* = 4 Hz, 4H).

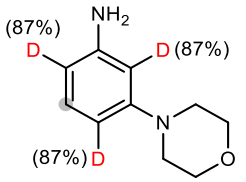

28b

Reaction conditions: 0.7 wt.% Pt_1/TiO_2-h (50 mg), substrate (17.8 mg, 0.1 mmol), D_2O (1.6 mL), acetone (0.4 mL), 410 nm LED (60 mW/cm^2), Ar (1 bar), 60 °C, 12 h. The product **28b** was obtained (Selectivity > 99%, detected by ^{1}H NMR).

Feed material 28a: ^{1}H NMR (400 MHz, $CDCl_3$) δ 7.06 (t, *J* = 8 Hz, 1H), 6.35 (d, *J* = 8 Hz, 1H), 6.23 (s, 2H), 3.84 (t, *J* = 4 Hz, 4H), 3.64 (s, 2H), 3.12 (t, *J* = 4 Hz, 4H).

Product 28b: ^{1}H NMR (400 MHz, $CDCl_3$) δ 7.06 (s, 0.86H), 6.35 (d, *J* = 8 Hz, 0.13H), 6.24 (t, *J* = 4 Hz, 0.25H), 3.84 (t, *J* = 4 Hz, 4H), 3.62 (s, 0.46H), 3.12 (t, *J* = 4 Hz, 4H).

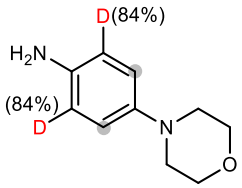

29b

Reaction conditions: 2.0 wt.% Pt_1/TiO_2-h (50 mg), substrate (17.8 mg, 0.1 mmol), D_2O (1.6 mL), acetone (0.4 mL), 410 nm LED (60 mW/cm^2), Ar (1 bar), 60 °C, 24 h. The product **29b** was obtained (Selectivity > 99%, detected by ^{1}H NMR).

Feed material 29a: ^{1}H NMR (400 MHz, $CDCl_3$) δ 6.80 (d, *J* = 8 Hz, 2H), 6.66 (d, *J* = 8 Hz, 2H), 3.85 (t, *J* = 4 Hz, 4H), 3.44 (s, 2H), 3.02 (t, *J* = 4 Hz, 4H).

Product 29b: ^{1}H NMR (400 MHz, $CDCl_3$) δ 6.80 (s, 1.90H), 6.66 (t, *J* = 4 Hz, 0.30H), 3.85 (t, *J* = 4 Hz, 4H), 3.35 (s, 0.92H), 3.02 (t, *J* = 4 Hz, 4H).

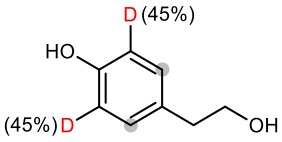

30b

Reaction conditions: 2.0 wt.% Pt_1/TiO_2-h (50 mg), substrate (13.8 mg, 0.1 mmol), D_2O (2.0 mL), 410 nm LED (60 mW/cm^2), Ar (1 bar), 60 °C, 24 h. The product **30b** was obtained (Selectivity > 99%, detected by ^{1}H NMR).

Feed material 30a: ^{1}H NMR (400 MHz, D_2O) δ 7.19 (d, *J* = 8 Hz, 2H), 6.88 (d, *J* = 12 Hz, 2H), 3.79 (t, *J* = 8 Hz, 2H), 2.79 (t, *J* = 8 Hz, 2H).

Product 30b: ^{1}H NMR (400 MHz, D_2O) δ 7.16 (t, *J* = 4 Hz, 1.88H), 6.84 (d, *J* = 8 Hz, 1.01H), 3.76 (t, *J* = 8 Hz, 2H), 2.75 (t, *J* = 8 Hz, 2H).

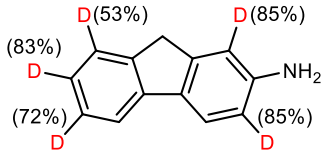

31b

Reaction conditions: 2.0 wt.% Pt_1/TiO_2-h (50 mg), substrate (18.1 mg, 0.1 mmol), D_2O (1.6 mL), acetone (0.4 mL), 410 nm LED (60 mW/cm^2), Ar (1 bar), 60 °C, 24 h. The product **31b** was obtained (Selectivity > 99%, detected by ^{1}H NMR).

Feed material 31a: ^{1}H NMR (400 MHz, DMSO-d_6) δ 7.60 (d, J = 8 Hz, 1H), 7.51 (d, J = 8 Hz, 1H), 7.43 (d, J = 8 Hz, 1H), 7.25 (t, J = 8 Hz, 1H), 7.11 (t, J = 8 Hz, 1H), 6.79 (s, 1H), 6.61 (d, J = 8 Hz, 1H), 5.19 (s, 2H), 3.74 (s, 2H).

Product 31b: ^{1}H NMR (400 MHz, DMSO-d_6) δ 7.60 (s, 1H), 7.52 (s, 1H), 7.43 (s, 0.46H), 7.25 (d, J = 8 Hz, 0.28H), 7.11 (s, 0.17H), 6.79 (s, 0.15H), 6.61 (d, J = 8 Hz, 0.15H), 5.39 (s, 1.49H), 3.74 (s, 2H).

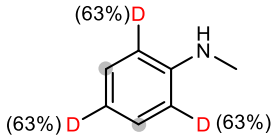

32b

Reaction conditions: 2.0 wt.% Pt_1/TiO_2-h (50 mg), substrate (10.7 mg, 0.1 mmol), D_2O (2.0 mL), 410 nm LED (60 mW/cm^2), Ar (1 bar), 60 °C, 24 h. The product **32b** was obtained (Selectivity > 99%, detected by ^{1}H NMR).

Feed material 32a: ^{1}H NMR (400 MHz, D_2O) δ 7.30 (t, J = 4 Hz, 2H), 6.90 – 6.85 (m, 3H), 2.75 (s, 3H).

Product 32b: ^{1}H NMR (400 MHz, D_2O) δ 7.32 (t, J = 4 Hz, 1.63H), 6.93 – 6.87 (m, 1.28H), 2.76 (s, 3.0H).

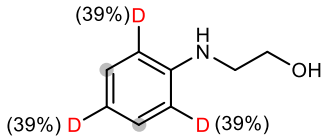

33b

Reaction conditions: 2.0 wt.% Pt_1/TiO_2-h (50 mg), substrate (13.7 mg, 0.1 mmol), D_2O (2.0 mL), 410 nm LED (60 mW/cm^2), Ar (1 bar), 60 °C, 24 h. The product **33b** was obtained (Selectivity > 99%, detected by ^{1}H NMR).

Feed material 33a: ^{1}H NMR (400 MHz, D_2O) δ 7.27 (t, J = 8 Hz, 2H), 6.87 – 6.82 (m, 2H), 3.73 (t, J = 8 Hz, 2H), 3.23 (t, J = 8 Hz, 2H).

Product 33b: ^{1}H NMR (400 MHz, D_2O) δ 7.30 – 7.26 (m, 1.82H), 6.90 – 6.85 (m, 1.72H), 3.75 (t, J = 8 Hz, 2H), 3.26 (t, J = 4 Hz, 2H).

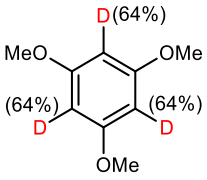

34b

Reaction conditions: 0.7 wt.% Pt_1/TiO_2-h (50 mg), substrate (16.8 mg, 0.1 mmol), D_2O (1.6 mL), acetone (0.4 mL), 410 nm LED (60 mW/cm^2), Ar (1 bar), 60 °C, 12 h. The product **34b** was obtained (Selectivity > 99%, detected by ^{1}H NMR).

Feed material 34a: ^{1}H NMR (400 MHz, $CDCl_3$) δ 6.09 (s, 3H), 3.77 (s, 9H).

Product 34b: ^{1}H NMR (400 MHz, $CDCl_3$) δ 6.09 (s, 1.05H), 3.77 (s, 9H).

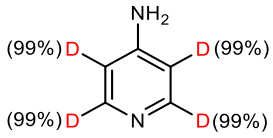

35b

Reaction conditions: 2.0 wt.% Pt_1/TiO_2-h (50 mg), substrate (9.4 mg, 0.1 mmol), D_2O (2.0 mL), 410 nm LED (60 mW/cm^2), Ar (1 bar), 60 °C, 24 h. The product **35b** was obtained (Selectivity > 99%, detected by ^{1}H NMR).

Feed material 35a: ^{1}H NMR (400 MHz, DMSO-d_6) δ 7.97 (d, J = 4 Hz, 2H), 6.45 (d, J = 8 Hz, 2H), 5.98 (s, 2H).

Product 35b: ^{1}H NMR (400 MHz, DMSO-d_6) δ 7.96 (s, 0.01H), 6.45 (s, 0.01H), 6.01 (s, 1.48H).

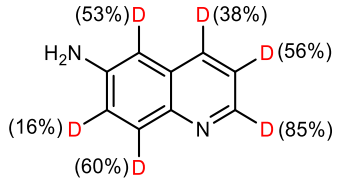

36b

Reaction conditions: 2.0 wt.% Pt_1/TiO_2-h (50 mg), substrate (14.4 mg, 0.1 mmol), D_2O (1.6 mL), acetone (0.4 mL), 410 nm LED (60 mW/cm^2), Ar (1 bar), 60 °C, 24 h. The product **36b** was obtained (Selectivity > 99%, detected by ^{1}H NMR).

Feed material 36a: ^{1}H NMR (400 MHz, DMSO-d_6) δ 8.47 (dd, J = 8, 4 Hz, 1H), 7.91 (d, J = 8 Hz, 1H), 7.71 (d, J = 12 Hz, 1H), 7.27 – 7.24 (m, 1H), 7.17 (dd, J = 12, 4 Hz, 1H), 6.80 (d, J = 4 Hz, 1H), 5.60 (s, 2H).

Product 36b: ^{1}H NMR (400 MHz, DMSO-d_6) δ 8.47 – 8.46 (m, 0.14H), 7.93 (t, J = 4 Hz, 0.84H), 7.70 (t, J = 4 Hz, 0.38H), 7.26 (t, J = 4 Hz, 0.44H), 7.17 (t, J = 4 Hz, 0.61H), 6.79 (s, 0.47H).

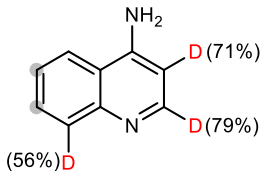

37b

Reaction conditions: 2.0 wt.% Pt_1/TiO_2-h (50 mg), substrate (14.4 mg, 0.1 mmol), D_2O (1.6 mL), acetone (0.4 mL), 410 nm LED (60 mW/cm^2), Ar (1 bar), 60 °C, 24 h. The product **37b** was obtained (Selectivity > 99%, detected by ^{1}H NMR).

Feed material 37a: ^{1}H NMR (400 MHz, DMSO-d_6) δ 8.31 (d, J = 4 Hz, 1H), 8.14 (d, J = 8 Hz, 1H), 7.75 (d, J = 8 Hz, 1H), 7.60 – 7.56 (m, 1H), 7.39 – 7.35 (m, 1H), 6.77 (s, 2H), 6.54 (d, J = 8 Hz, 1H).

Product 37b: ^{1}H NMR (400 MHz, DMSO-d_6) δ 8.31 (t, J = 4 Hz, 0.21H), 8.16 (t, J = 4 Hz, 1H), 7.77 (d, J = 12 Hz, 0.44H), 7.61 – 7.57 (m, 0.89H), 7.40 – 7.36 (m, 0.92H), 6.85 (s, 1.38H), 6.56 (t, J = 4 Hz, 0.29H).

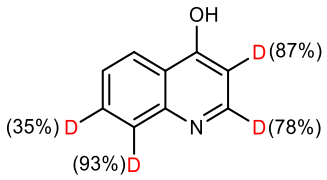

38b

Reaction conditions: 2.0 wt.% Pt_1/TiO_2-h (50 mg), substrate (14.5 mg, 0.1 mmol), D_2O (1.6 mL), acetone (0.4 mL), 410 nm LED (60 mW/cm^2), Ar (1 bar), 60 °C, 24 h. The product **38b** was obtained (Selectivity > 99%, detected by ^{1}H NMR).

Feed material 38a: ^{1}H NMR (400 MHz, DMSO-d_6) δ 11.79 (s, 1H), 8.10 (dd, J = 8, 4 Hz, 1H), 7.92 – 7.89 (m, 1H), 7.65 – 7.61 (m, 1H), 7.54 (d, J = 8 Hz, 1H), 7.32 – 7.28 (m, 1H), 6.04 (d, J = 8 Hz, 1H).

Product 38b: ^{1}H NMR (400 MHz, DMSO-d_6) δ 11.79 (s, 0.85H), 8.09 (d, J = 8 Hz, 1H), 7.90 (s, 0.22H), 7.64 (d, J = 4 Hz, 0.65H), 7.54 (t, J = 4 Hz, 0.07H), 7.33 – 7.29 (m, 1H), 6.04 (t, J = 4 Hz, 0.12H).

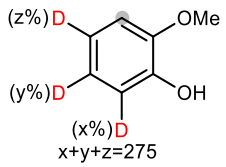

39b

Reaction conditions: 0.7 wt.% Pt_1/TiO_2-h (50 mg), substrate (12.4 mg, 0.1 mmol), D_2O (2.0 mL), 410 nm LED (60 mW/cm^2), Ar (1 bar), 60 °C, 12 h. The product **39b** was obtained (Selectivity > 99%, detected by ^{1}H NMR).

Feed material 39a: ^{1}H NMR (400 MHz, D_2O) δ 7.01 (d, J = 8 Hz, 1H), 6.94 – 6.86 (m, 1H), 3.82 (s, 3H).

Product 39b: ^{1}H NMR (400 MHz, D_2O) δ 7.07 (s, 0.91H), 6.98 – 6.94 (m, 0.23H), 3.87 (s, 3H).

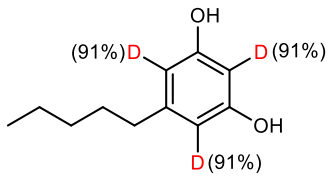

40b

Reaction conditions: 2.0 wt.% Pt_1/TiO_2-h (50 mg), substrate (18.0 mg, 0.1 mmol), D_2O (1.6 mL), acetone (0.4 mL), 410 nm LED (60 mW/cm^2), Ar (1 bar), 60 °C, 24 h. The product **40b** was obtained (Selectivity > 99%, detected by ^{1}H NMR).

Feed material 40a: ^{1}H NMR (400 MHz, DMSO-d_6) δ 8.99 (s, 2H), 6.02 (s, 3H), 2.36 (t, J = 8 Hz, 2H), 1.52 – 1.45 (m, 2H), 1.33 – 1.19 (m, 4H), 0.85 (t, J = 8 Hz, 3H).

Product 40b: ^{1}H NMR (400 MHz, DMSO-d_6) δ 9.00 (s, 1.34H), 6.01 (s, 0.28H), 2.36 (t, J = 8 Hz, 2H), 1.52 – 1.45 (m, 2H), 1.33 – 1.20 (m, 4H), 0.85 (t, J = 8 Hz, 3H).

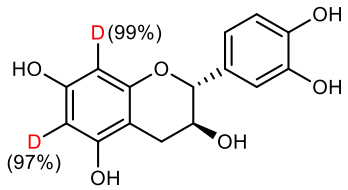

41b

Reaction conditions: 0.7 wt.% Pt_1/TiO_2-h (50 mg), substrate (29.0 mg, 0.1 mmol), D_2O (2.0 mL), 410 nm LED (60 mW/cm^2), Ar (1 bar), 60 °C, 12 h. The product **41b** was obtained (Selectivity > 99%, detected by ^{1}H NMR).

Feed material 41a: ^{1}H NMR (400 MHz, D_2O) δ 6.95 (d, *J* = 12 Hz, 2H), 6.87 (d, *J* = 8 Hz, 1H), 6.11 (s, 1H), 6.02 (s, 1H), 4.74 (d, *J* = 4 Hz, 1H), 4.19 (q, *J* = 16, 8 Hz, 1H), 2.88 (dd, *J* = 16, 8 Hz, 1H), 2.54 (dd, *J* = 16, 8 Hz, 1H).

Product 41b: ^{1}H NMR (400 MHz, D_2O) δ 6.93 (d, *J* = 12 Hz, 2H), 6.85 (d, *J* = 8 Hz, 1H), 6.09 (s, 0.01H), 6.00 (s, 0.02H), 4.68 (d, *J* = 8 Hz, 1H), 4.15 (q, *J* = 12, 8 Hz, 1H), 2.87 (dd, *J* = 16, 4 Hz, 1H), 2.51 (dd, *J* = 16, 8 Hz, 1H).

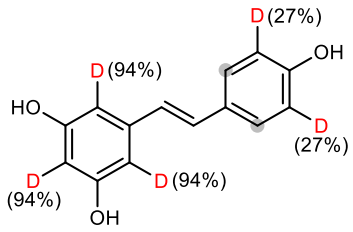

42b

Reaction conditions: 0.7 wt.% Pt_1/TiO_2-h (50 mg), substrate (22.8 mg, 0.1 mmol), D_2O (1.6 mL), acetone (0.4 mL), 410 nm LED (60 mW/cm^2), Ar (1 bar), 60 °C, 12 h. The product **42b** was obtained (Selectivity > 99%, detected by ^{1}H NMR).

Feed material 42a: ^{1}H NMR (400 MHz, DMSO-d_6) δ 9.53 (s, 1H), 9.20 (s, 2H), 7.39 (d, *J* = 8 Hz, 2H), 6.94 (d, *J* = 16 Hz, 1H), 6.82 (d, *J* = 16 Hz, 1H), 6.76 (d, *J* = 8 Hz, 2H), 6.40 (s, 2H), 6.13 (s, 1H).

Product 42b: ^{1}H NMR (400 MHz, DMSO-d_6) δ 9.54 (s, 0.59H), 9.18 (s, 1.22H), 7.39 (d, *J* = 8 Hz, 1.76H), 6.92 (d, *J* = 16 Hz, 1H), 6.81 (d, *J* = 16 Hz, 1H), 6.75 (d, *J* = 8 Hz, 1.42H), 6.38 (s, 0.11H), 6.11 (s, 0.06H).

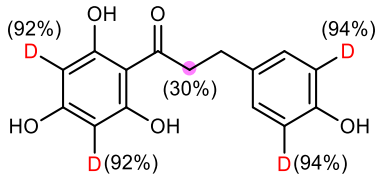

43b

Reaction conditions: 0.7 wt.% Pt_1/TiO_2-h (50 mg), substrate (27.4 mg, 0.1 mmol), D_2O (1.6 mL), acetone (0.4 mL), 410 nm LED (60 mW/cm^2), Ar (1 bar), 60 °C, 12 h. The product **43b** was obtained (Selectivity > 99%, detected by ^{1}H NMR).

Feed material 43a: ^{1}H NMR (400 MHz, DMSO-d_6) δ 12.25 (s, 2H), 10.36 (s, 1H), 9.15 (s, 1H), 7.01 (d, J = 8 Hz, 2H), 6.66 (d, J = 8 Hz, 2H), 5.80 (s, 2H), 3.21 (t, J = 8 Hz, 2H), 2.76 (t, J = 8 Hz, 2H).

Product 43b: ^{1}H NMR (400 MHz, DMSO-d_6) δ 12.25 (d, J = 8 Hz, 1.16H), 10.36 (s, 0.58H), 9.14 (s, 0.60H), 7.02 (s, 2H), 6.66 (d, J = 8 Hz, 0.13H), 5.82 (s, 0.16H), 3.24 – 3.16 (m, 1.46H), 2.77 (t, J = 8 Hz, 2H).

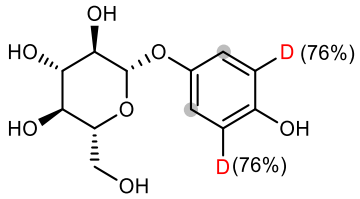

44b

Reaction conditions: 2.0 wt.% Pt_1/TiO_2-h (50 mg), substrate (27.2 mg, 0.1 mmol), D_2O (2.0 mL), 410 nm LED (60 mW/cm^2), Ar (1 bar), 60 °C, 24 h. The product **44b** was obtained (Selectivity > 99%, detected by ^{1}H NMR).

Feed material 44a: ^{1}H NMR (400 MHz, D_2O) δ 7.04 (d, J = 8 Hz, 2H), 6.86 (d, J = 8 Hz, 2H), 4.96 (d, J = 8 Hz, 1H), 3.91 (d, J = 16 Hz, 1H), 3.75 (dd, J = 12, 8 Hz, 1H), 3.61 – 3.46 (m, 4H).

Product 44b: ^{1}H NMR (400 MHz, D_2O) δ 7.05 (s, 1.79H), 6.87 (d, J = 8 Hz, 0.45H), 4.98 (d, J = 8 Hz, 1H), 3.92 (dd, J = 12, 4 Hz, 1H), 3.75 (dd, J = 12, 4 Hz, 1H), 3.61 – 3.46 (m, 4H).

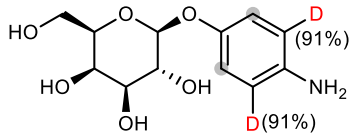

45b

Reaction conditions: 2.0 wt.% Pt_1/TiO_2-h (50 mg), substrate (27.1 mg, 0.1 mmol), D_2O (1.6 mL), acetone (0.4 mL), 410 nm LED (60 mW/cm^2), Ar (1 bar), 60 °C, 24 h. The product **45b** was obtained (Selectivity > 99%, detected by ^{1}H NMR).

Feed material 45a: ^{1}H NMR (400 MHz, DMSO-d_6) δ 6.75 (d, J = 8 Hz, 2H), 6.48 (d, J = 12 Hz, 2H), 5.05 (d, J = 4 Hz, 1H), 4.78 (d, J = 4 Hz, 1H), 4.67 (s, 2H), 4.60 (t, J = 4 Hz, 1H), 4.53 (d, J = 8 Hz, 1H), 4.43 (d, J = 4 Hz, 1H), 3.66 (t, J = 4 Hz, 1H), 3.57 – 3.42 (m, 4H), 3.37 – 3.32 (m, 1H).

Product 45b: ^{1}H NMR (400 MHz, DMSO-d_6) δ 6.75 (s, 1.71H), 6.49 (t, J = 8 Hz, 0.17H), 5.06 (d, J = 4 Hz, 0.43H), 4.79 (d, J = 4 Hz, 1H), 4.61 (s, 0.48H), 4.54 (d, J = 8 Hz, 1H), 4.44 (d, J = 4 Hz, 0.45H), 3.66 (d, J = 4 Hz, 1H), 3.56 – 3.43 (m, 4H), 3.36 – 3.33 (m, 1H).

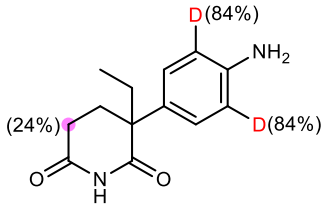

46b

Reaction conditions: 2.0 wt.% Pt_1/TiO_2-h (50 mg), substrate (23.2 mg, 0.1 mmol), D_2O (1.6 mL), acetone (0.4 mL), 410 nm LED (60 mW/cm^2), Ar (1 bar), 60 °C, 24 h. The product **46b** was obtained (Selectivity > 99%, detected by ^{1}H NMR).

Feed material 46a: ^{1}H NMR (400 MHz, DMSO-d_6) δ 10.71 (s, 1H), 6.91 (d, J = 8 Hz, 2H), 6.54 (d, J = 8 Hz, 2H), 5.05 (s, 2H), 2.41 (d, J = 16 Hz, 1H), 2.26 – 2.02 (m, 3H), 1.83 – 1.67 (m, 2H), 0.73 (t, J = 8 Hz, 3H).

Product 46b: ^{1}H NMR (400 MHz, DMSO-d_6) δ 8.22 (s, 0.15H), 4.44 (t, J = 4 Hz, 2H), 3.97 (t, J = 4 Hz, 2H), 3.51 (d, J = 8 Hz, 2H).

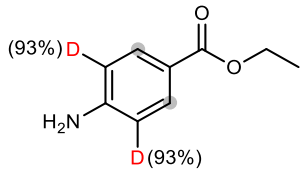

47b

Reaction conditions: 2.0 wt.% Pt_1/TiO_2-h (50 mg), substrate (16.5 mg, 0.1 mmol), D_2O (1.6 mL), acetone (0.4 mL), 410 nm LED (60 mW/cm^2), Ar (1 bar), 60 °C, 24 h. The product **47b** was obtained (Selectivity > 99%, detected by ^{1}H NMR).

Feed material 47a: ^{1}H NMR (400 MHz, $CDCl_3$) δ 7.85 (d, *J* = 8 Hz, 2H), 6.63 (d, *J* = 8 Hz, 2H), 4.31 (q, *J* = 16, 8 Hz, 2H), 4.07 (s, 2H), 1.35 (t, *J* = 8 Hz, 3H).

Product 47b: ^{1}H NMR (400 MHz, $CDCl_3$) δ 7.85 (s, 1.83H), 6.63 (d, *J* = 8 Hz, 0.13H), 4.31 (q, *J* = 16, 8 Hz, 2H), 4.04 (s, 1.06H), 1.36 (t, *J* = 8 Hz, 3H).

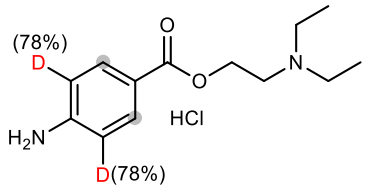

48b

Reaction conditions: 2.0 wt.% Pt_1/TiO_2-h (50 mg), substrate (27.2 mg, 0.1 mmol), D_2O (2.0 mL), 410 nm LED (60 mW/cm^2), Ar (1 bar), 60 °C, 24 h. The product **48b** was obtained (Selectivity > 99%, detected by ^{1}H NMR).

Feed material 48a: ^{1}H NMR (400 MHz, D_2O) δ 7.79 (d, *J* = 8 Hz, 2H), 6.81 (d, *J* = 12 Hz, 2H), 4.55 (t, *J* = 4 Hz, 2H), 3.57 (t, *J* = 4 Hz, 2H), 3.33 (q, *J* = 16, 8 Hz, 4H), 1.34 (t, *J* = 8 Hz, 6H).

Product 48b: ^{1}H NMR (400 MHz, D_2O) δ 7.84 (s, 1.89H), 6.82 (d, *J* = 8 Hz, 0.43H), 4.61 (t, *J* = 4 Hz, 2H), 3.62 (t, *J* = 4 Hz, 2H), 3.35 (q, *J* = 12, 8 Hz, 4H), 1.34 (t, *J* = 8 Hz, 6H).

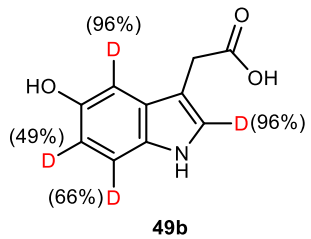

49b

Reaction conditions: 2.0 wt.% Pt_1/TiO_2-h (50 mg), substrate (19.1 mg, 0.1 mmol), D_2O (1.6 mL), acetone (0.4 mL), 410 nm LED (60 mW/cm^2), Ar (1 bar), 60 °C, 24 h. The product **49b** was obtained (Selectivity > 99%, detected by ^{1}H NMR).

Feed material 49a: ^{1}H NMR (400 MHz, DMSO-d_6) δ 12.03 (s, 1H), 10.57 (s, 1H), 8.65 (s, 1H), 7.14 (d, J = 8 Hz, 1H), 7.11 (s, 1H), 6.81 (s, 1H), 6.60 (dd, J = 12, 4 Hz, 1H), 3.54 (s, 2H).

Product 49b: ^{1}H NMR (400 MHz, DMSO-d_6) δ 12.04 (s, 0.31H), 10.57 (s, 0.47H), 8.61 (s, 0.49H), 7.13 (t, J = 4 Hz, 0.34H), 7.11 (s, 0.04H), 6.81 (s, 0.04H), 6.59 (t, J = 8 Hz, 0.52H), 3.53 (s, 2H).

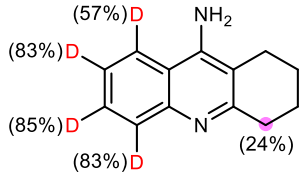

50b

Reaction conditions: 2.0 wt.% Pt_1/TiO_2-h (50 mg), substrate (19.8 mg, 0.1 mmol), D_2O (1.6 mL), acetone (0.4 mL), 410 nm LED (60 mW/cm^2), Ar (1 bar), 60 °C, 24 h. The product **50b** was obtained (Selectivity > 99%, detected by ^{1}H NMR).

Feed material 50a: ^{1}H NMR (400 MHz, DMSO-d_6) δ 8.14 (d, J = 8 Hz, 1H), 7.63 (d, J = 8 Hz, 1H), 7.47 (t, J = 8 Hz, 1H), 7.27 (t, J = 8 Hz, 1H), 6.32 (s, 2H), 2.82 (t, J = 8 Hz, 2H), 2.56 (t, J = 8 Hz, 2H), 1.83 – 1.79 (m, 4H).

Product 50b: ^{1}H NMR (400 MHz, DMSO-d_6) δ 8.14 (t, J = 8 Hz, 0.43H), 7.63 (t, J = 4 Hz, 0.16H), 7.48 (t, J = 4 Hz, 0.15H), 7.27 (t, J = 8 Hz, 0.17H), 6.37 (s, 0.91H), 2.84 – 2.78 (m, 1.52H), 2.55 (t, J = 8 Hz, 2H), 1.83 – 1.77 (m, 4H).

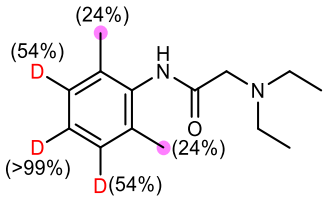

51b

In order to facilitate the determination of the D incorporation rate, we synthesized non-D labeled compound **51a** as reference. The product **51b** was obtained in 89% isolated yield.

Reference material 51a: ^{1}H NMR (400 MHz, DMSO-d_6) δ 9.16 (s, 1H), 7.07 (s, 3H), 3.14 (s, 2H), 2.62 (q, J = 16, 8 Hz, 4H), 2.14 (s, 6H), 1.08 (t, J = 8 Hz, 6H).

Product 51b: ^{1}H NMR (400 MHz, DMSO-d_6) δ 9.17 (s, 1H), 7.08 (s, 0.98H), 3.15 (s, 2H), 2.64 (q, J = 16, 8 Hz, 4H), 2.17 (s, 4.57H), 1.10 (t, J = 8 Hz, 6H).

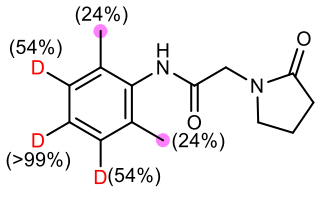

52b

In order to facilitate the determination of the D incorporation rate, we synthesized non-D labeled compound **52a** as reference. The product **52b** was obtained in 86% isolated yield.

Reference material 52a: ^{1}H NMR (400 MHz, DMSO-d_6) δ 9.31 (s, 1H), 7.07 (s, 3H), 4.03 (s, 2H), 3.46 (t, J = 8 Hz, 2H), 2.27 (t, J = 8 Hz, 2H), 2.13 (s, 6H), 2.02 – 1.94 (m, 2H).

Product 52b: ^{1}H NMR (400 MHz, DMSO-d_6) δ 9.32 (s, 1H), 7.08 (s, 0.98H), 4.05 (s, 2H), 3.47 (t, J = 8 Hz, 2H), 2.28 (t, J = 8 Hz, 2H), 2.15 (s, 4.57H), 2.02 – 1.94 (m, 2H).

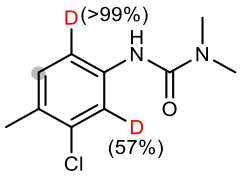

53b

In order to facilitate the determination of the D incorporation rate, we synthesized non-D labeled compound **53a** as reference. The product **53b** was obtained in 75% isolated yield.

Reference material 53a: ^{1}H NMR (400 MHz, DMSO-d_6) δ 8.35 (s, 1H), 7.66 (d, J = 4 Hz, 1H), 7.34 (dd, J = 8, 4 Hz, 1H), 7.15 (d, J = 8 Hz, 1H), 2.91 (s, 6H), 2.23 (s, 3H).

Product 53b: ^{1}H NMR (400 MHz, DMSO-d_6) δ 8.35 (s, 1H), 7.64 (s, 0.40H), 7.16 (s, 0.86H), 2.91 (s, 6H), 2.23 (s, 3H).

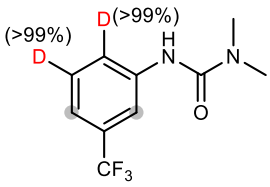

54b

In order to facilitate the determination of the D incorporation rate, we synthesized non-D labeled compounds **54a** as reference. The product **54b** was obtained in 62% isolated yield.

Reference material 54a: ^{1}H NMR (400 MHz, DMSO-d_6) δ 8.61 (s, 1H), 7.94 (s, 1H), 7.56 (d, J = 8 Hz, 1H), 7.44 (t, J = 8 Hz, 1H), 7.24 (d, J = 8 Hz, 1H), 2.94 (s, 6H).

Product 54b: ^{1}H NMR (400 MHz, DMSO-d_6) δ 8.61 (s, 1H), 7.93 (s, 0.88H), 7.24 (s, 0.87H), 2.94 (s, 6H).

8. NMR spectra for substrates and products

^{1}H NMR (400 MHz, D_2O) of feed material **1a**

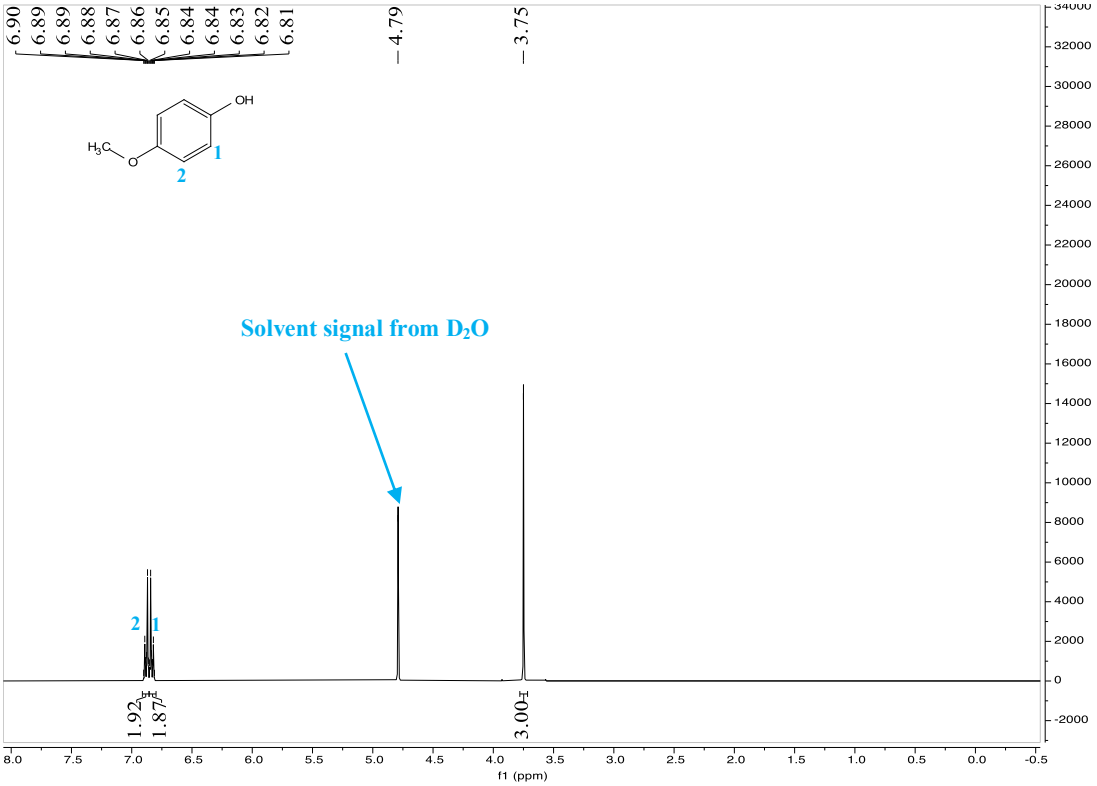

^{1}H NMR (400 MHz, D_2O) of product **1b**

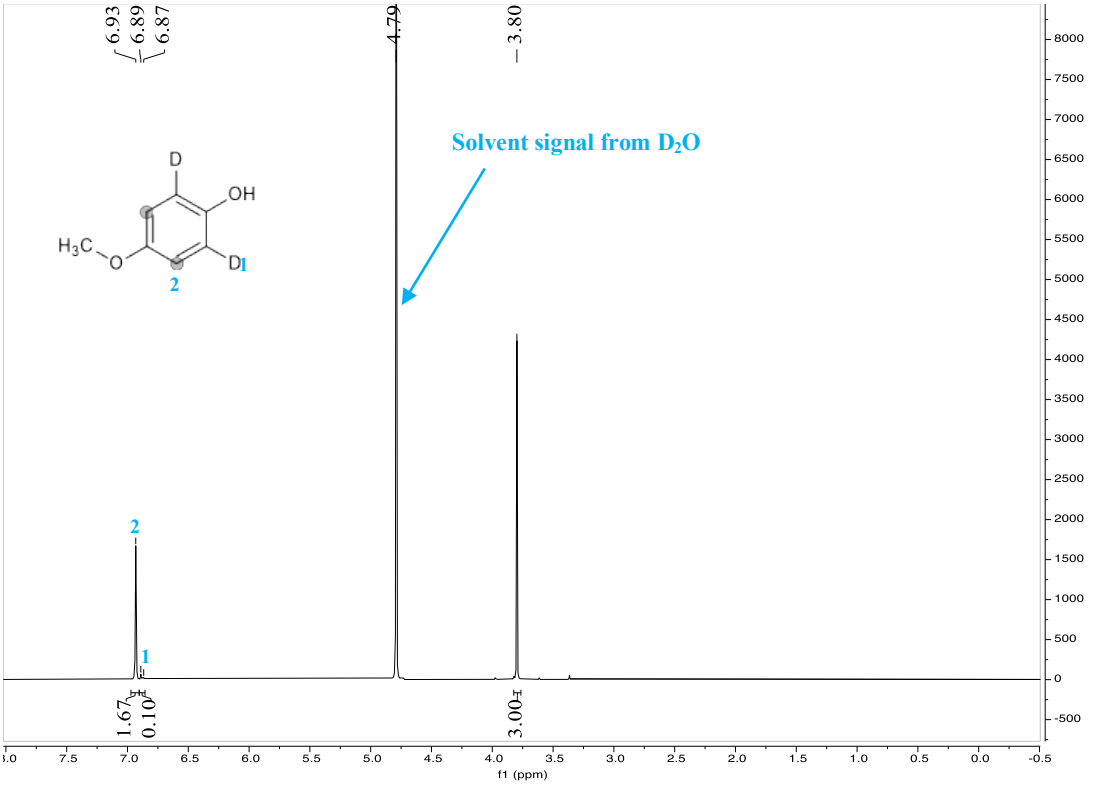

^{1}H NMR (400 MHz, D_2O) of feed material **2a**

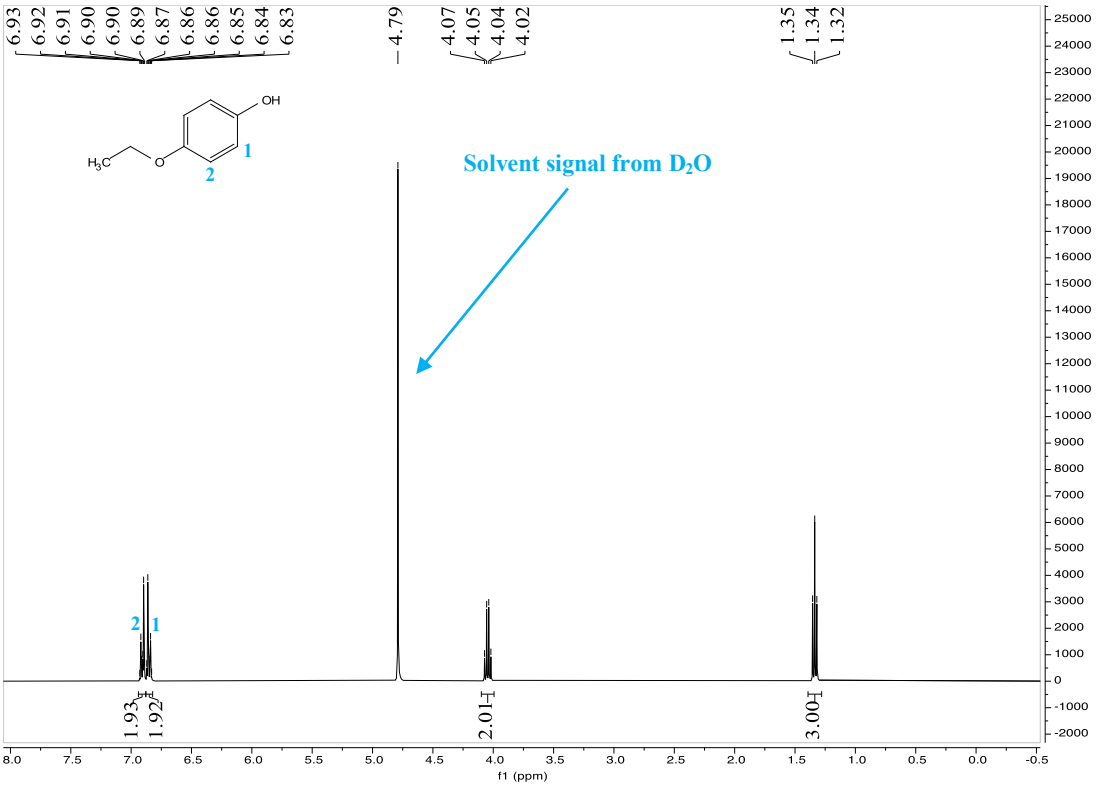

^{1}H NMR (400 MHz, D_2O) of product **2b**

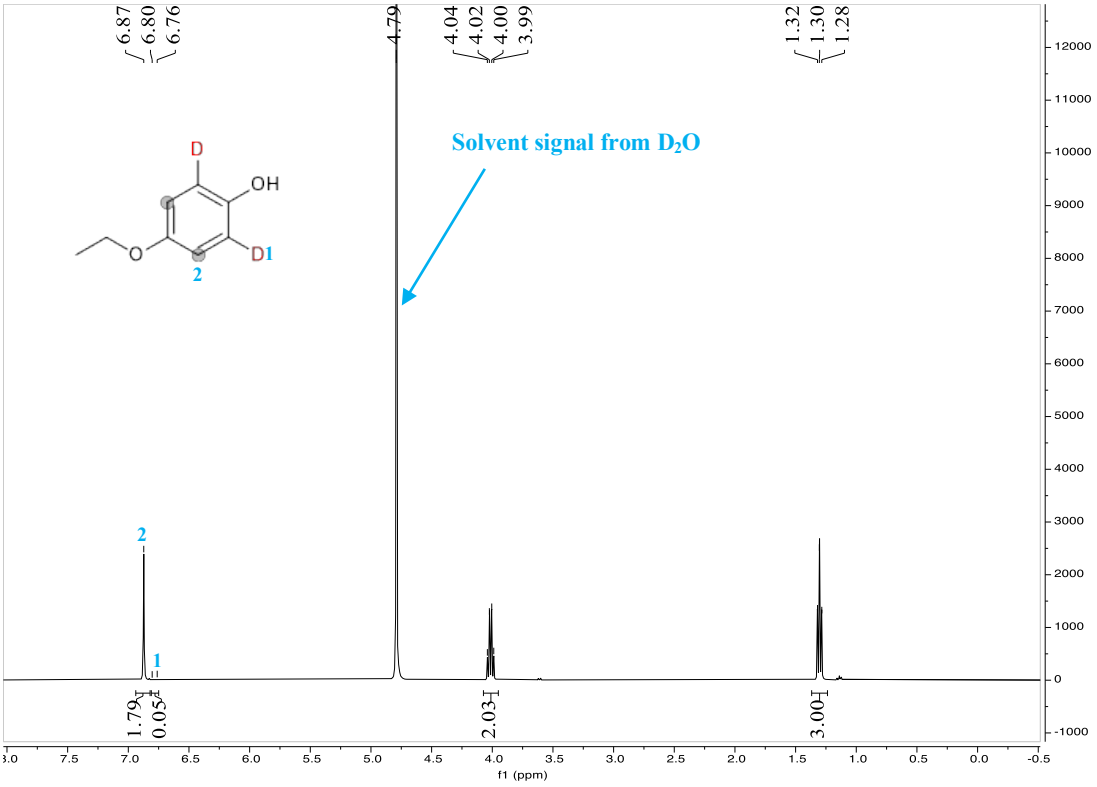

^{1}H NMR (400 MHz, D_2O) of feed material **3a**

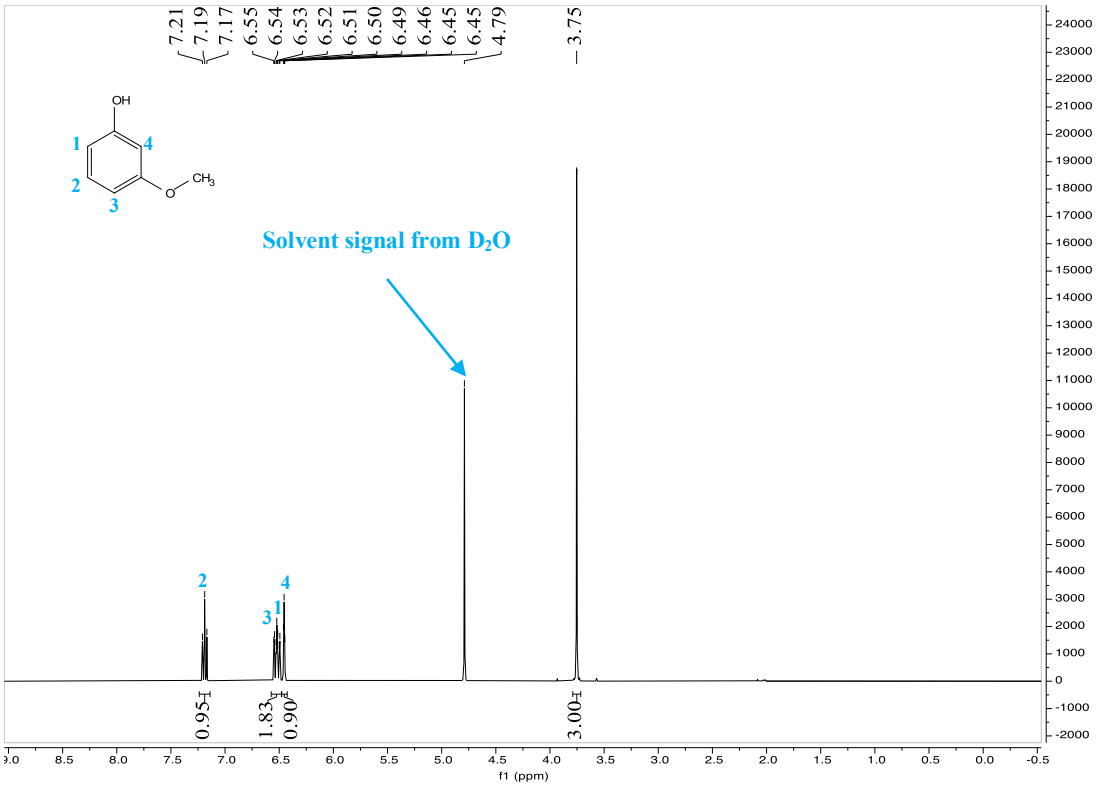

^{1}H NMR (400 MHz, D_2O) of product **3b**

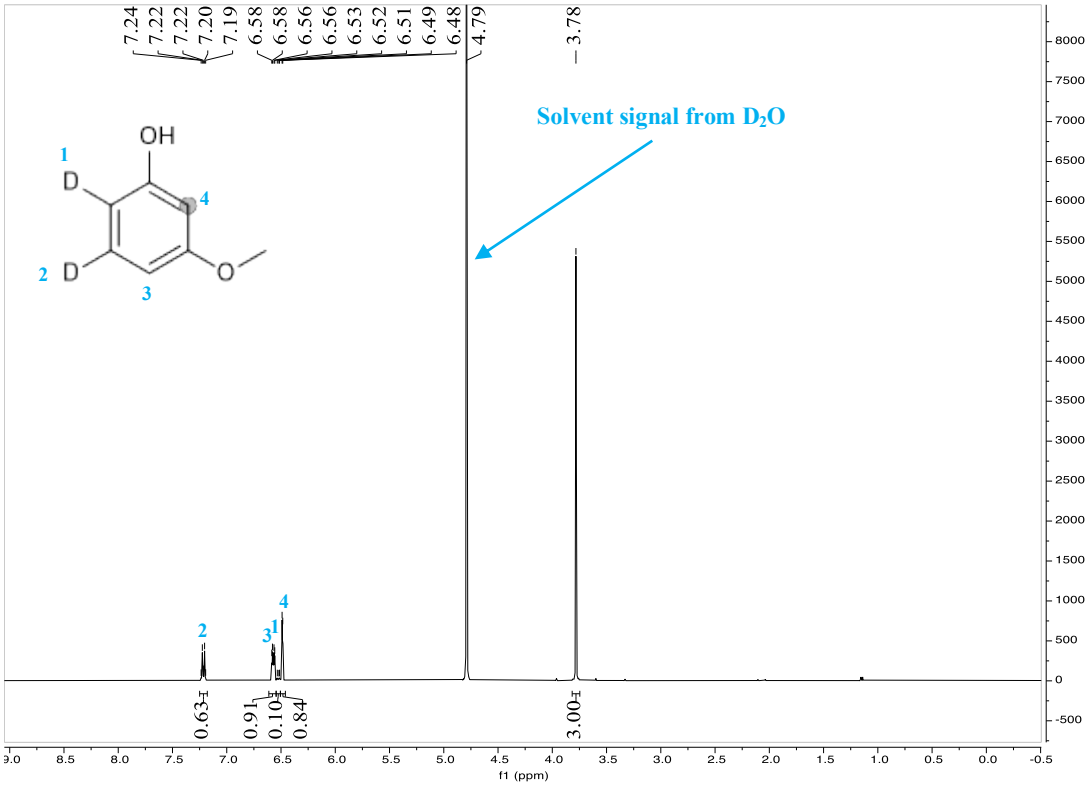

^{1}H NMR (400 MHz, D_2O) of feed material **4a**

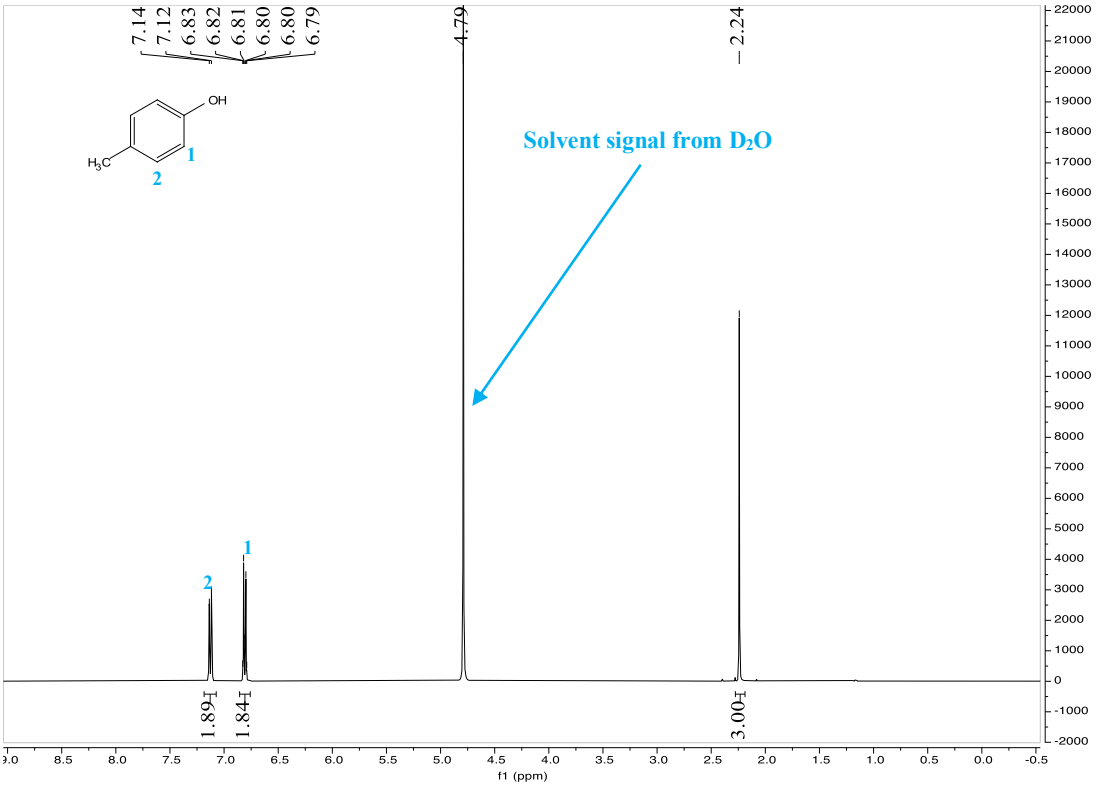

^{1}H NMR (400 MHz, D_2O) of product **4b**

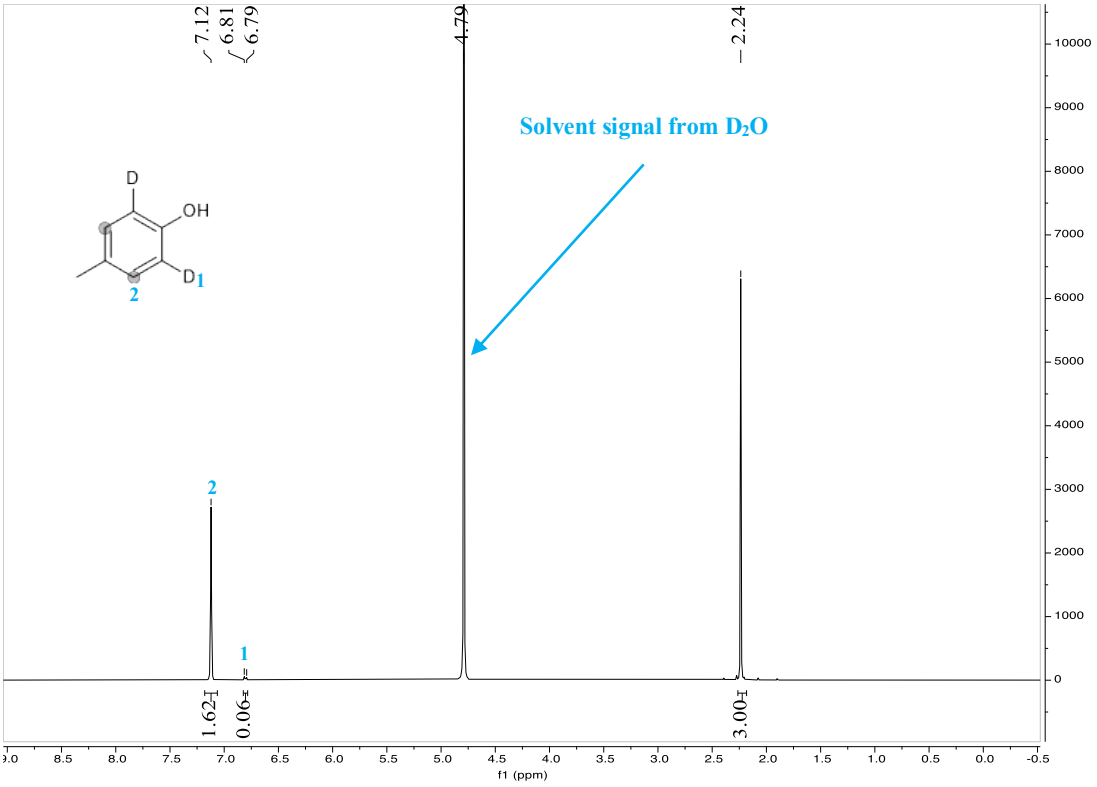

^{1}H NMR (400 MHz, D_2O) of feed material **5a**

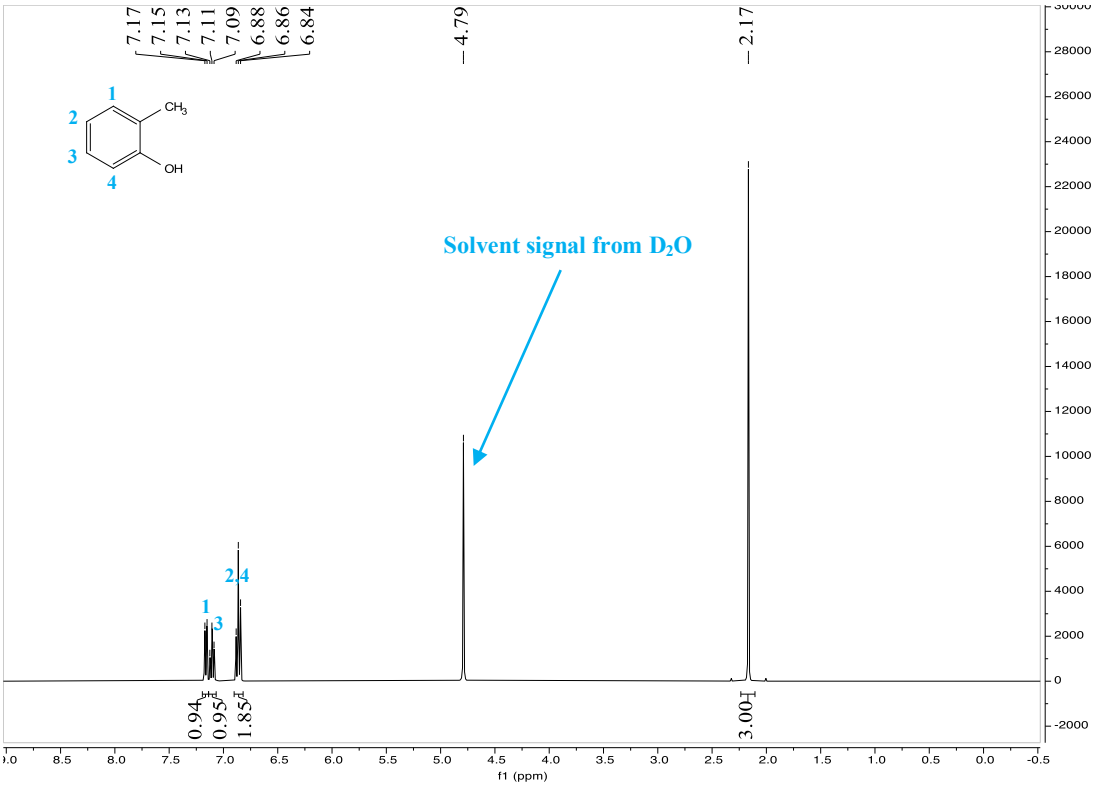

^{1}H NMR (400 MHz, D_2O) of product **5b**

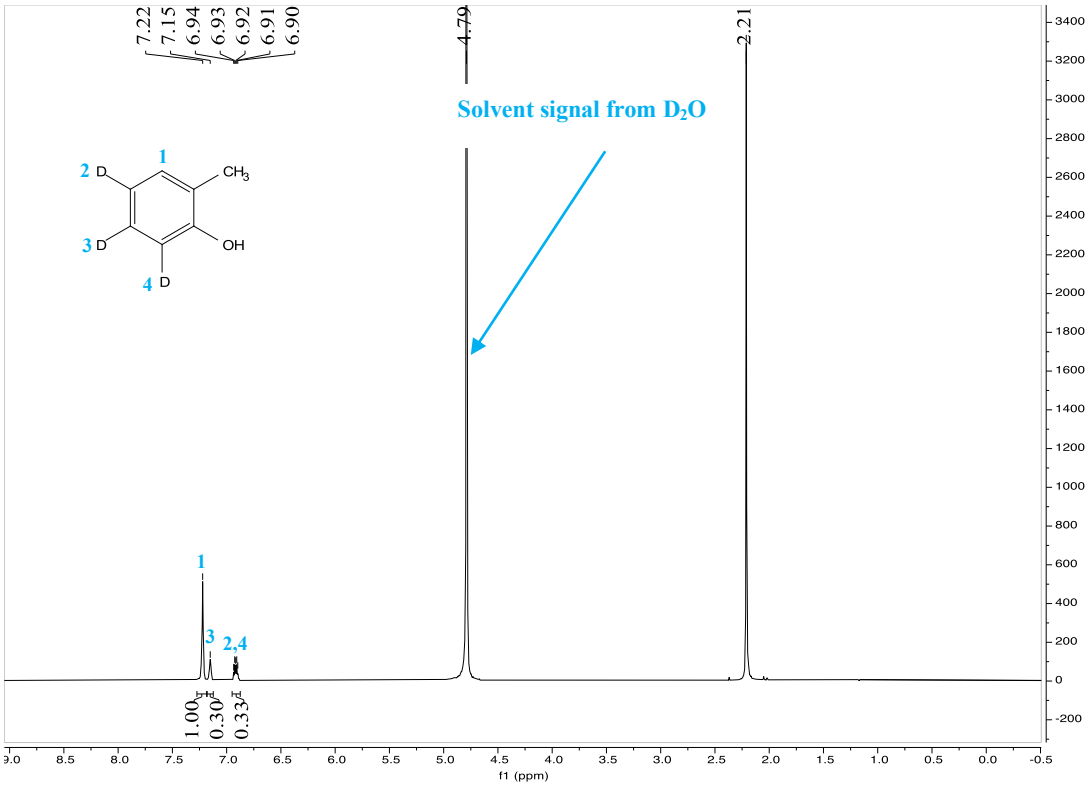

^{1}H NMR (400 MHz, D_2O) of feed material **6a**

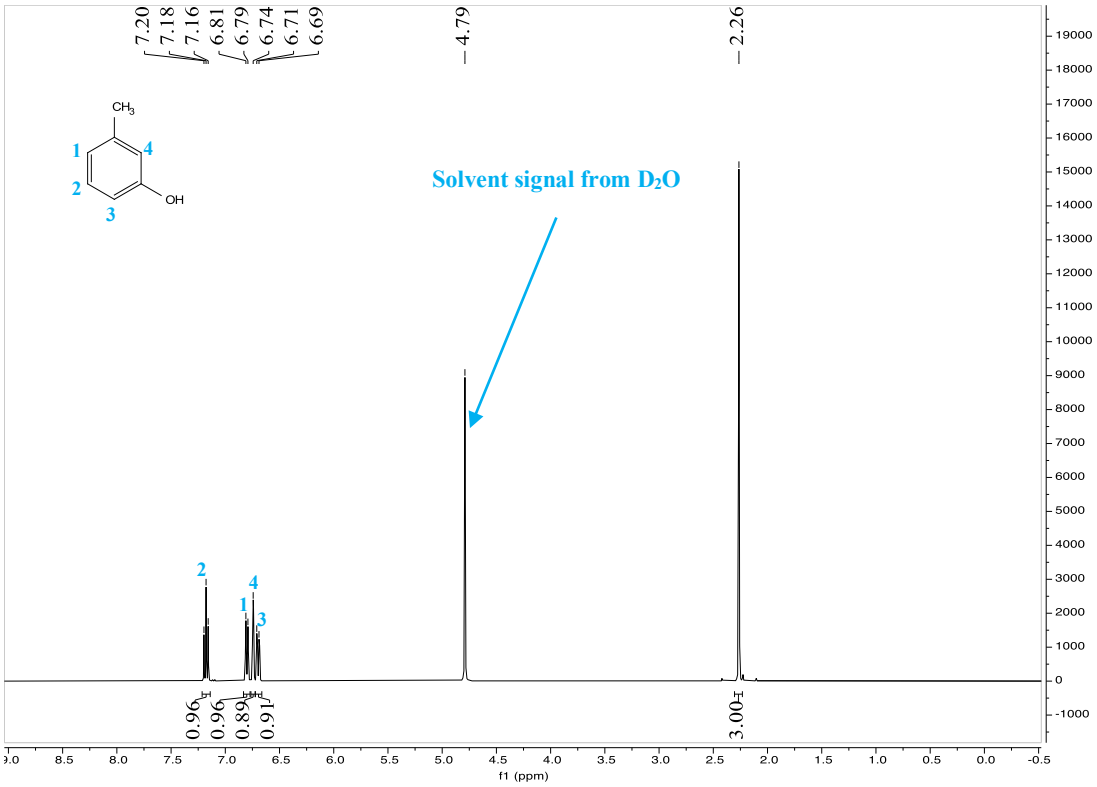

^{1}H NMR (400 MHz, D_2O) of product **6b**

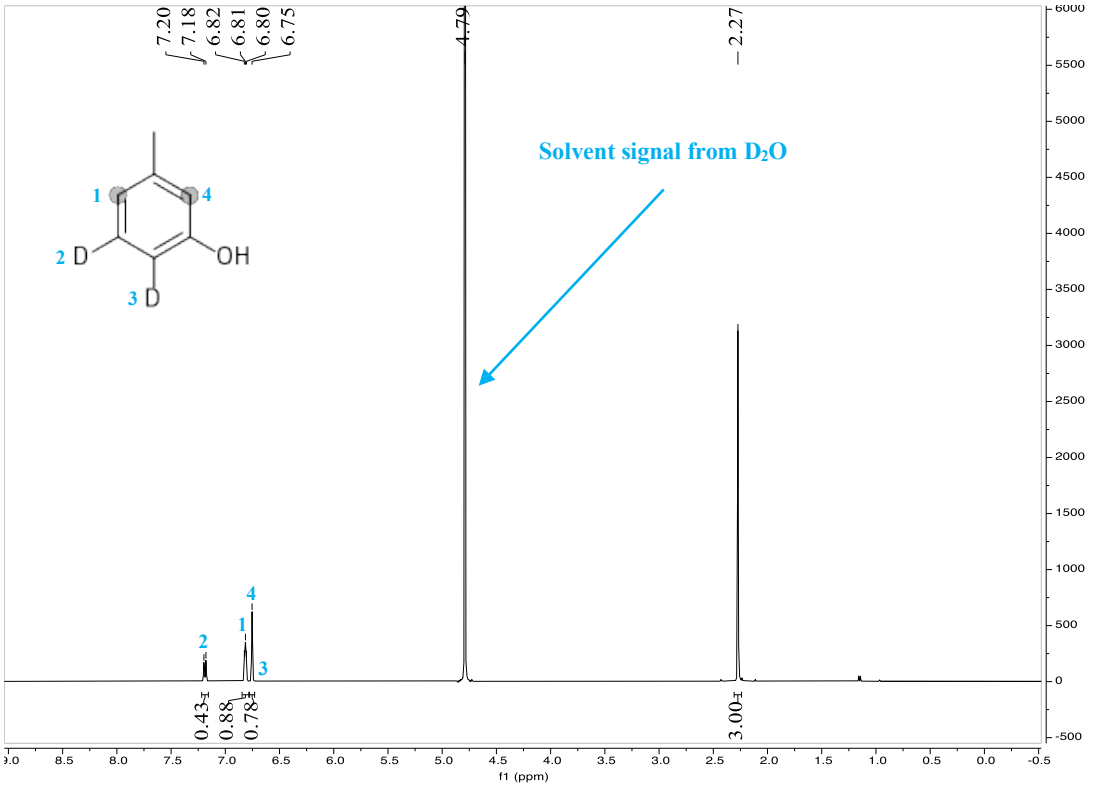

^{1}H NMR (400 MHz, DMSO-d_6) of feed material **7a**

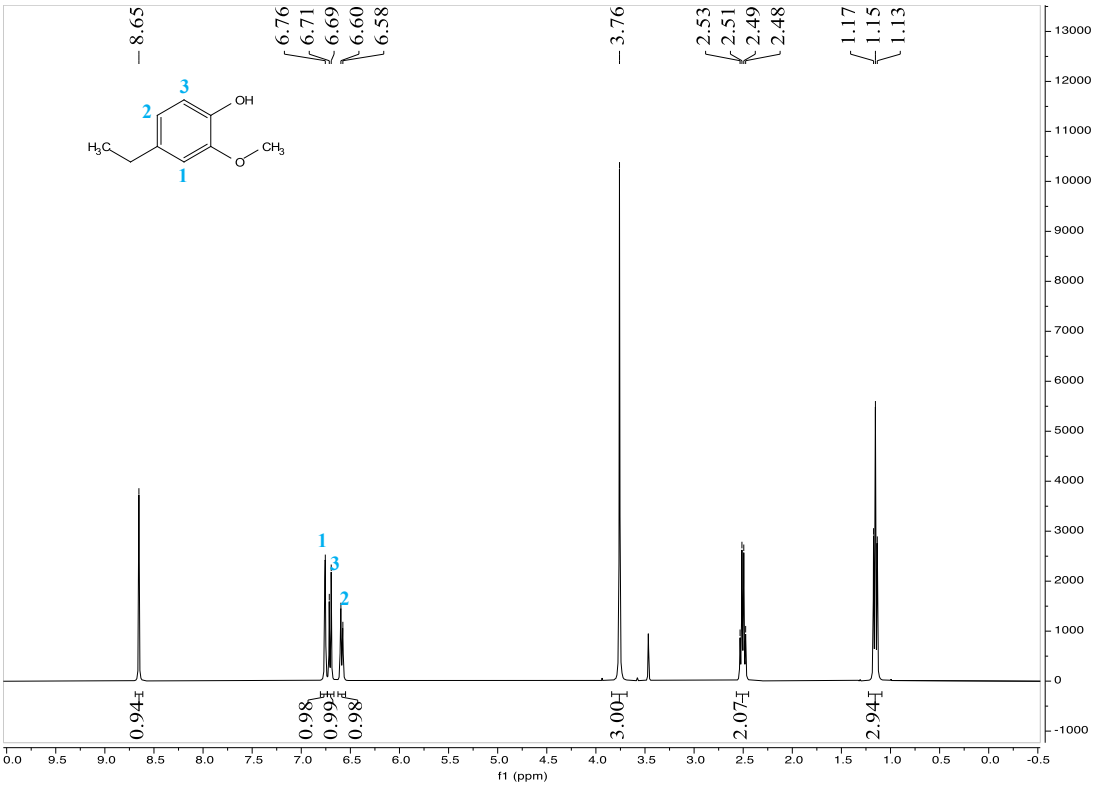

^{1}H NMR (400 MHz, D_2O) of product **7b**

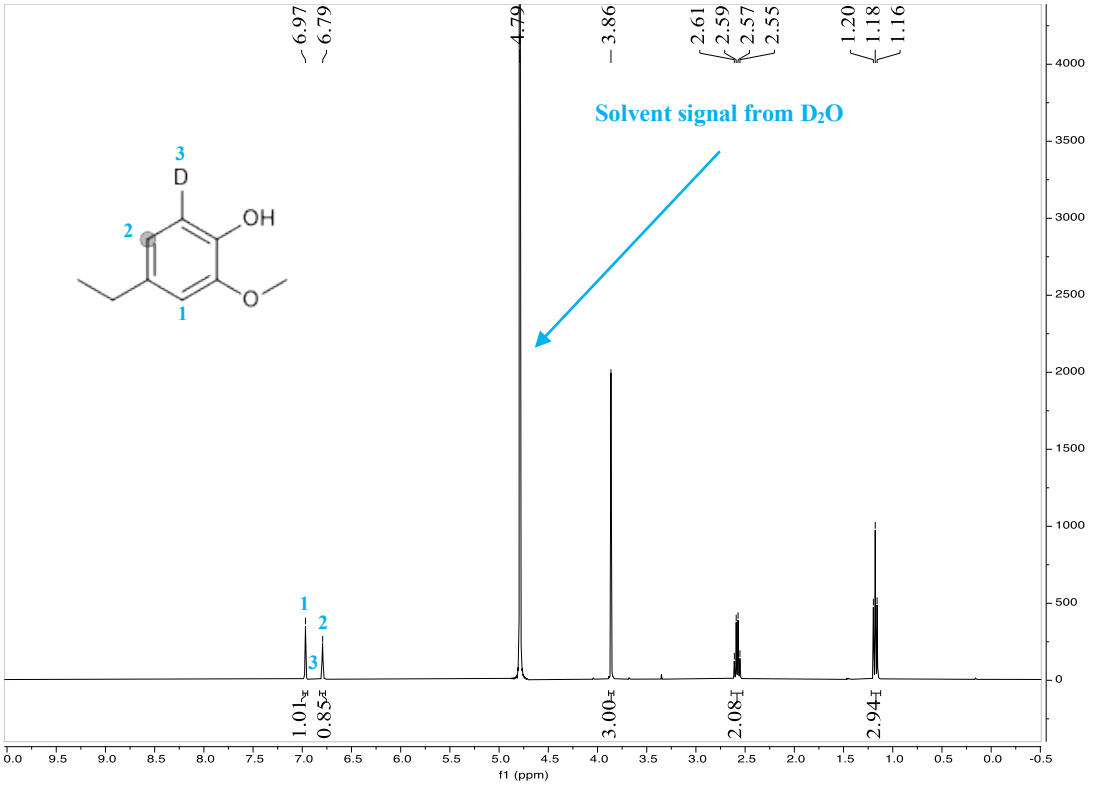

^{1}H NMR (400 MHz, D_2O) of feed material **8a**

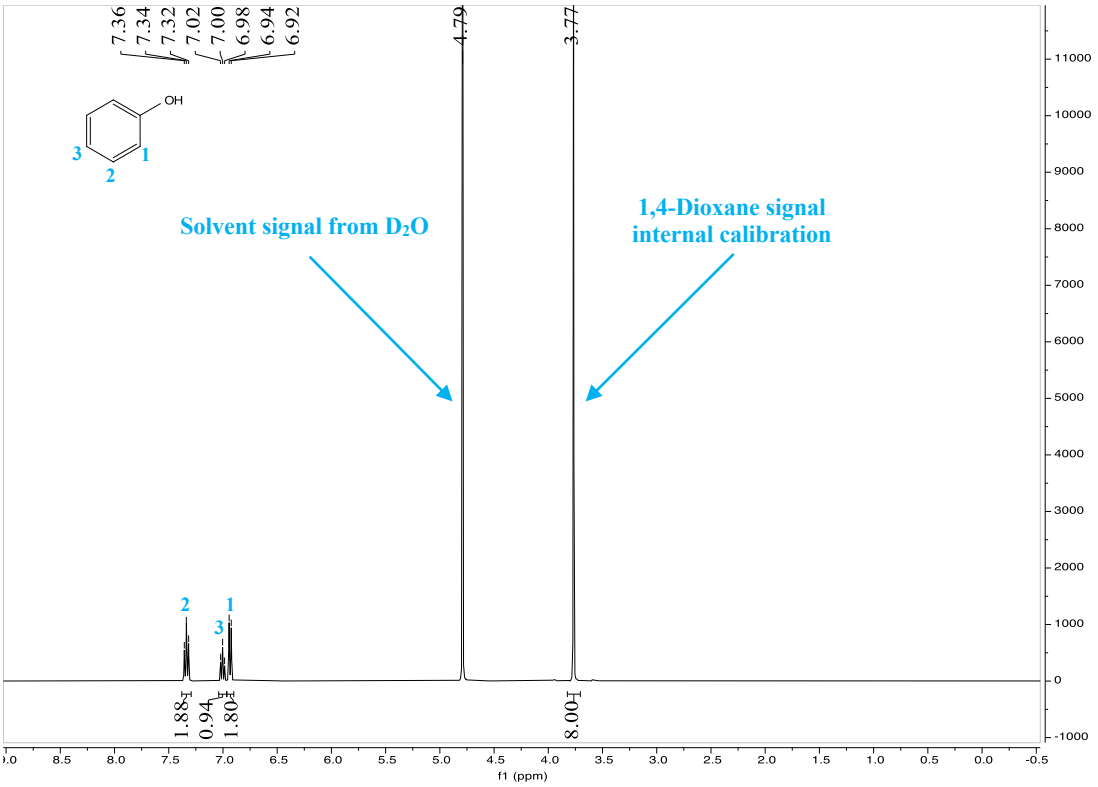

^{1}H NMR (400 MHz, D_2O) of product **8b**

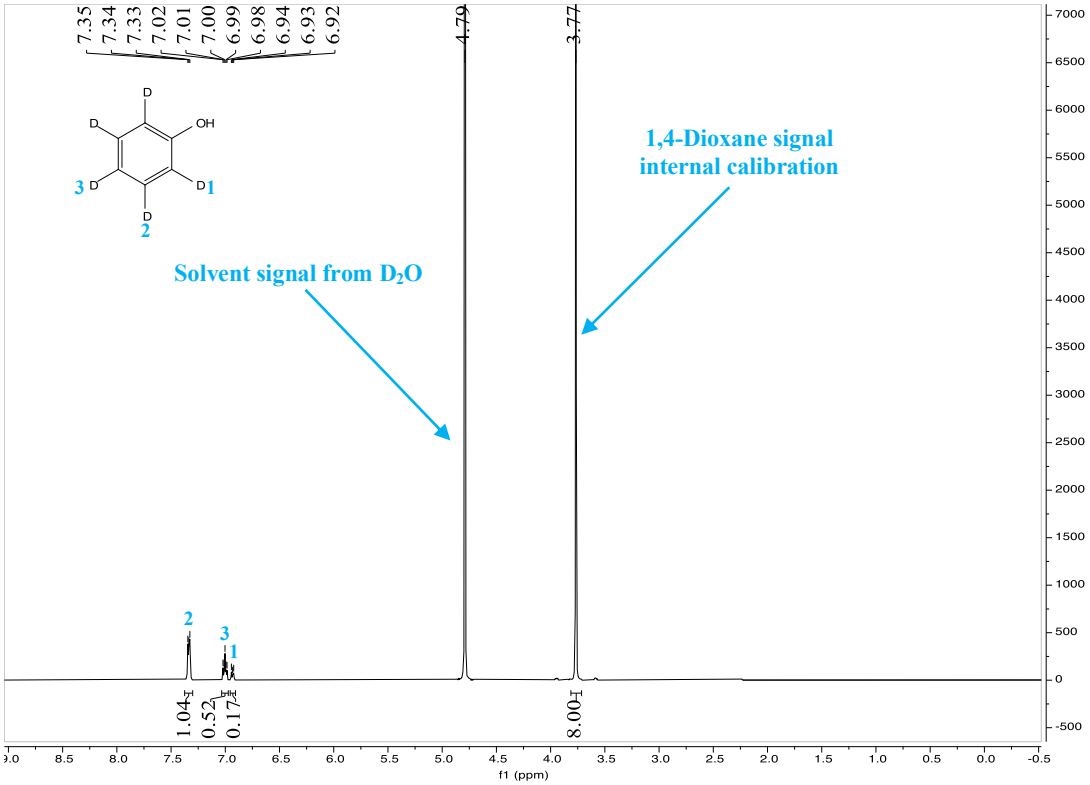

^{1}H NMR (400 MHz, D_2O) of feed material **9a**

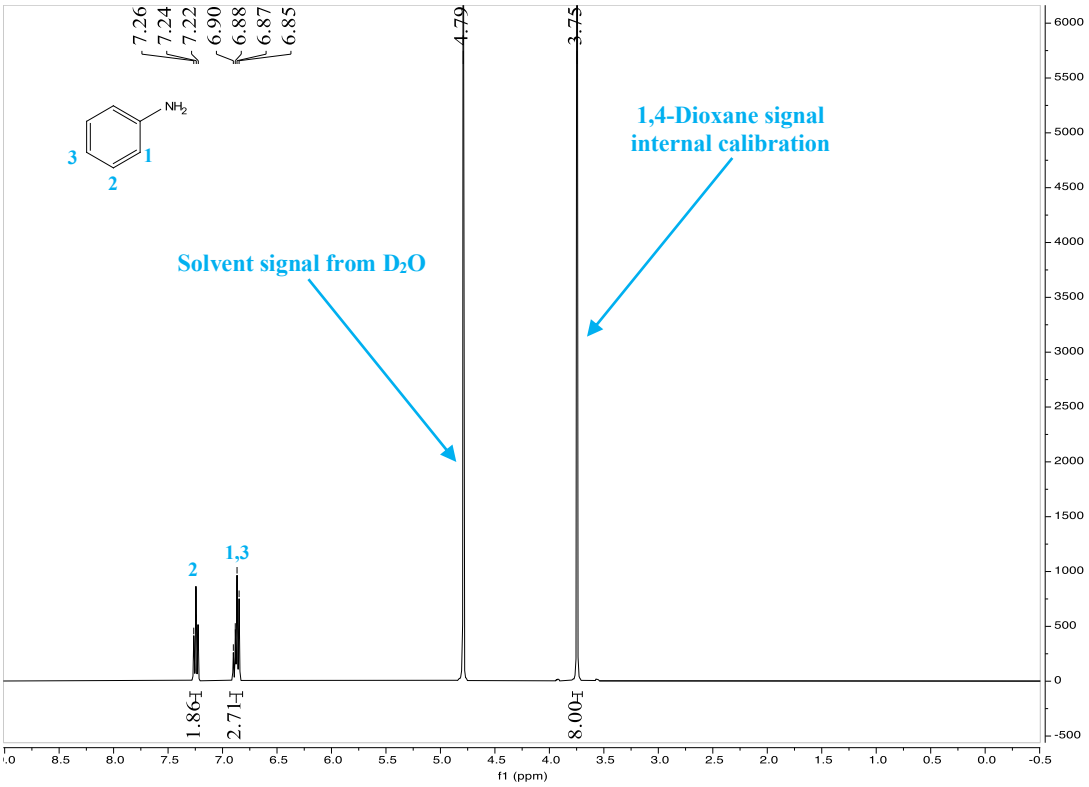

^{1}H NMR (400 MHz, D_2O) of product **9b**

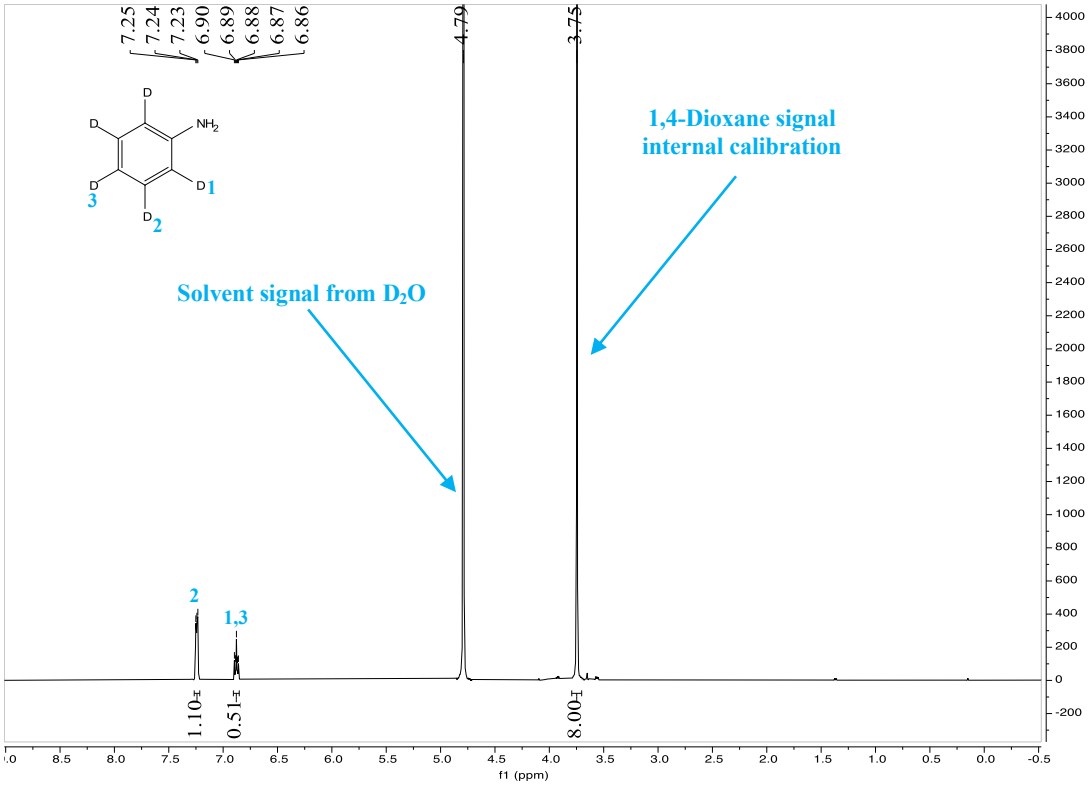

^{1}H NMR (400 MHz, D_2O) of feed material **10a**

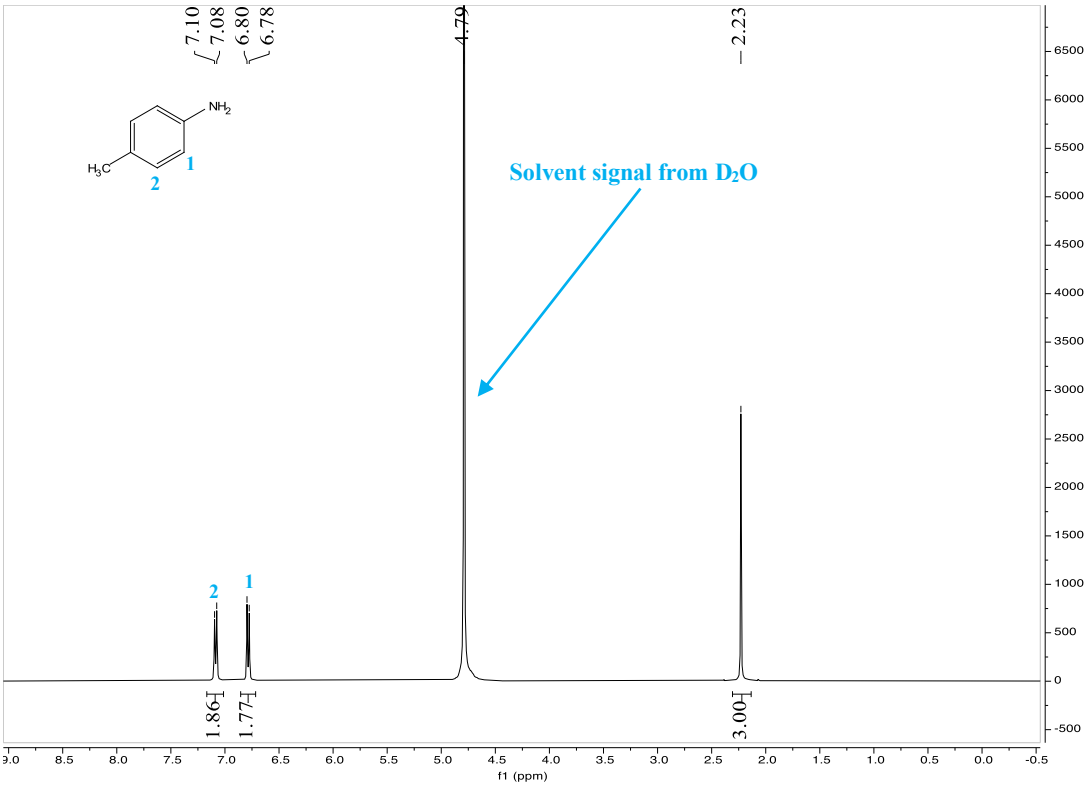

^{1}H NMR (400 MHz, D_2O) of product **10b**

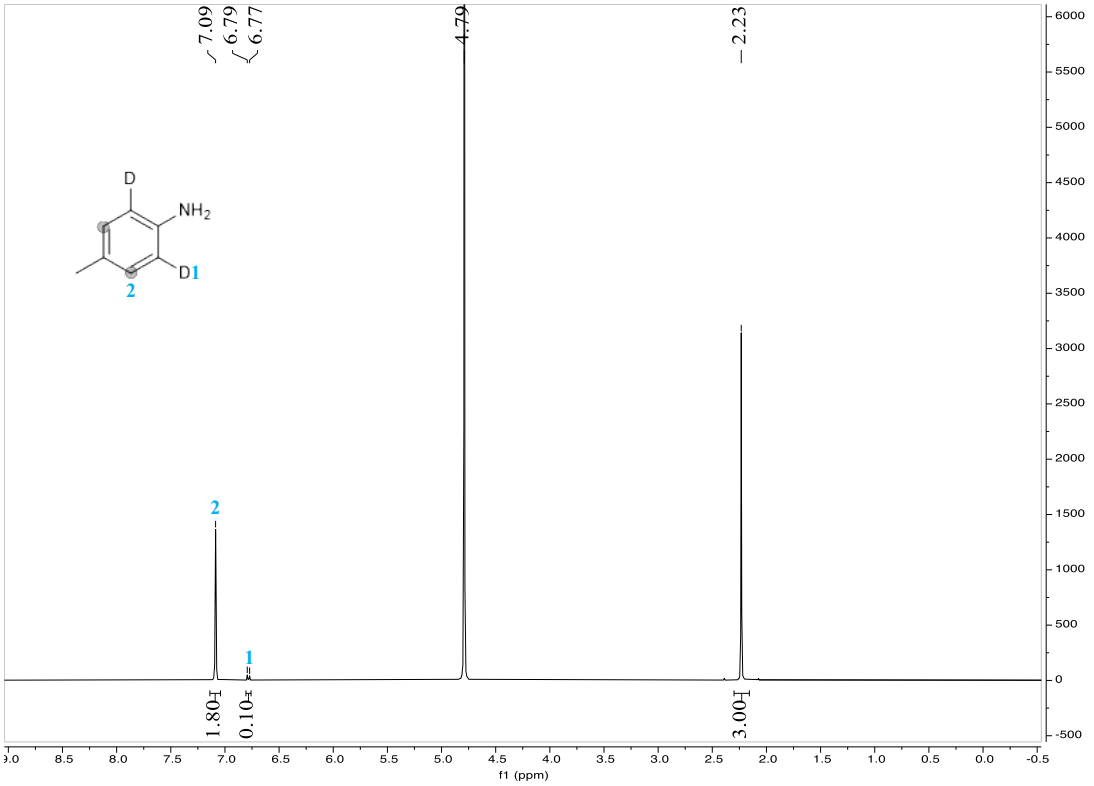

^{1}H NMR (400 MHz, D_2O) of feed material **11a**

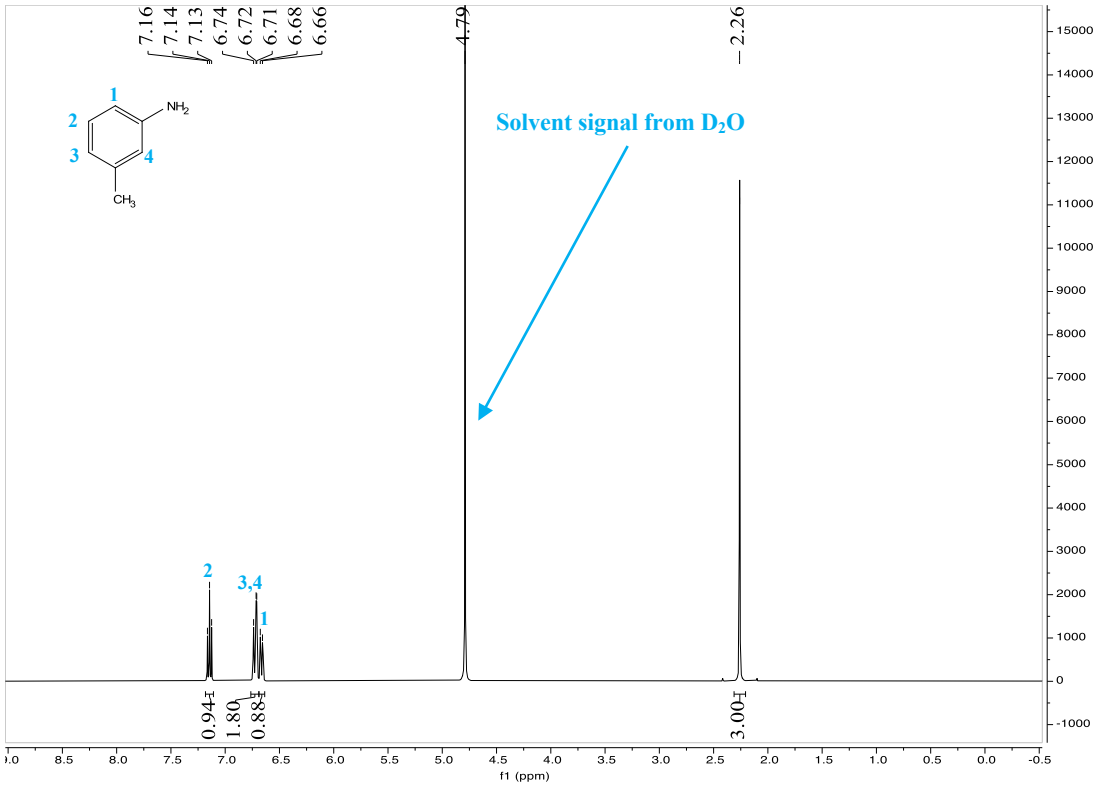

^{1}H NMR (400 MHz, D_2O) of product **11b**

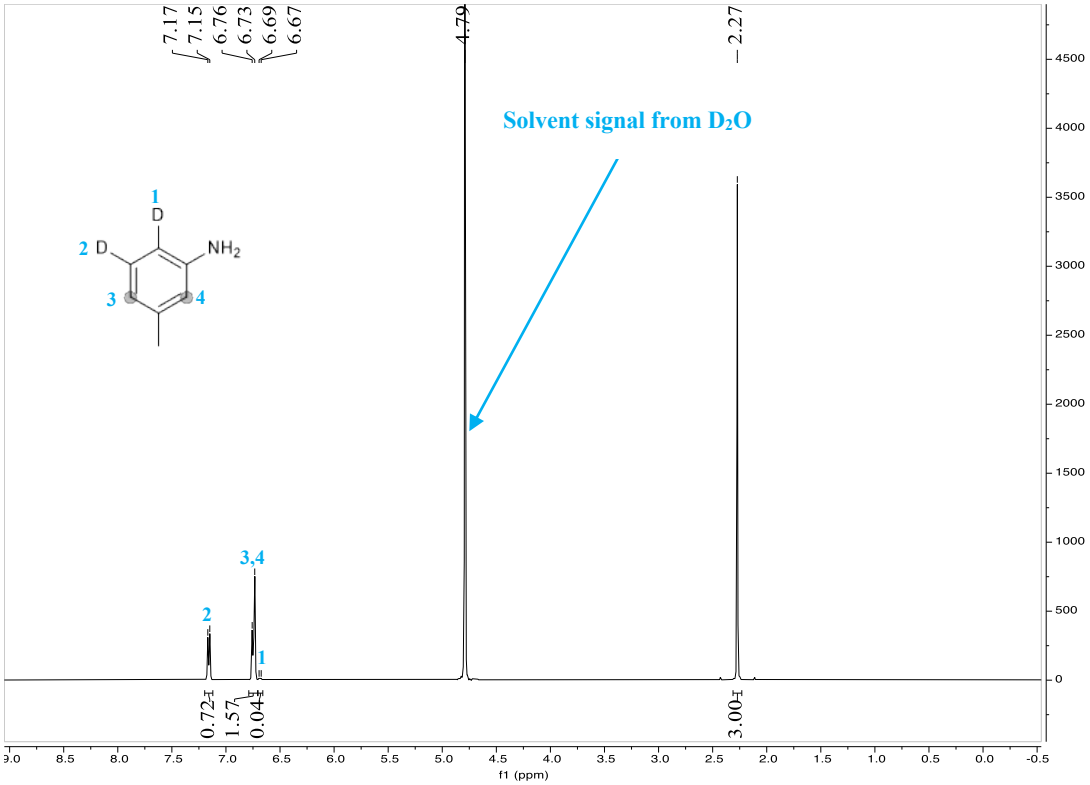

^{1}H NMR (400 MHz, D_2O) of feed material **12a**

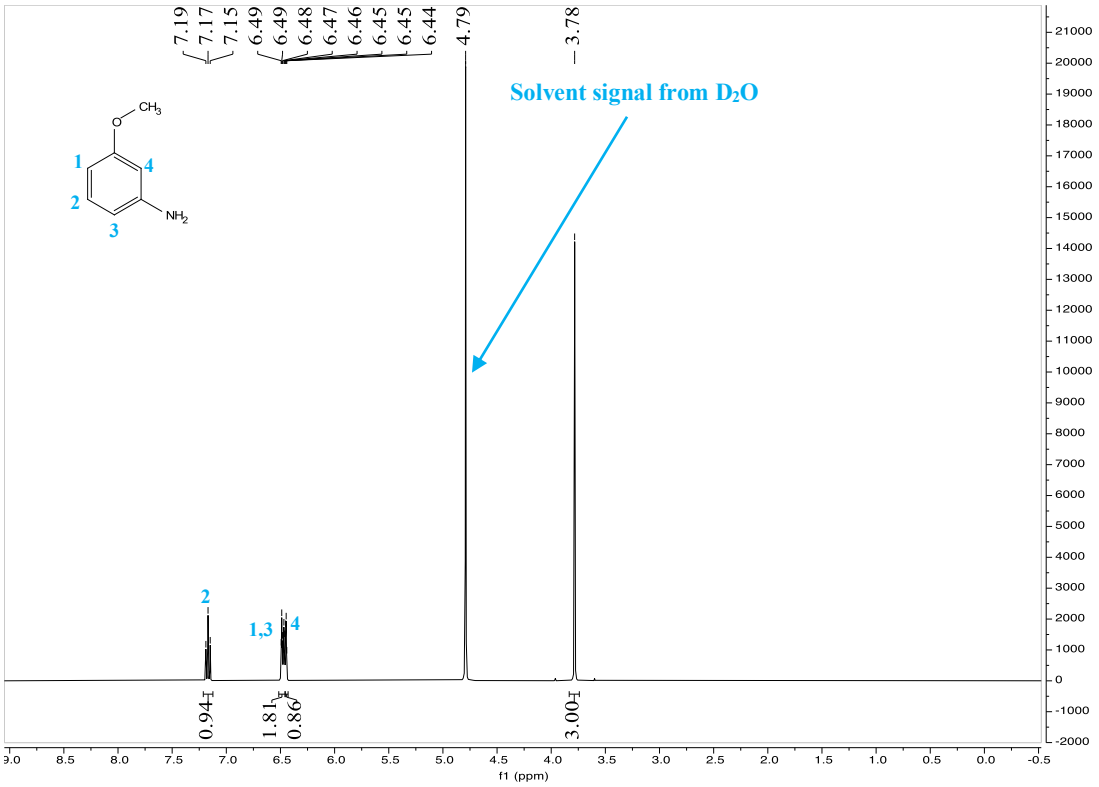

^{1}H NMR (400 MHz, D_2O) of product **12b**

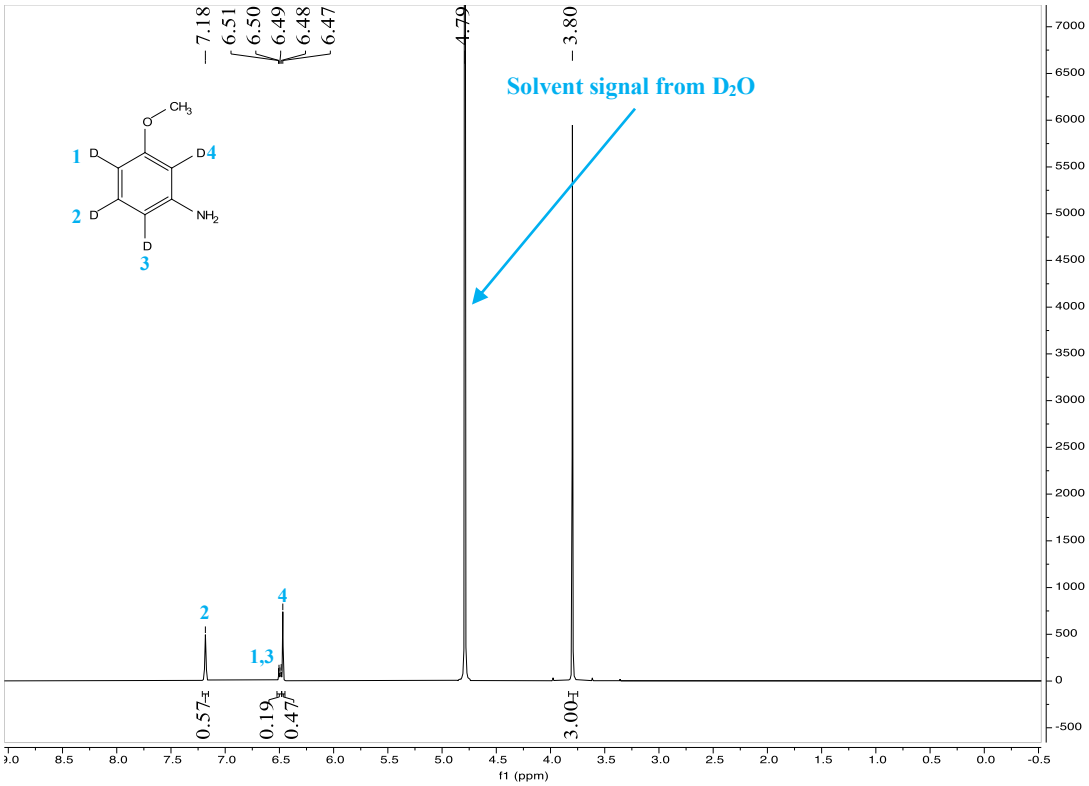

^{1}H NMR (400 MHz, D_2O) of feed material **13a**

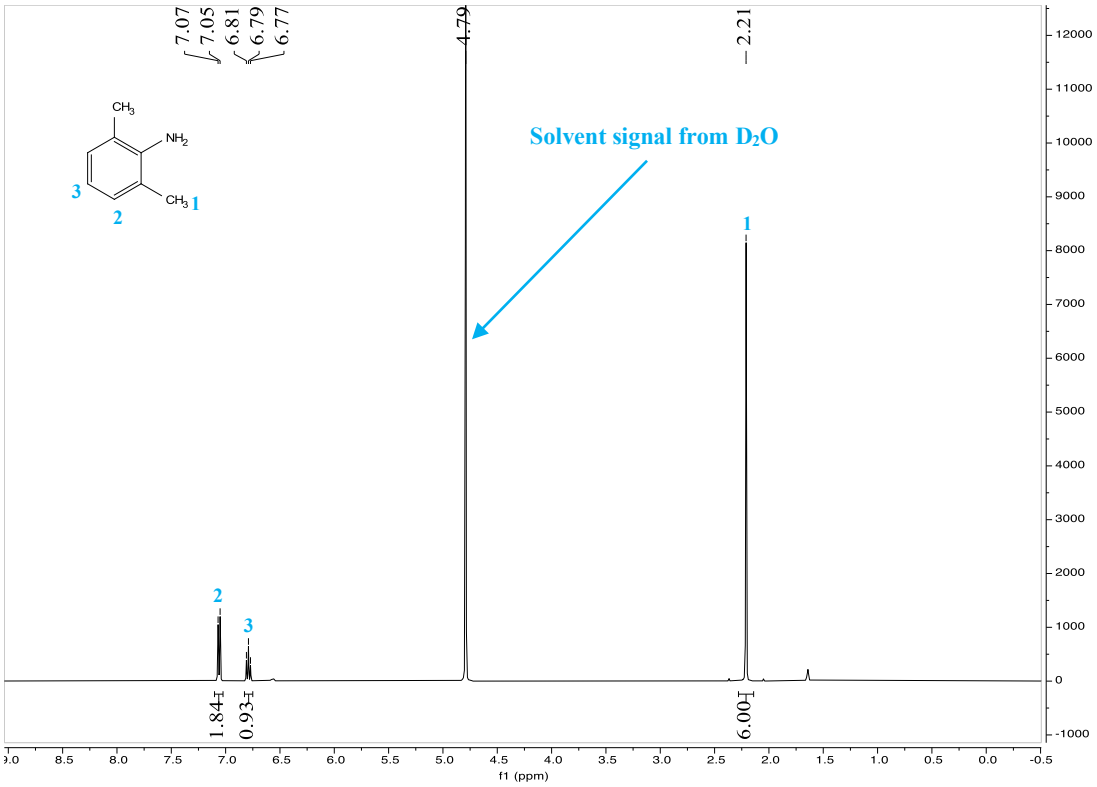

^{1}H NMR (400 MHz, D_2O) of product **13b**

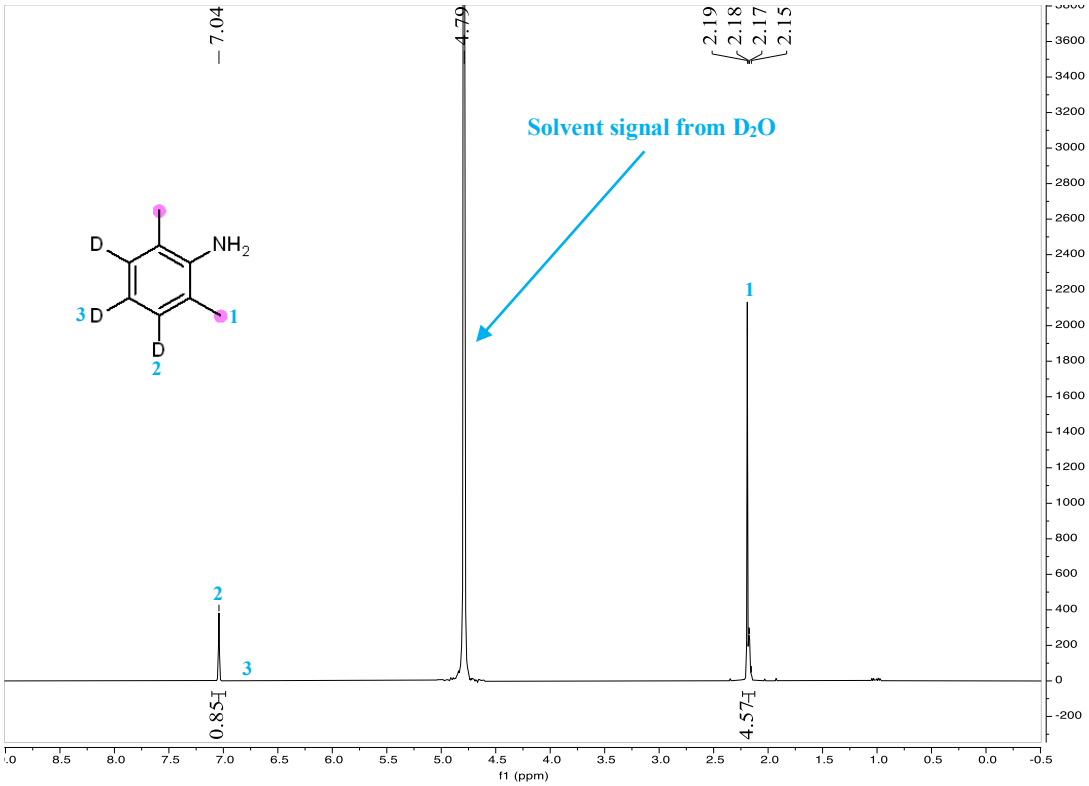

^{1}H NMR (400 MHz, D_2O) of feed material **14a**

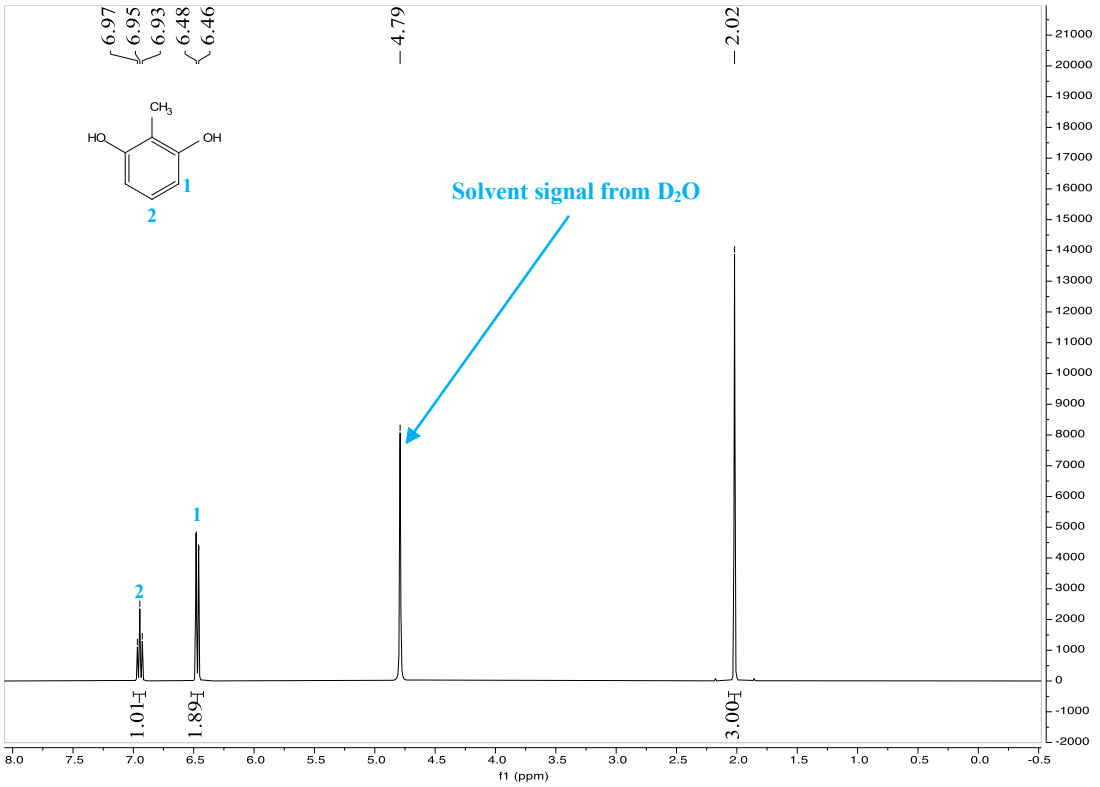

^{1}H NMR (400 MHz, D_2O) of product **14b**

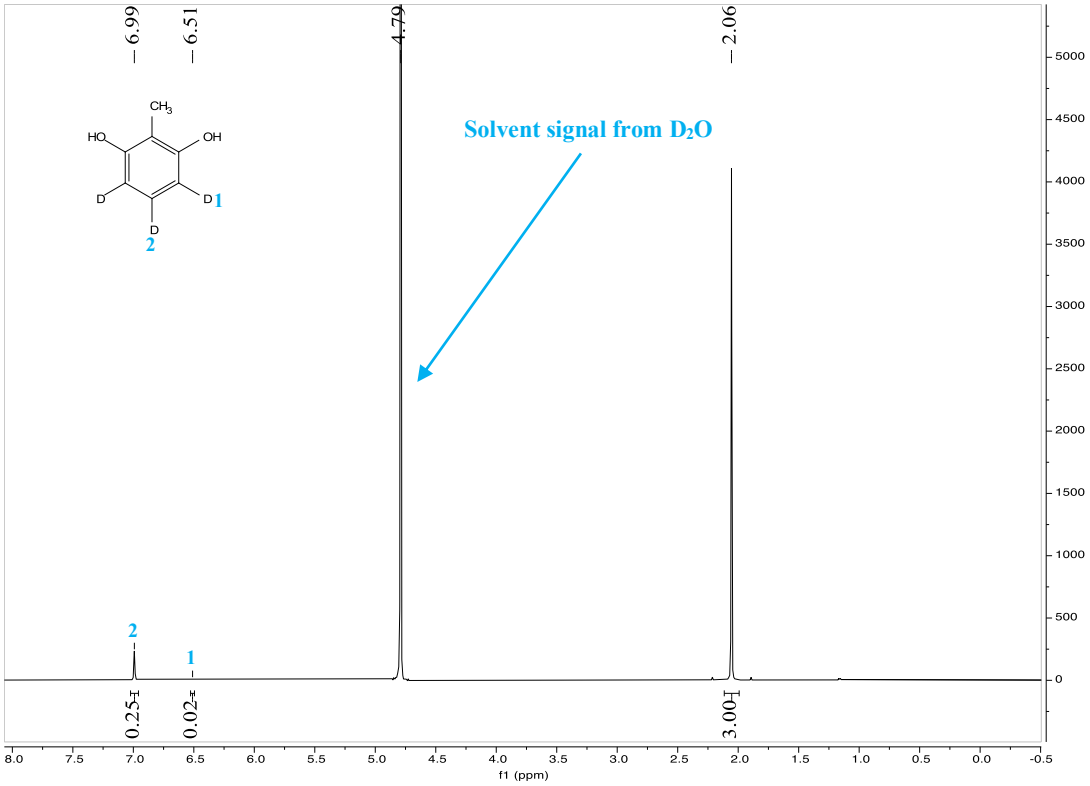

^{1}H NMR (400 MHz, D_2O) of feed material **15a**

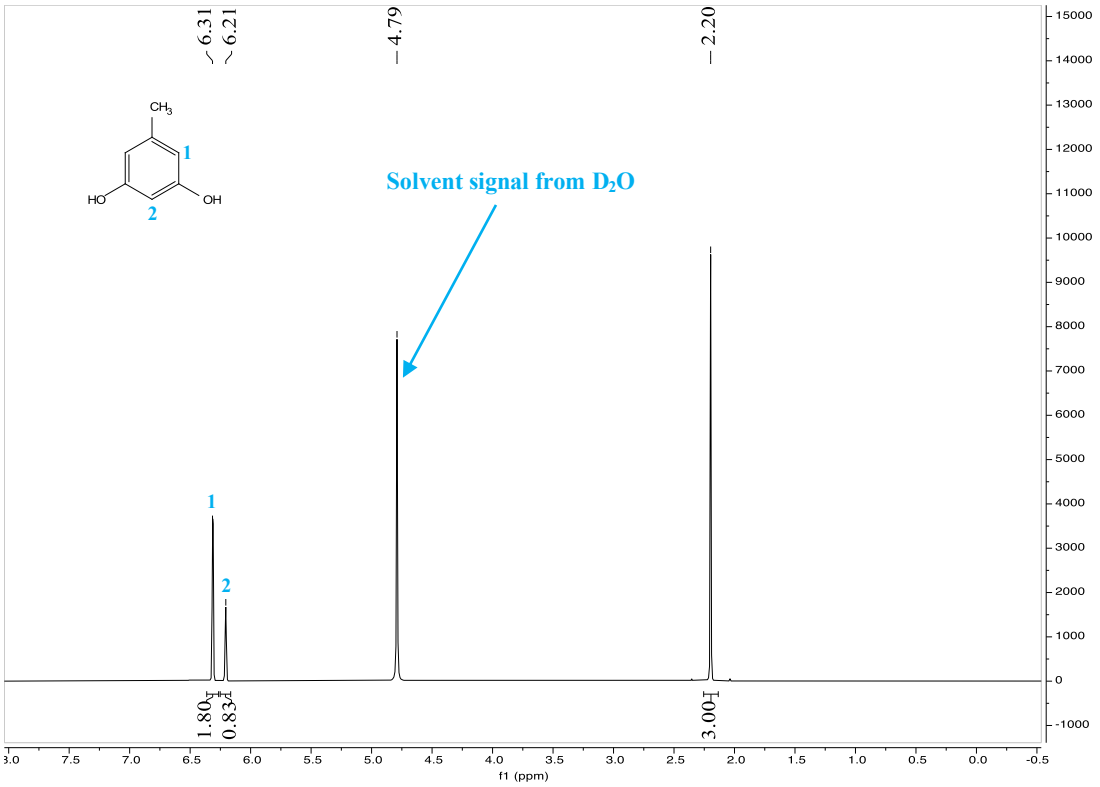

^{1}H NMR (400 MHz, D_2O) of product **15b**

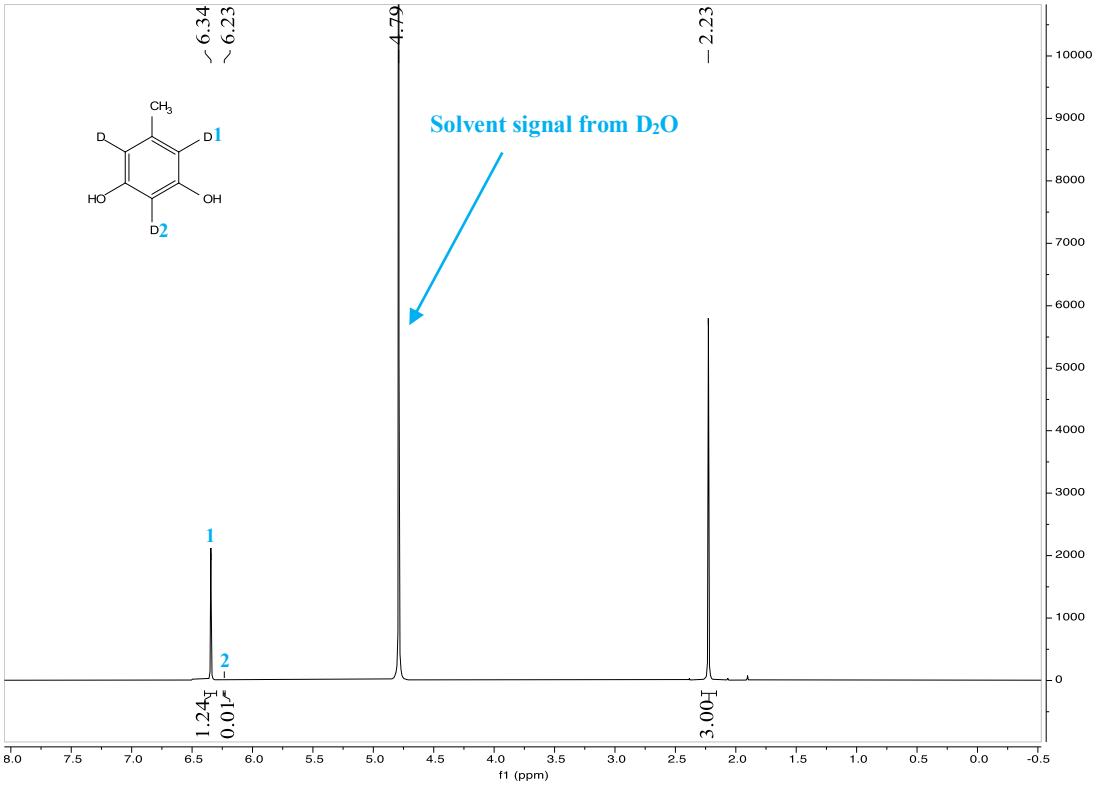

^{1}H NMR (400 MHz, D_2O) of feed material **16a**

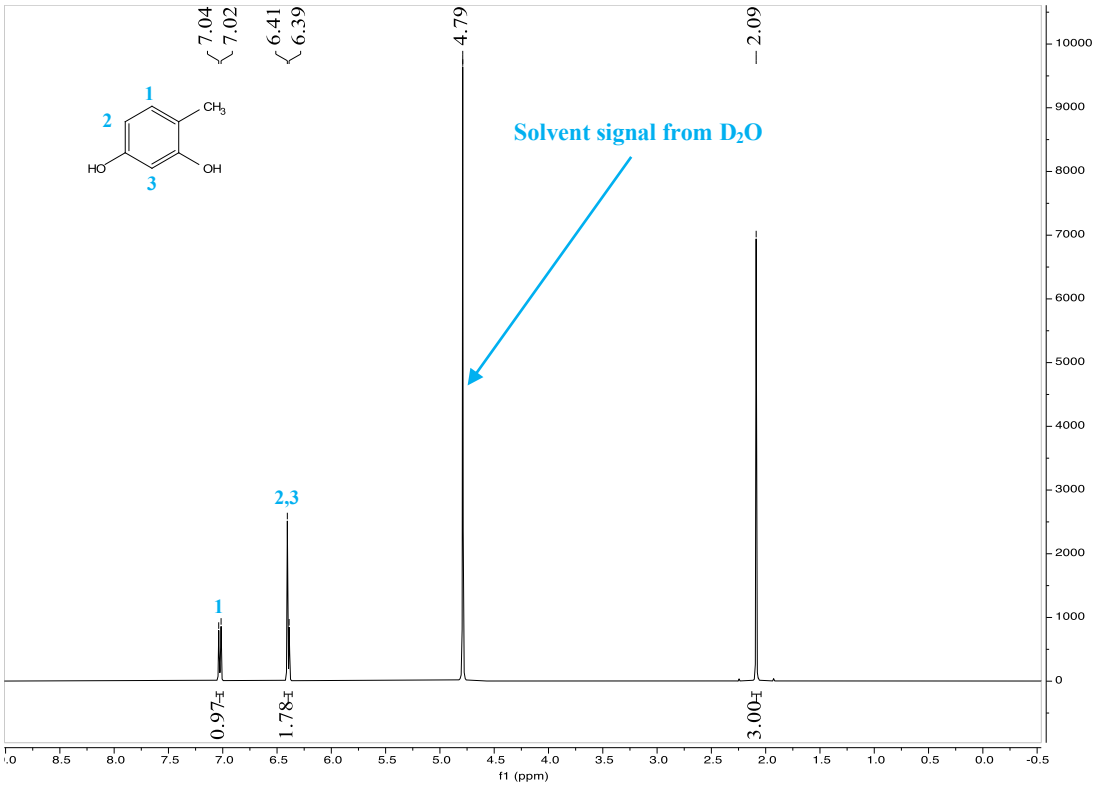

^{1}H NMR (400 MHz, D_2O) of product **16b**

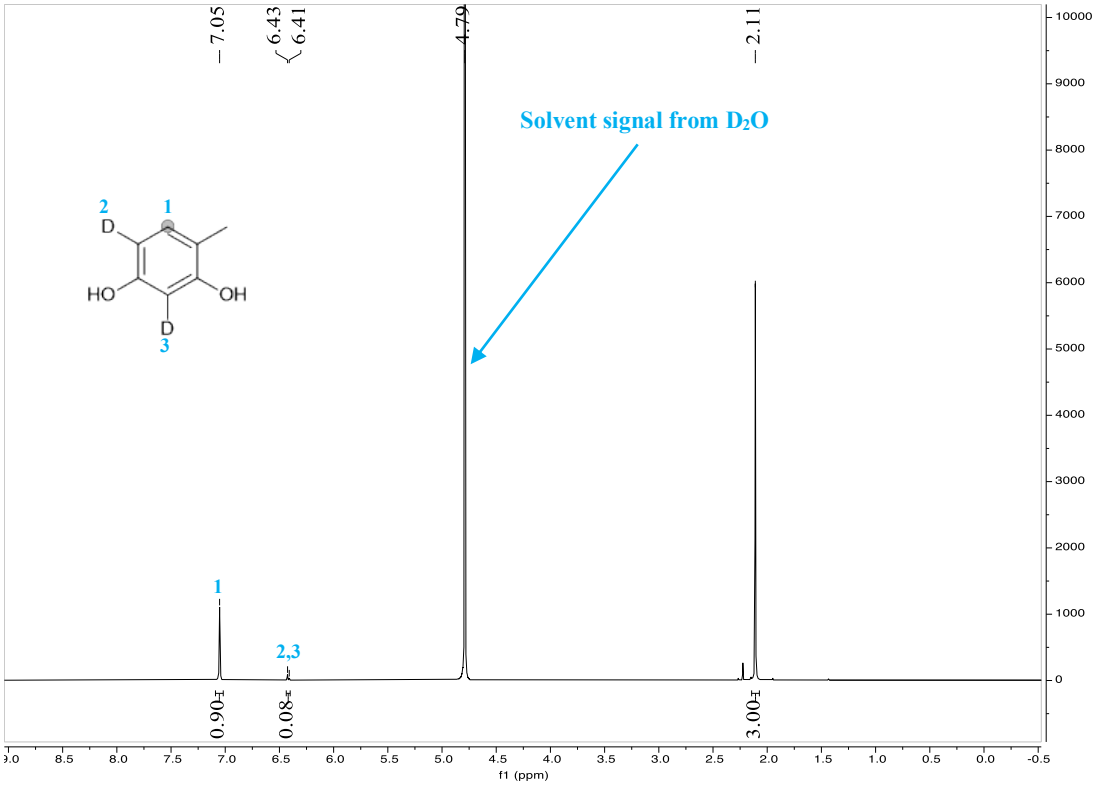

^{1}H NMR (400 MHz, D_2O) of feed material **17a**

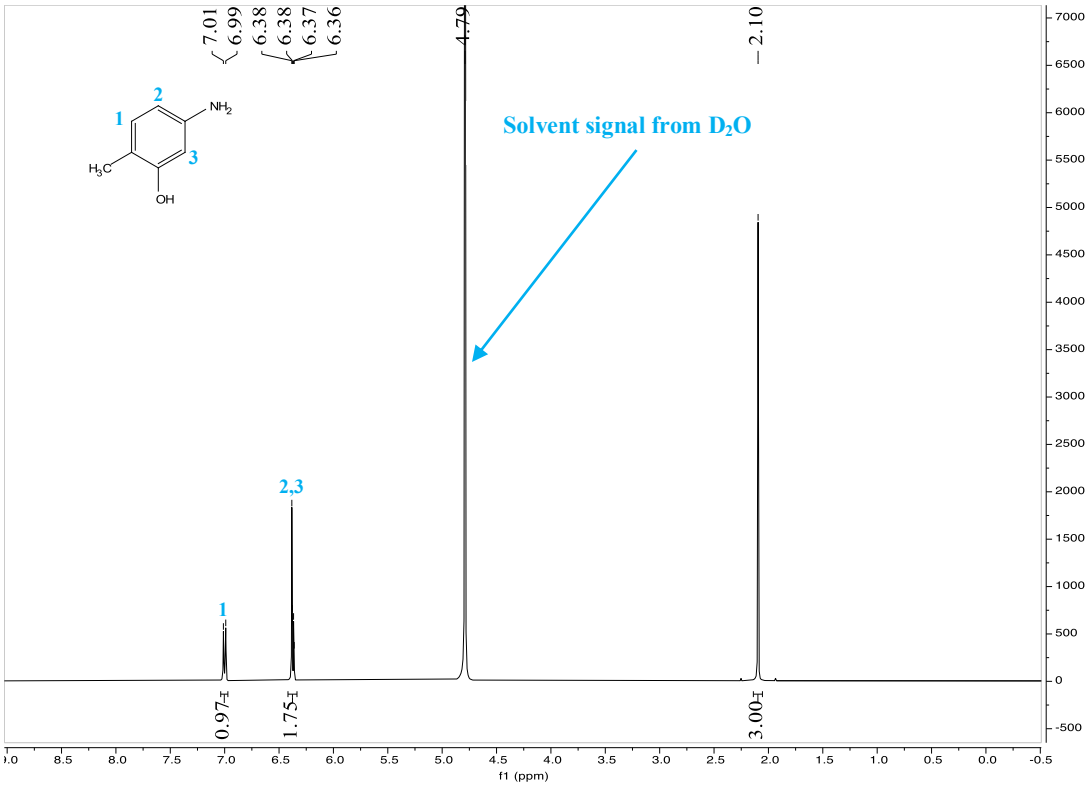

^{1}H NMR (400 MHz, D_2O) of product **17b**

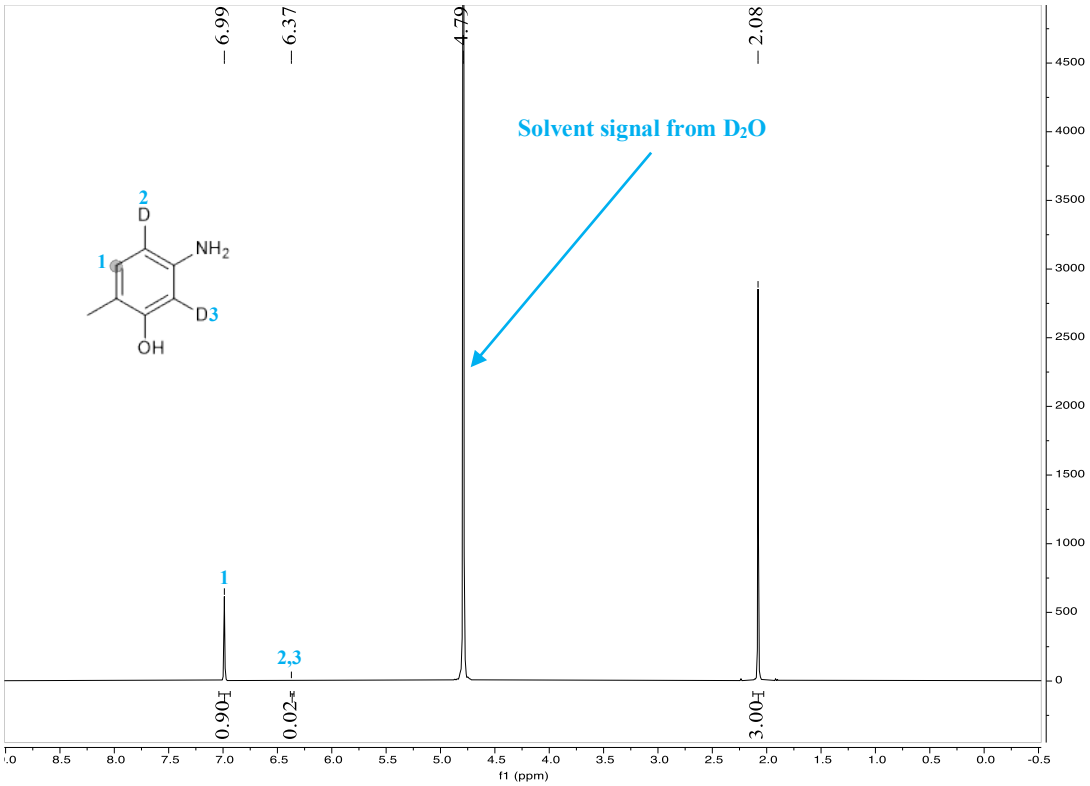

^{1}H NMR (400 MHz, D_2O) of feed material **18a**

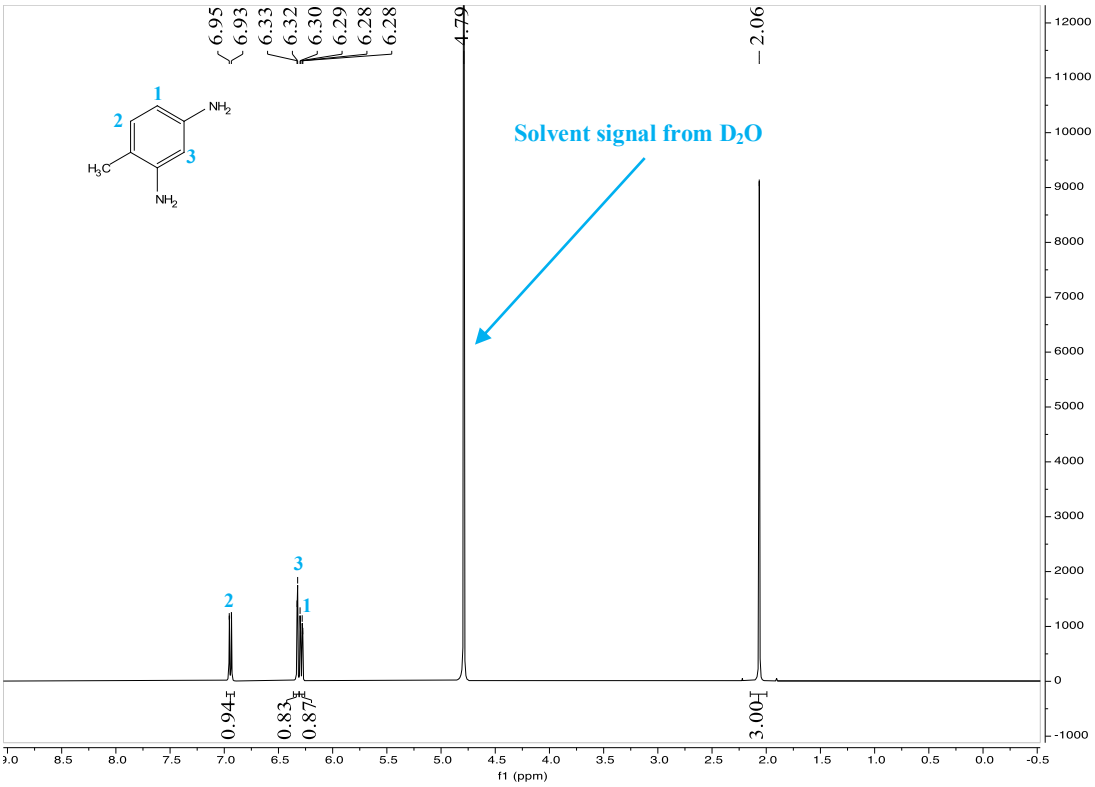

^{1}H NMR (400 MHz, D_2O) of product **18b**

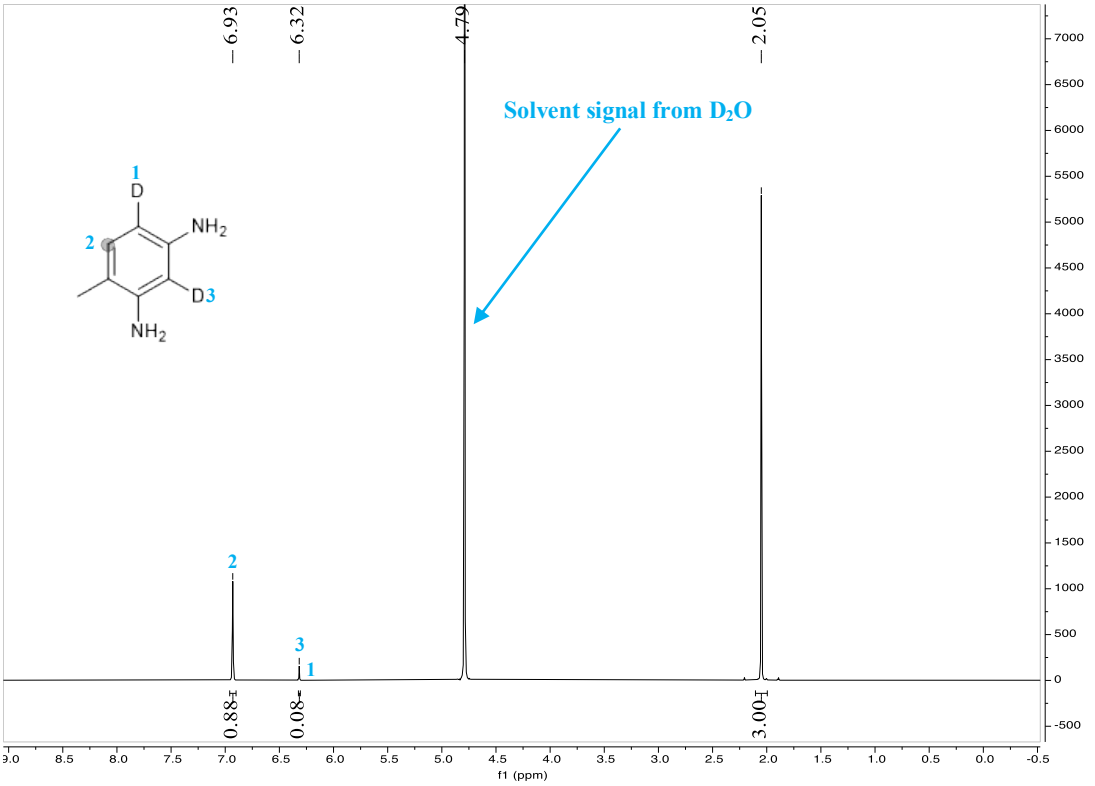

[1]H NMR (400 MHz, DMSO-d_6) of feed material **19a**

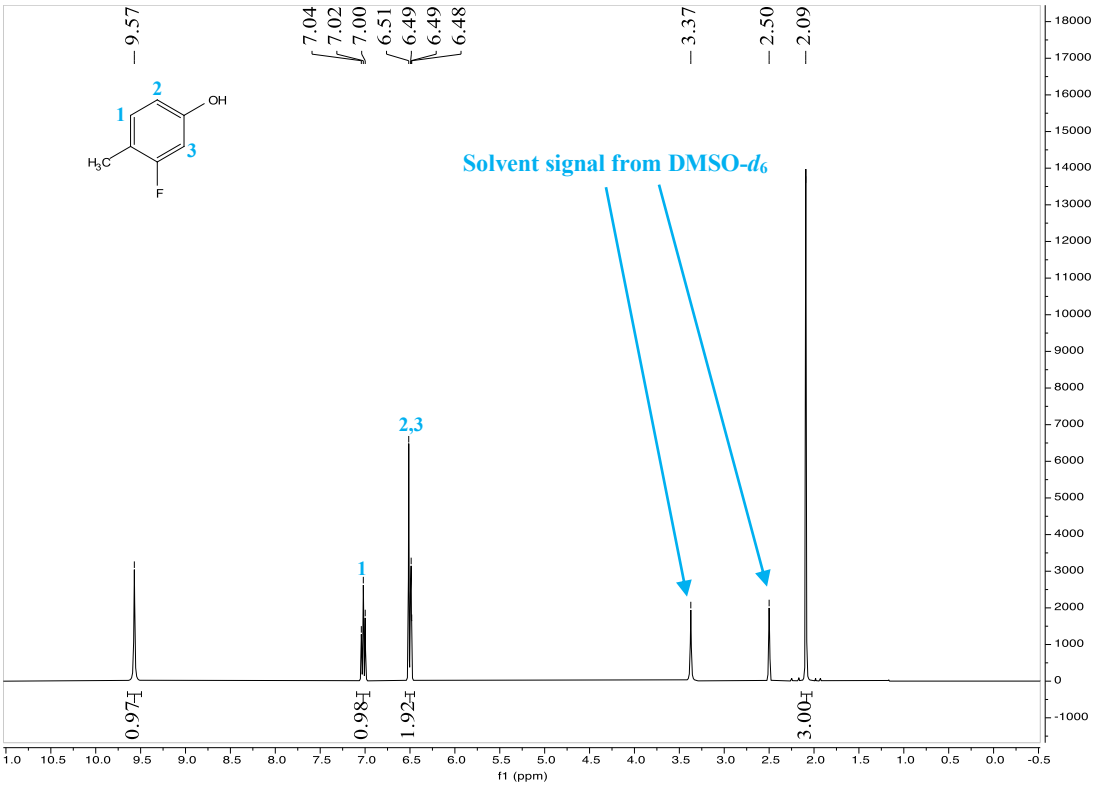

[19]F NMR (376 MHz, DMSO-d_6) of feed material **19a**

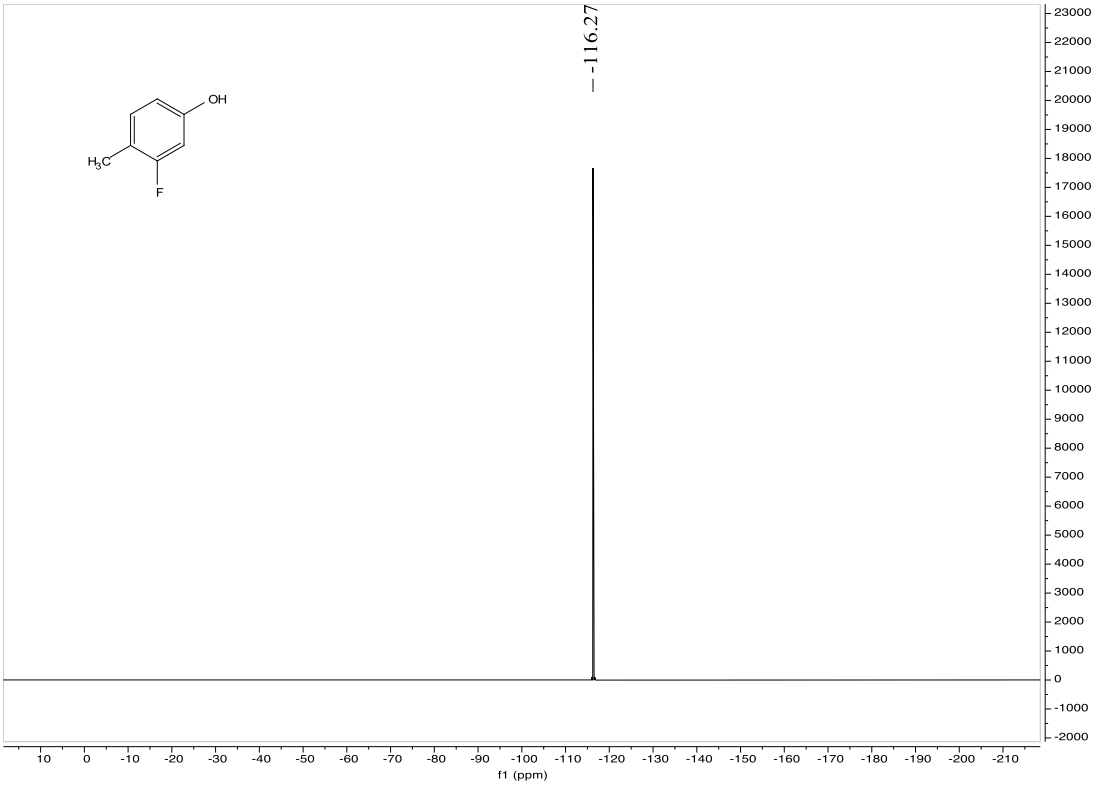

^{1}H NMR (400 MHz, D_2O) of product **19b**

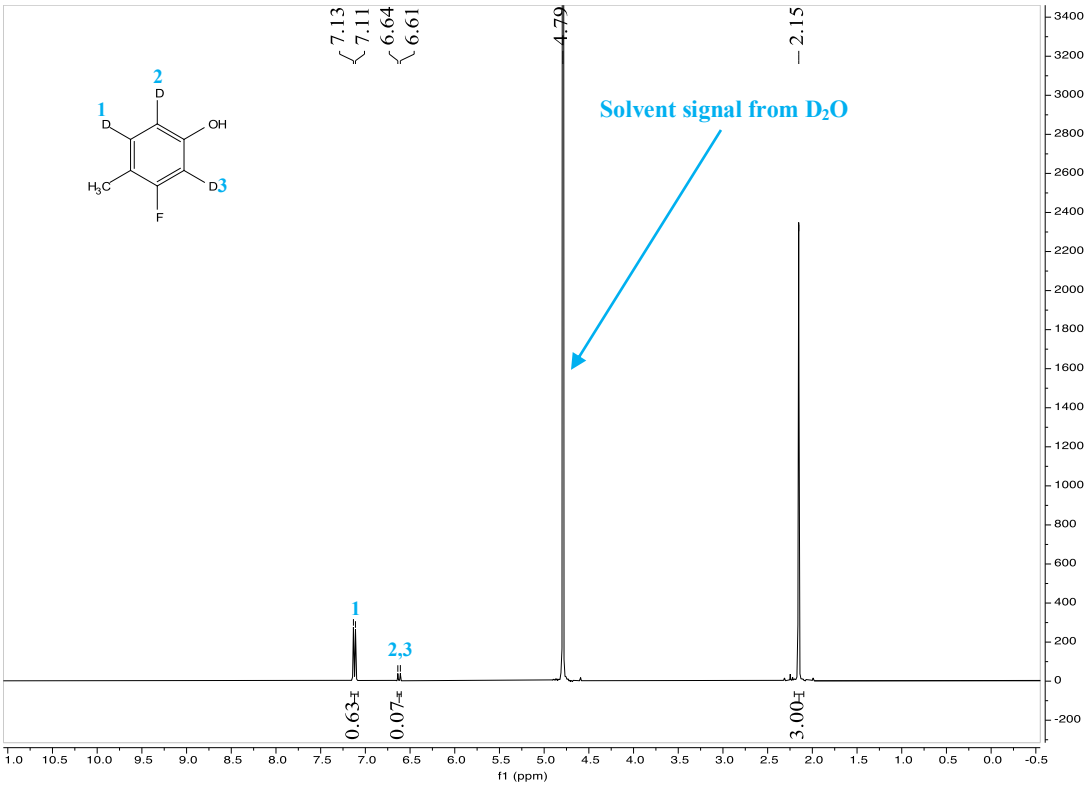

^{19}F NMR (376 MHz, D_2O) of product **19b**

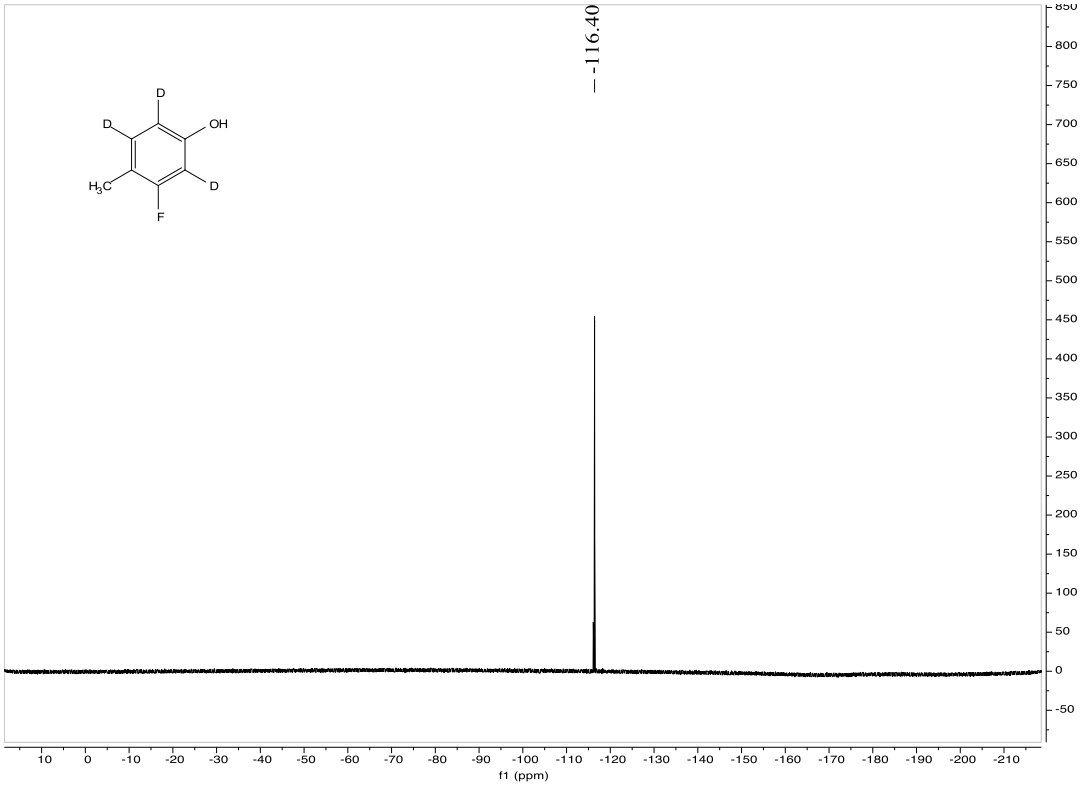

^{1}H NMR (400 MHz, DMSO-d_6) of feed material **20a**

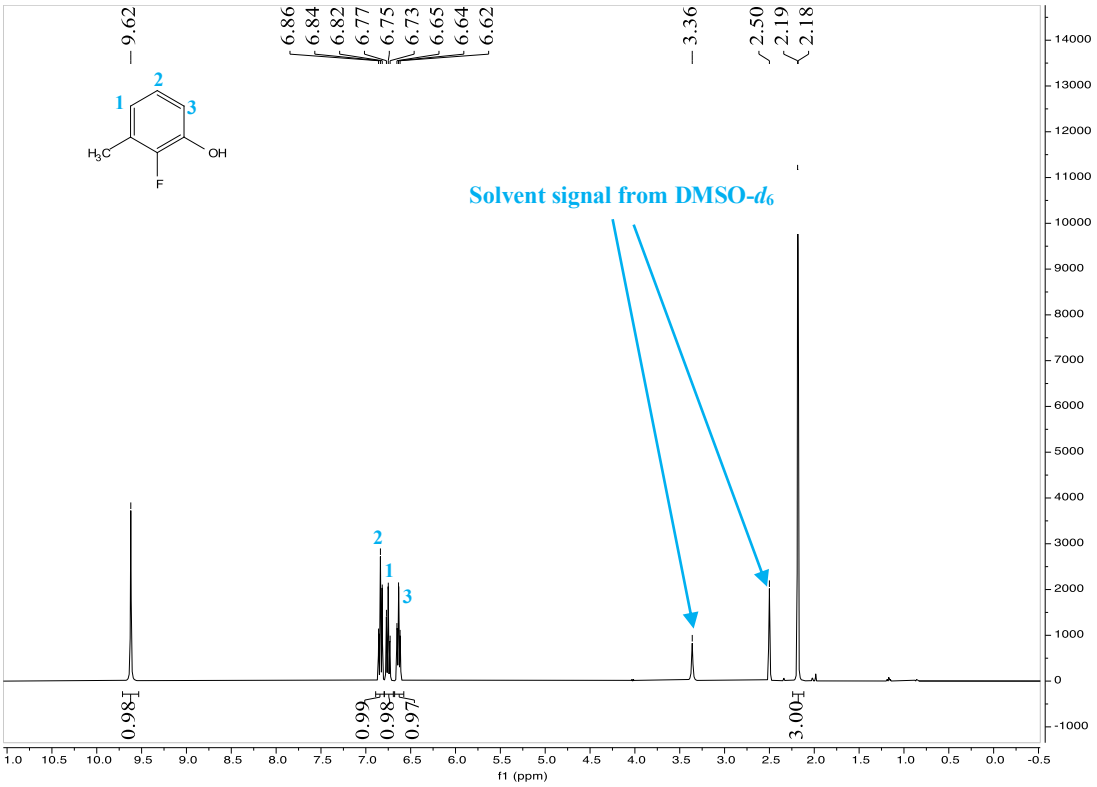

^{19}F NMR (376 MHz, DMSO-d_6) of feed material **20a**

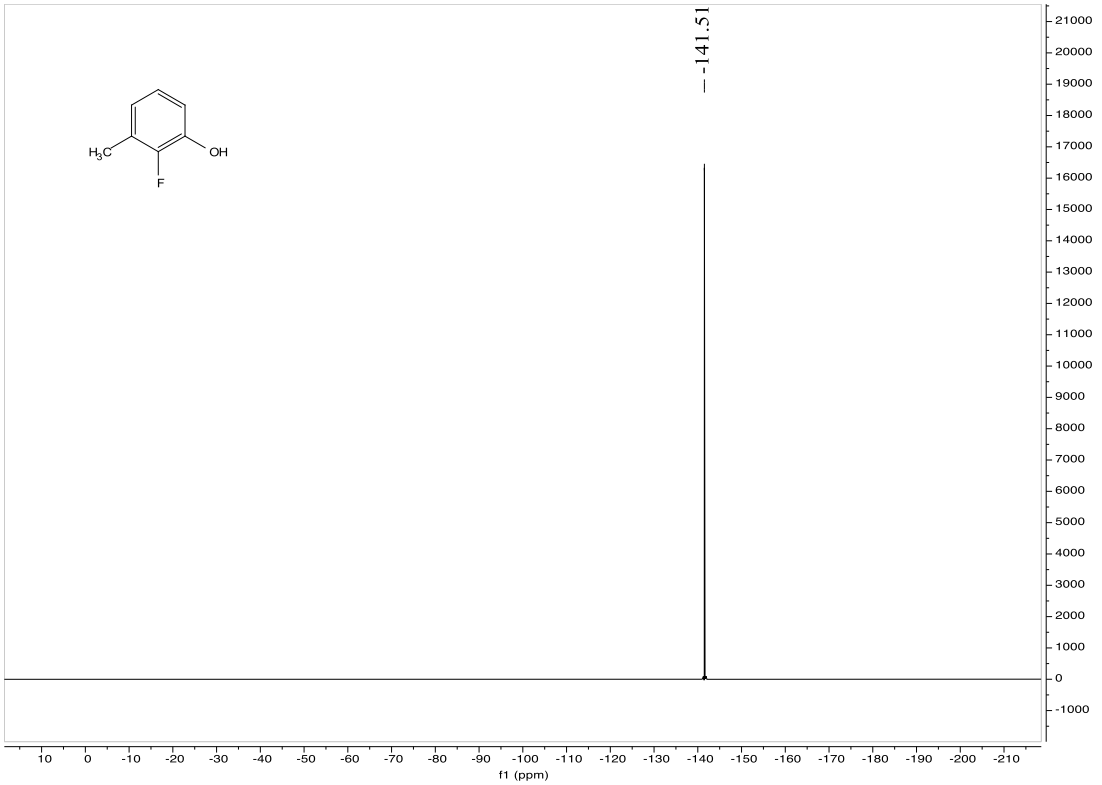

^{1}H NMR (400 MHz, D_2O) of product **20b**

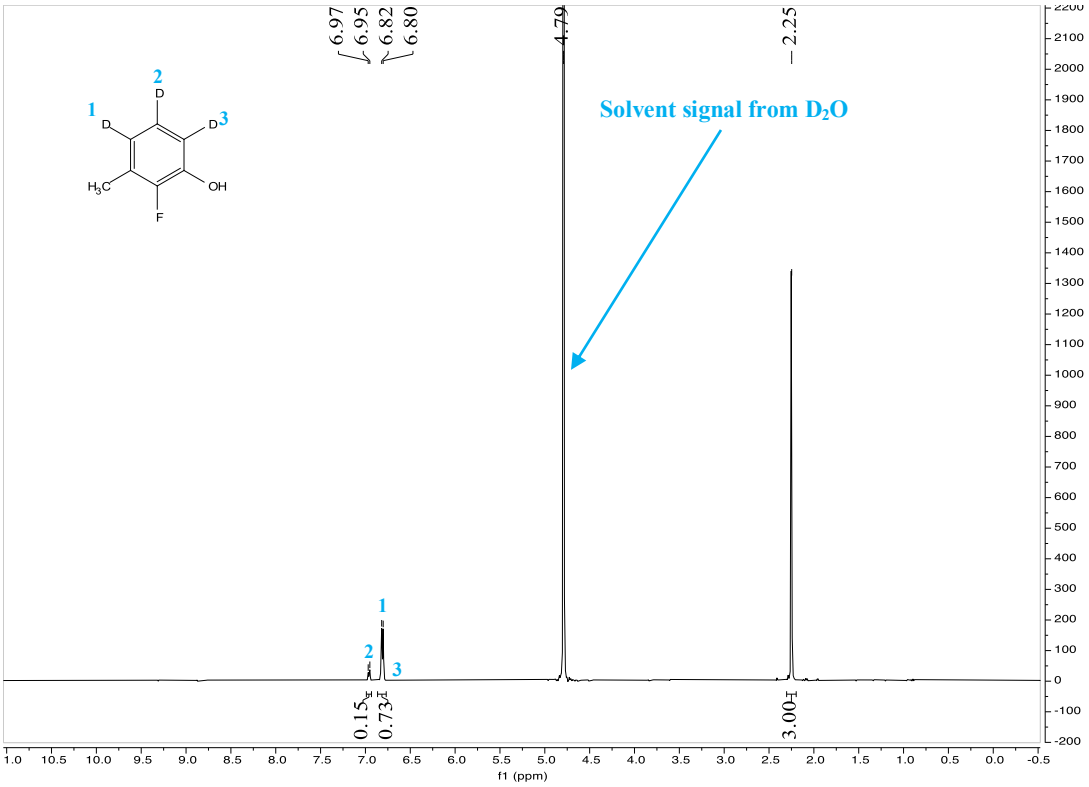

^{19}F NMR (376 MHz, D_2O) of product **20b**

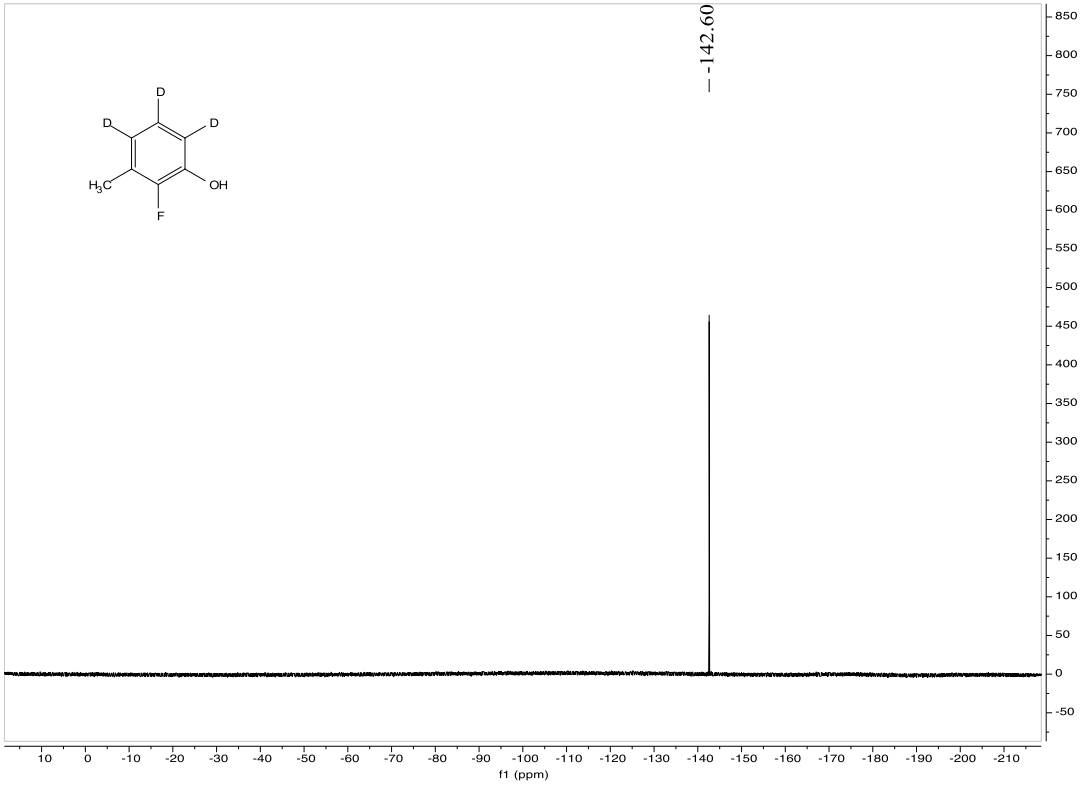

^{1}H NMR (400 MHz, DMSO-d_6) of feed material **21a**

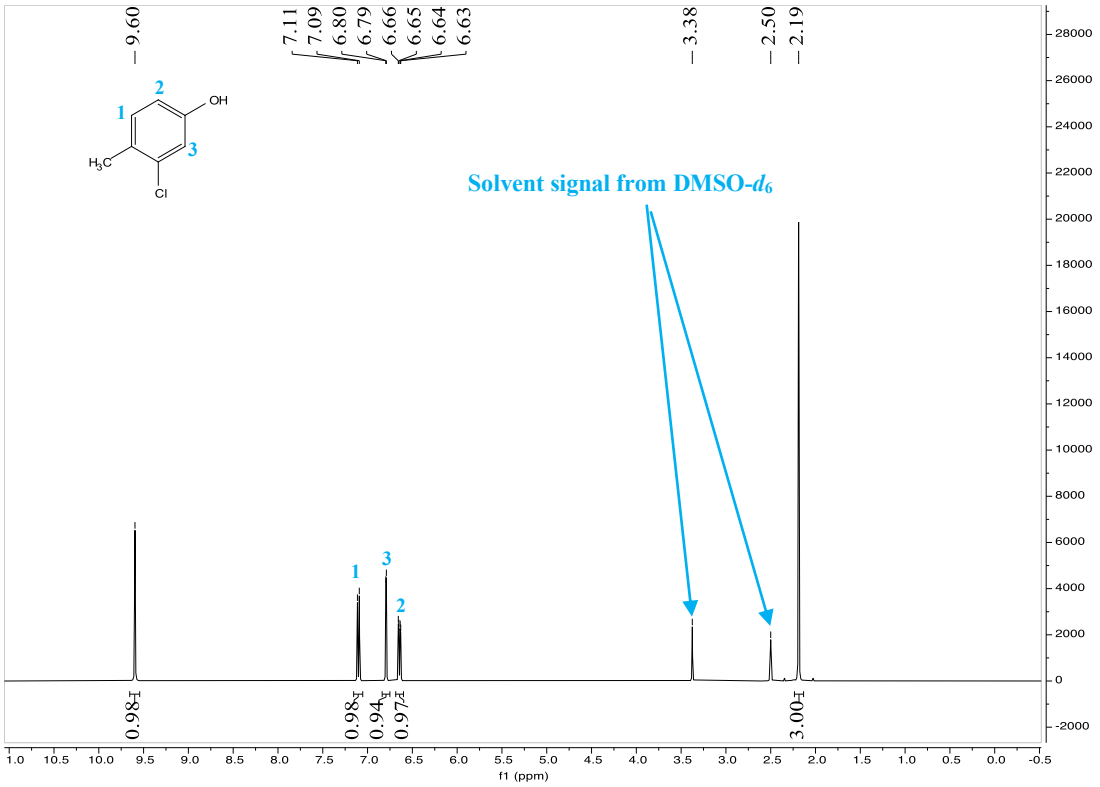

^{1}H NMR (400 MHz, D_2O) of product **21b**

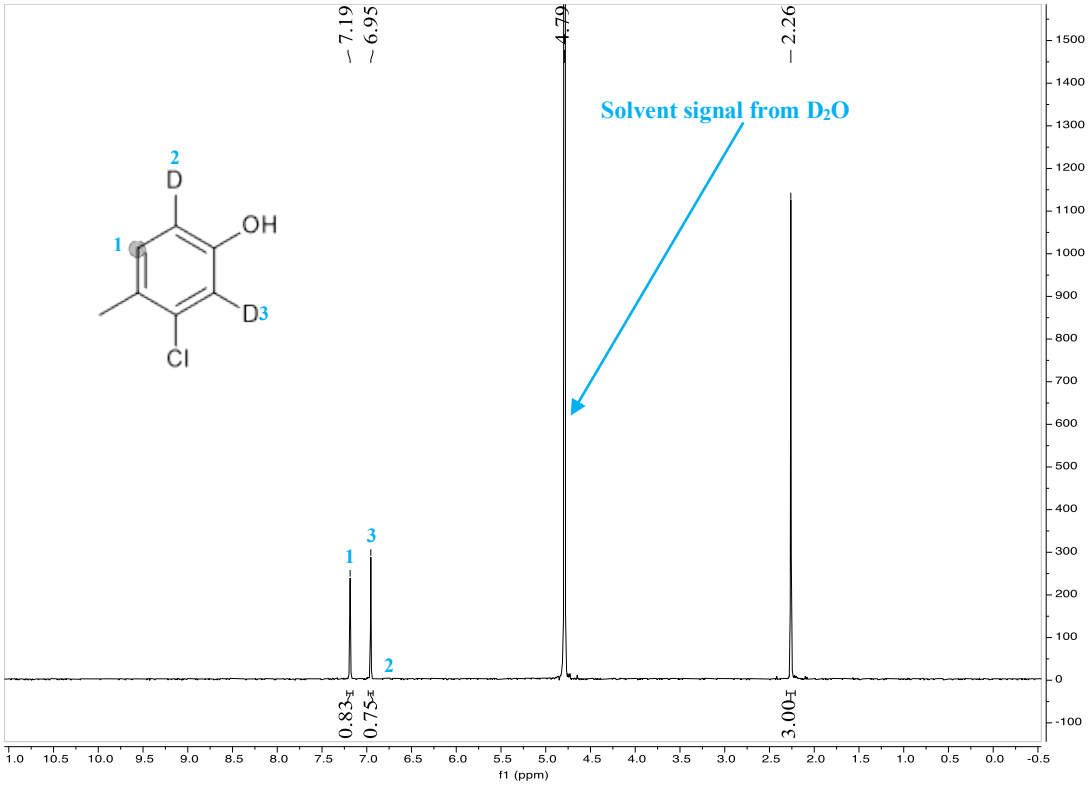

^{1}H NMR (400 MHz, D_2O) of feed material **22a**

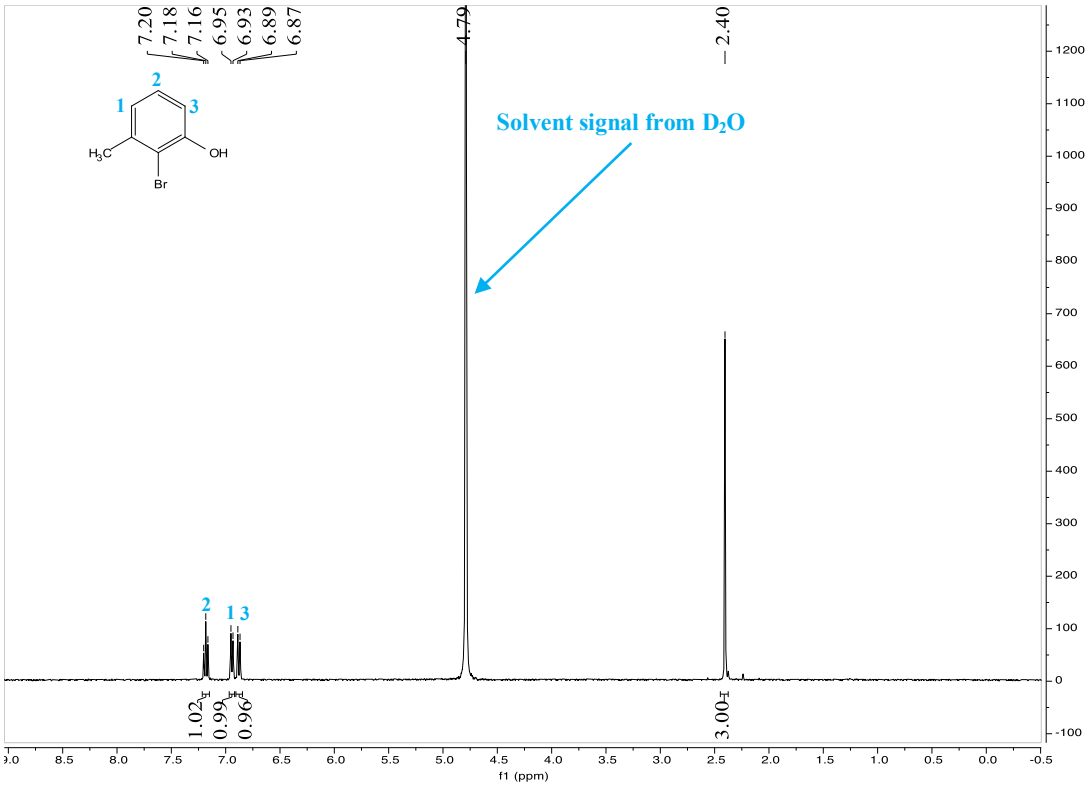

^{1}H NMR (400 MHz, D_2O) of product **22b**

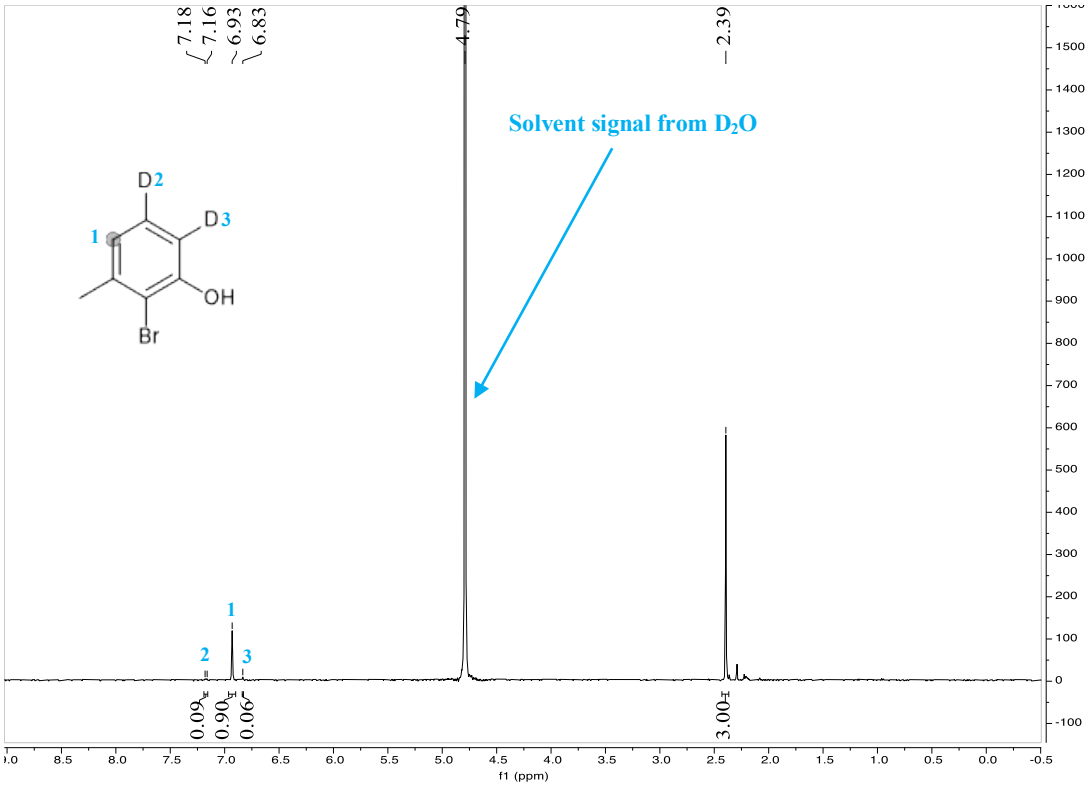

^{1}H NMR (400 MHz, D_2O) of feed material **23a**

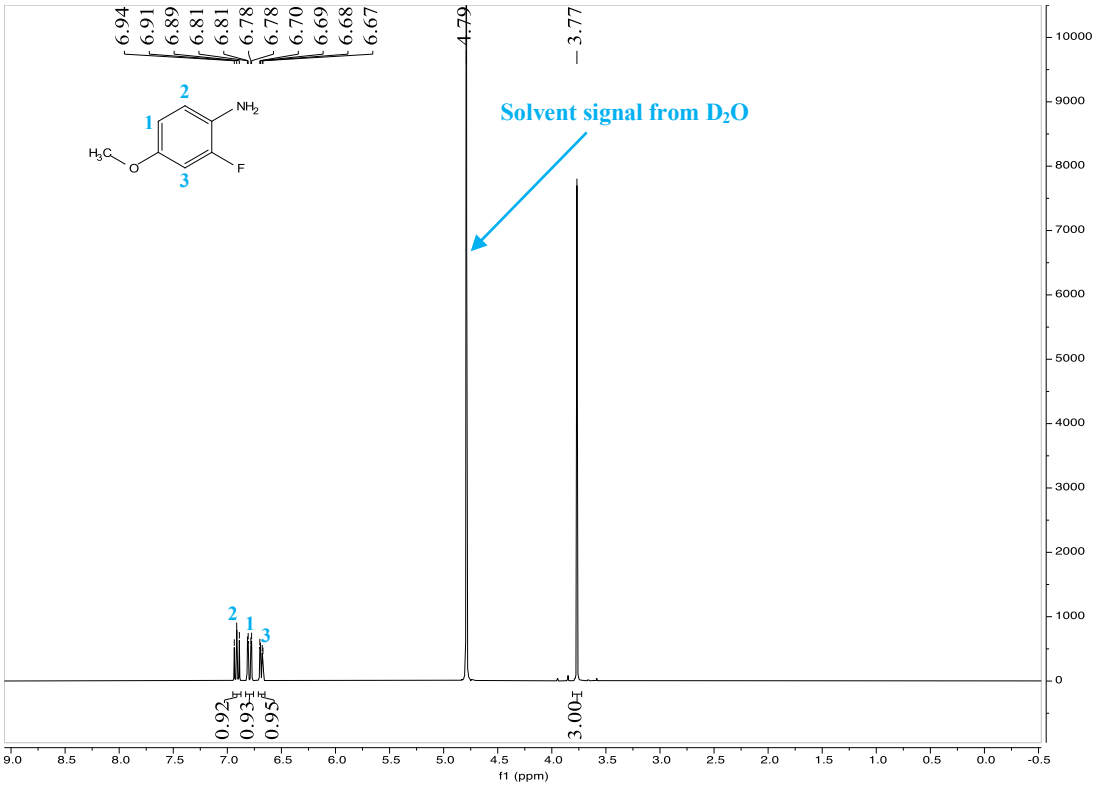

^{19}F NMR (376 MHz, D_2O) of feed material **23a**

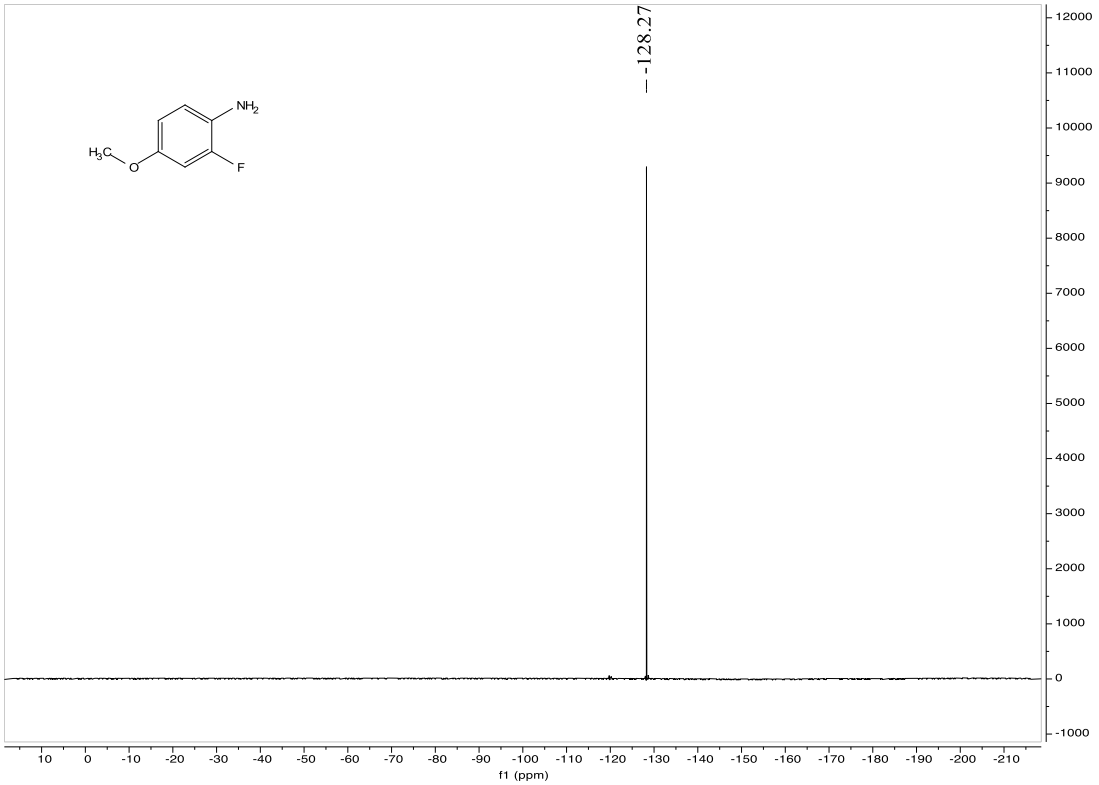

^{1}H NMR (400 MHz, D_2O) of product **23b**

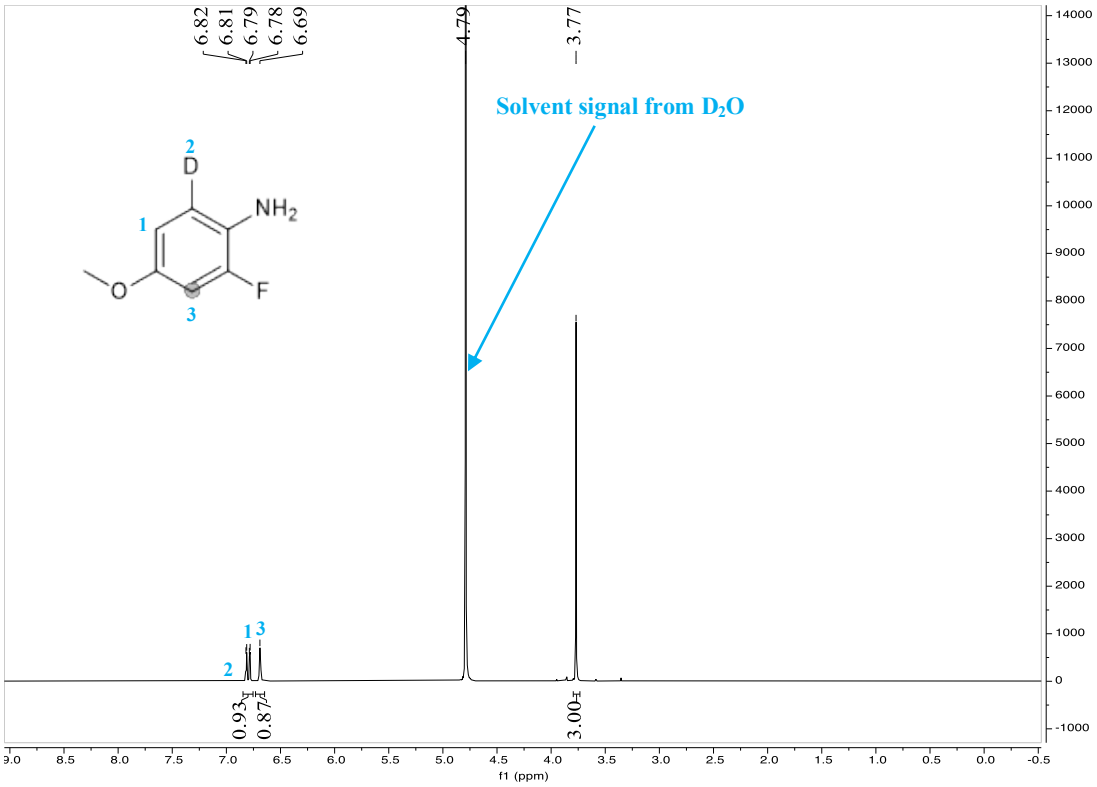

^{19}F NMR (376 MHz, D_2O) of product **23b**

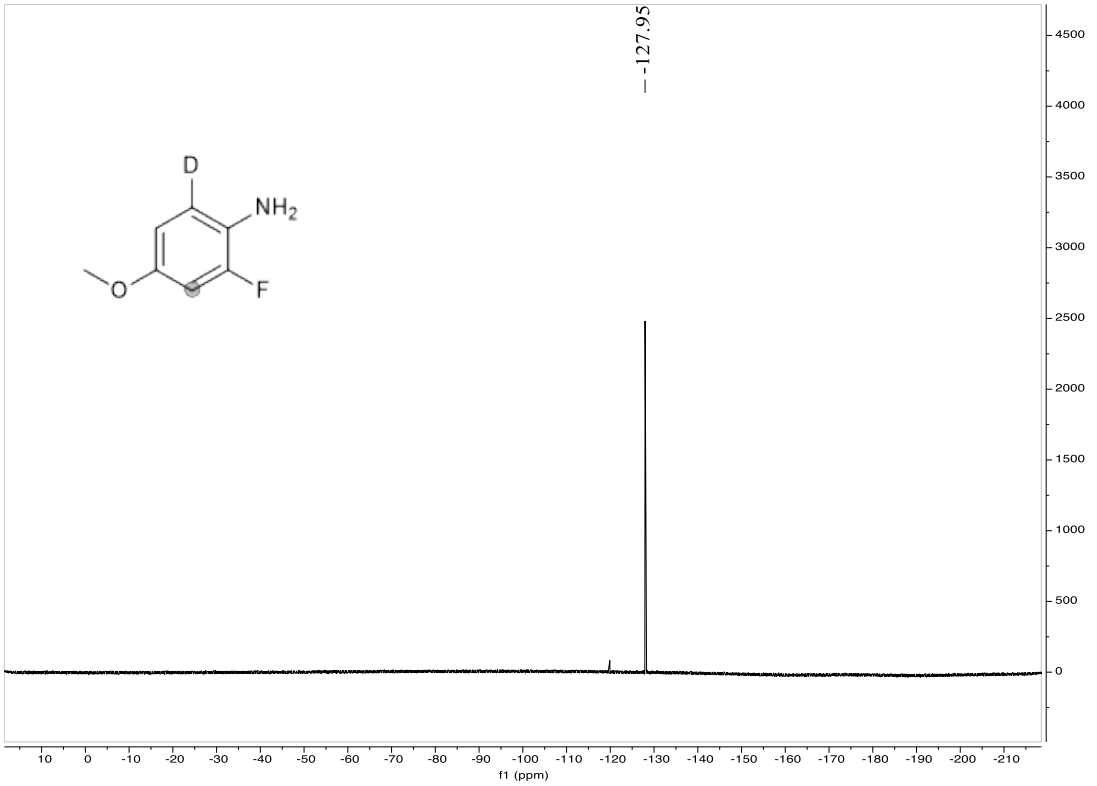

^{1}H NMR (400 MHz, D_2O) of feed material **24a**

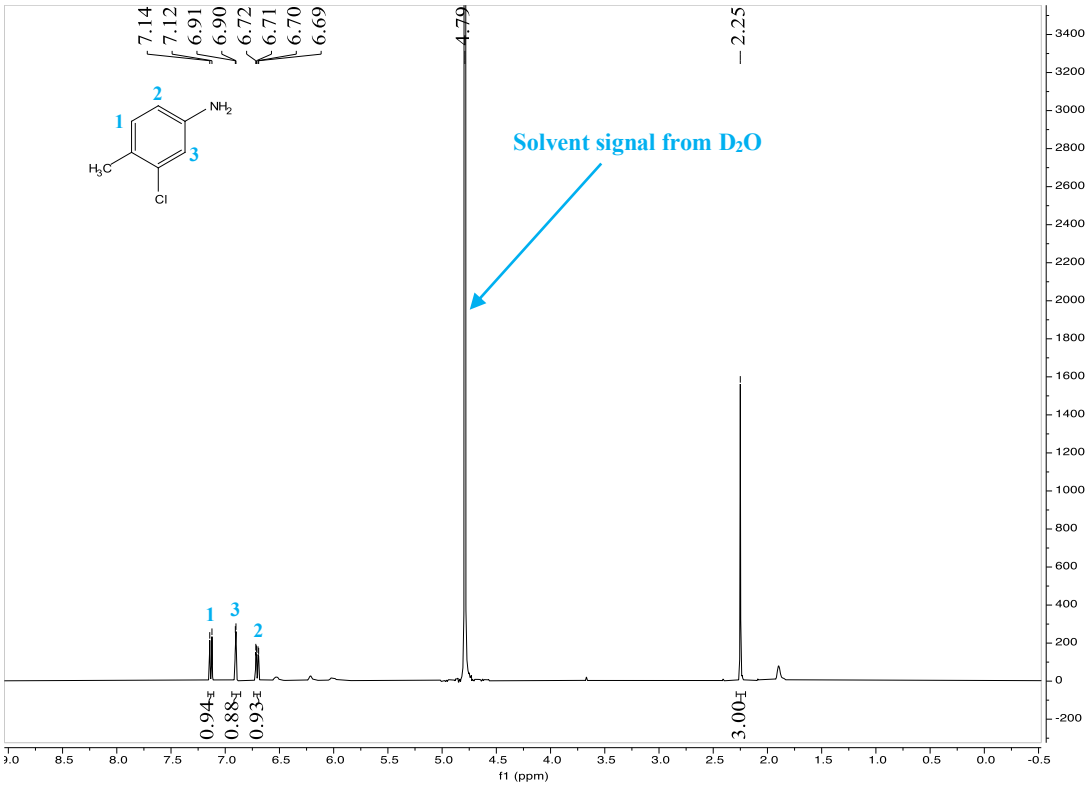

^{1}H NMR (400 MHz, D_2O) of product **24b**

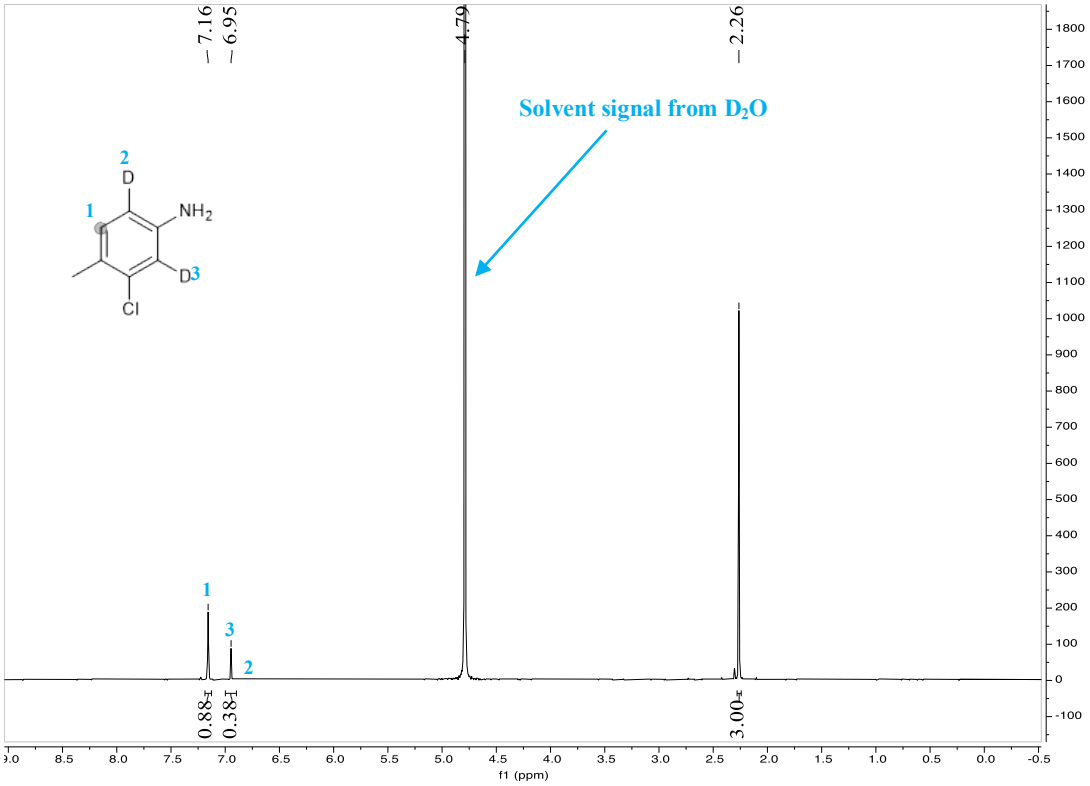

^{1}H NMR (400 MHz, DMSO-d_6) of feed material **26a**

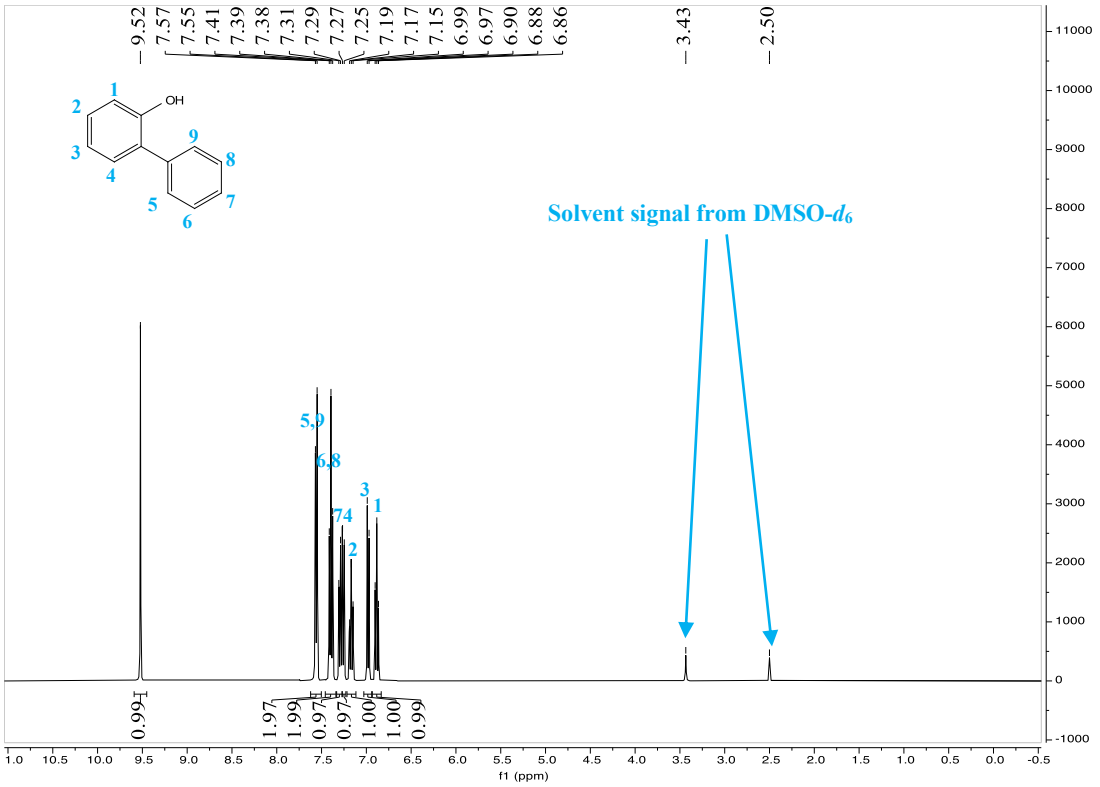

^{1}H NMR (400 MHz, DMSO-d_6) of product **26b**

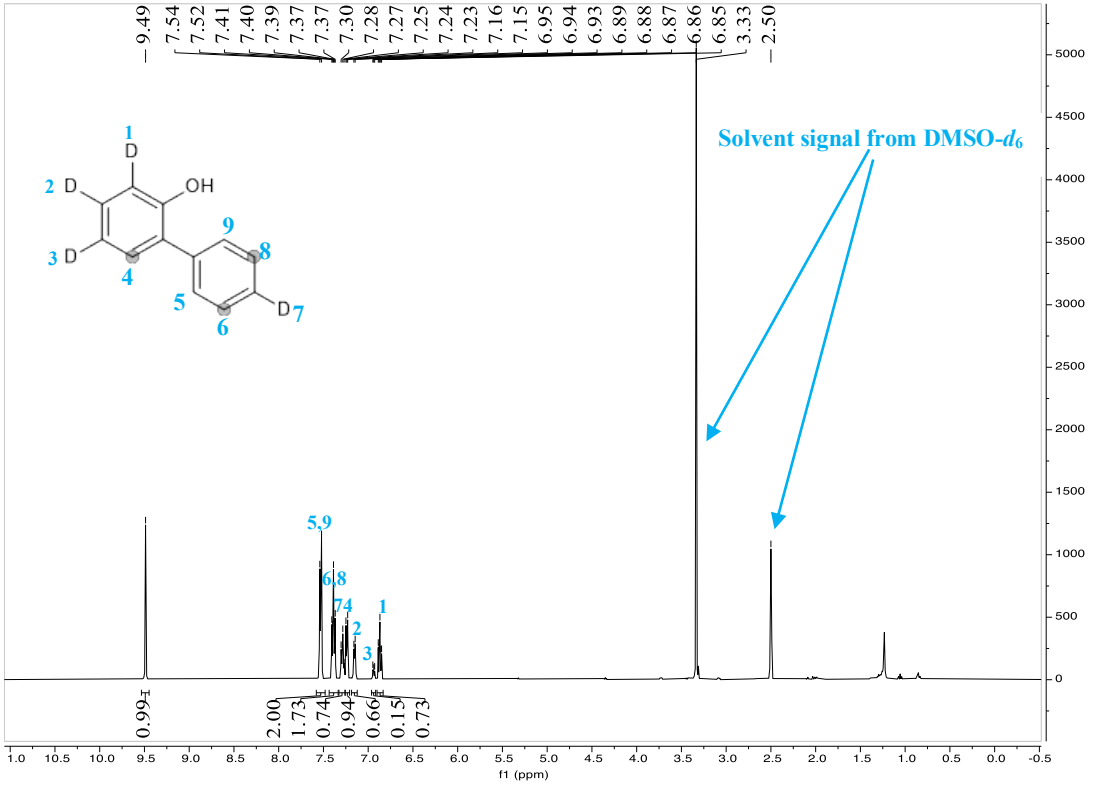

^{1}H NMR (400 MHz, $CDCl_3$) of feed material **27a**

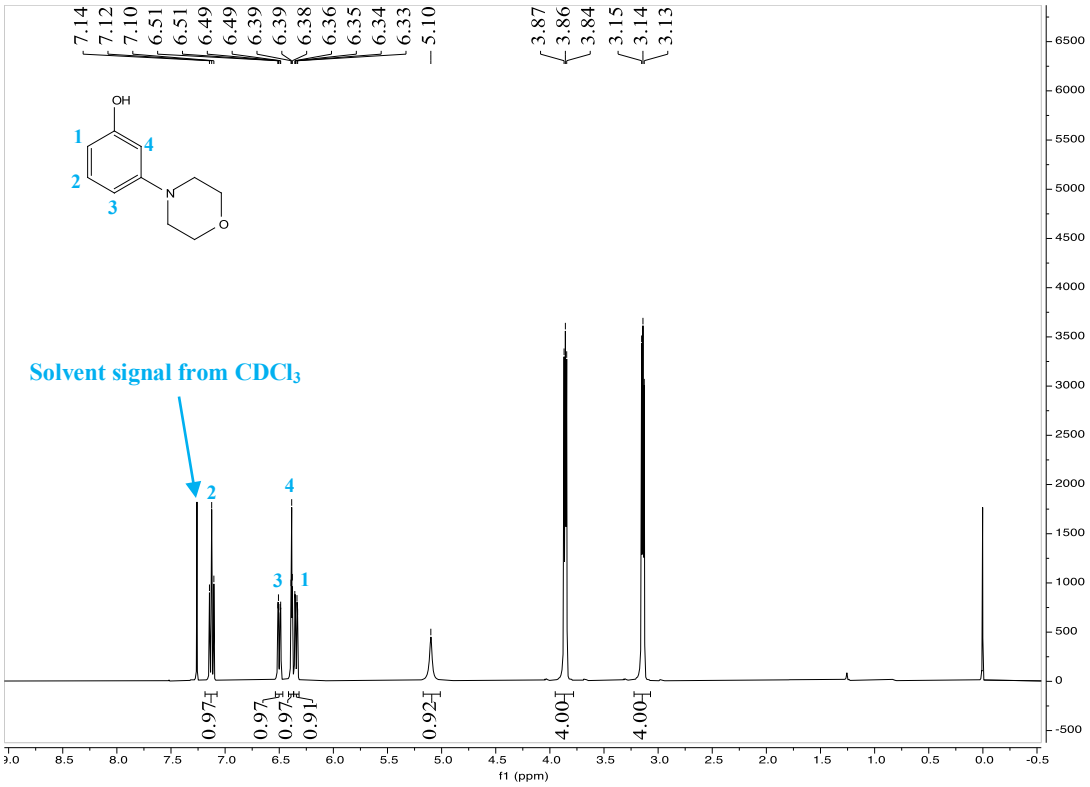

^{1}H NMR (400 MHz, $CDCl_3$) of product **27b**

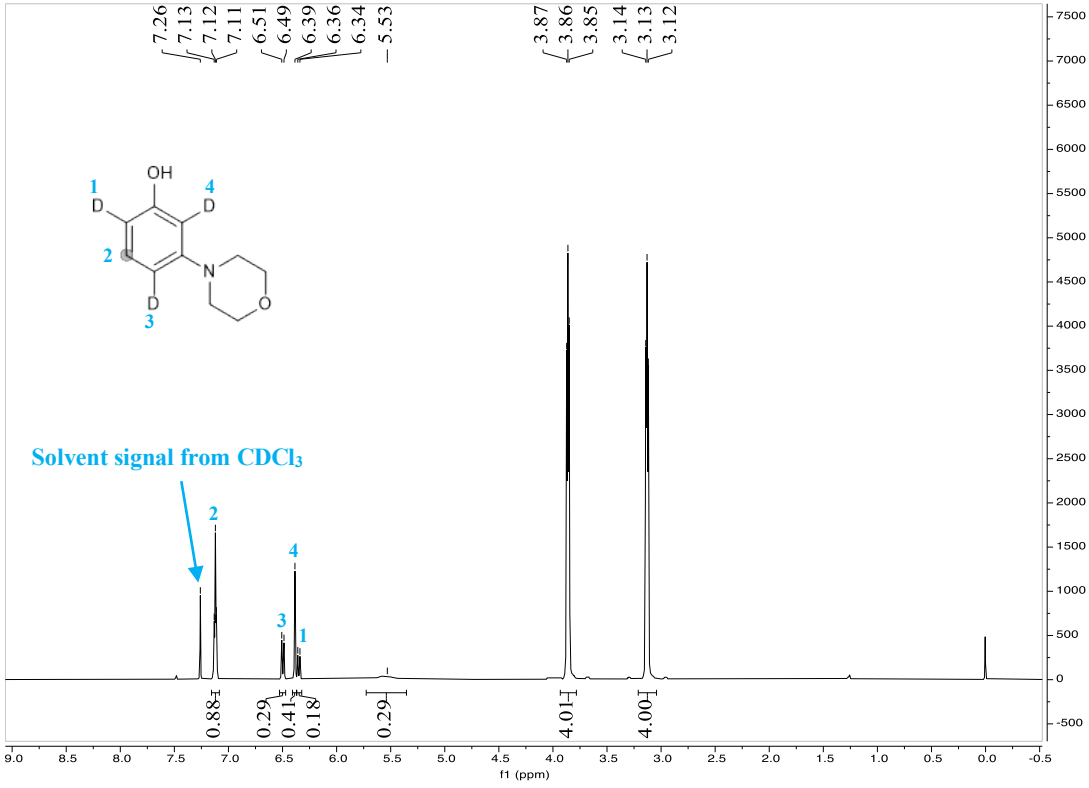

^{1}H NMR (400 MHz, $CDCl_3$) of feed material **28a**

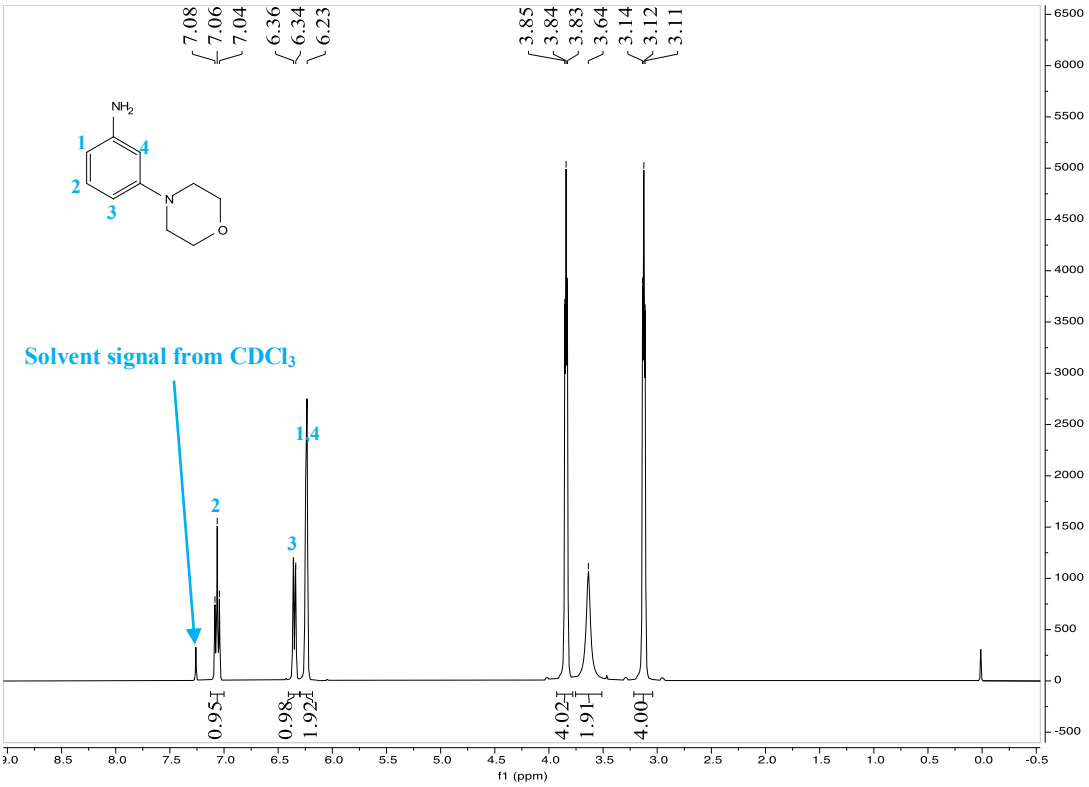

^{1}H NMR (400 MHz, $CDCl_3$) of product **28b**

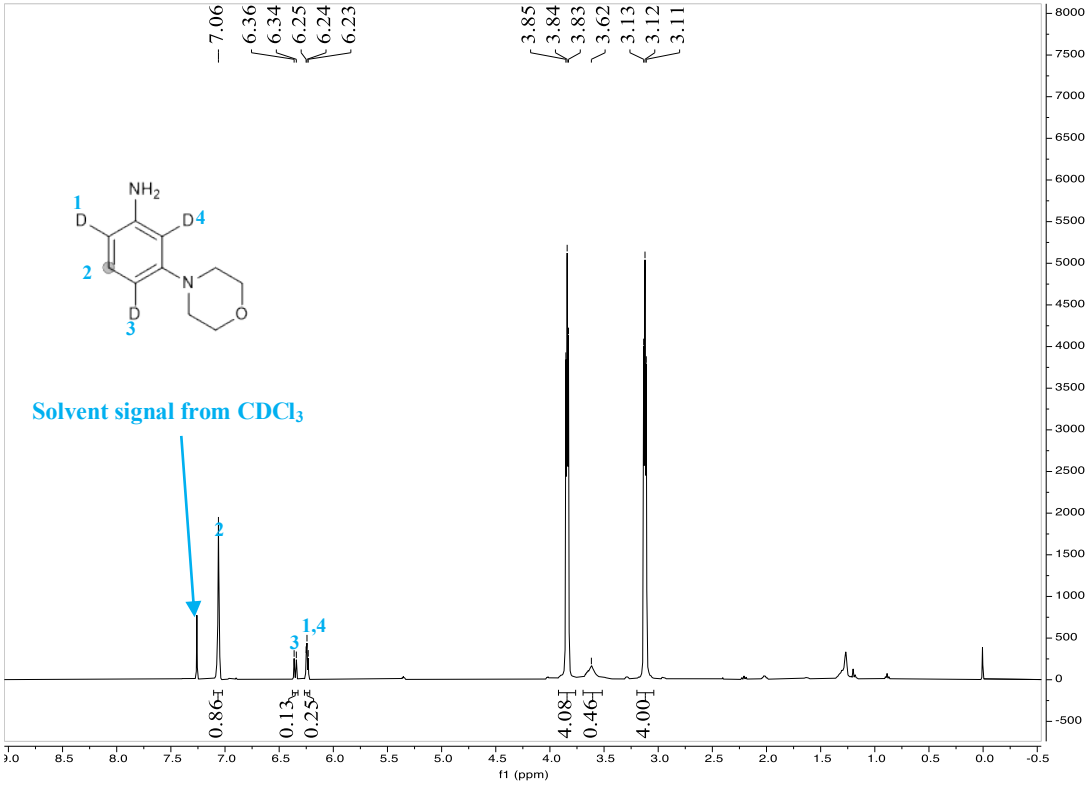

^{1}H NMR (400 MHz, $CDCl_3$) of feed material **29a**

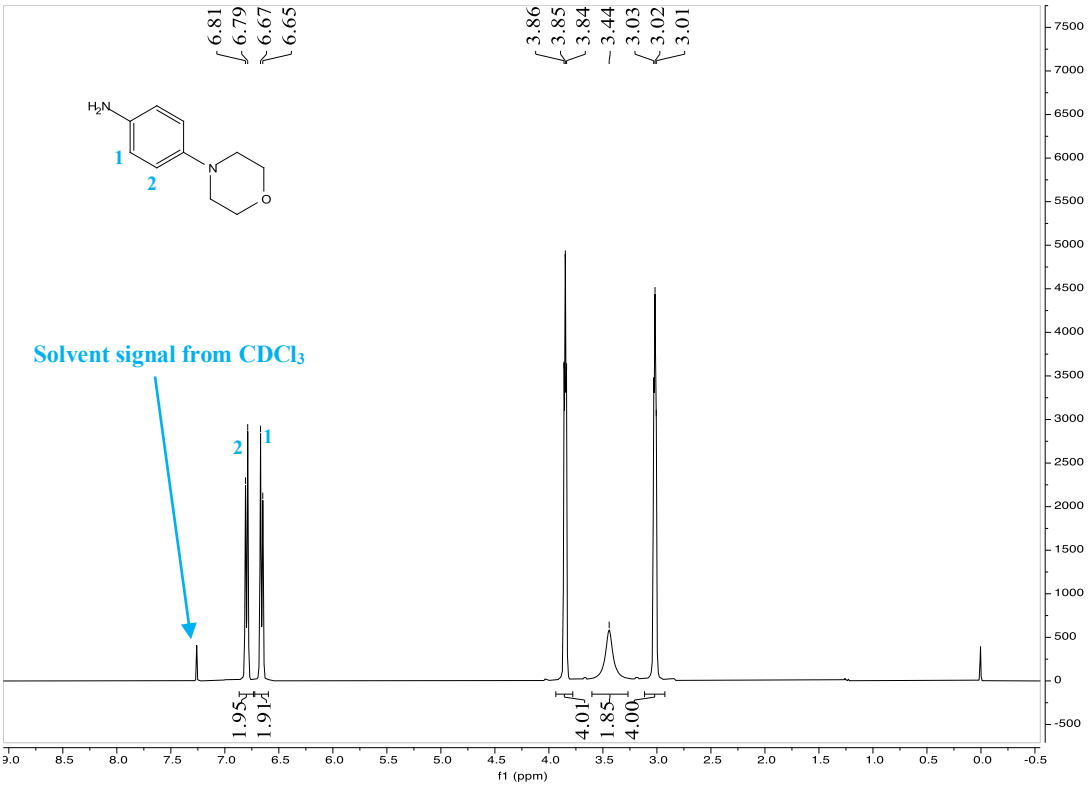

^{1}H NMR (400 MHz, $CDCl_3$) of product **29b**

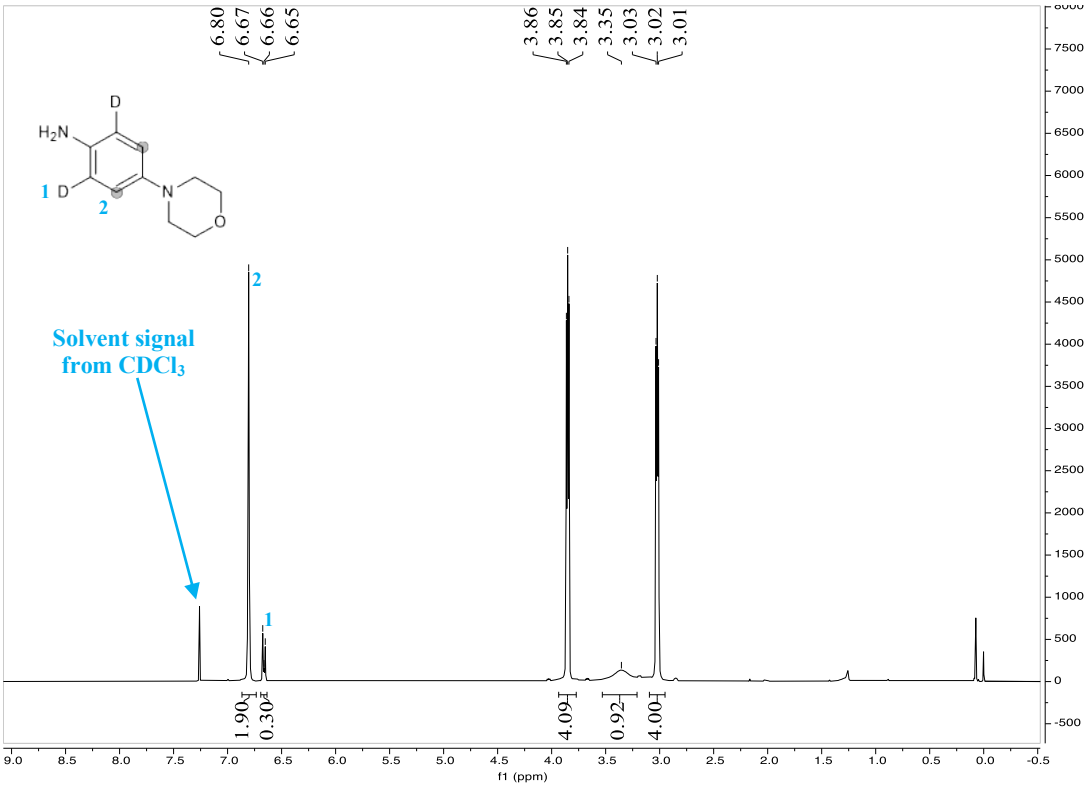

^{1}H NMR (400 MHz, D_2O) of feed material **30a**

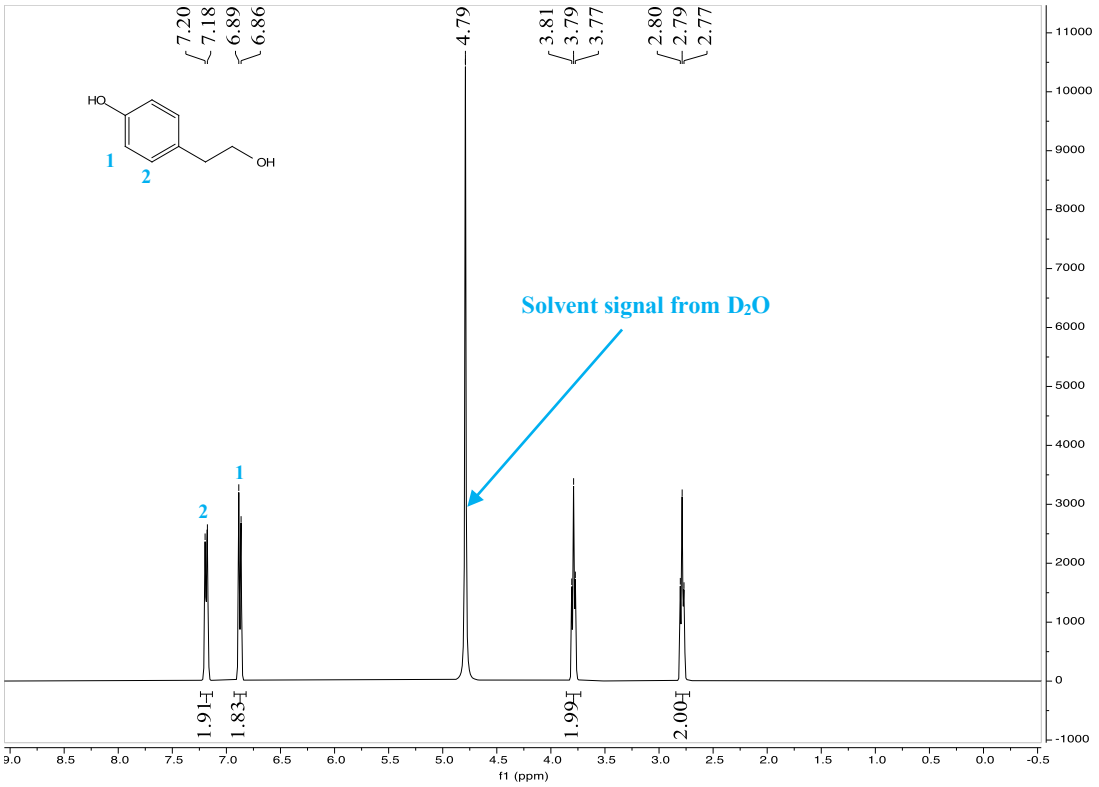

^{1}H NMR (400 MHz, D_2O) of product **30b**

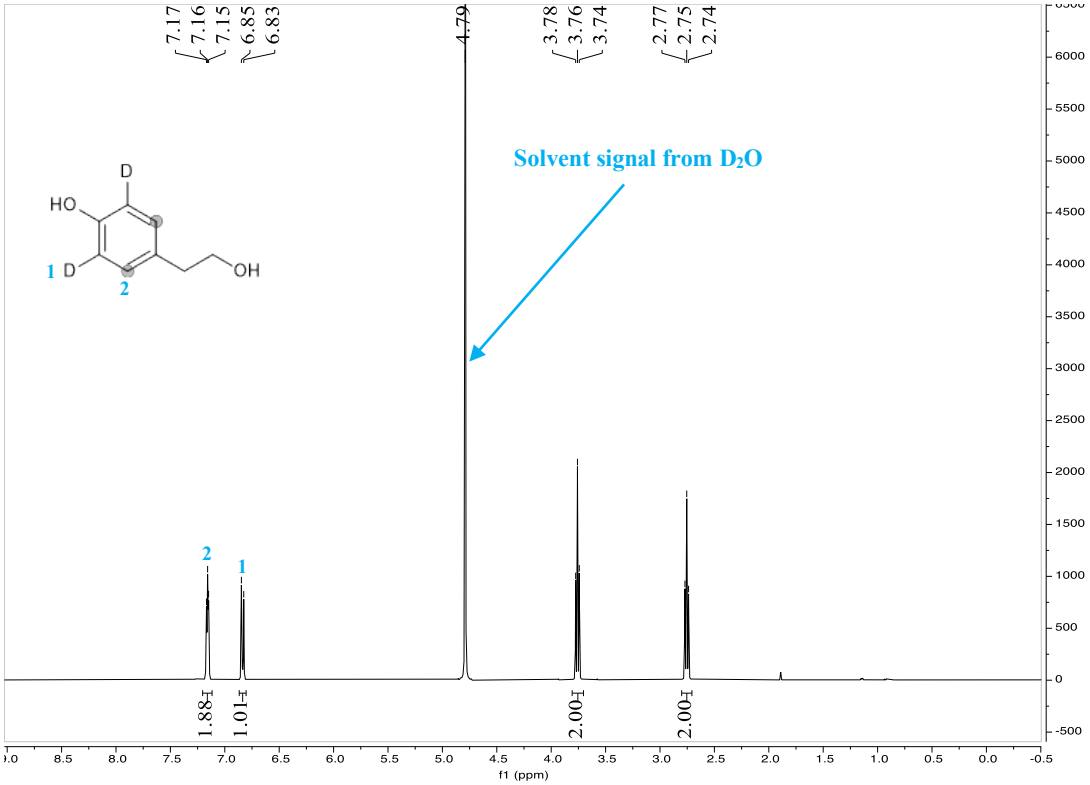

^{1}H NMR (400 MHz, DMSO-d_6) of feed material **31a**

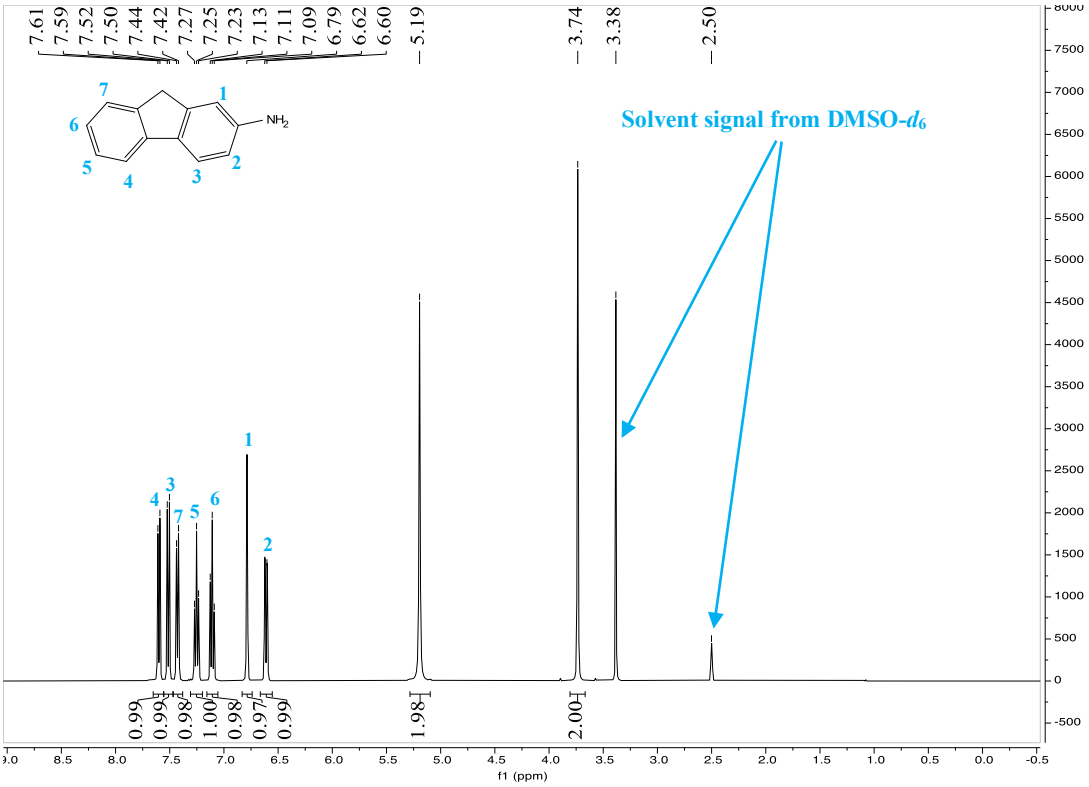

^{1}H NMR (400 MHz, DMSO-d_6) of product **31b**

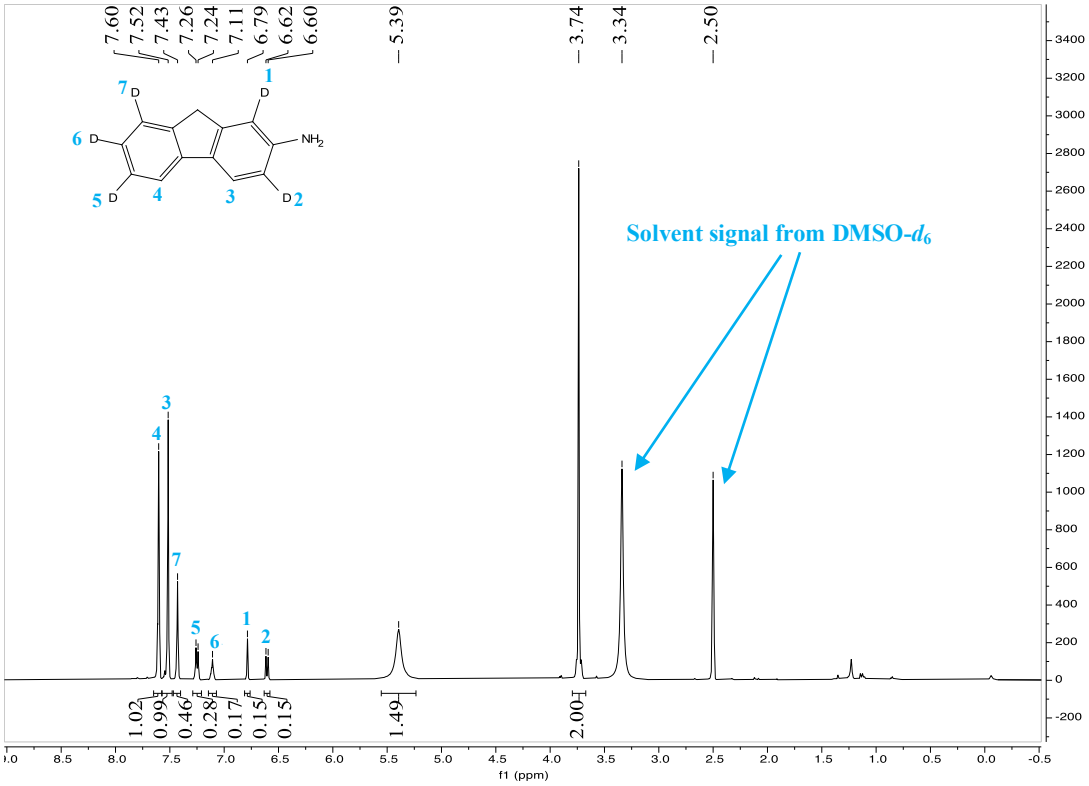

^{1}H NMR (400 MHz, D_2O) of feed material **32a**

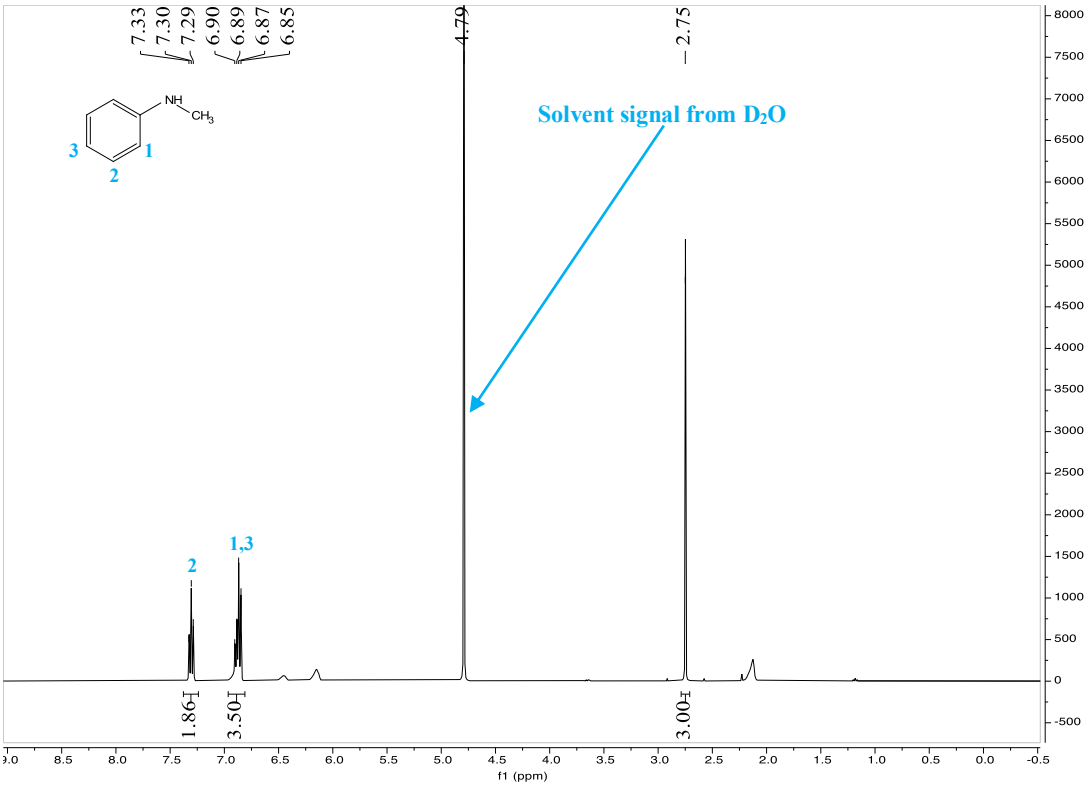

^{1}H NMR (400 MHz, D_2O) of product **32b**

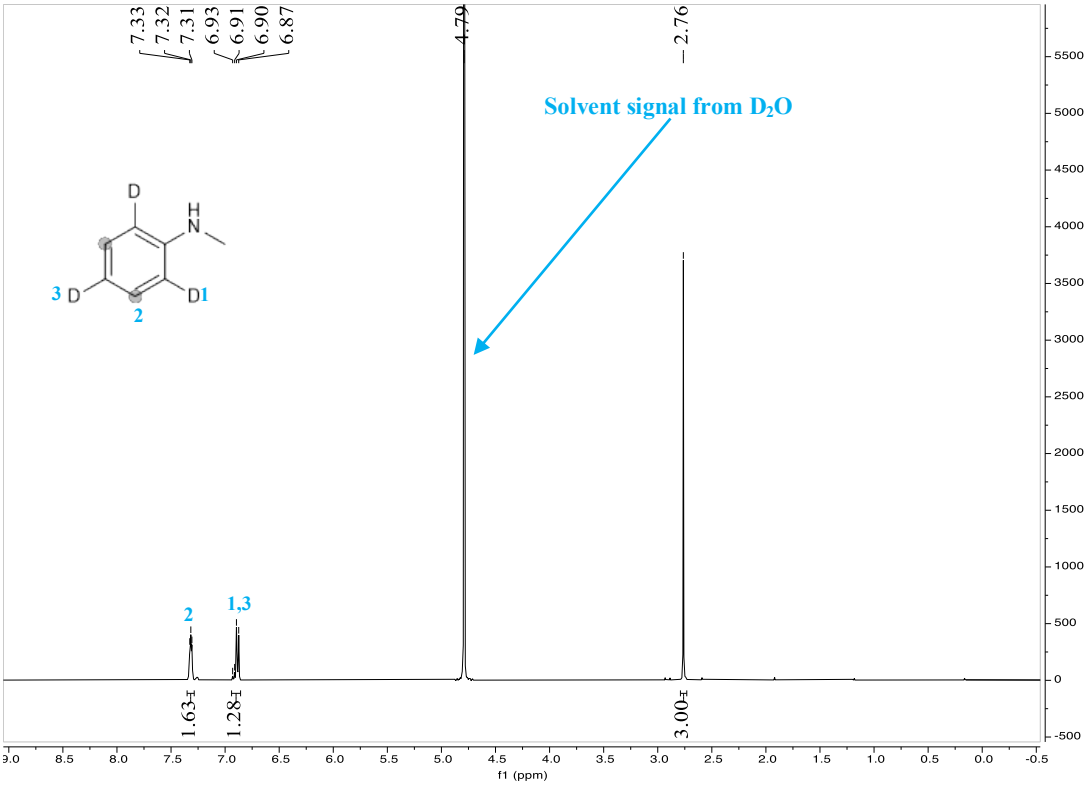

^{1}H NMR (400 MHz, D_2O) of feed material **33a**

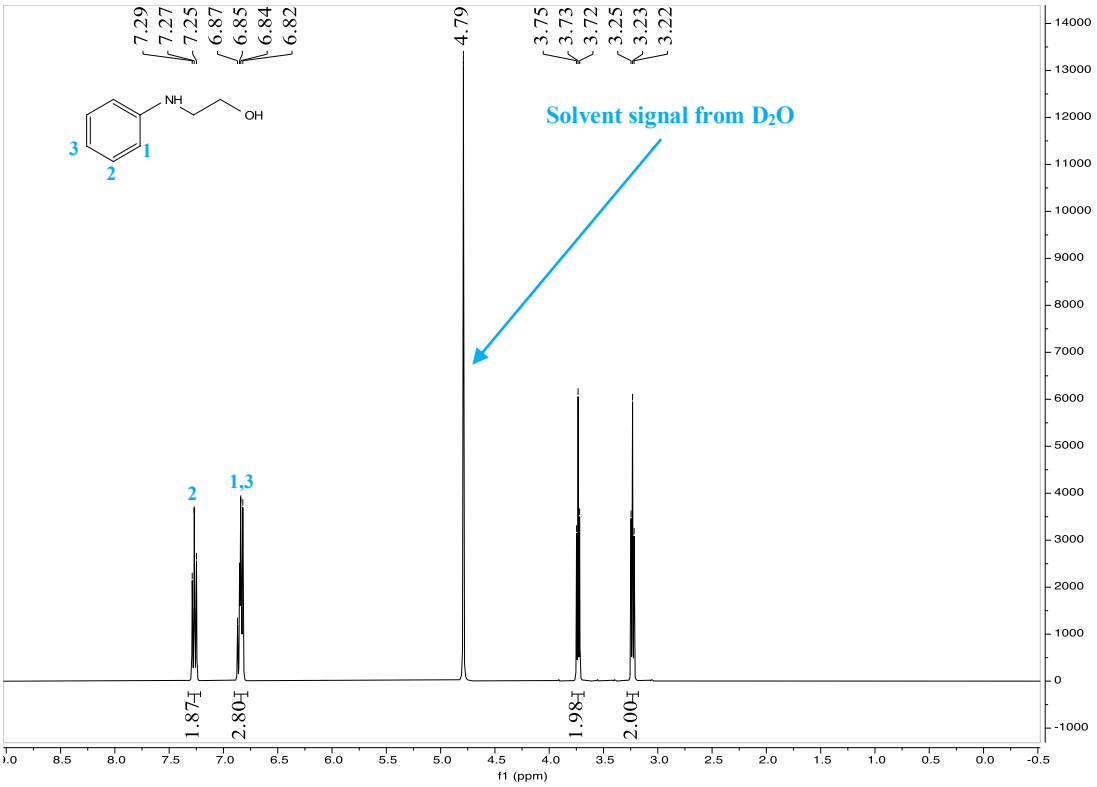

^{1}H NMR (400 MHz, D_2O) of product **33b**

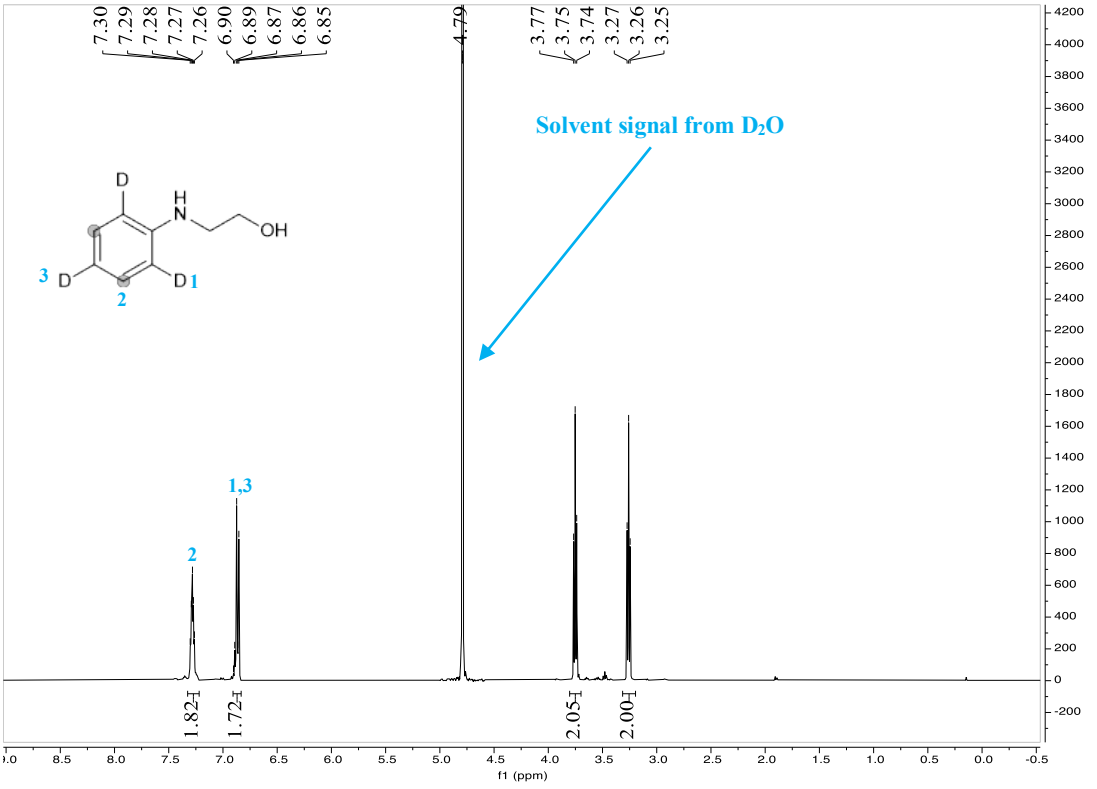

^{1}H NMR (400 MHz, $CDCl_3$) of feed material **34a**

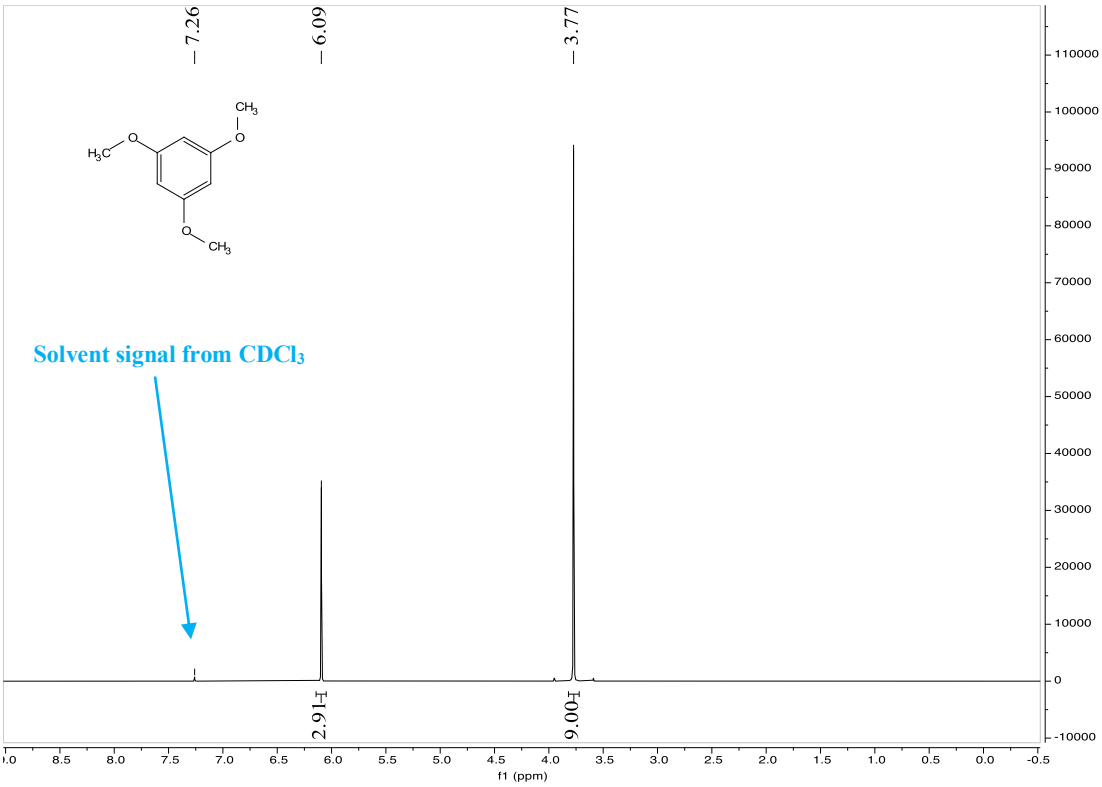

^{1}H NMR (400 MHz, $CDCl_3$) of product **34b**

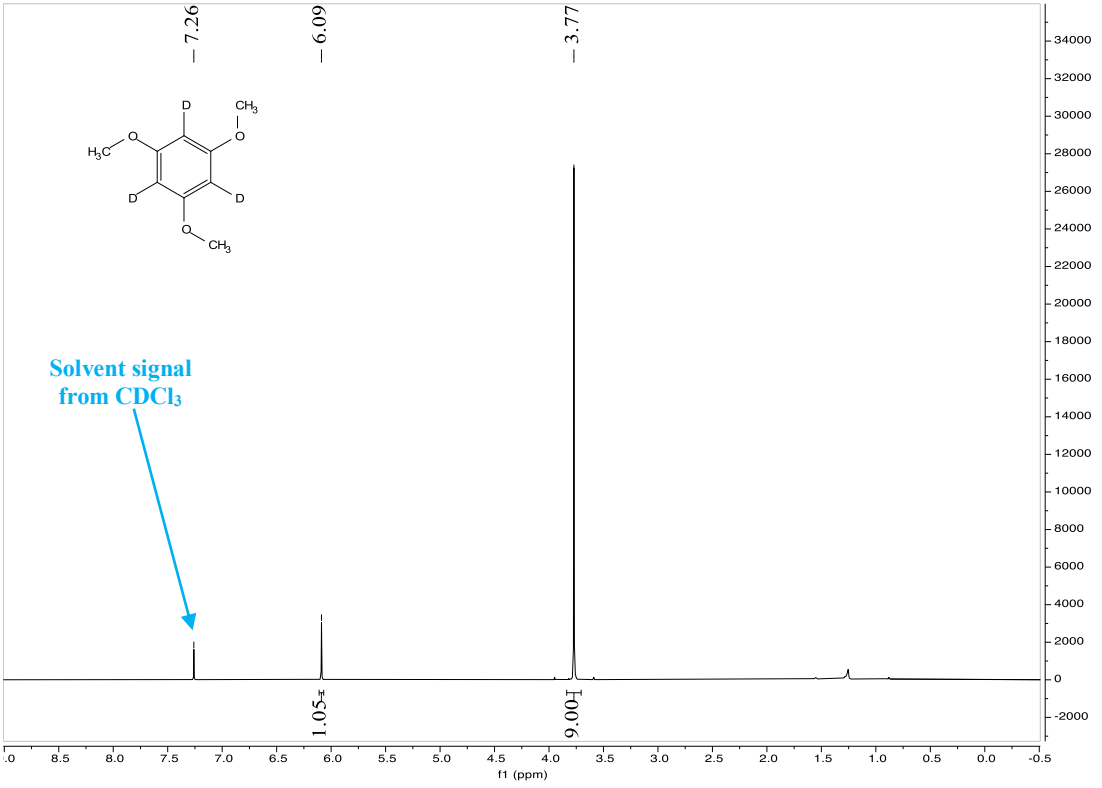

^{1}H NMR (400 MHz, DMSO-d_6) of feed material **35a**

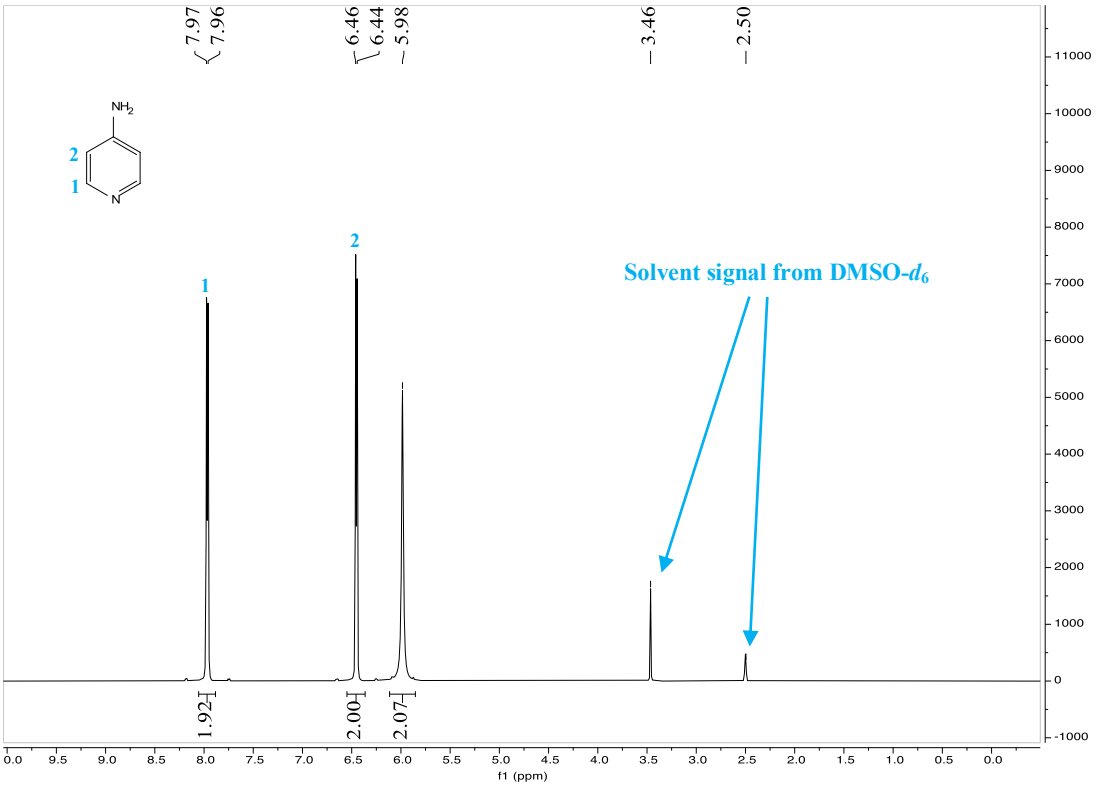

^{1}H NMR (400 MHz, DMSO-d_6) of product **35b**

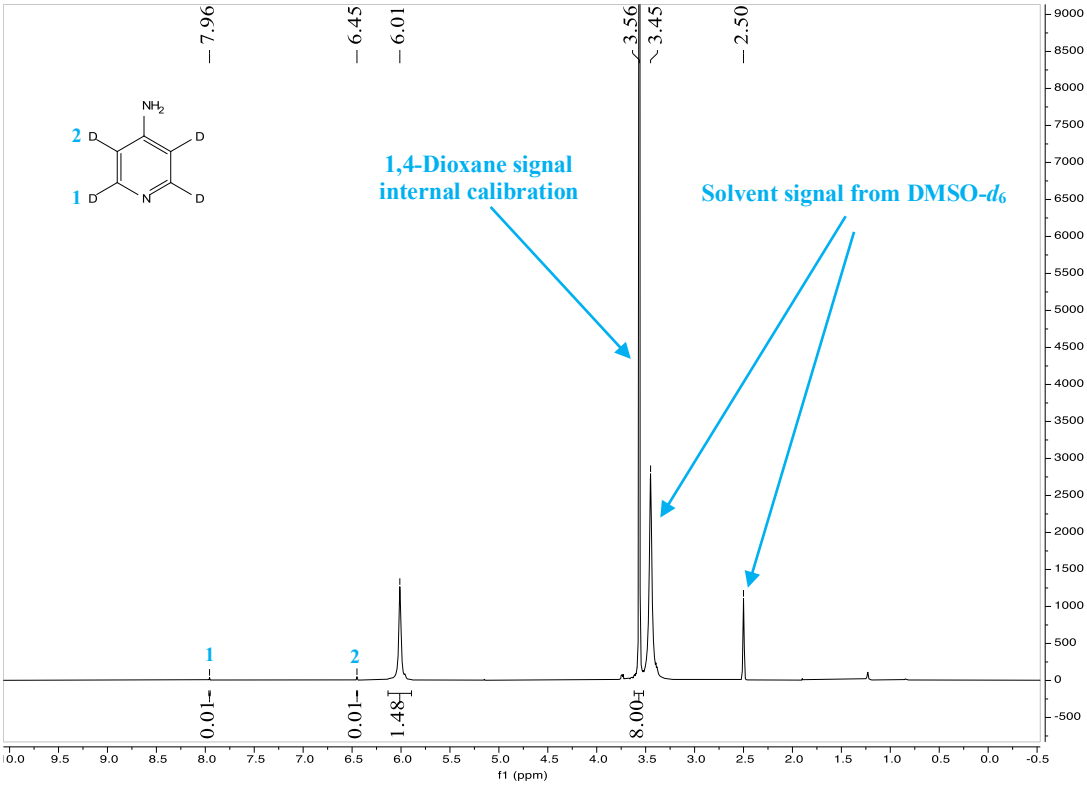

^{1}H NMR (400 MHz, DMSO-d_6) of feed material **36a**

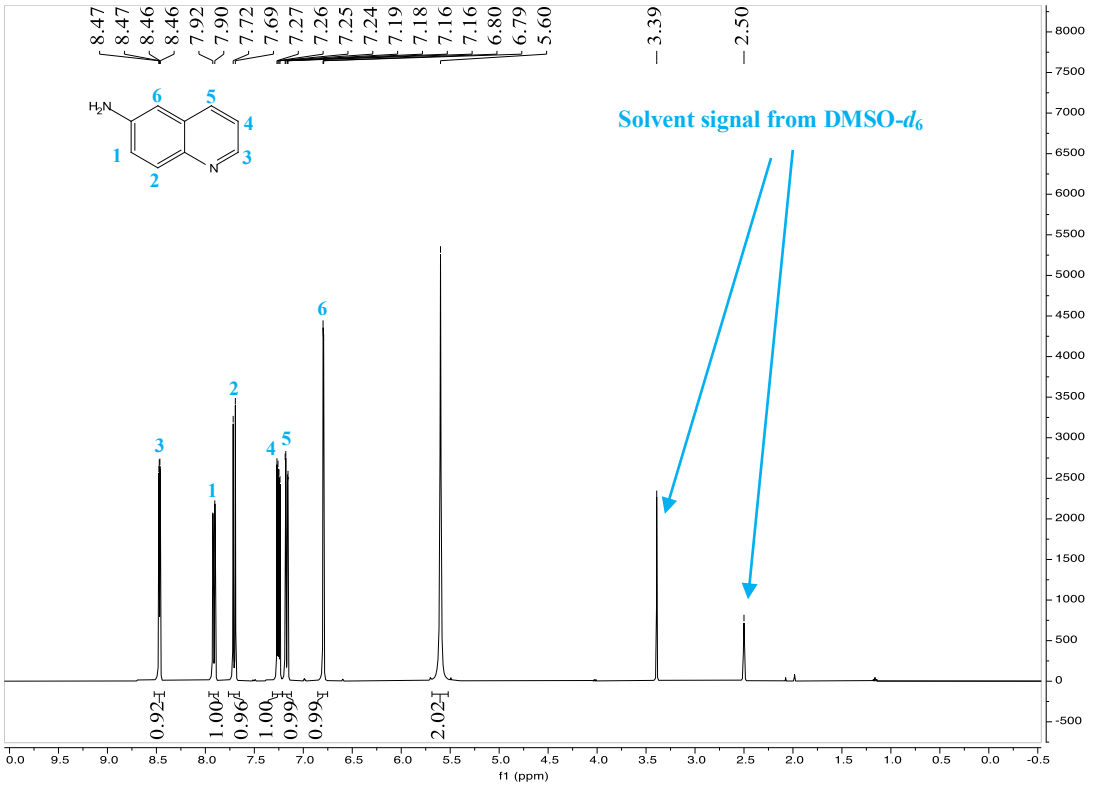

^{1}H NMR (400 MHz, DMSO-d_6) of product **36b**

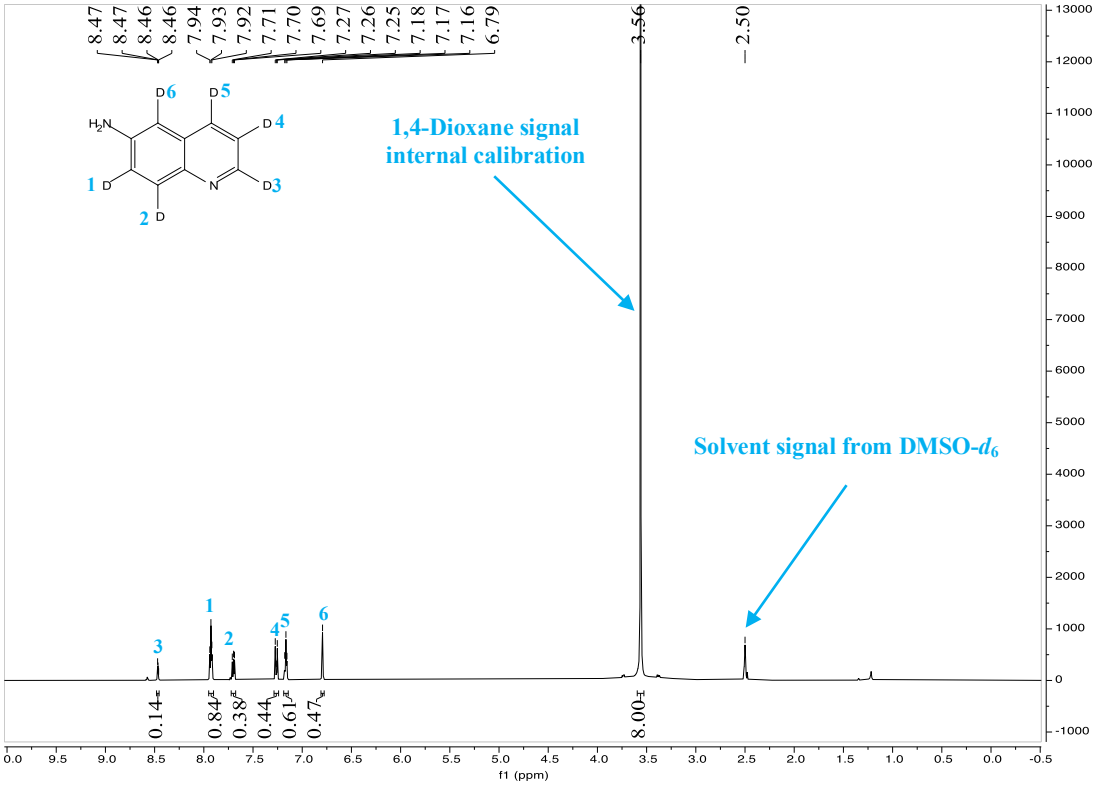

^{1}H NMR (400 MHz, DMSO-d_6) of feed material **37a**

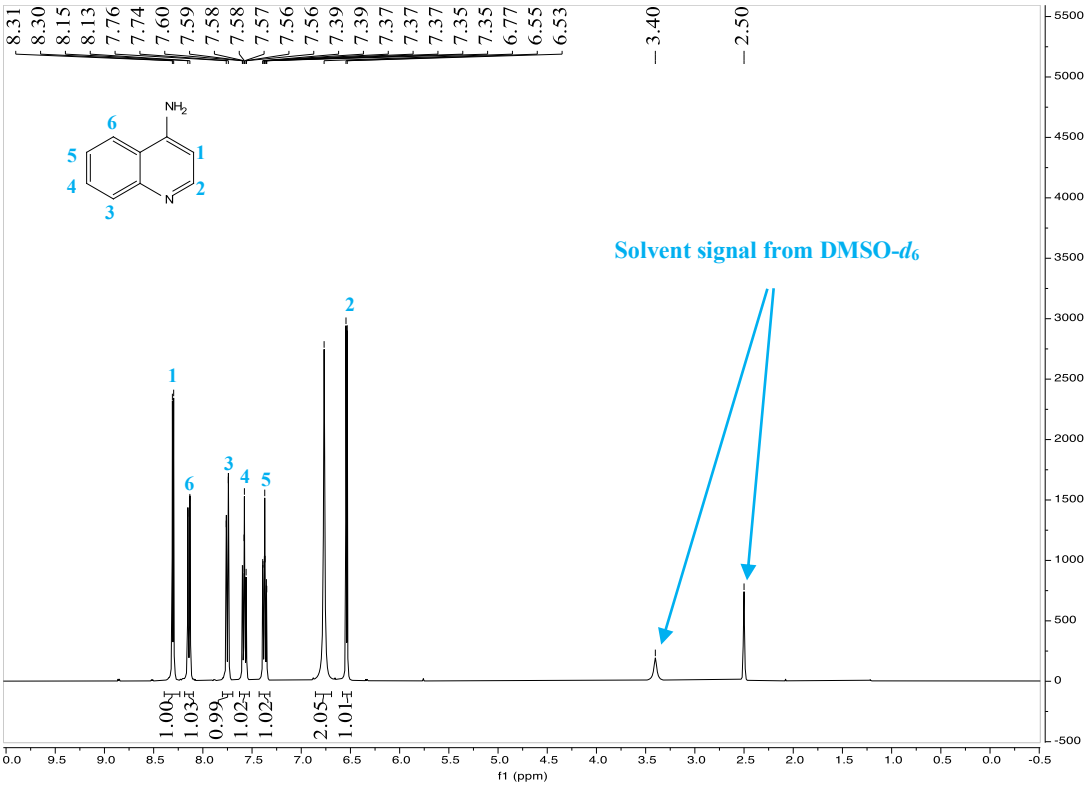

^{1}H NMR (400 MHz, DMSO-d_6) of product **37b**

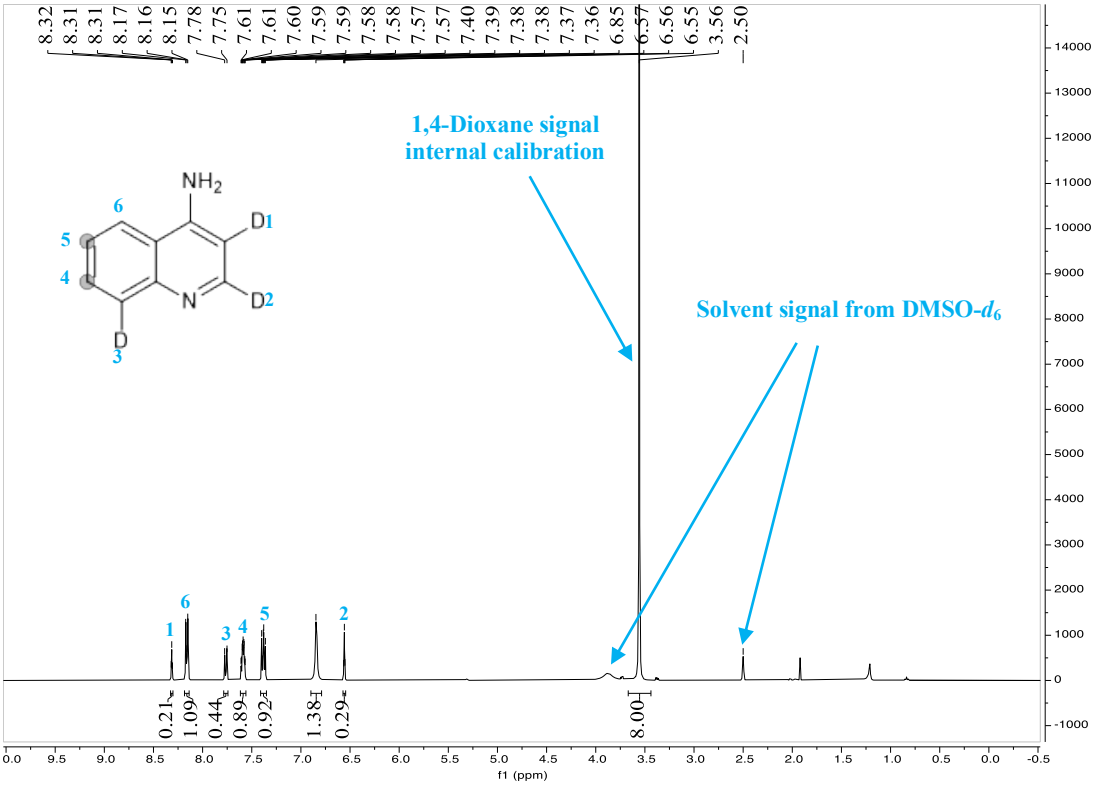

^{1}H NMR (400 MHz, DMSO-d_6) of feed material **38a**

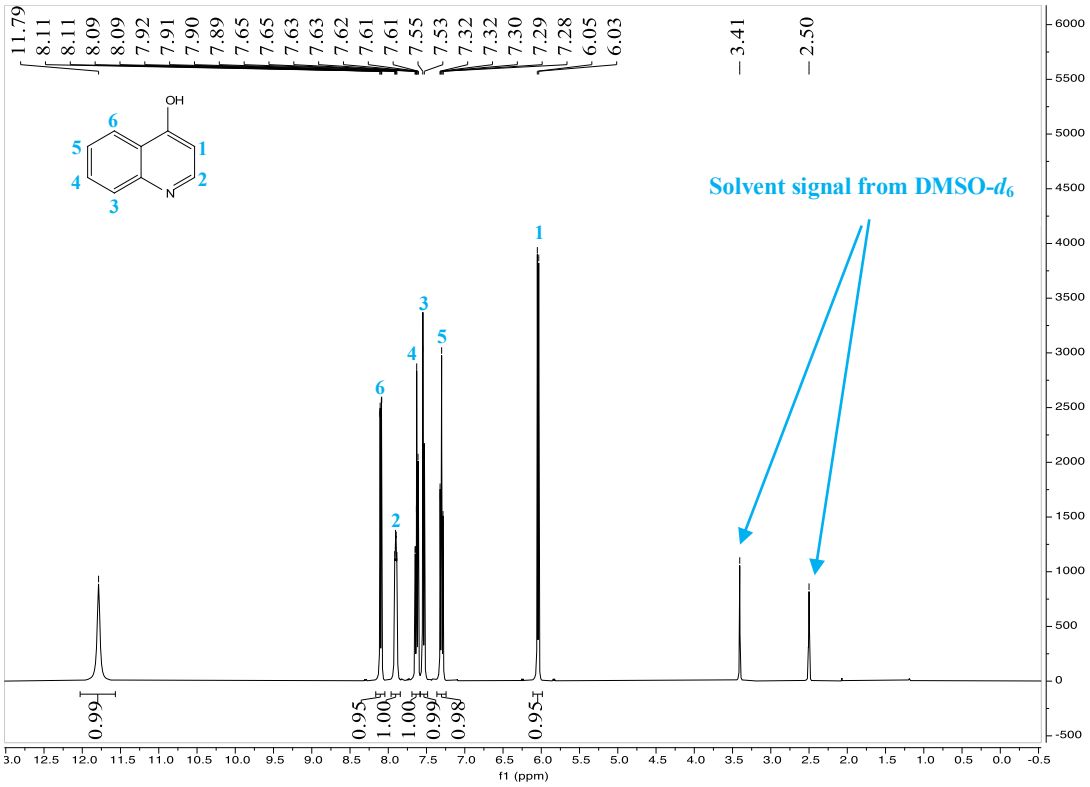

^{1}H NMR (400 MHz, DMSO-d_6) of product **38b**

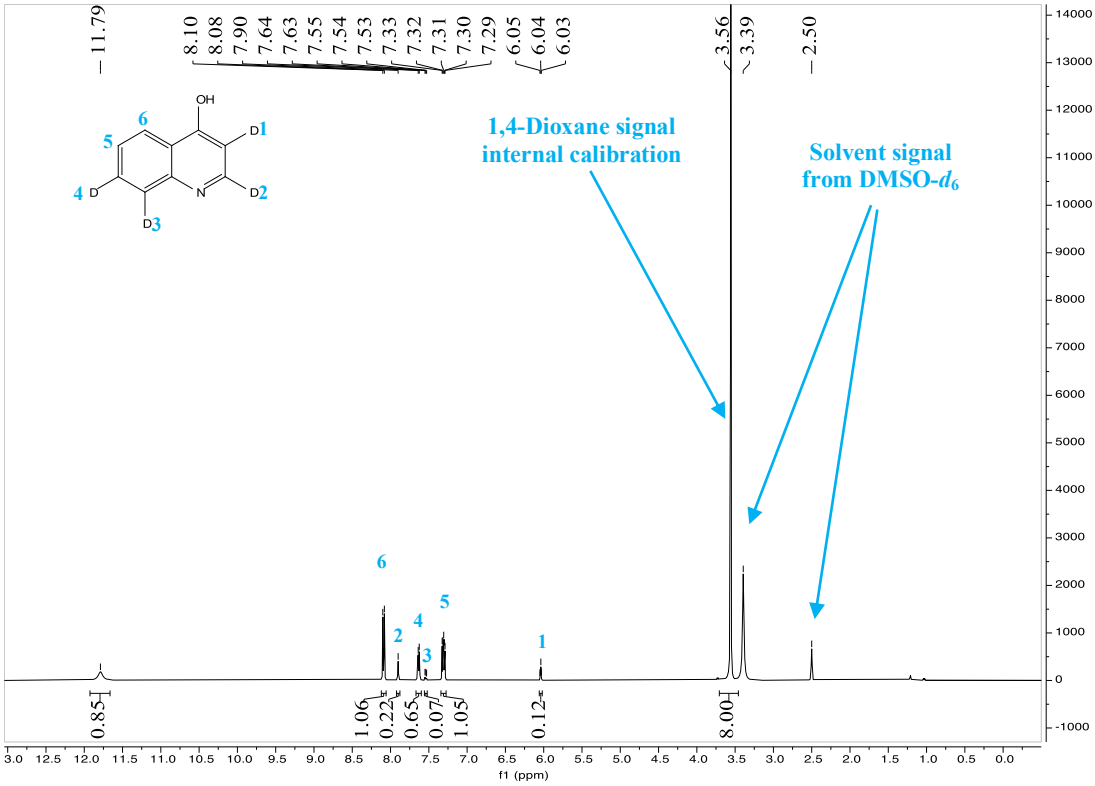

^{1}H NMR (400 MHz, D_2O) of feed material **39a**

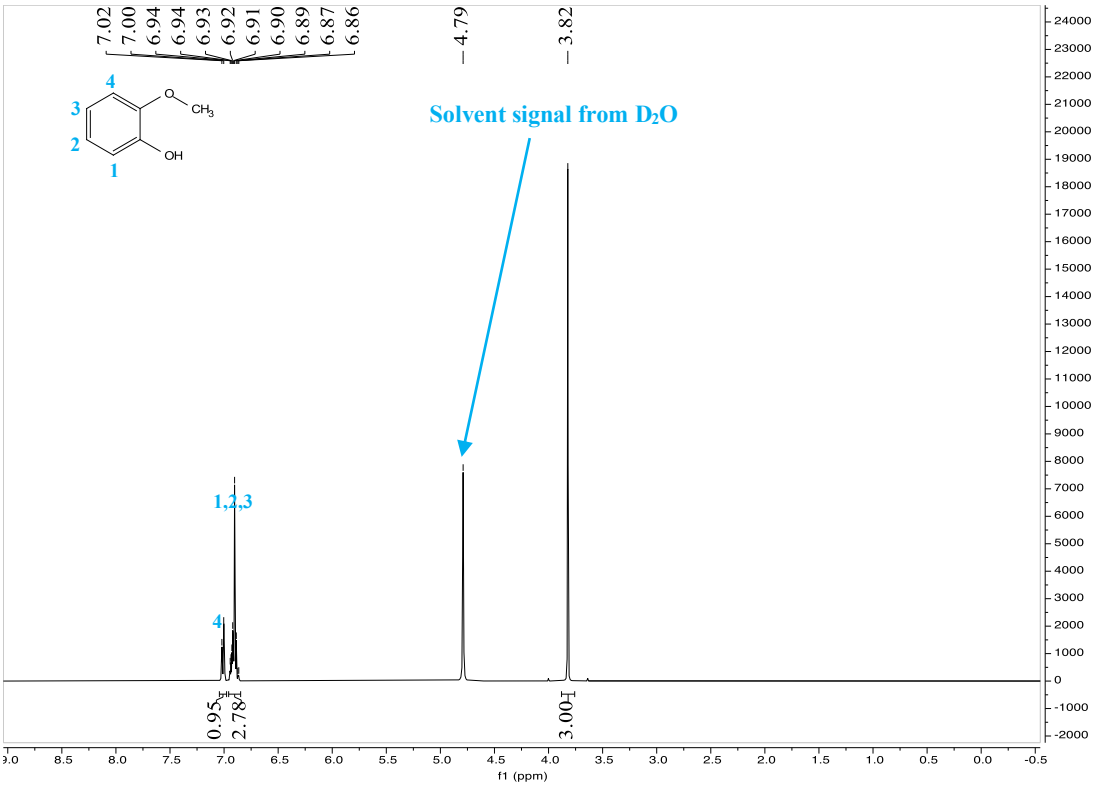

^{1}H NMR (400 MHz, D_2O) of product **39b**

^{1}H NMR (400 MHz, DMSO-d_6) of feed material **40a**

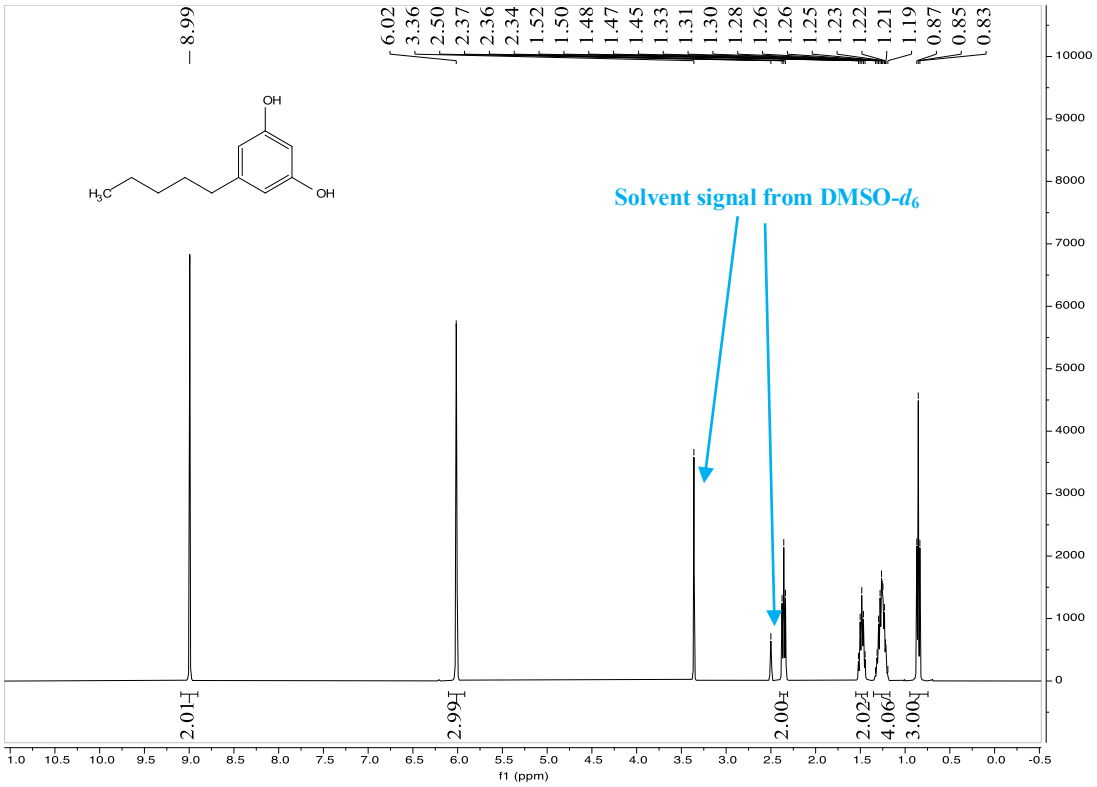

^{1}H NMR (400 MHz, DMSO-d_6) of product **40b**

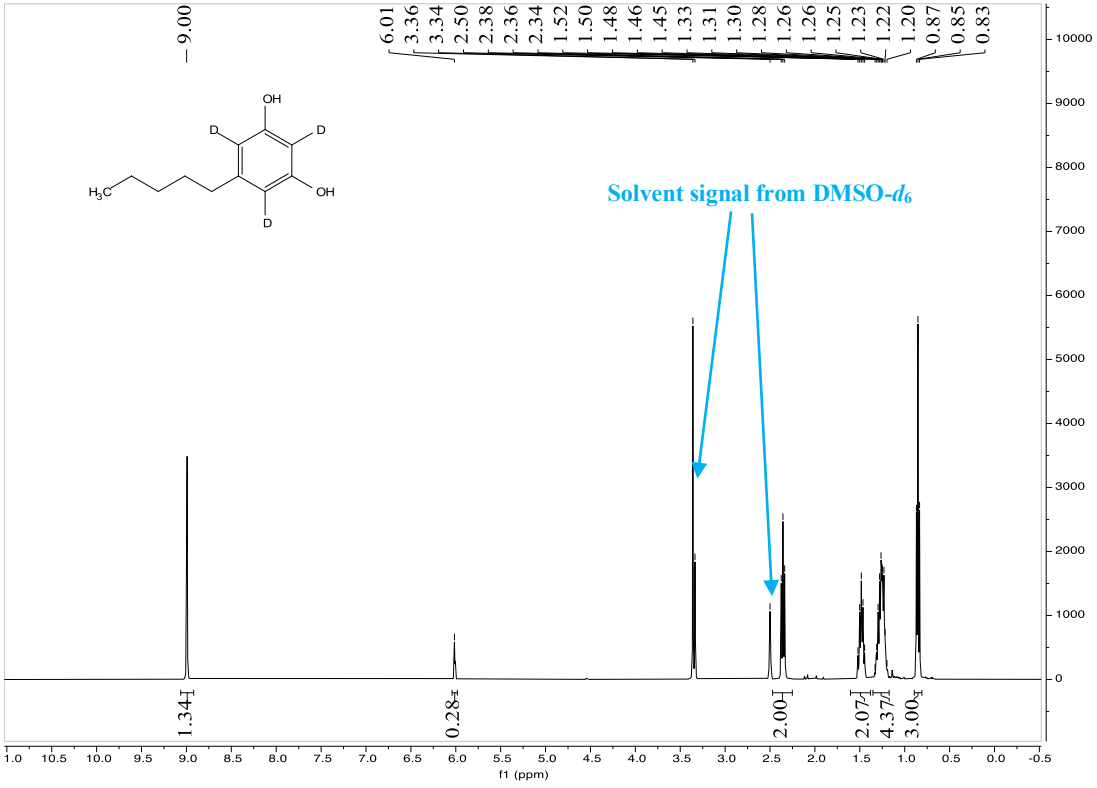

^{1}H NMR (400 MHz, D_2O) of feed material **41a**

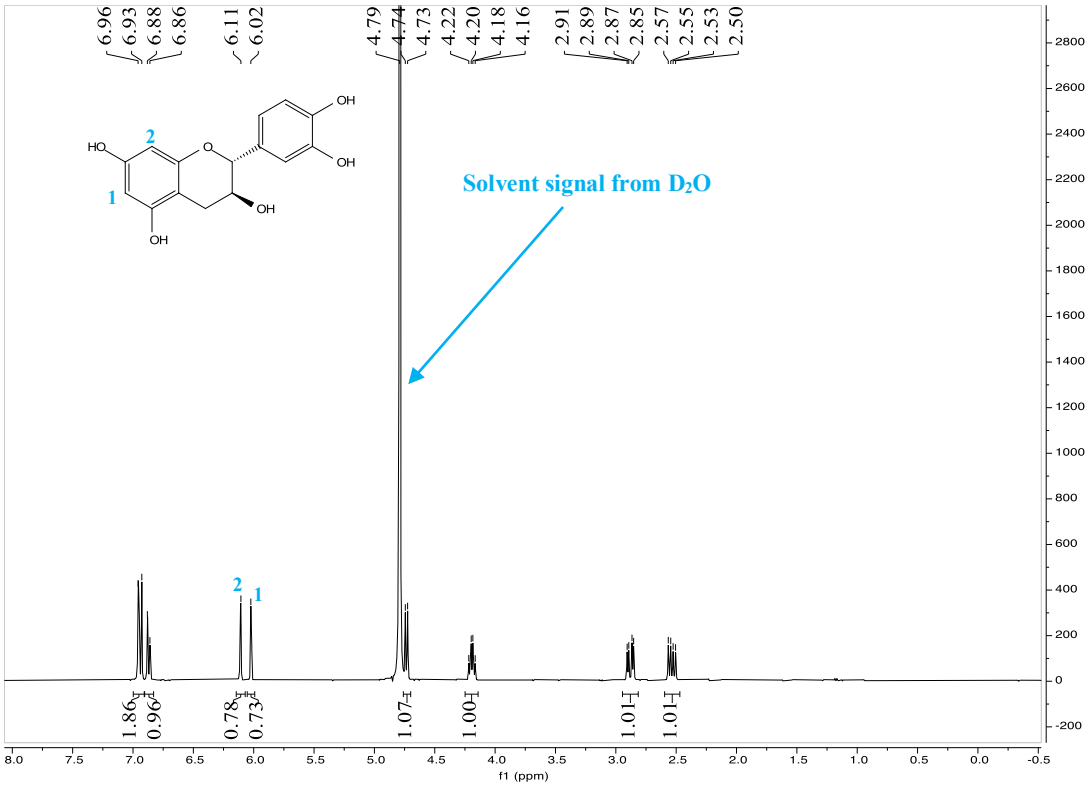

^{1}H NMR (400 MHz, D_2O) of product **41b**

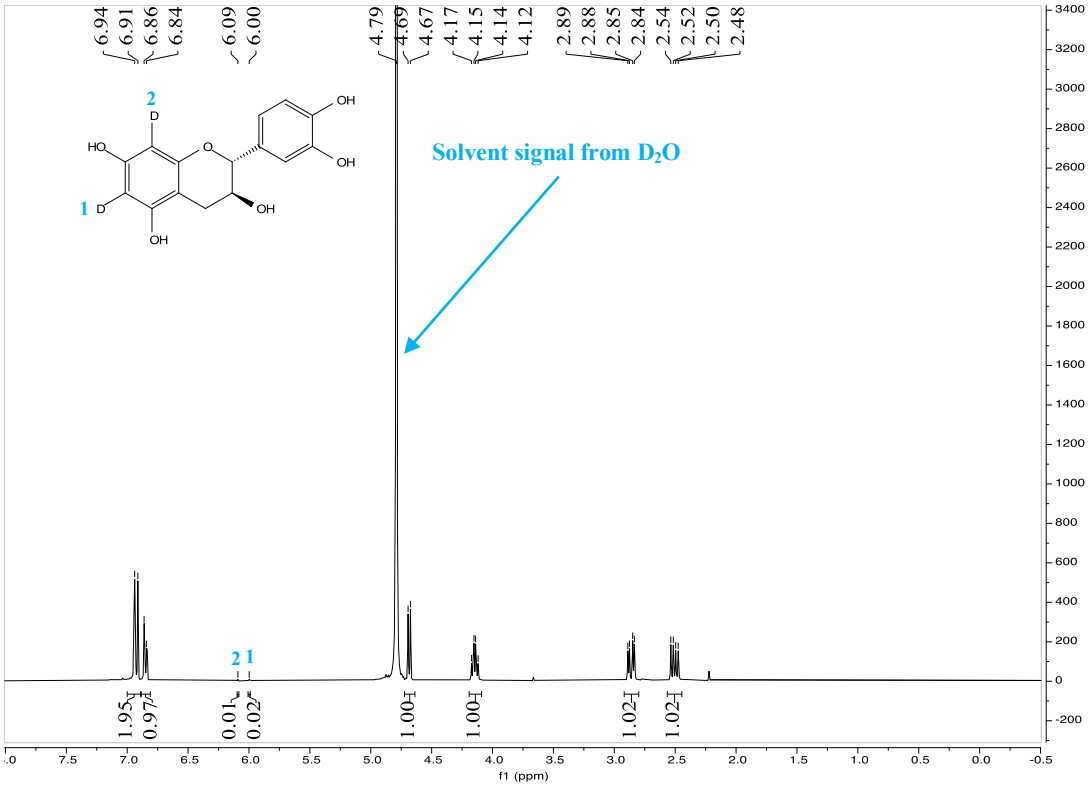

^{1}H NMR (400 MHz, DMSO-d_6) of feed material **42a**

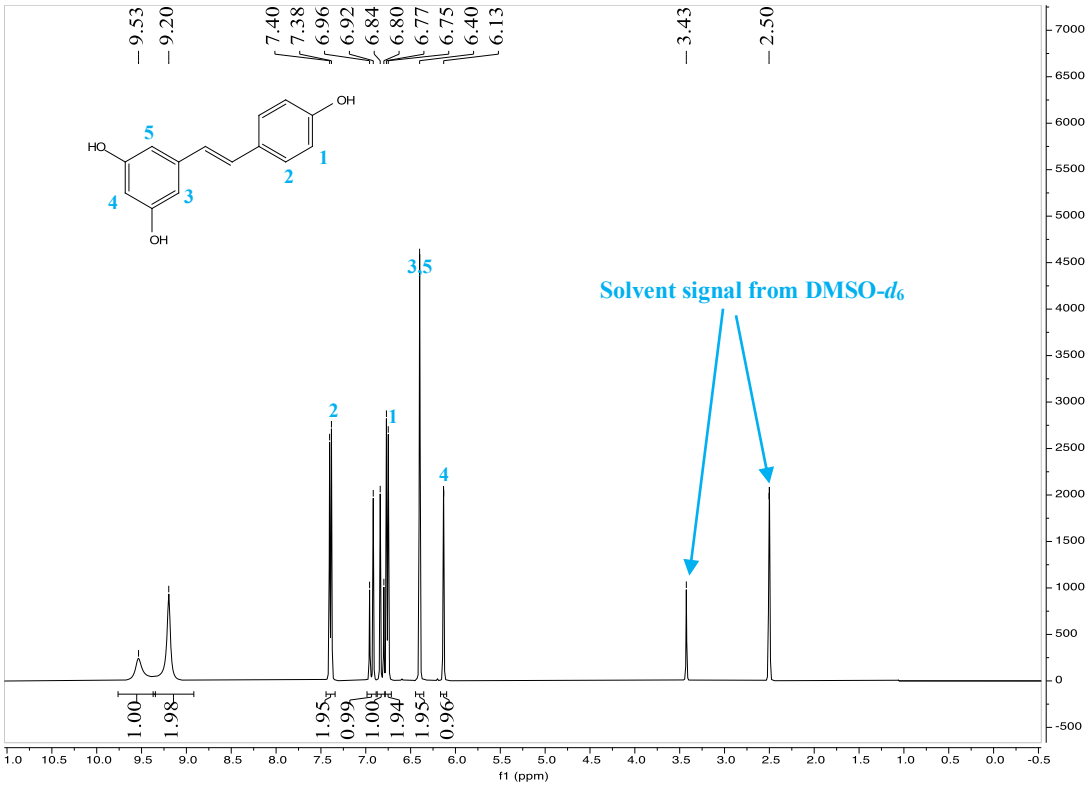

^{1}H NMR (400 MHz, DMSO-d_6) of product **42b**

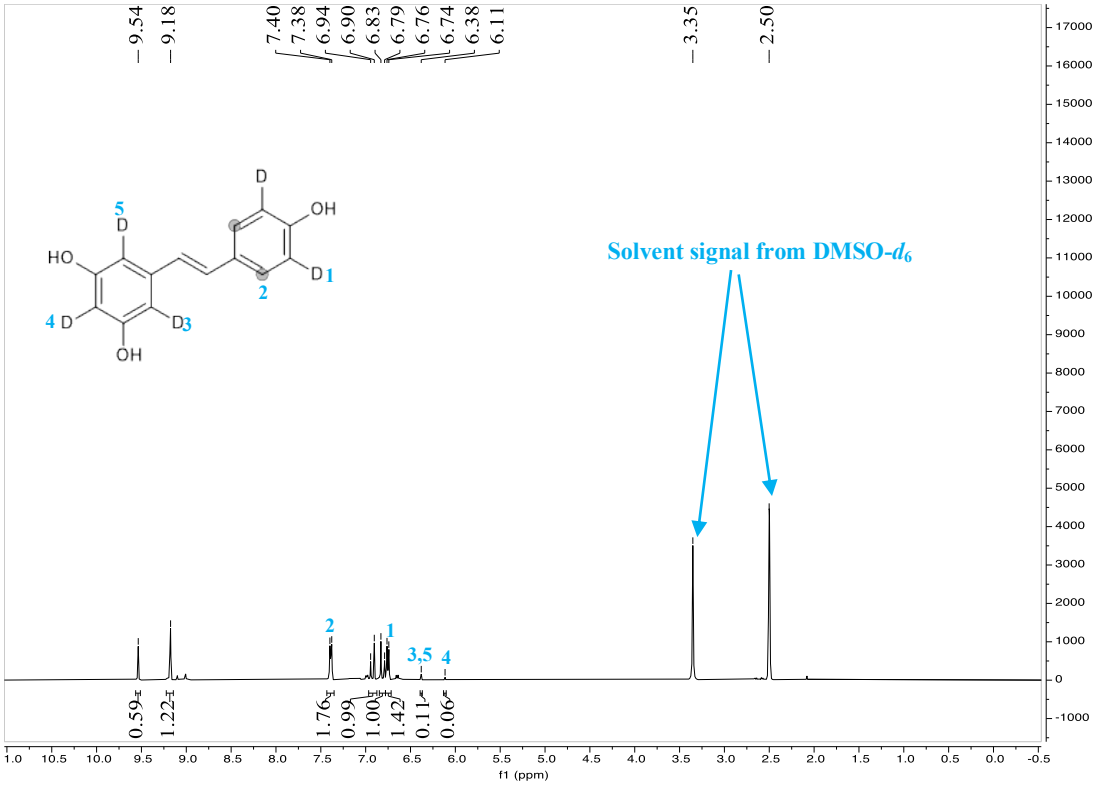

^{1}H NMR (400 MHz, DMSO-d_6) of feed material **43a**

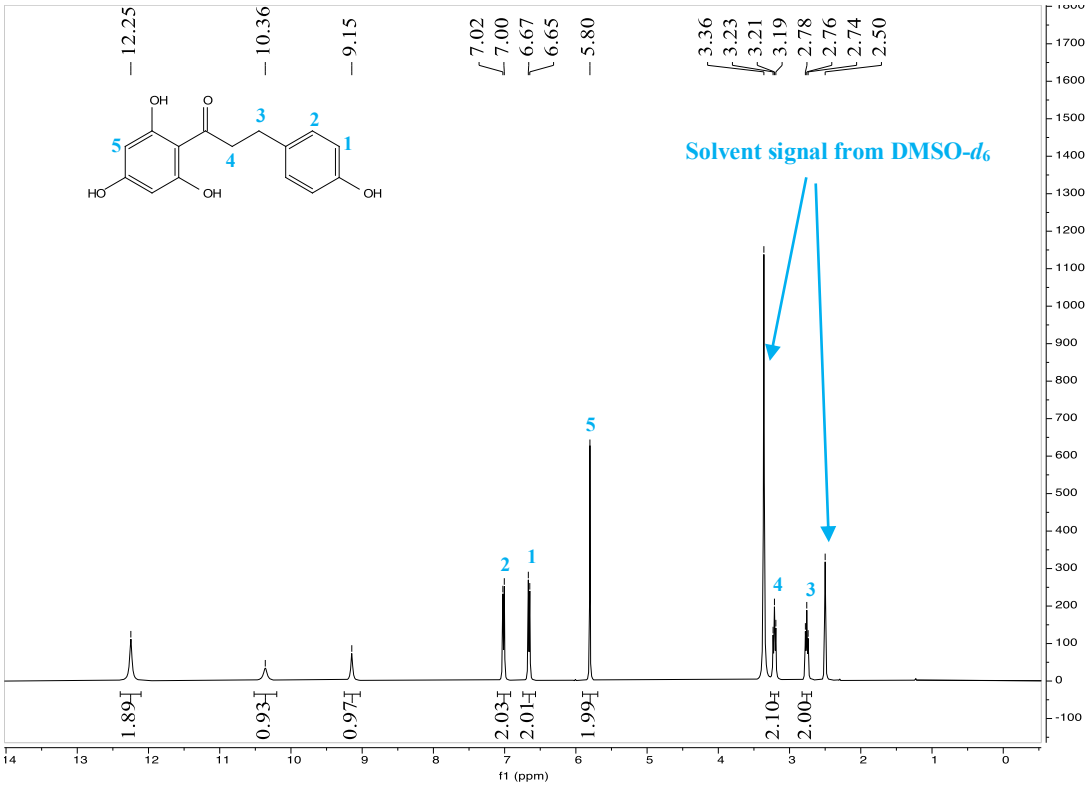

^{1}H NMR (400 MHz, DMSO-d_6) of product **43b**

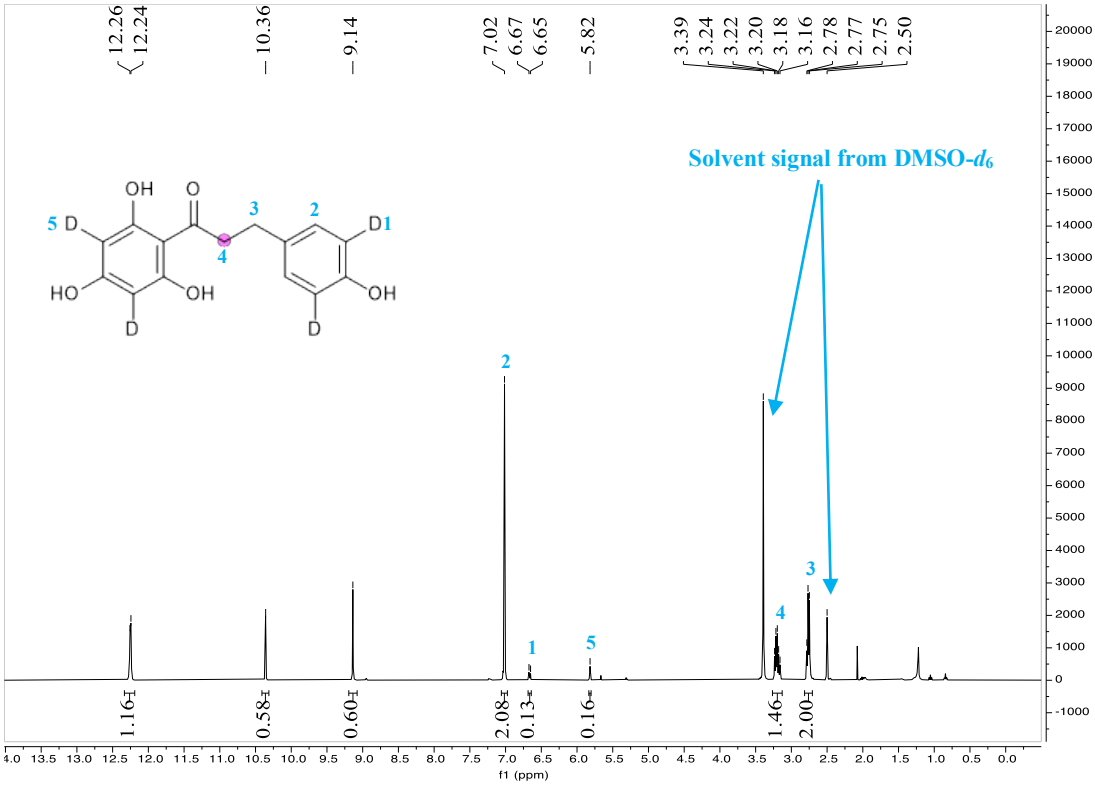

^{1}H NMR (400 MHz, D_2O) of feed material **44a**

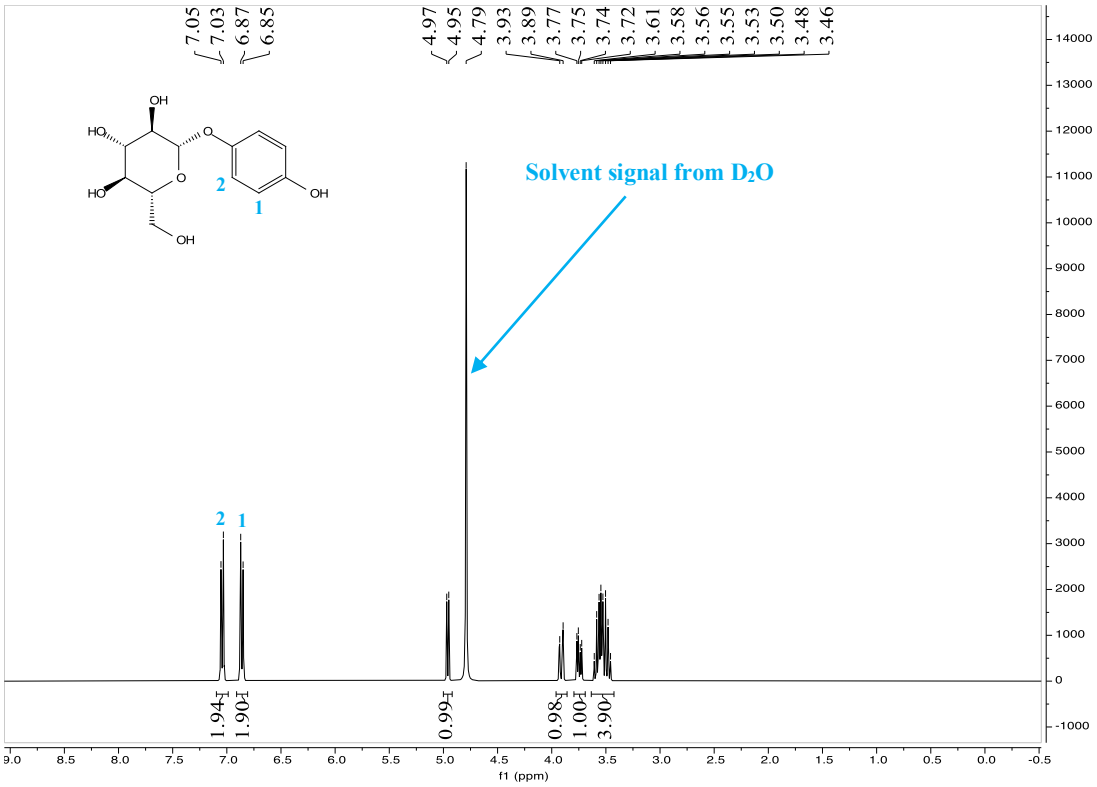

^{1}H NMR (400 MHz, D_2O) of product **44b**

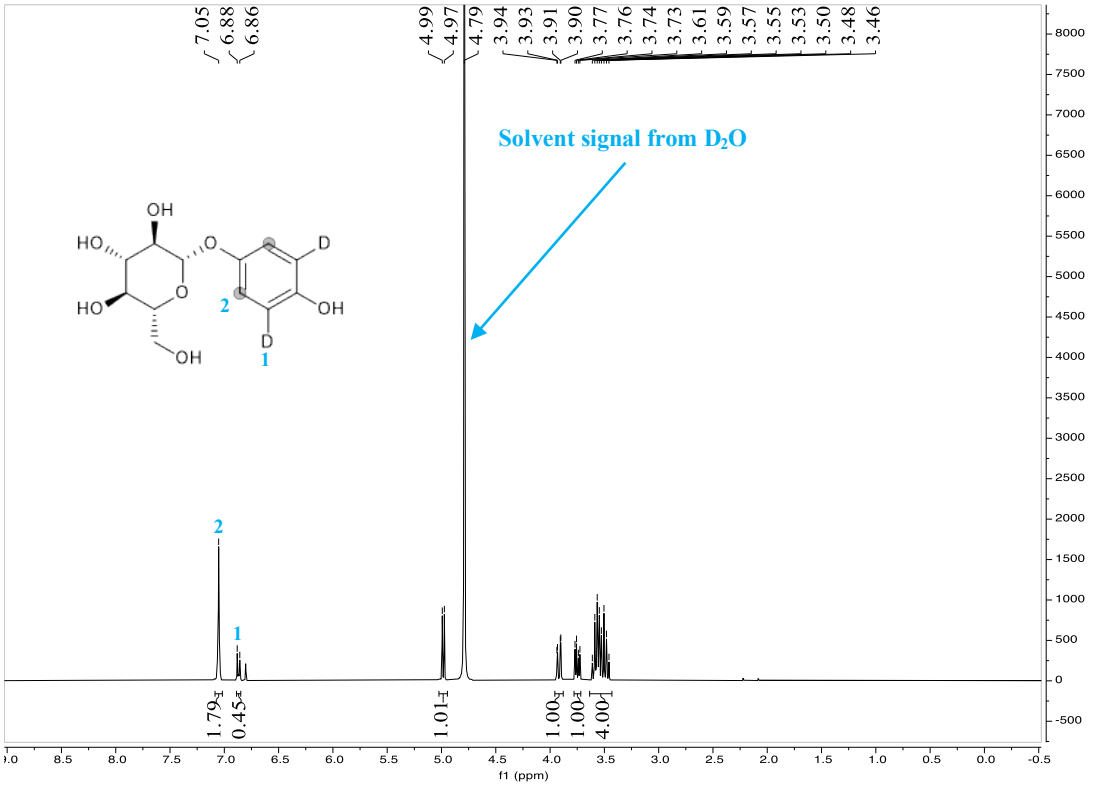

^{1}H NMR (400 MHz, DMSO-d_6) of feed material **45a**

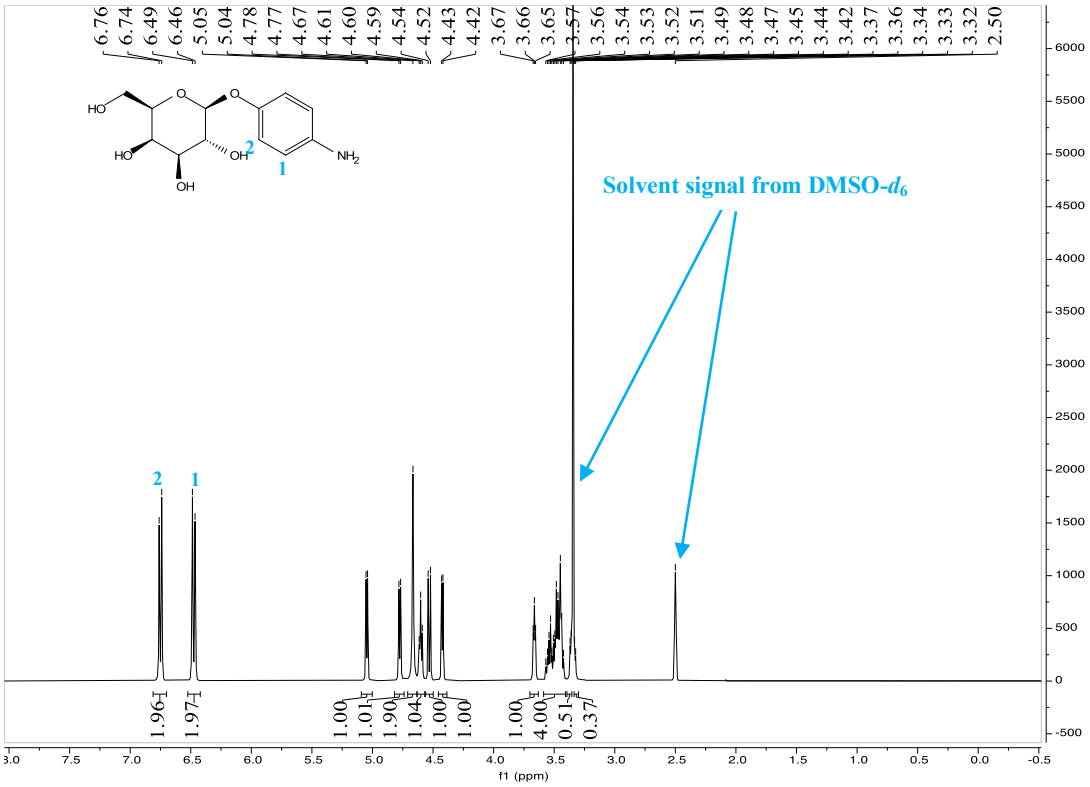

^{1}H NMR (400 MHz, DMSO-d_6) of product **45b**

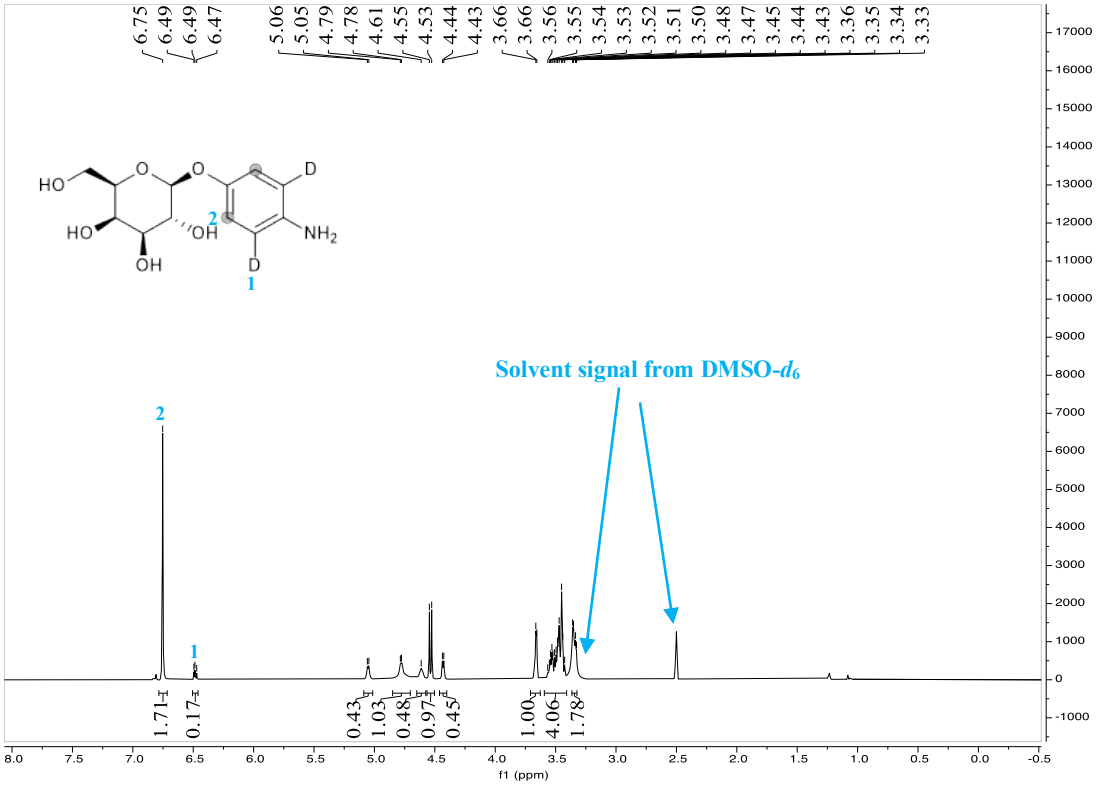

^{1}H NMR (400 MHz, DMSO-d_6) of feed material **46a**

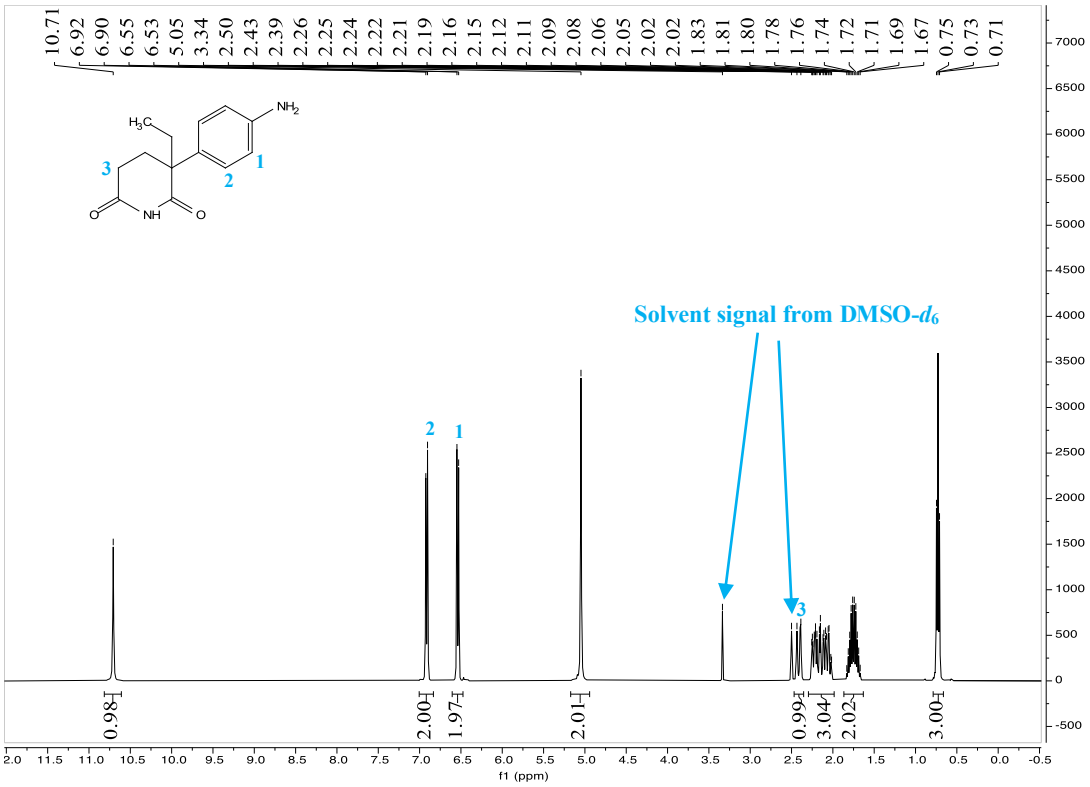

^{1}H NMR (400 MHz, DMSO-d_6) of product **46b**

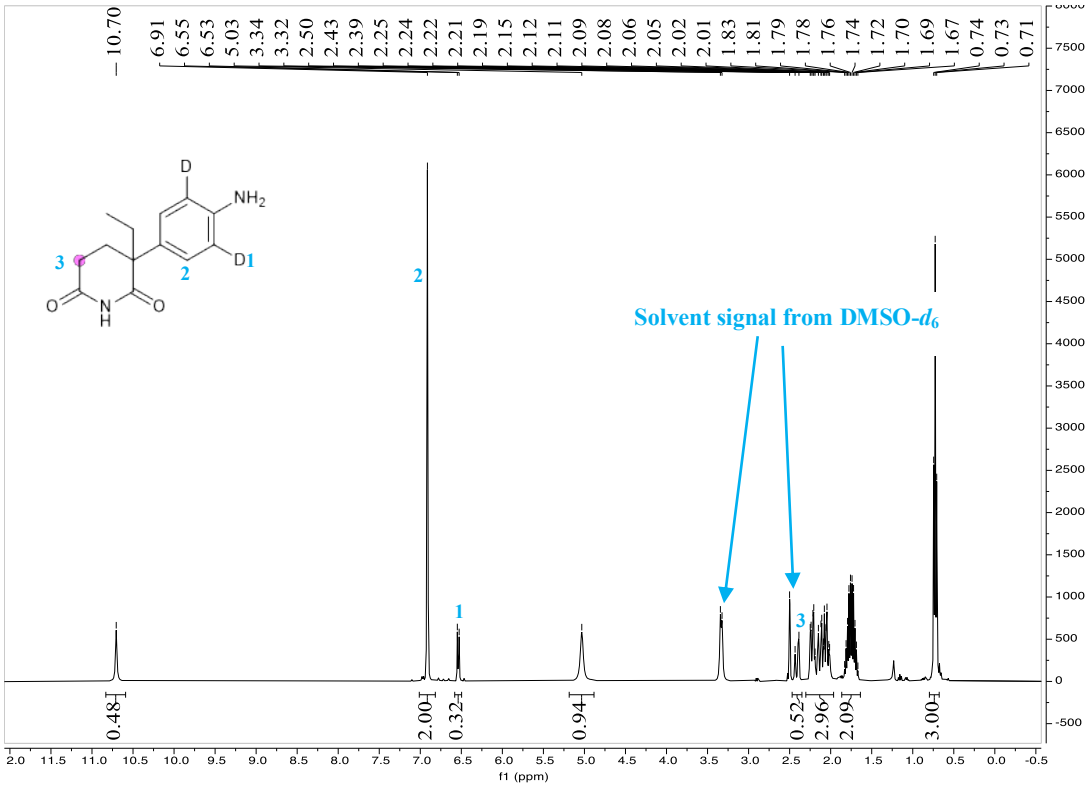

^{1}H NMR (400 MHz, $CDCl_3$) of feed material **47a**

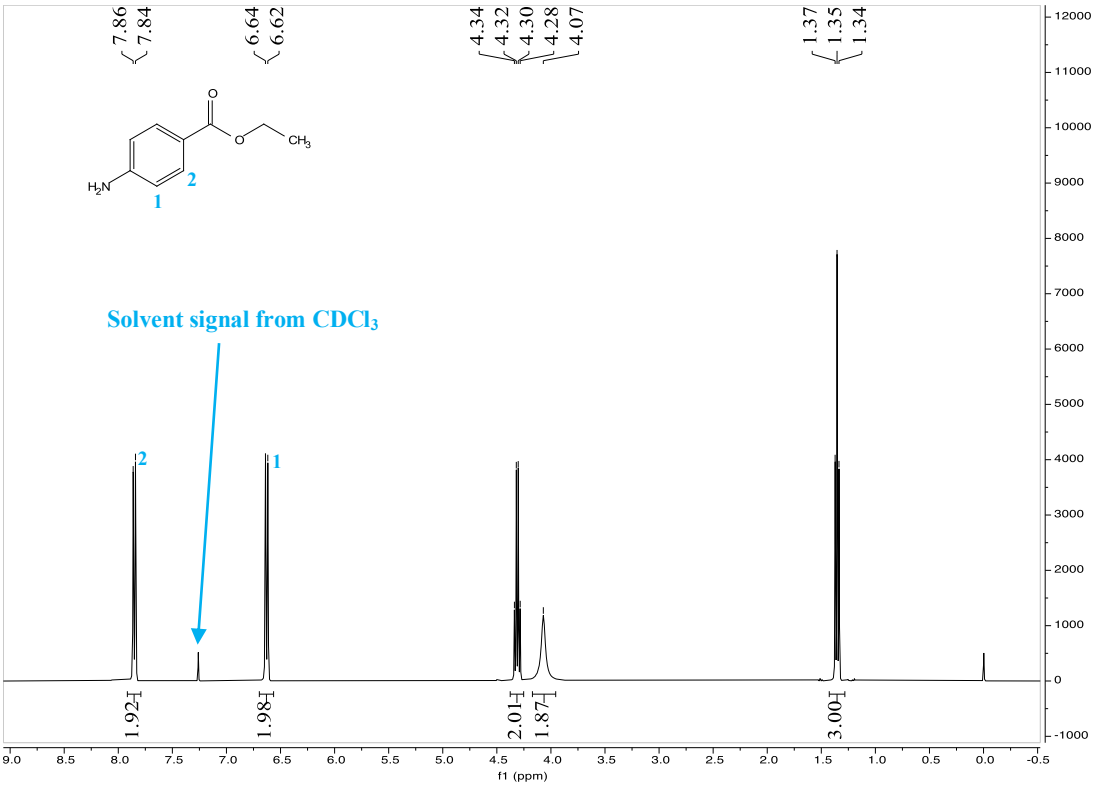

^{1}H NMR (400 MHz, $CDCl_3$) of product **47b**

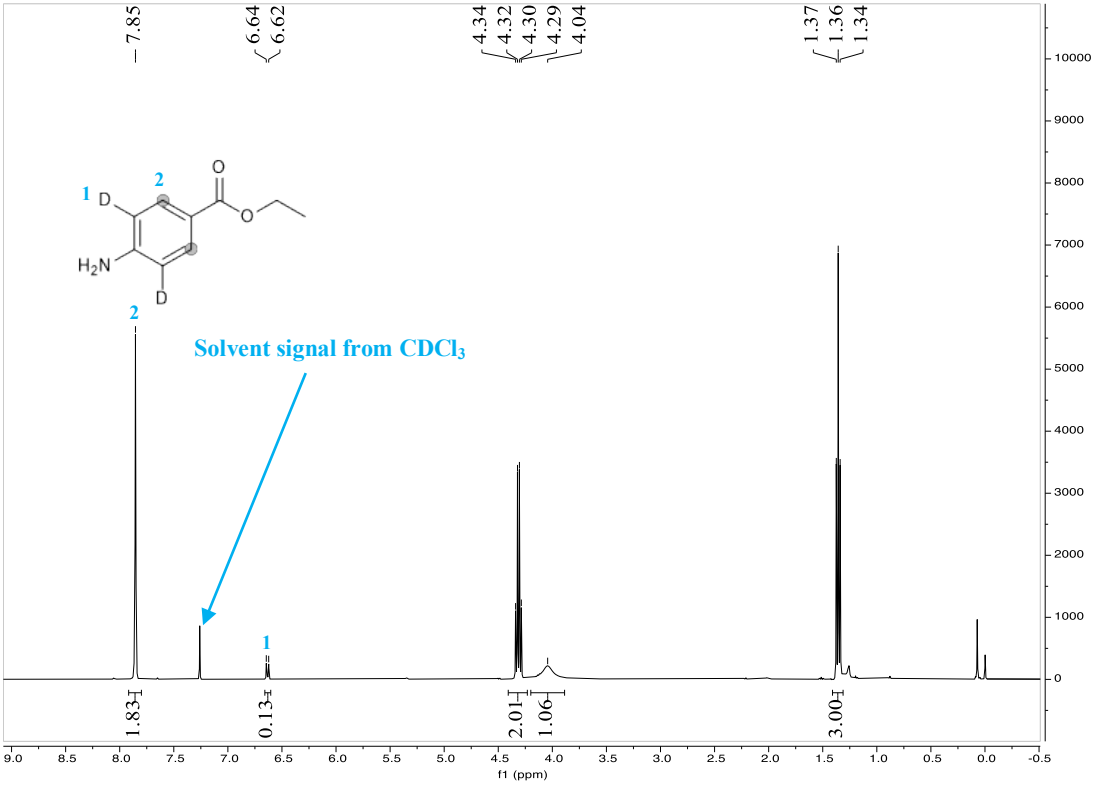

^{1}H NMR (400 MHz, D_2O) of feed material **48a**

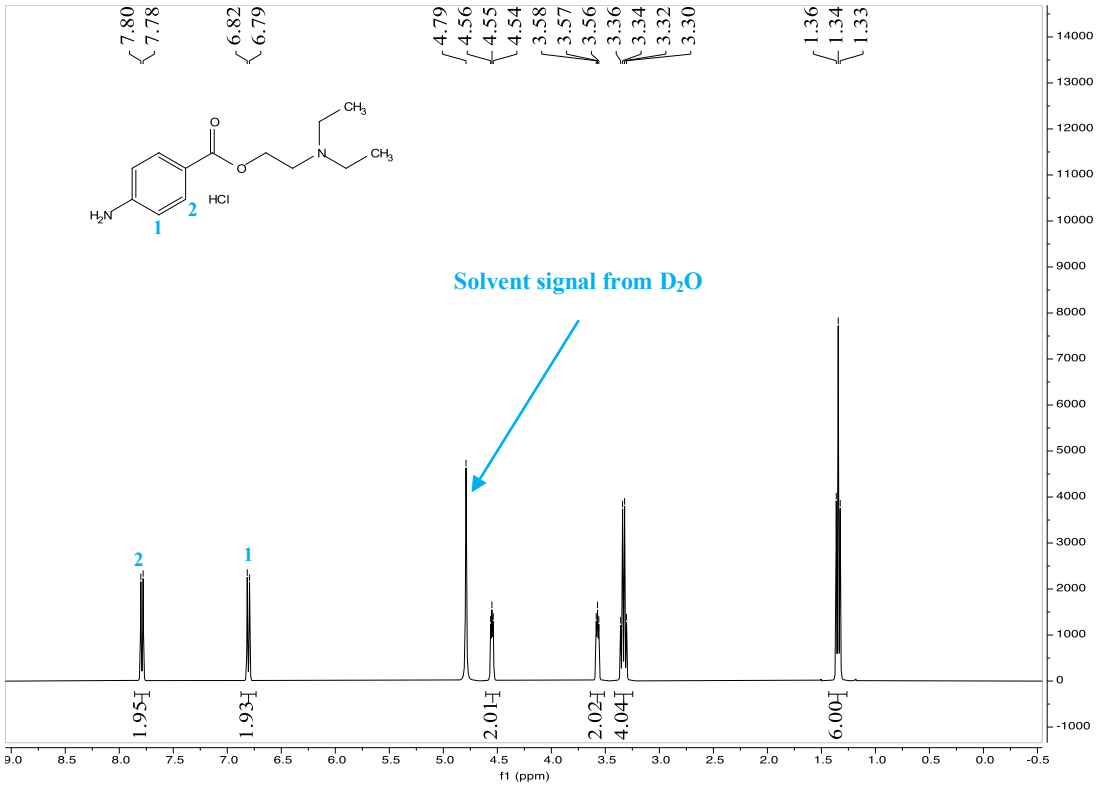

^{1}H NMR (400 MHz, D_2O) of product **48b**

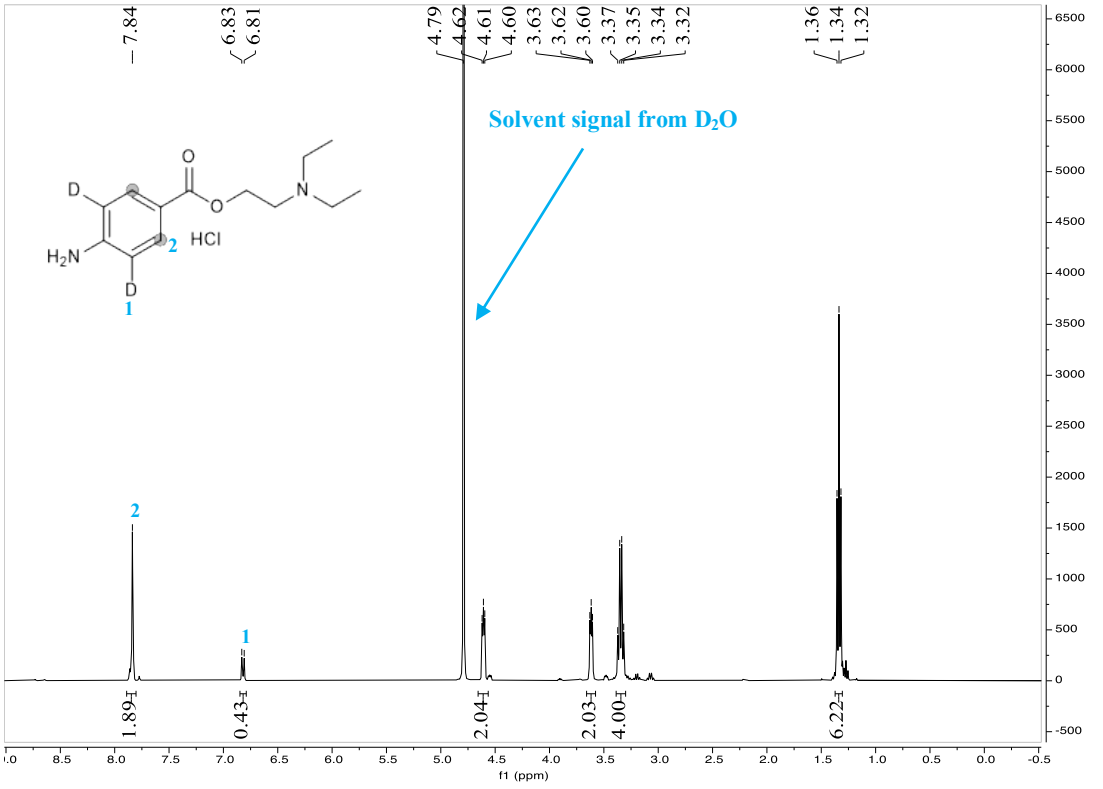

^{1}H NMR (400 MHz, DMSO-d_6) of feed material **49a**

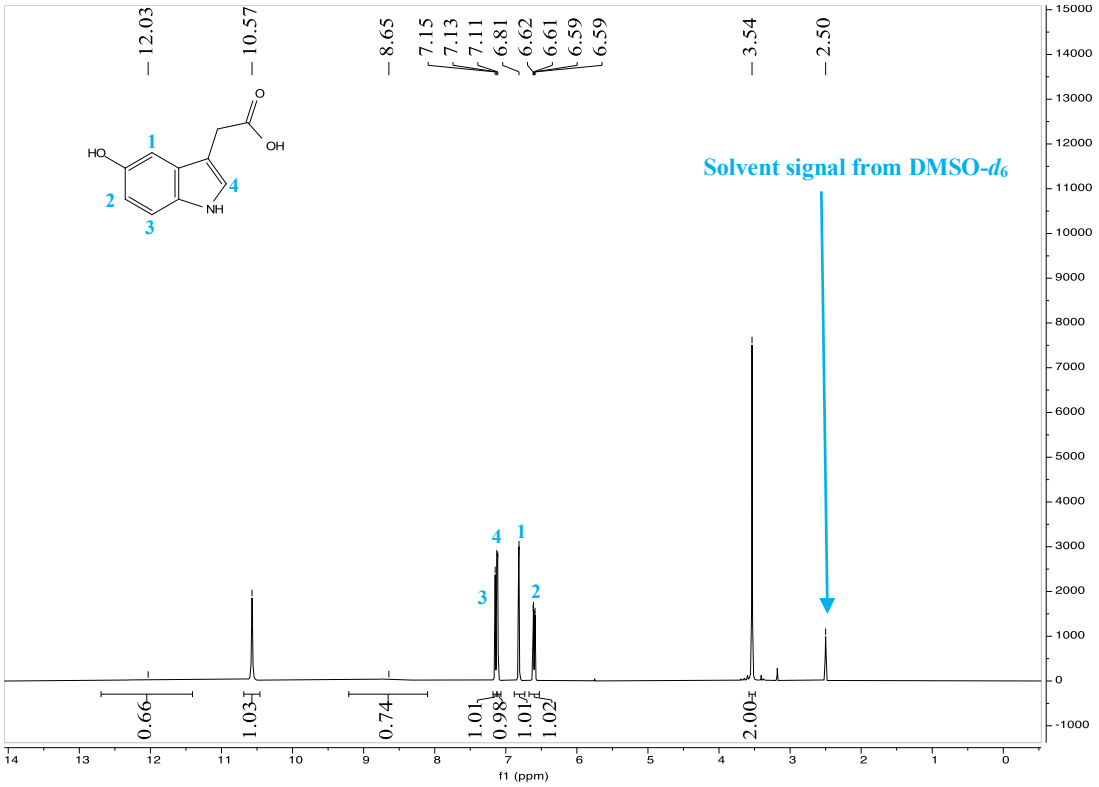

^{1}H NMR (400 MHz, DMSO-d_6) of product **49b**

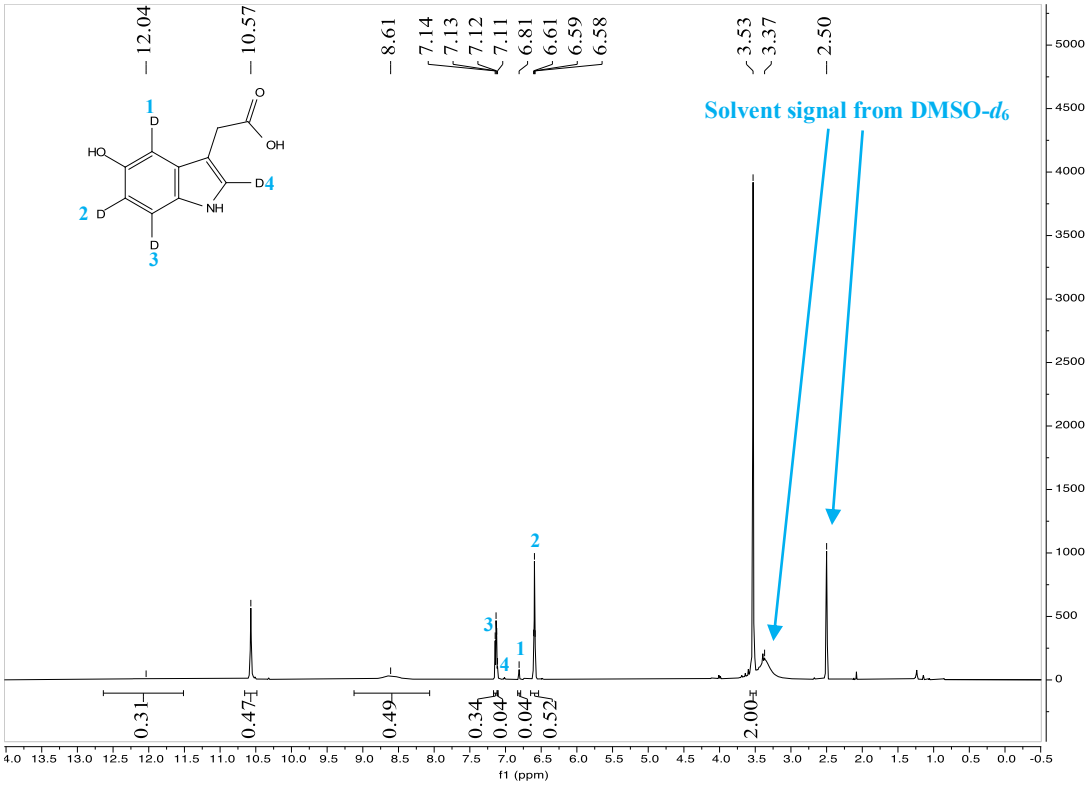

^{1}H NMR (400 MHz, DMSO-d_6) of feed material **50a**

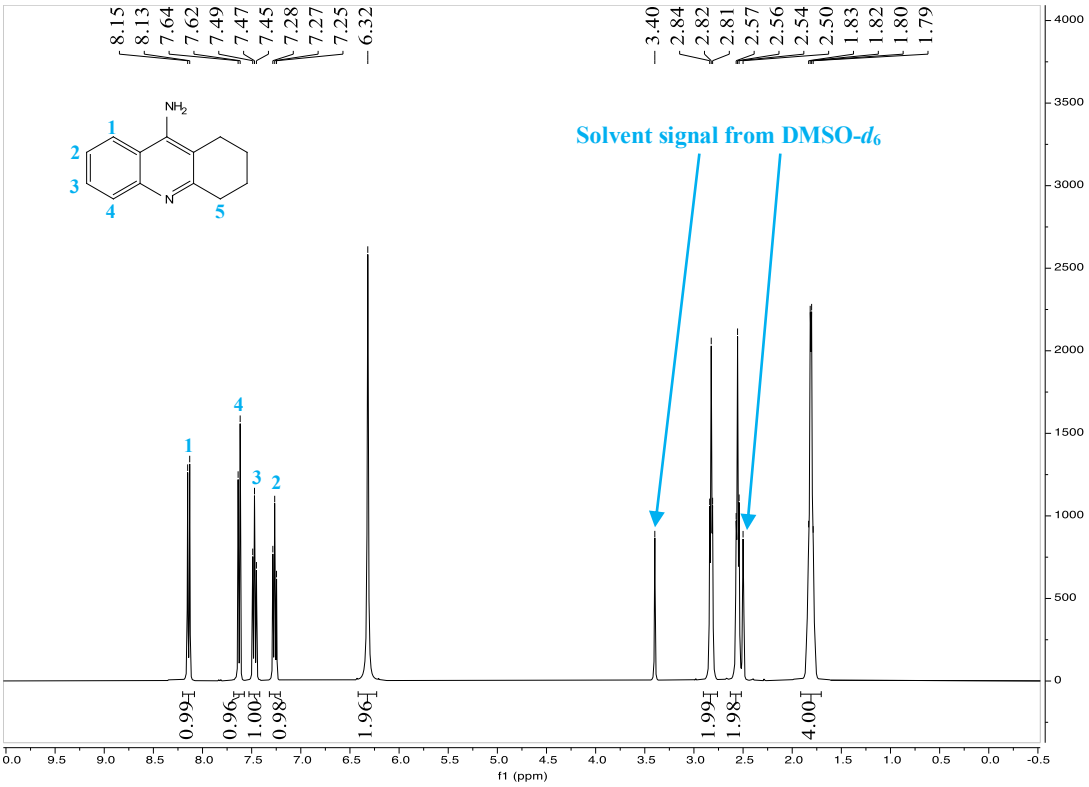

^{1}H NMR (400 MHz, DMSO-d_6) of product **50b**

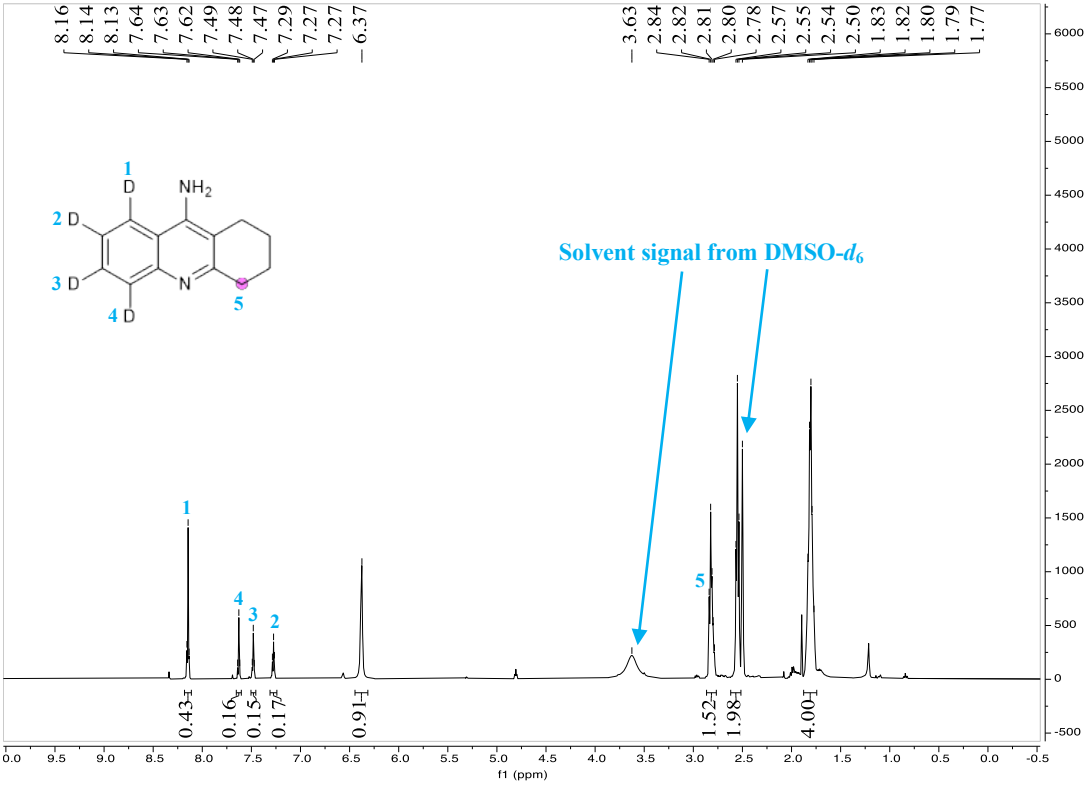

^{1}H NMR (400 MHz, DMSO-d_6) of reference material **51a**

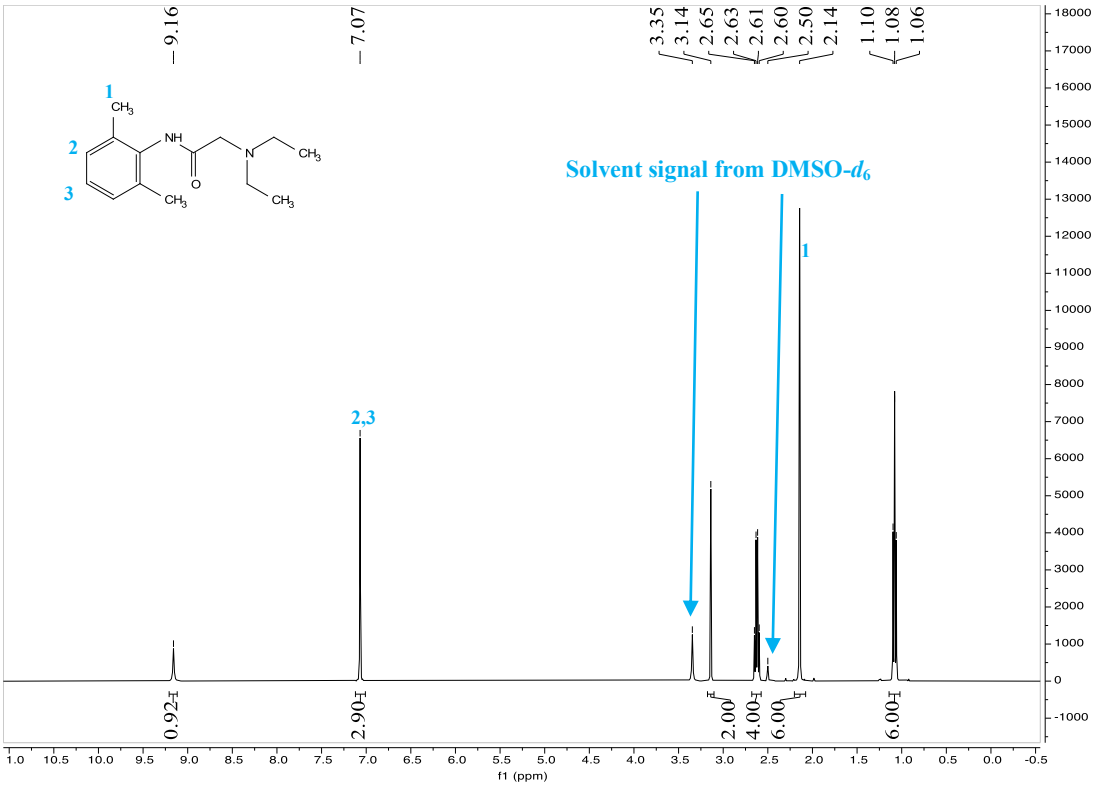

^{1}H NMR (400 MHz, DMSO-d_6) of product **51b**

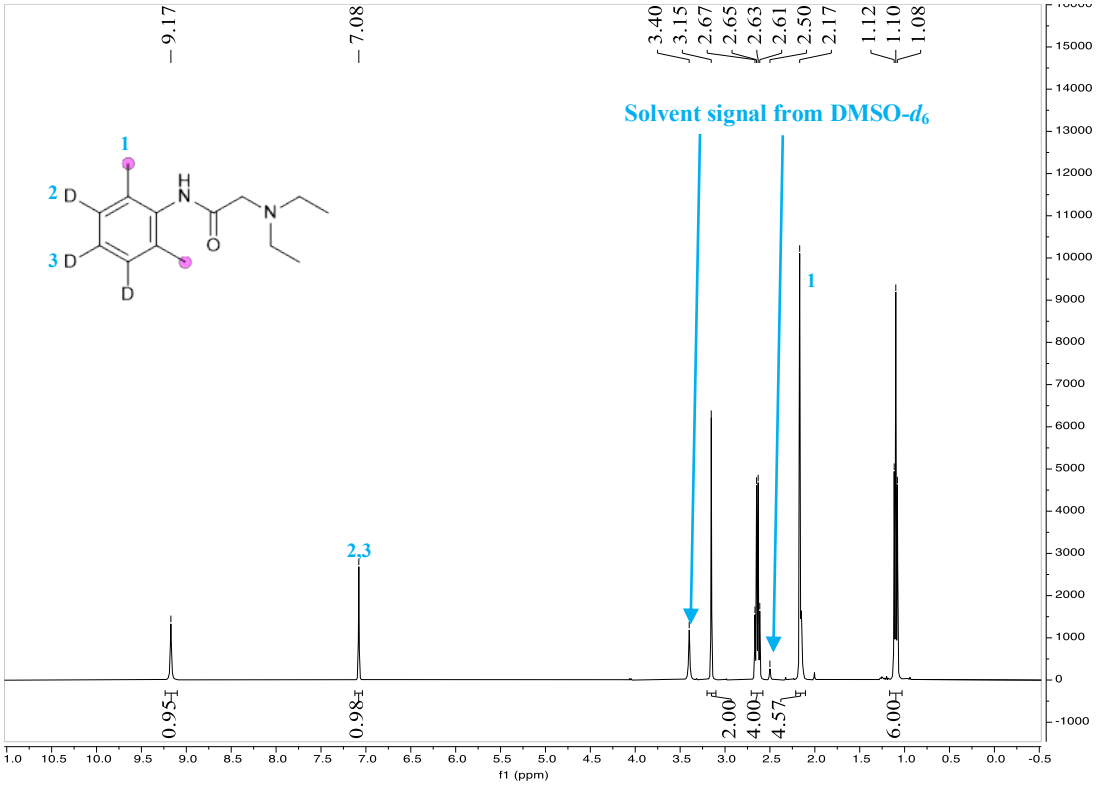

^{1}H NMR (400 MHz, DMSO-d_6) of reference material **52a**

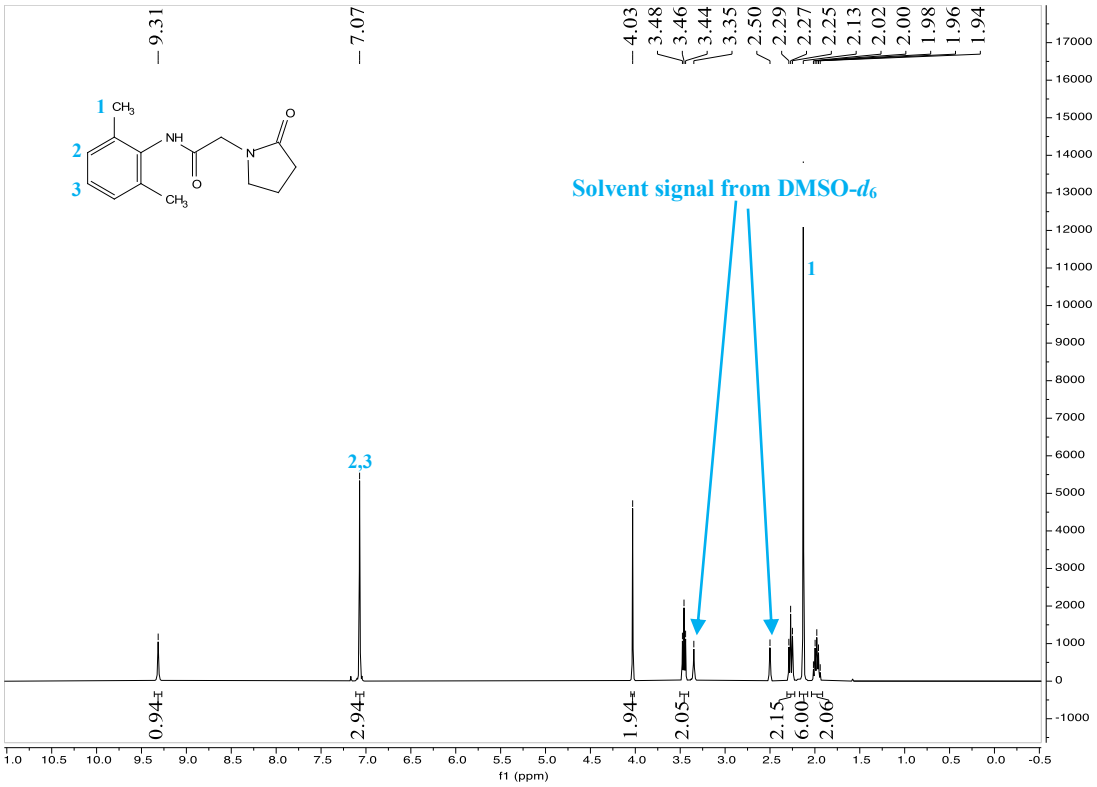

^{1}H NMR (400 MHz, DMSO-d_6) of product **52b**

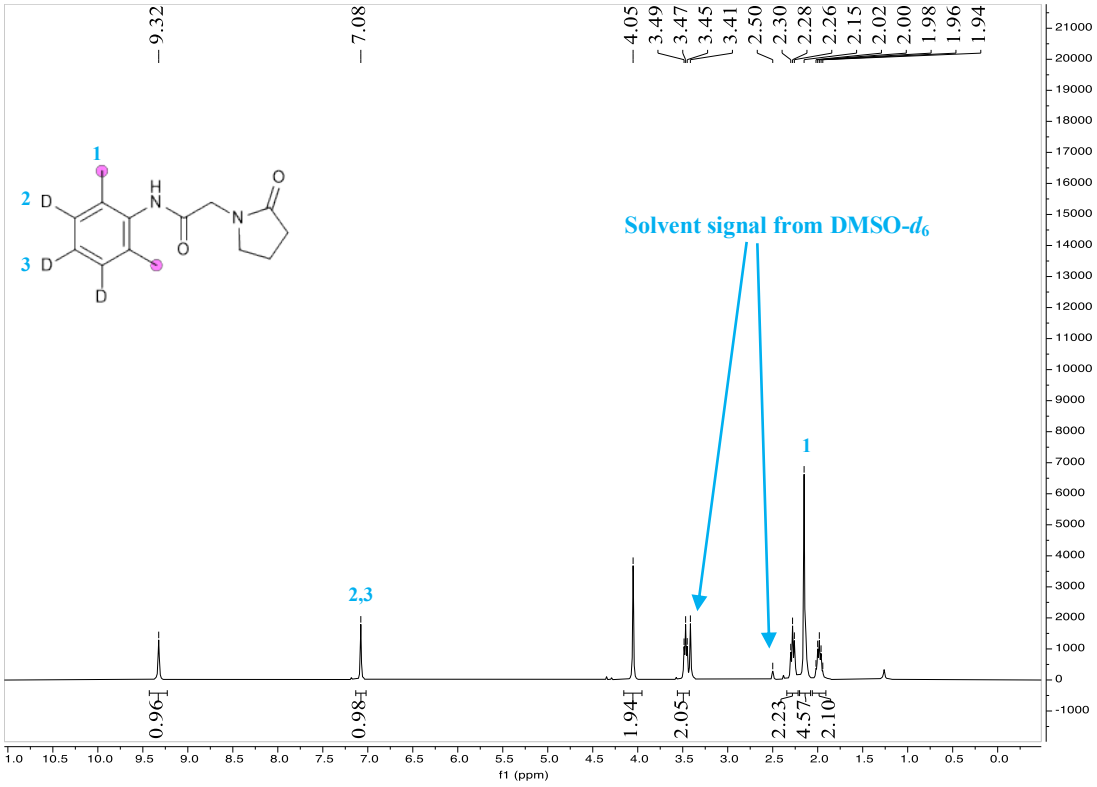

^{1}H NMR (400 MHz, DMSO-d_6) of reference material **53a**

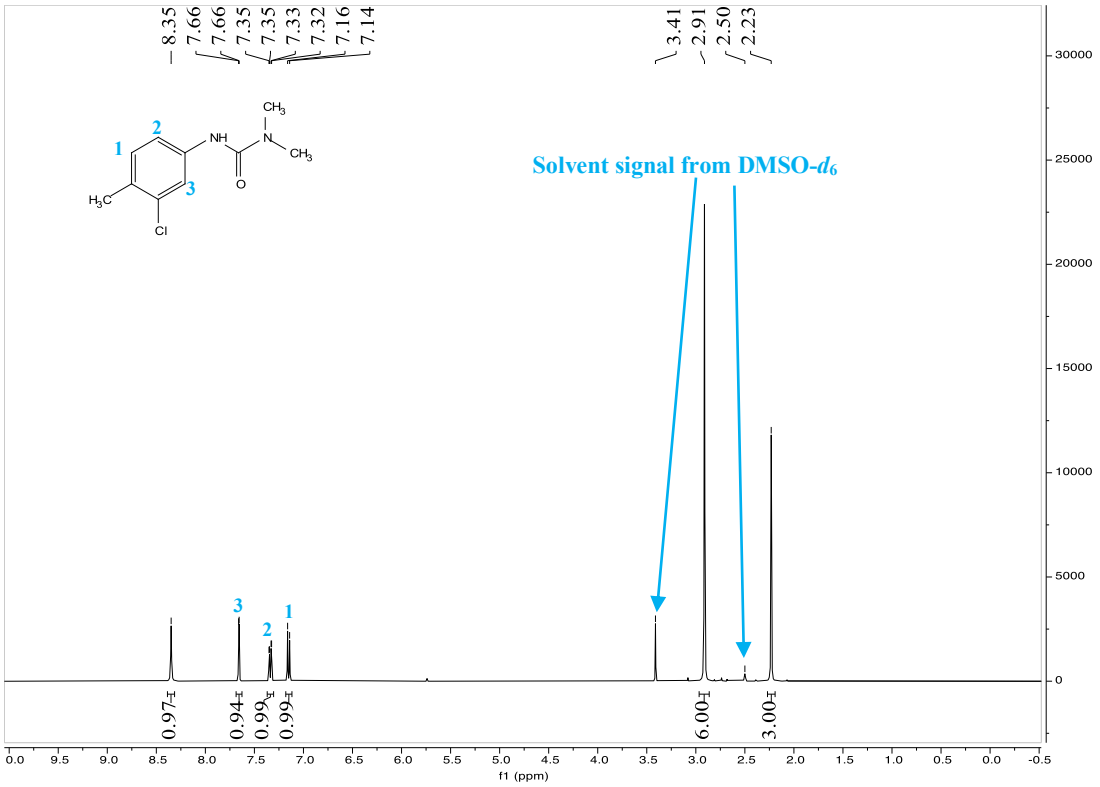

^{1}H NMR (400 MHz, DMSO-d_6) of product **53b**

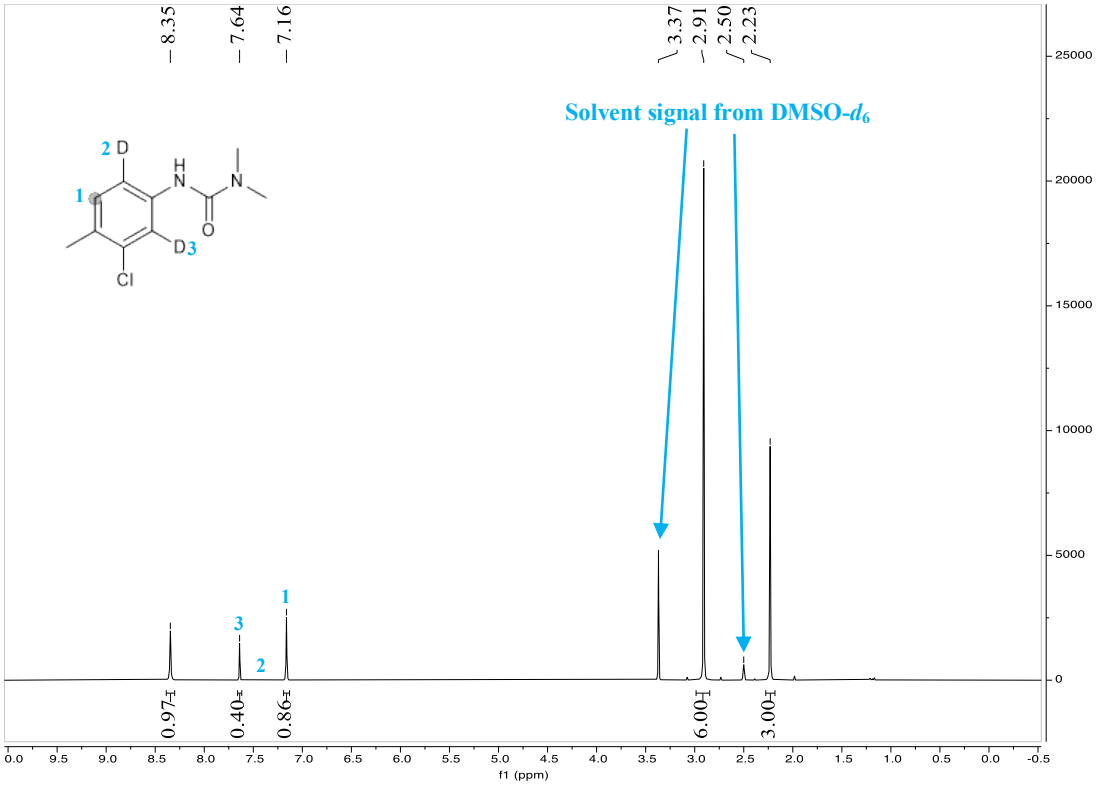

^{1}H NMR (400 MHz, DMSO-d_6) of reference material **54a**

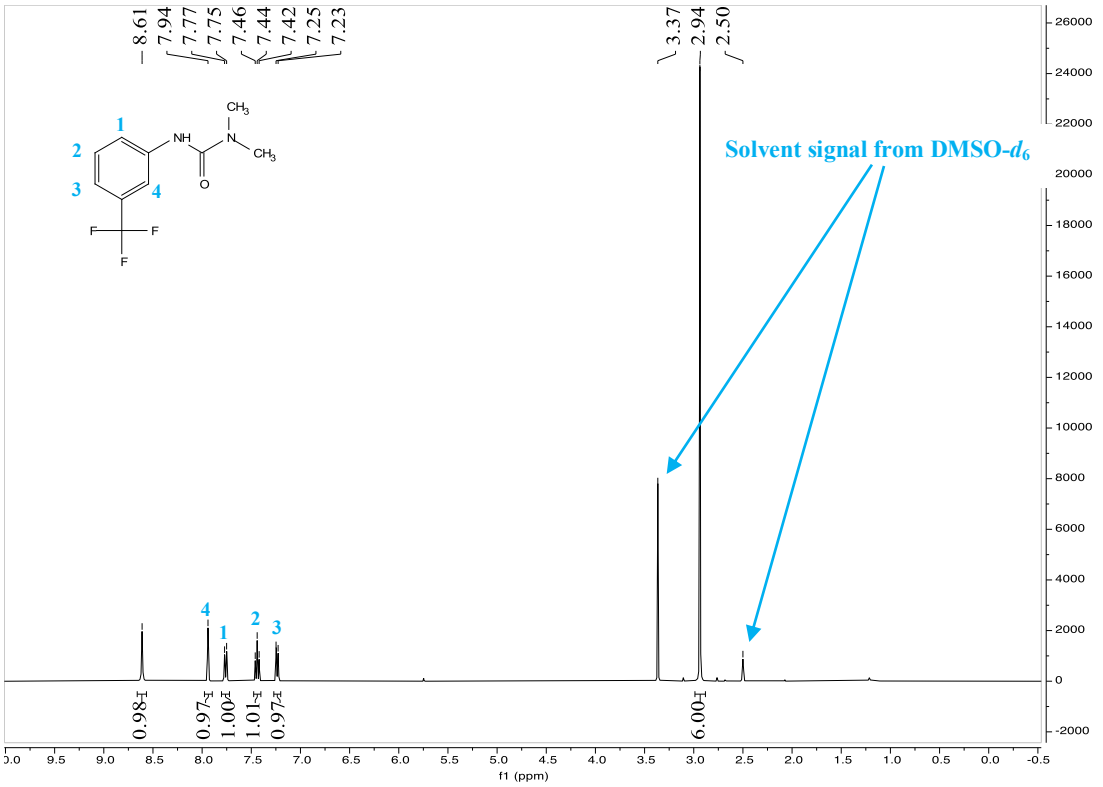

^{19}F NMR (376 MHz, DMSO-d_6) of reference material **54a**

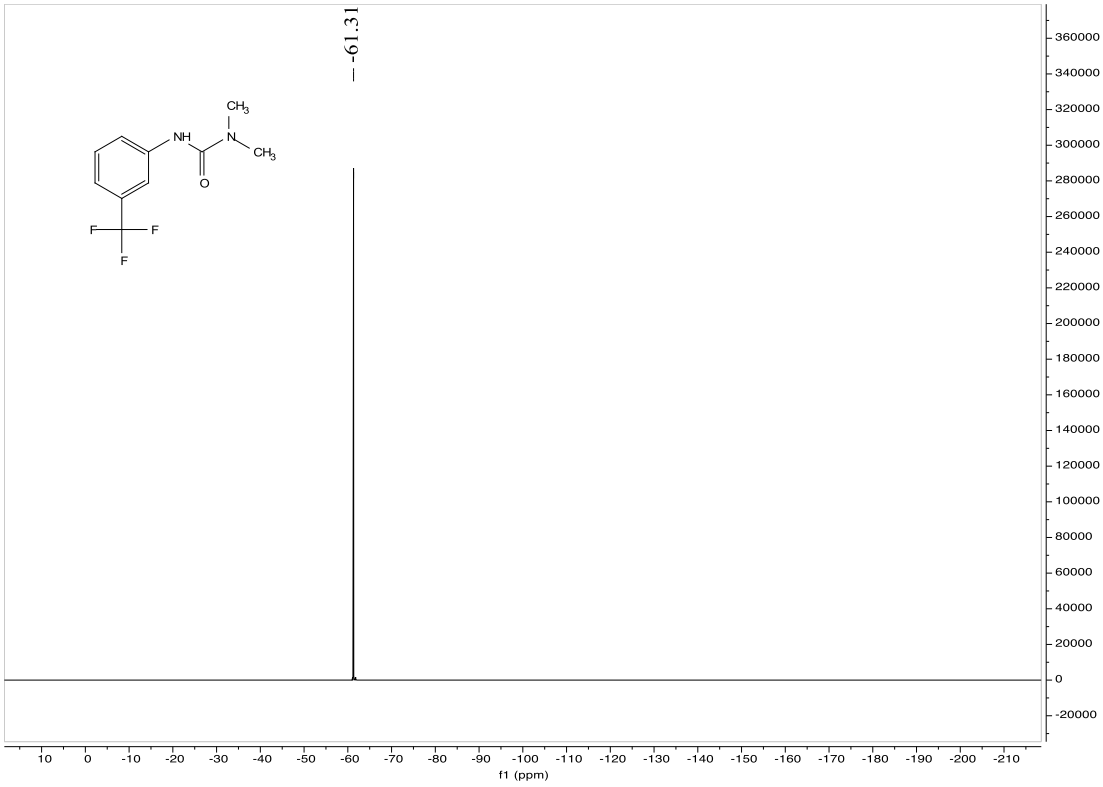

^{1}H NMR (400 MHz, DMSO-d_6) of product **54b**

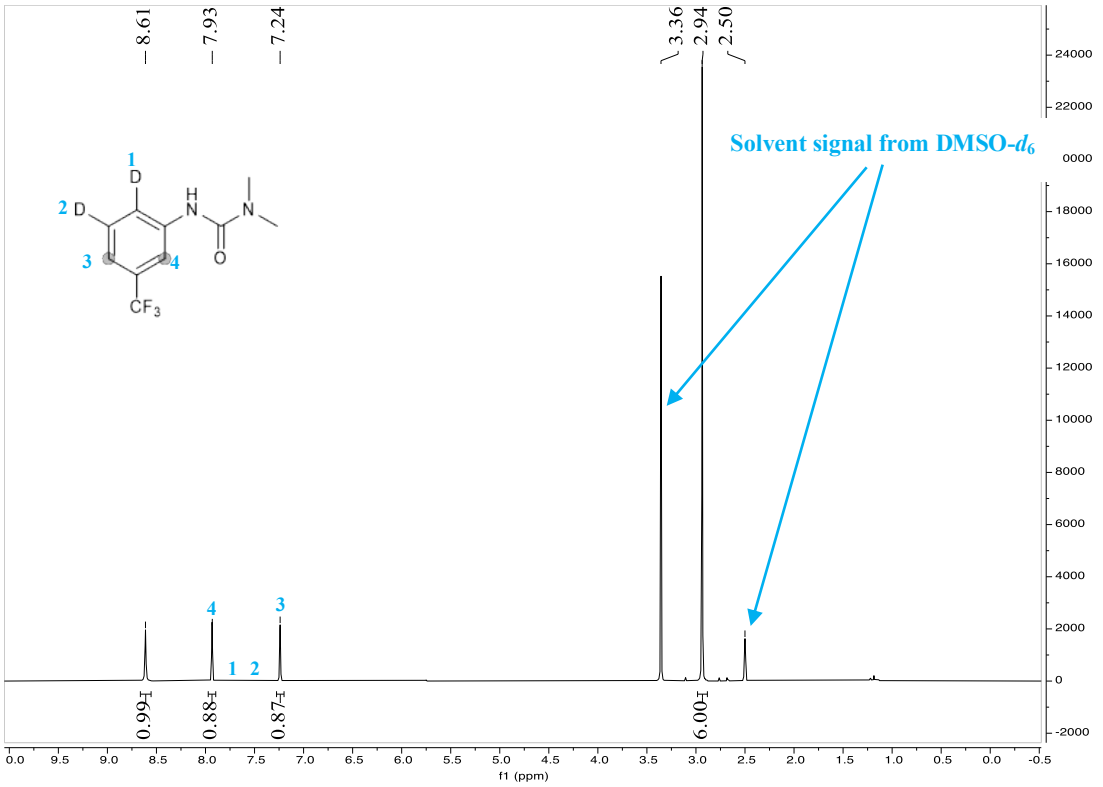

^{19}F NMR (376 MHz, DMSO-d_6) of product **54b**

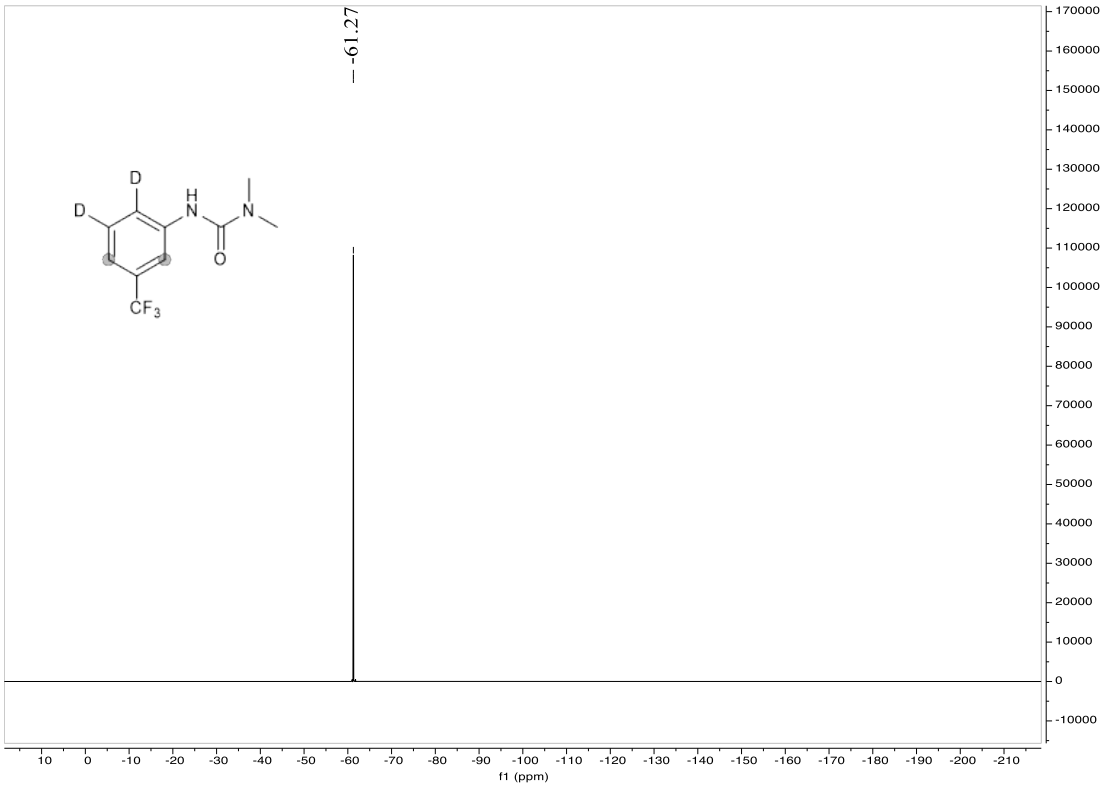

9. Supplementary References

1 Wu, S.-M. *et al.* Pt Single Atoms on TiO_2 Can Catalyze Water Oxidation in Photoelectrochemical Experiments. *J. Am. Chem. Soc.* **146**, 16363–16368 (2024).

2 Jiang, X., Li, M., Li, H. & Jin, Z. ZIF-9 derived cobalt phosphide and In_2O_3 as co-catalysts for efficient hydrogen production. *Mol. Catal.* **507**, 111551 (2021).

3 Dai, Y. *et al.* Light-tuned selective photosynthesis of azo- and azoxy-aromatics using graphitic C_3N_4. *Nat. Commun.* **9**, 60 (2018).

4 Lang, X., Chen, X. & Zhao, J. Heterogeneous visible light photocatalysis for selective organic transformations. *Chem. Soc. Rev.* **43**, 473–486 (2014).

5 Mansfeldova, V. *et al.* Work Function of TiO_2 (Anatase, Rutile, and Brookite) Single Crystals: Effects of the Environment. *J. Phys. Chem. C* **125**, 1902–1912 (2021).

6 de Souza, P. M. *et al.* Hydrodeoxygenation of Phenol over Pd Catalysts. Effect of Support on Reaction Mechanism and Catalyst Deactivation. *ACS Catal.* **7**, 2058–2073 (2017).

7 Wu, R. *et al.* Electrochemical Strategy for the Simultaneous Production of Cyclohexanone and Benzoquinone by the Reaction of Phenol and Water. *J. Am. Chem. Soc.* **144**, 1556–1571 (2022).

8 He, C. *et al.* Regulating Atomically-Precise Pt Sites for Boosting Light-Driven Dry Reforming of Methane. *Angew. Chem. Int. Ed.* **63**, e202412308 (2024).

9 Lei, H. *et al.* Thermally Triggered Redox Flexibility of Pt/CeO_2 Cluster Catalyst Against In-Situ Atomic Redispersion. *Angew. Chem. Int. Ed.* **64**, e202509239 (2025).

10 Qiao, B. *et al.* Single-atom catalysis of CO oxidation using Pt_1/FeOx. *Nat. Chem.* **3**, 634–641 (2011).

11 Zhang, Z. *et al.* Thermally stable single atom Pt/m-Al_2O_3 for selective hydrogenation and CO oxidation. *Nat. Commun.* **8**, 16100 (2017).

12 Mino, L., Zecchina, A., Martra, G., Rossi, A. M. & Spoto, G. A surface science approach to TiO_2 P25 photocatalysis: An in situ FTIR study of phenol photodegradation at controlled water coverages from sub-monolayer to multilayer. *Appl. Catal. B-Environ.* **196**, 135–141 (2016).

13 Fujisawa, J.-i., Kato, S. & Hanaya, M. Detailed study of a TiO_2-phenol complex using deuterated phenol. *Chem. Phys. Lett.* **803**, 139833–139839 (2022).

14 Fujisawa, J.-i., Matsumura, S. & Hanaya, M. A single Ti-O-C linkage induces interfacial charge-transfer transitions between TiO_2 and a π-conjugated molecule. *Chem. Phys. Lett.* **657**, 172–176 (2016).

15 Higashimoto, S. *et al.* Characteristics of the charge transfer surface complex on titanium(IV) dioxide for the visible light induced chemo-selective oxidation of benzyl alcohol. *RSC Adv.* **2**, 669–676 (2012).

16 Giuliano, B. M., Reva, I., Lapinski, L. & Fausto, R. Infrared spectra and ultraviolet-tunable laser induced photochemistry of matrix-isolated phenol and phenol-d_5. *J. Chem. Phys.* **136**, 024505 (2012).

17 Belhadj, H., Hakki, A., Robertson, P. K. J. & Bahnemann, D. W. In situ ATR-FTIR study of H_2O and D_2O adsorption on TiO_2 under UV irradiation. *Phys. Chem. Chem. Phys.* **17**, 22940–22946 (2015).

18 Yang, D. *et al.* Rapid Identification of Hydrogen Isotopes in Water Mixtures by FTIR Spectroscopy. *ACS Omega* **10**, 25801–25809 (2025).

19 Teng, Z. *et al.* Atomically dispersed low-valent Au boosts photocatalytic hydroxyl radical production. *Nat. Chem.* **16**, 1250–1260 (2024).

20 Fitzpatrick, D. E., Maujean, T., Evans, A. C. & Ley, S. V. Across-the-World Automated Optimization and Continuous-Flow Synthesis of Pharmaceutical Agents Operating Through a Cloud-Based Server. *Angew. Chem. Int. Ed.* **57**, 15128–15132 (2018).

21 Knight, N. M. L. *et al.* Iridium-Catalysed C(sp^3)−H Activation and Hydrogen Isotope Exchange via Nitrogen-Based Carbonyl Directing Groups. *Adv. Synth. Catal.* **366**, 2577–2586 (2024).

22 Baruah, K. *et al.* Stabilization of Azapeptides by Namide···H–N_{amide} Hydrogen Bonds. *Org. Lett.* **23**, 4949–4954 (2021).